DANMARKS OG GRØNLANDS GEOLOGISKE UNDERSØGELSE RAPPORT 2016/38

Geology and Mineral Potential of South-East Greenland

Jochen Kolb, Bo Møller Stensgaard, Thomas F. Kokfelt (eds)

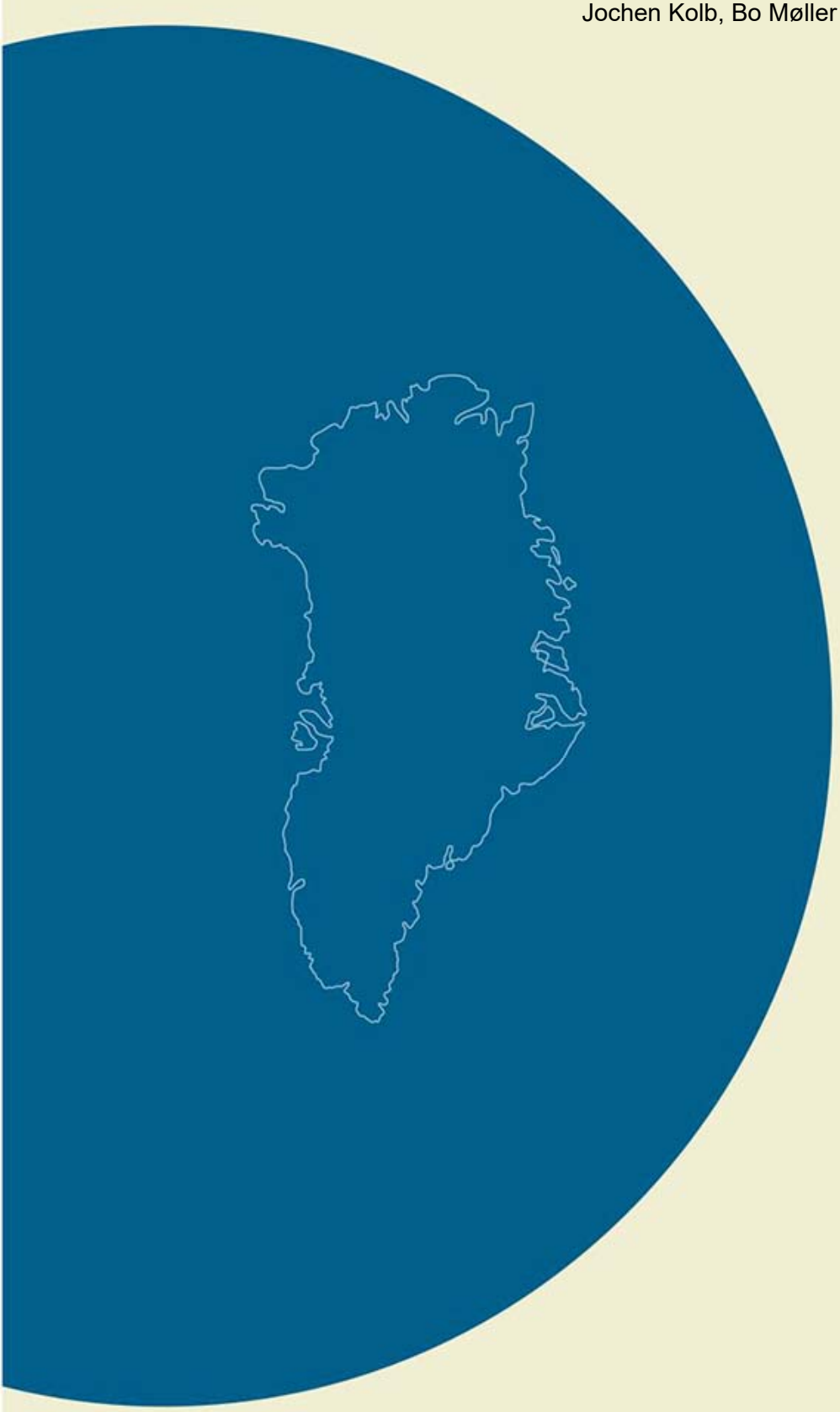

GEOLOGICAL SURVEY OF DENMARK AND GREENLAND
DANISH MINISTRY OF ENERGY, UTILITIES AND CLIMATE

GEUS

DANMARKS OG GRØNLANDS GEOLOGISKE UNDERSØGELSE RAPPORT 2016/38

Geology and Mineral Potential of South-East Greenland

Final report from the South-East Greenland Mineral ENdownment Task (SEGMENT)

Jochen Kolb, Bo Møller Stensgaard & Thomas F. Kokfelt (eds)

GEOLOGICAL SURVEY OF DENMARK AND GREENLAND
DANISH MINISTRY OF ENERGY, UTILITIES AND CLIMATE

GEUS

Content

1 Introduction

South-East Greenland between 62°30'N and 66°30'N was before 2009 one of the most poorly known areas of Greenland. Following expeditions in the early 20st Century, geologists from British Universities mapped the area from the shore in the 1960s. The Greenland Geological Survey (GGU) joined these geological mapping expeditions in the late 1960s, early 1970s and early 1980s. Helicopter and fixed-wing aircraft support was first available in 1986 and 1987, where areas further inland could be mapped. These expeditions resulted in two 1:500 000 scale map sheets and continued geological research in collaboration with researchers from several universities. Regional geochemical or geophysical data sets were not compiled and in very poor resolution. Two efforts by universities and GGU were accomompained by only limited mineral exploration. Kryolitselskabet Øresund A/S and Nordisk Mineselskab A/S carried out helicopter supported prospecting of the area and at Kialineq (Kialeq) in 1963 and 1971, respectively. Graphite mineralisation north of Tasiilaq was discovered during GGU campaigns and were briefly mapped and studied by Mineral Development International A/S in 1992 (Kalvig 1992). Nickel-PGE sulphide mineralisation in the Ammassalik Intrusive Complex (AIC) close to Tasiilaq area has received most attention with a more detailed exploration program since 1996 by various companies (Lie 1997).

When the **S**outh-**E**ast **G**reenland **M**ineral **EN**dowment **T**ask (**SEGMENT**) project was organized in late 2008 and early 2009 in collaboration between the Geological Survey of Denmark and Greenland (GEUS) and the Bureau of Minerals and Petroleum (BMP, now Ministry of Mineral Resources, MMR) the main aims were jointly formulated as:

- Compiling a regional stream sediment geochemical and till indicator mineral survey;
- Compiling a regional aeromagnetic survey of South-East Greenland;
- Conduct geological field investigations in order to characterise the main lithology and as the basis for geological research, including petrology, structural geology, geochemistry and geochronology;
- Evaluate economic geology and mineral potential through field investigations, using geological parameter in order to be able to predict possible mineralisation;
- Revise the existing 1:500 000 geological map of South-East Greenland; and
- Integrated data interpretation to describe and provide a geological model for the geological evolution of South-East Greenland and assess the mineral of potential of the region.

In this report, we summarize the data collected and the main research results that are based on intense field expeditions in the previous years aimed at reaching the main goals listed above. The report aims at providing an overview of all rock units and events encountered in the area covered by the SEGMENT project. Consequently, to gain the most of the report it is suggested that it is used in conjunction with the reviesed 1:500 000 scale map which is accessible and printable from on the 'SEGMENT Data Package' that is accessible on the memory-stick which is enclosed to this report (see also section '2 SEGMENT Data Package').

This report represents the status at the time of writing, and numerous ongoing joint research projects will continue to publish new data on the area between 62°N and 66°30'N. Not all researchers or institutes that have been involved in collaborative projects under the SEGMENT framework are represented in this report, but it should be emphasized that without their contribution and scientific discussion, this project would not have been successful. The large-scale effort that was made during the SEGMENT project including costly field expeditions, thus, not only yields a return in the form of new data generated during the project, but also has a more sustainable aspect in continued research within joint research projects between mainly GEUS, MMR and various university partners based on the collected data.

During the SEGMENT project, the 1:500 000 scale maps have been continuously updated with corrections and new data. This report is organized chronologically starting with the Archaean and describes the main map units. It should, therefore, be read together with the updated map sheets. Brief chapters summarize our current understanding of the geological evolution, mainly during the Archaean and Palaeoproterozoic, where most of the study area was transformed into a stable shield with limited reactivation in the Mesoproterozoic and the Tertiary continental breakup in the north. The regional geochemical and geophysical data sets are briefly described, and the report ends with a description of mineralisation and mineralising processes. This report can only give a summary and brief overview of the data and research results, which are already published in GEUS reports and international peer-reviewed journals. We aimed at a comprehensive reference list so the interested reader is able to continue his or hers research in the relevant articles.

2 SEGMENT Data Package

Símun D. Olsen & Bo Møller Stensgaard

A collection of data produced during the South-East Greenland Mineral Endowment Task (SEGMENT) project from 2009–2016 have been compiled on the memory-stick enclosed to this report. Included also is also the digital version of the revised 1:500 000 geological map which has been produced during the SEGMENT project as well as a printable pdf version of the map (print scaled to A0).

2.1 Access to the data

The data is stored in the SEG_2016 folder on the USB memory-stick which is enclosed in the report.

Access to the data is possible via ESRI's ArcGIS system (ArcMap an ArCatalog) v. 10 to 10.4, and file manager in Windows based computer systems. Machintosh and Linux systems will also do. However, access and reading of geodatabase filesystems requires ArcGIS systems. Version 10 is used in this project.

The ArcMap project file (SEG_2016.mxd or SEG_2016_v10_0.mxd) hosts all the data that is provided on the USB flash drive. The size of the data provided here is c. 44.2 GB.

The ellipsoid and datum used is the WGS84, UTM zone 24N (i.e. Central Meridian is 39°West) and False Easting is 500 000. Most of the data is recorded with geographic coordinates, using decimal degrees.

2.2 Contents of the SEGMENT Data Package

The USB memory-stick contains the following datasets.

- Revised 1:500 000 scale geological map
- Localities and oblique photos
- Structural measurements
- Digital Field Data - description of localities, samples, etc.
- Lithogeochemistry
- Fine-fraction sediment sample geochemistry
- Stream- and surface water chemistry
- Scanned maps from previous field campaigns

More details on the above datasets can be found in Appendix I.

3 Archaean granite-gneiss complexes

Jochen Kolb & Leon Bagas

Most of the area studied in South-East Greenland between 62°N and 67°N is underlain by Archaean granite-gneiss complexes of mainly Meso- to NeoArchaean age (Andrews *et al.* 1973, Andrews *et al.* 1971, Bagas *et al.* 2013, Bridgwater and Gormsen 1968, Bridgwater and Gormsen 1969, Escher and Nielsen 1983, Kalsbeek 1989, Kolb *et al.* 2013, Nielsen and Escher 1985, Stensgaard *et al.* 2010, Wright *et al.* 1973). Two different cratonic areas, the North Atlantic Craton (NAC) in the south and the East Greenland Archaean (EGA) in the north that possibly is correlated with the Rae Craton westward, are separated by the NW-trending Palaeoproterozoic Nagssugtoqidian Orogen (in Kalsbeck 1989 referred to as "the Ammassalik mobile belt") between approx. 65°N and 67°N (Andrews et al. 1973, Bridgwater 1976, Bridgwater et al. 1990, Bridgwater et al. 1976, Bridgwater et al. 1977, Bridgwater et al. 1978, Bridgwater et al. 1973, Bridgwater and Gormsen 1968, Bridgwater and Gormsen 1969, Bridgwater and Myers 1979, Kalsbeek 1989, Kalsbeek et al. 1993, Kolb 2014, Myers 1984, Myers 1987, Myers et al. 1979b, Nutman et al. 2008b, Wright et al. 1973).

3.1 North Atlantic Craton (NAC)

The NAC in the study area, the Thrym Complex, is dominated by felsic orthogneiss with only 0.5-1 km wide and several km long dismembered belts of metamorphosed mafic, ultramafic and sedimentary rocks (Fig. 3.1). It is thus difficult to define a basement for the precursor igneous rocks of the felsic gneiss. A few preserved intrusive relationships indicate that the felsic rocks intruded a mafic to ultramafic basement of unknown age.

3.1.1 Metamorphosed mafic, ultramafic and sedimentary rocks

The metamorphosed mafic, ultramafic and sedimentary rocks occur in dismembered belts and as xenoliths in orthogneiss (Fig. 3.1). They were not mapped in detail, and stratigraphy and geochronology are difficult due to the high-grade metamorphic nature of the rocks. One mafic granulite from inner Graah Fjord (Lommen) yields a formation age of 2859 ± 6 Ma contemporaneous with the early orthogneiss (Bagas *et al.* 2016). Metasedimentary rocks from Helge Halvø and Jættefjord contain *c.* 2800 Ma and *c.* 2840 Ma detrital zircons, indicating that they may represent erosion products of the ≥ 2800 Ma mafic and felsic rocks (Berger *et al.* 2014). Generally the rocks have been metamorphosed at granulite facies peak conditions and were subsequently variably retrogressed in the amphibolite facies. Greenschist facies overprint is localized to metre-scale shear zones. The ultramafic and mafic rocks include dunite, peridotite, hornblendite, pyroxenite, mafic granulite, amphibolite and paragneiss (Andrews *et al.* 1973, Bridgwater and Gormsen 1969, Kolb *et al.* 2013, Nielsen and Escher 1985).

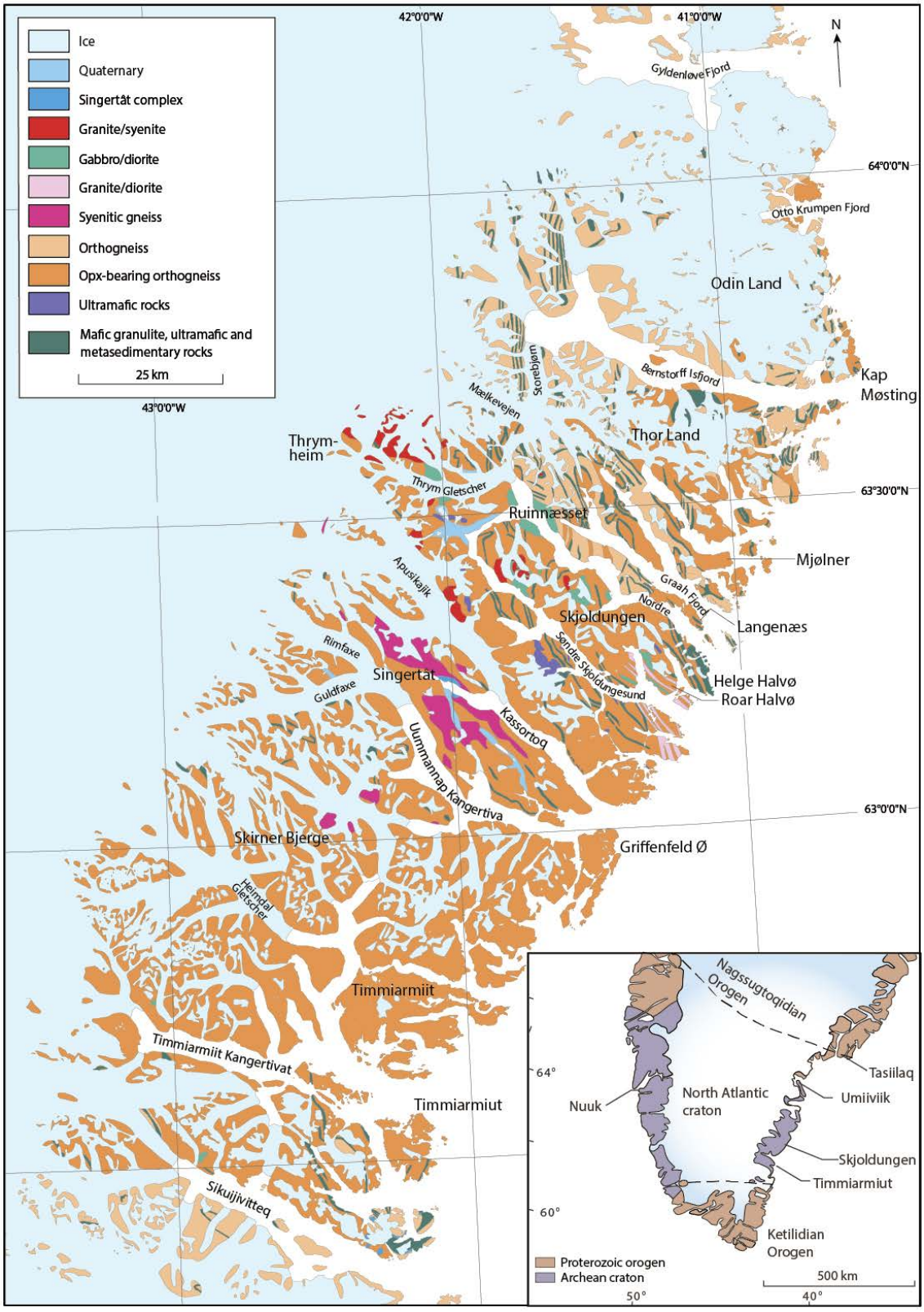

Figure 3.1 *Geological map of the Thrym Complex of the North Atlantic Craton in the Timmiarmiut-Skjoldungen area, South-East Greenland (Kolb* et al. *2013).*

Mafic granulite and amphibolite

The most common rock type is dark, medium-grained, well-foliated mafic granulite composed of orthopyroxene, clinopyroxene, plagioclase, quartz, magnetite, and, locally, ilmenite, biotite and hornblende (Kolb *et al.* 2013). It has abundant leucosomes, which are coarser-grained and contain plagioclase, quartz, clinopyroxene, orthopyroxene and garnet (Fig. 3.2A). Coarse-grained mafic granulite represents a possible meta-gabbro and contains plagioclase, hornblende, orthopyroxene, and magnetite, whereby plagioclase has a cumulate texture (Kolb *et al.* 2013).

Figure 3.2 *Photographs of the field appearance of **A.** mafic granulite, **B.** ultramafic rocks and **C.** banded paragneiss (Kolb* et al. *2013).*

Mafic granulite has a basaltic composition with a Mg# between 44 and 67, and a flat or enriched REE pattern. Meta-gabbro has a Mg# of 55, a slightly LREE enriched pattern, and negative Pb, P as well as positive Nb, Ta, Sr and Ti anomalies (Kolb *et al.* 2013). Two geochemical types are distinguished (Fig. 3.3) (Bagas *et al.* 2016): (M1) rocks with a distinctly fractionated chondrite-normalised heavy rare earth element (HREE) and a variable light rare earth element (LREE) signature with pronounced negative Eu anomaly in some of them. They are overall enriched in highly incompatible elements. Platinum group element patterns are positively fractionated; and (M2) rocks with consistently flat and unfractionated HREE pattern, rather flat or mildly enriched LREE signature, with an overall lower abundance of incompatible elements. They consistently display a negative Nb-Ta anomaly, but

no Eu anomaly. Platinum group element patterns are more fractionated and commonly display higher Au contents (Bagas *et al.* 2016).

Ultramafic rocks
The dunite is composed of olivine, spinel, magnetite, hornblende, sulphides and biotite (Kolb *et al.* 2013). The peridotite is fine-grained equigranular and contains olivine, orthopyroxene, clinopyroxene, pargasitic to kaersutitic amphibole, green spinel, opaque minerals and serpentine (Bagas *et al.* 2016). The pyroxenite is darker blue-black and varies from fine-grained to coarse-grained (Fig. 3.2B). The fine-grained end-member consists of clinopyroxene, orthopyroxene, olivine, amphibole, minor biotite and quartz, and interstitial opaque minerals. The coarse-grained end-member consists of pyroxene replaced by amphibole, which is in turn replaced by biotite (Bagas *et al.* 2016).

A significant scatter in the major element data for peridotite and pyroxenite is explained by variable modal mineral abundances (Kolb *et al.* 2013). Similar to the mafic granulite, two compositional groups are distinguished (Fig. 3.3) (Bagas *et al.* 2016, Kolb *et al.* 2013): (UM1) rocks with a fractionated chondrite normalised HREE signature and a commonly fractionated and enriched LREE signature, and generally negative Eu anomaly. The rocks are overall enriched in highly incompatible elements; and (UM2) rock with a consistently flat and unfractionated HREE pattern, a commonly flat or mildly enriched LREE signature, and an overall lower abundance of highly incompatible elements. Most rocks display a negative Nb-Ta anomaly. Platinum group element patterns display mildly fractionated patterns and are not consistently different between the two groups (Bagas *et al.* 2016).

Paragneiss
The paragneisses are medium-grained light grey to white with a brownish rusty weathering surface and show locally a primary layering on the decimetre- to millimetre-scale (Fig. 3.2C) (Berger *et al.* 2014, Kolb *et al.* 2013). The layers are quartz- or biotite-rich with narrow heavy mineral layers (e.g. apatite, zircon and monazite). The paragneisses can be subdivided into three groups related to their protoliths (Berger *et al.* 2014): (1) meta-psammite; (2) meta-semipelite; and (3) restitic rocks with undefined protolith. They vary in $KAlO_3/(FeO+MgO)/Al_2O_3$ ratios, whereas the Mg# is more constant between 0.40 and 0.55. The Post-Archaean Australian average Shale (PAAS) normalized REE patterns are relatively flat (Kolb *et al.* 2013).

The meta-psammite contains quartz, K-feldspar, plagioclase, garnet and biotite with accessory zircon, monazite and apatite. Rutile and sillimanite occur as inclusions in garnet. Garnet is not zoned and has similar composition from grain to grain with ~ $X_{Alm}0.55$, $X_{Py}0.39$, $X_{Gr}0.04$. Biotite has a X_{Mg} of 0.75 and the TiO_2 content is ~ 5.5 wt% (Berger *et al.* 2014, Kolb *et al.* 2013).

The impure meta-semipelite contains quartz, perthitic K-feldspar, plagioclase, sillimanite, garnet, biotite, cordierite and rutile with accessory zircon, monazite and apatite (Kolb *et al.* 2013). Garnet is locally elongated parallel to the foliation and has strongly lobate grain boundaries. All garnets contain quartz and feldspar inclusions. Some garnet includes sillimanite needles in the centre, which indicate an apparent zonation, but they show no compositional zonation with similar compositions (~ $X_{Alm}0.47$, $X_{Py}0.43$, $X_{Gr}0.04$). Cordierite (X_{Mg}

of 0.82) shows different intensity of pinnitization. The restitic rocks contain quartz, antiperthitic plagioclase, K-feldspar, biotite and orthopyroxene (Berger *et al.* 2014). Abundant leucosomes form patches of coarse-grained K-feldspar, quartz and plagioclase are deformed (Kolb *et al.* 2013).

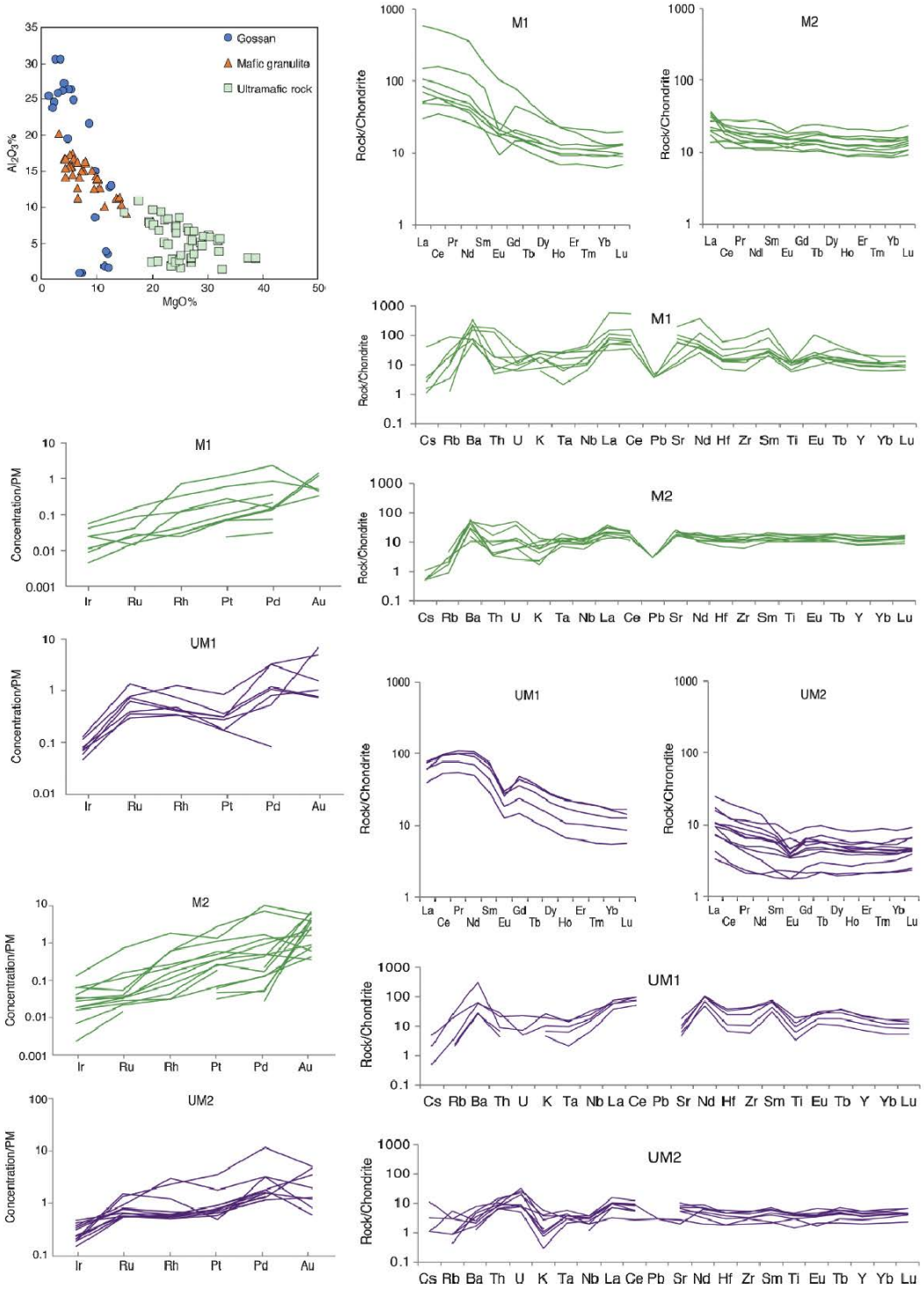

Figure 3.3 *Compilation of geochemical data of the mafic and ultramafic rocks of the Thrym Complex (Bagas* et al. *2016).*

3.1.2 Felsic orthogneiss

Felsic orthogneiss is the dominant rock type of the area where they range in composition from tonalite to monzogranite. Based on geochronology, mineralogy and fabric, several generations of orthogneiss are distinguished in the field (Kolb *et al.* 2013). Orthogneisses vary considerably from dioritic to monzogranitic compositions. They have a Mg# between 21 and 62, a K/Na ratio between 0.2 and 1.2, and an A/CNK ratio (molecular Al/(Ca + Na + K) around 1.0 (Kolb *et al.* 2013). The trace element patterns are not easily compared with typical Archaean tonalite-trondhjemite-granodiorite (TTG), because many of them represent anatectic rocks (Bagas *et al.* 2013, Kolb *et al.* 2013).

*Early- to syn-tectonic orthogneiss (*c. *2860-2780 Ma)*
Early- to syn-tectonic orthogneiss is medium-grained, banded, greenish grey and composed of orthopyroxene, antiperthitic and perthitic feldspars, quartz, magnetite and, locally, clinopyroxene, biotite and pyrite (Fig. 3.4A–B) (Kolb *et al.* 2013). They are the main rock type of the Thrym Complex. The leucosomes consist of 1-2 cm sized feldspar with perthitic K-feldspar cores and antiperthitic feldspar rims, biotite and quartz. Porphyritic orthogneiss is characterised by 1-2 cm sized feldspar porphyroclasts, quartz, biotite, clinopyroxene, magnetite and ilmenite (Kolb et al. 2013). The rocks are commonly referred to as tonalite, trondhjemite, granodiorite (TTG) and monzogranite although only few bulk compositions fall in the tonalite field. They also have unusual trace element compositions (Fig. 3.5), and both characteristics may reflect the complex evolution during emplacement and anatexis at granulite facies peak metamorphism (Bagas *et al.* 2013, Kolb *et al.* 2013).

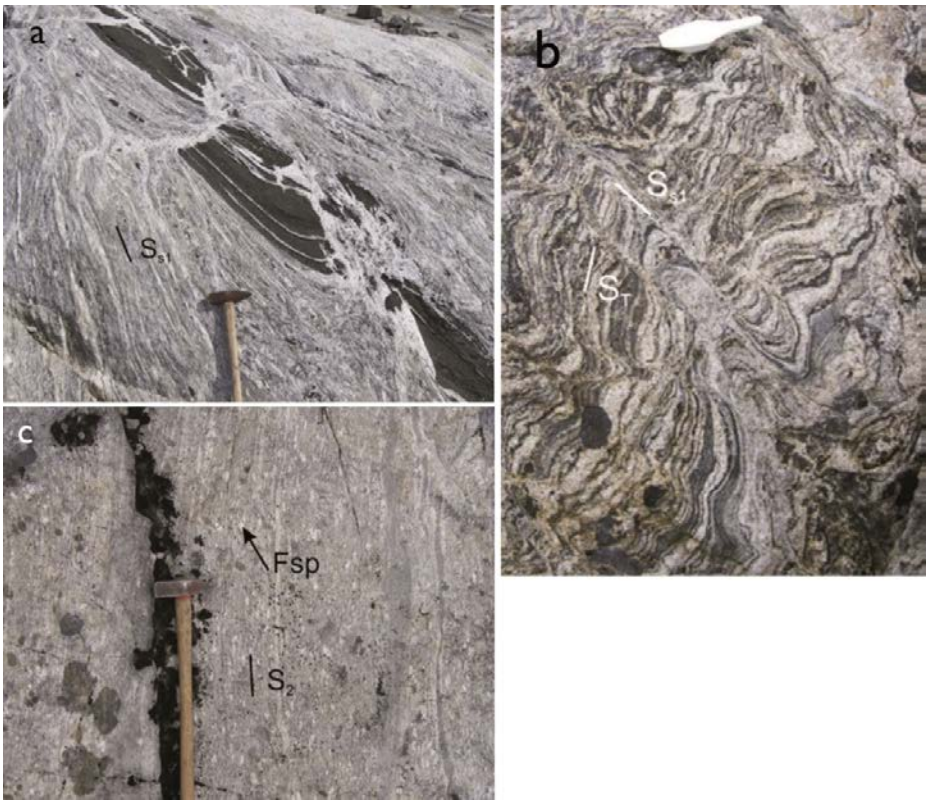

Figure 3.4 *Field photographs of early- to syn-tectonic orthogneiss:* ***A.*** *orthogneiss with leucosomes and mafic granulite xenoliths;* ***B.*** *banded orthogneiss; and* ***C.*** *porphyritic orthogneiss (Kolb* et al. *2013).*

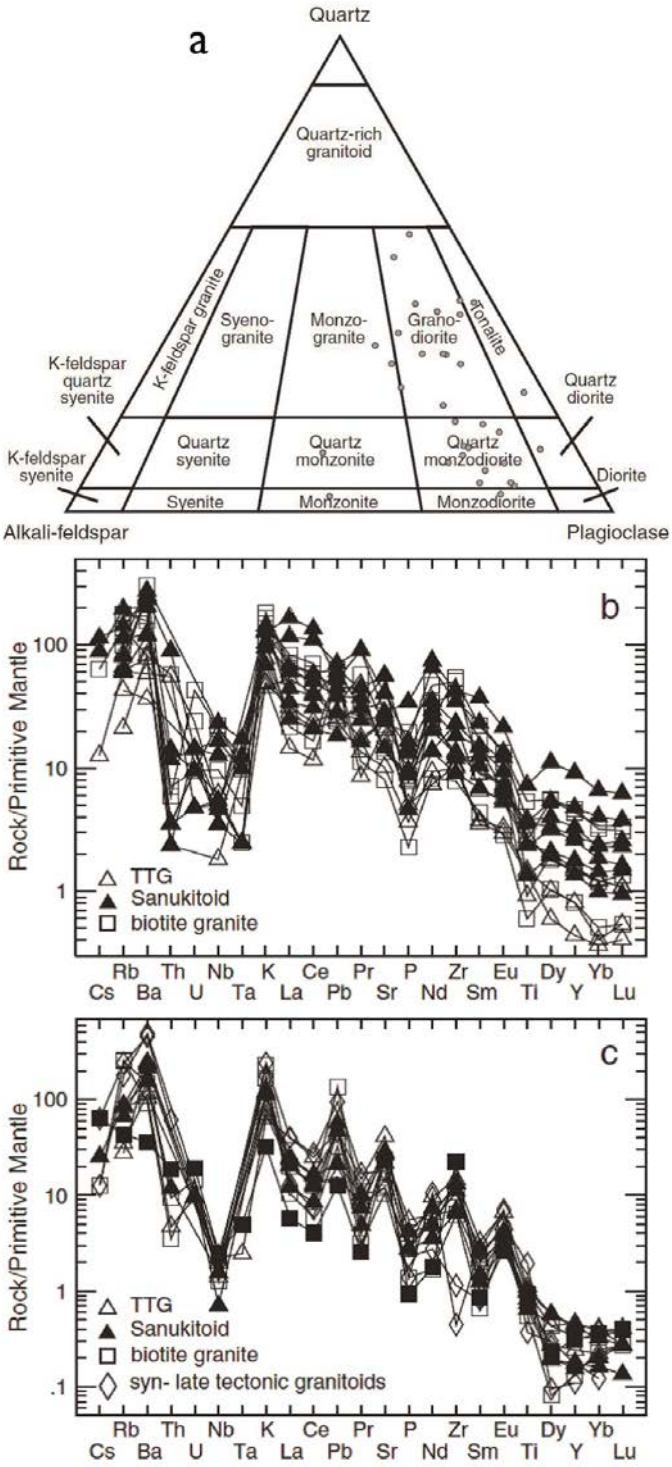

Figure 3.5 ***A.*** *Discrimination and,* ***B.*** *and* ***C.*** *trace element diagrams for the various orthogneisses (Kolb* et al. *2013).*

*Syn- to late-tectonic orthogneiss (*c. *2750-2740 Ma)*

Syn- to late-tectonic monzogranite and syenite are medium- to coarse-grained and contain plagioclase, K-feldspar, biotite, muscovite, quartz, magnetite, ilmenite and, locally, clinopyroxene and garnet (Fig. 3.4C) (Kolb *et al.* 2013). They share geochemical characteristics with sanukitoids and biotite monzogranites (Fig. 3.5). The trace element patterns of many

of the sanukitoid-like granites are, however, similar to those of the biotite monzogranite and leucogranite with only higher Zr and Hf (Fig. 3.5) (Bagas *et al.* 2013, Kolb *et al.* 2013).

3.2 East Greenland Archaean (EGA) or Rae Craton

The Archaean granite-gneiss terrane that lies north of Tasiilaq is interpreted to be located north of an interpreted Palaeoproterozoic suture at the northern margin of the NAC and its Thrym Complex (Kolb 2014, Nutman *et al.* 2008b). As such it may represent the Eastward continuation of the Rae craton. The Archaean rocks are either strongly overprinted by Palaeoproterozoic deformation and metamorphism or only very little investigated, especially north and northeast of Helheim and Kangertitivatsiaq Fjords (Kolb 2014, Nutman *et al.* 2008b).

The MesoArchaean Blokken Gneiss is an orthogneiss dated at 3035 ± 14 Ma and *c.* 2960-2920 Ma (Kalsbeek *et al.* 1993, Nutman *et al.* 2008b). The orthogneiss consists of a suite of less deformed tonalite, granodiorite and diorite composed of quartz, plagioclase, K-feldspar, biotite and hornblende (Dawes *et al.* 1989a). Metamorphic zircon rims yield 2723 ± 49 Ma for NeoArchaean metamorphism (Nutman *et al.* 2008b). To the west, the orthogneiss is migmatitic with polyphase leucosomes and pegmatite bands, and consists of quartz, plagioclase, K-feldspar, biotite and hornblende (Fig. 3.6A) (Dawes 1989). One orthogneiss yields an upper intercept TIMS U-Pb age of 2636 +22/-18 Ma (Kalsbeek *et al.* 1993). Amphibolites form 10-100 m wide lenses and layers with pinch-and-swell structures parallel to the main gneissosity (Dawes 1989). The amphibolite is variable in modal abundance of plagioclase, hornblende, garnet and quartz, and locally has greenish, clinopyroxene-rich centres in the bands and lenses.

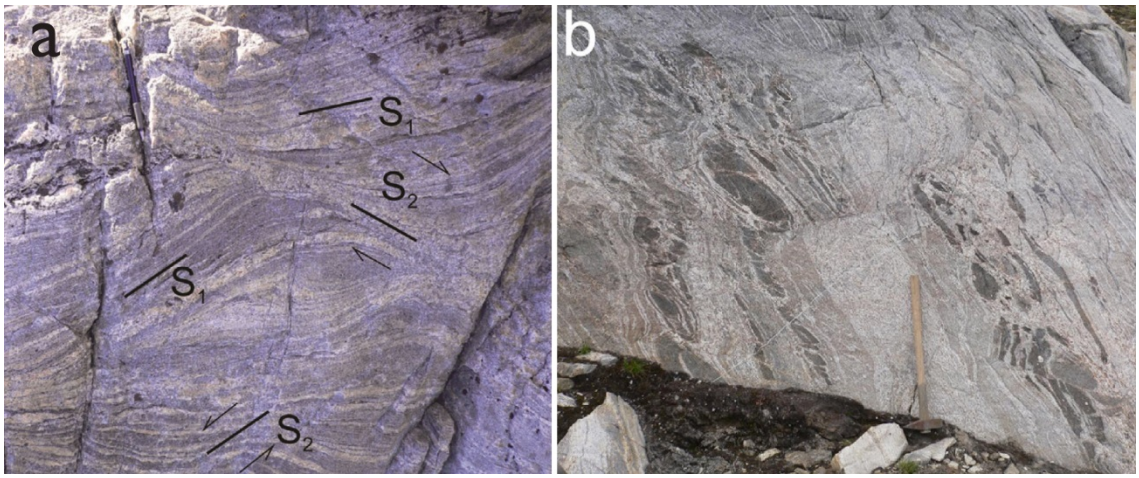

Figure 3.6 *Field appearance of felsic orthogneiss from EGA:* ***A.*** *migmatitic, banded orthogneiss; and* ***B.*** *strongly migmatitic, orthopyroxene-bearing orthogneiss (Kolb 2014).*

Further north in the hanging wall of the Niflheim Thrust north of Helheim Fjord, the orthogneiss is brown and consists of quartz, plagioclase, K-feldspar, and clino- and orthopyroxene, indicating granulite facies metamorphism (Fig. 3.6) (Dawes 1989, Escher and Hall 1989). The orthogneiss was dated at 2835 +6/-8 Ma (U-Pb TIMS upper intercept; Kalsbeek

et al. 1993), and has SHRIMP zircon U-Pb dates of 2863 ± 11 Ma, 2756 ± 6 Ma and 2734 ± 34 Ma, confirming the polyphase nature of the rocks (Kalsbeek *et al.* 1993, Nutman *et al.* 2008b). Pegmatites with Rb-Sr whole rock dates of 2630 ± 65 Ma intruded the orthogneiss during retrograde amphibolite facies metamorphism (Pedersen and Bridgwater 1979). Mafic rocks form narrow bands in orthogneiss (Bridgwater and Myers 1979, Dawes *et al.* 1989b, Myers 1984, Myers 1987).

4 Skjoldungen Alkaline Province

Thomas Find Kokfelt, Kristine Thrane, Martin Broman Klausen & Christian Tegner

4.1 Geological background

The Archaean Skjoldungen Alkaline Province, or SAP (Nielsen and Rosing 1990, Blichert-Toft *et al.* 1995), situated at 63º30'N in South-East Greenland, is part of the North Atlantic Craton (Fig. 4.1). Archaean alkaline rocks are noticeable rare worldwide, therefore the SAP offers an opportunity to study alkaline magmatism in the early Earth system (Blichert-Toft *et al.* 1996). The SAP constitutes a number of mildly alkaline intrusions of mafic and ultramafic to intermediate and evolved compositions including highly alkaline and carbonatite bearing rocks which were emplaced syn- to post-tectonically in the 2790-2700 Ma Skjoldungen Orogeny (Berger *et al.* 2014, Kolb *et al.* 2013). The alkaline rocks intruded a basement of felsic orthogneiss containing dismembered units of mafic-ultramafic granulites and amphibolites as kilometre-sized lensoidal belts. These older rocks of MesoArchaean age are commonly invaded by felsic partial melts.

The majority of the SAP intrusions occur within a large area of *c.* 2400 km^2 centered at the WNW-trending Skjoldungen Island, but syenitic gneiss intrusions, also belonging to the province as defined by Nielsen and Rosing (1990), occur further to the south between Kasertoq Fjord and Skirner Bjerge (Fig. 4.1). Based on the current knowledge and new geochronological data, the province can be divided into two stages: A main stage at *c.* 2750-2690 Ma, which comprises mildly alkaline rocks, and a second stage at *c.* 2680-2664 Ma, referred to by Kolb *et al.* (2013) as the Singertât stage, which is highly alkaline and comprises nephelinitic and carbonatitic rocks (Kokfelt *et al.* 2016c, Kolb *et al.* 2013, Nielsen and Rosing 1990, Nutman and Rosing 1994). The first stage overlaps with the main orogenic mountain building event with regional compression followed by orogenic collapse and rapid exhumation (Berger *et al.* 2014), whereas the second stage that possibly relates to a period of regional extension (Kolb *et al.* 2013). The oldest SAP intrusions often bear evidence of being emplaced syn-tectonically (Nielsen and Rosing 1990), in an orogenic belt under regional NE-SW-oriented compression, as these rocks are characterised by gneissic fabrics (Kolb et al. 2013). It can therefore be difficult to distinguish syn-tectonically deformed felsic SAP rocks in the field from the surrounding gneiss basement. The younger SAP intrusions, on the other hand, show pristine and undeformed magmatic textures. Some of the late mafic intrusions, such as the Vend Om Intrusion, show well-preserved magmatic layering, cross-bedding, drop stone structures and intrusive contacts (Klausen and Kokfelt 2014, Maarupgaard 2015).

The extensive geochronological work that has been carried out within the SEGMENT project places new constraints on the timing of formation of the SAP (see Chapter 5 for details). The new U-Pb age data support the view that the SAP developed during the Skjoldungen Orogeny, beginning at a syn-tectonic stage at *c.* 2750 Ma with the intrusion of mainly syenitic plutons in the southern part of the province, and continuing until a post-tectonic stage at < 2700 Ma with the emplacement of several mafic plutons like the Ruinnæsset and Vend Om Intrusion. The new age data also indicate that the SAP magmatism migrated northwards during the initial time period and relatively quickly was concentrated

along the main WNW-ESE trending axis defined by the Skjoldungen Island (Kokfelt *et al.* 2016c).

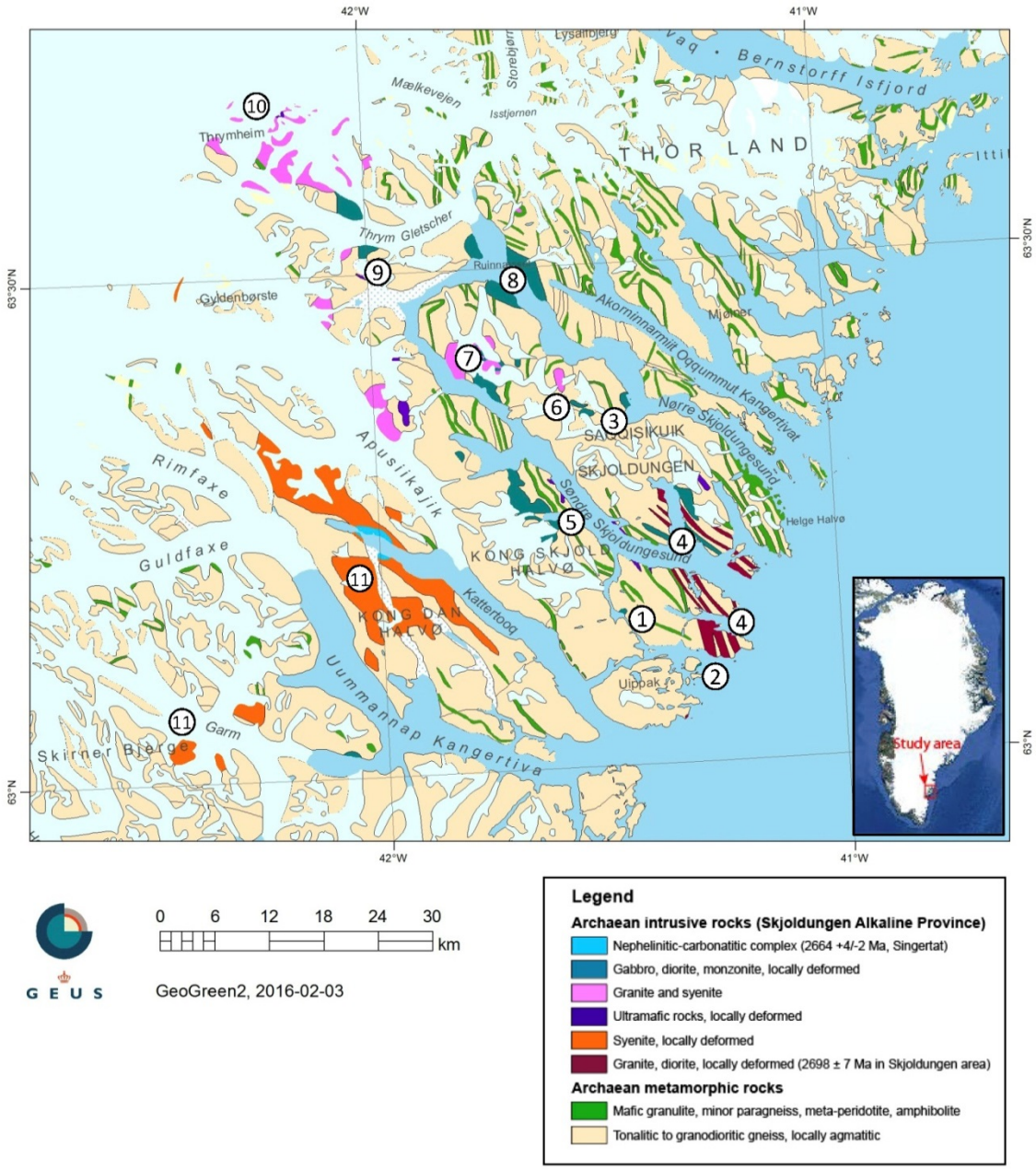

Figure 4.1 *Geological map of the Skjoldungen Alkaline Province (modified from Escher (1990)). Encircled numbers (1-11) relate to the investigated areas during the SEGMENT field work, and as reported by Klausen and Kokfelt (2014) and Kokfelt* et al. *(2016c): (1) Vend Om Intrusion, (2) Iglermiut, (3) Hermods Vig and Njords Gletscher, (4) Halvdans Fjord, Anarnitsoq Island and Kong Skjold Halvø, (5) Stærkodder Vig, (6) Central Skjoldungen Island, (7) Sfinksen area, (8) Ruinnæsset, (9) Tværdalen, (10) Thrymheim ('nunatak') area, (11) Kong Dan Halvø and Skirner Bjerge.*

One of the overall goals of the current work in the Skjoldungen area is to develop a more detailed understanding of the geological evolution of the SAP, as well as an evaluation of its economic potential. This was done through detailed field work within selected key areas,

including (but not restricted to) the following intrusions: Vend Om Intrusion, Halvdans Fjord Gabbro, Hermods Vig Diorite 1 and 2, the Sfinksen, Tværdalen and Thrymheim areas, and Ruinnæsset Intrusion (Fig. 4.1). The key objectives of the work included the time-frame for the emplacement of SAP, as well as the characterisation of its geological evolution and geotectonic setting. To this end, we conveyed an ambitious zircon U-Pb dating program involving ~ 50 samples of felsic to intermediate compositions that were dated by LA-ICPMS at GEUS (Kokfelt et al. 2016c). A large set of whole rock geochemical data (n = 500) have been compiled to better understand the geochemical signature of the SAP magmas and their evolution in crustal magma chambers. In addition, Hf isotope analyses on zircon and whole rock samples have also been undertaken on a subset of SAP samples in order to constrain nature of the mantle source(s) for the province (Kokfelt et al. 2016a).

4.2 Previous work on the Skjoldungen Alkaline Province

Prior to the SEGMENT project, the SAP was studied to some extent by Nielsen and Rosing (1990), Blichert-Toft *et al.* (1995) and Thomsen (1998), reflecting the work effort in the area by GGU in the 1980's and 1990's. The original geological mapping of the larger Skjoldungen region by GGU resulted in the 1:500 000 scale geological map compiled by Escher (1990). Whereas much of the regional mapping was carried out at a reconnaissance scale, the mapping of the SAP was done at considerably higher level of detail; mapping by Troels Nielsen and Minik Rosing resulted in a number of field maps at scale 1:50 000. These unpublished field maps provided a valuable basis during the SEGMENT fieldwork and often proved to be 'correct'. Previous zircon U/Pb TIMS age determinations of the Ruinnæsset Intrusion by Nutman and Rosing (1994) indicate an age of 2700 Ma, placing it to be late in the general sequence of SAP intrusions. Blichert-Toft *et al.* (1995) presented whole rock Sm-Nd (and Rb-Sr) data, and were able to construct rough isochrons for several of the SAP intrusions corroborating an age of around 2720 to 2700 Ma.

Based on the initial geochemical characterisation of the SAP intrusions, Blichert-Toft *et al.* (1995) suggested derivation from shoshonitic (high-K, calc-alkaline) parental melts, which most commonly are found along active, convergent margins (Meen 1987). They also found that high Mg# and high LILE/HFSE ratios of the most primitive SAP compositions would be consistent with hydrous melting of a mantle wedge source that had been metasomatized by hydrous fluids from a subducting oceanic slab.

4.3 Description of selected key intrusions

Here, we briefly describe some of the main features characterising three selected key SAP intrusions: (1) the Ruinnæsset Intrusion, which is the largest intrusion within the province, (2) the Vend Om Intrusion in the south-eastern part of the province, (3) the syenitic/granitic Sfinksen Intrusion in the western part of the province, in addition to (4) 'Meta-dykes' or 'deformed dykes' of the Skjoldungen Island region, and (5) the Singertât Complex. Further descriptions of these, and other intrusions in the province, can be found in Klausen and Kokfelt (2014).

4.3.1 Ruinnæsset Intrusion

The Ruinnæsset Intrusion defines a ~ 3 × 3 km large, well-preserved, rhomb-shaped intrusion dominated by coarse-grained gabbroic and monzonitic to syenitic and granitic rocks (Fig. 4.2). The main lithology is constituted by coarse-grained gabbro/monzonite that commonly shows modal layering as defined from ~ 5-20 cm thick layers rich in hornblende, pyroxene and Fe-Ti oxides. The intrusion is cut by multiple generations of dykes, sheets and leucocratic pegmatites and aplites. Some of the cross-cutting intrusions constitute irregular bodies with cuspate contacts to the host rocks, indicating that they intruded at a late magmatic stage when interstitial melt was still present in the main solidifying magma body (Fig. 4.2). These dykes are often rich in large feldspar phenocrysts and in cases are seen to grade into more massive gabbro/monzonite. There is a systematic distribution of rock types within the intrusion, with the western part mainly being comprised of syenites and monzonites, whereas the eastern part also comprises more mafic lithologies, such as gabbros and diorites, as well as pyroxenites that occur as xenolithic domains or rafts in the host rock (Fig. 4.2). An eastern extension of the complex was discovered in 2012 and investigated further in a petrological Honours thesis (Geldenhuys 2015). It may, however, also represent a separate (Kokkefars Hat) intrusion, made up of a concentric distribution of outer monzonites, cut by plagioclase-bearing hornblende pyroxenites and subsequently a central hornblende gabbro core.

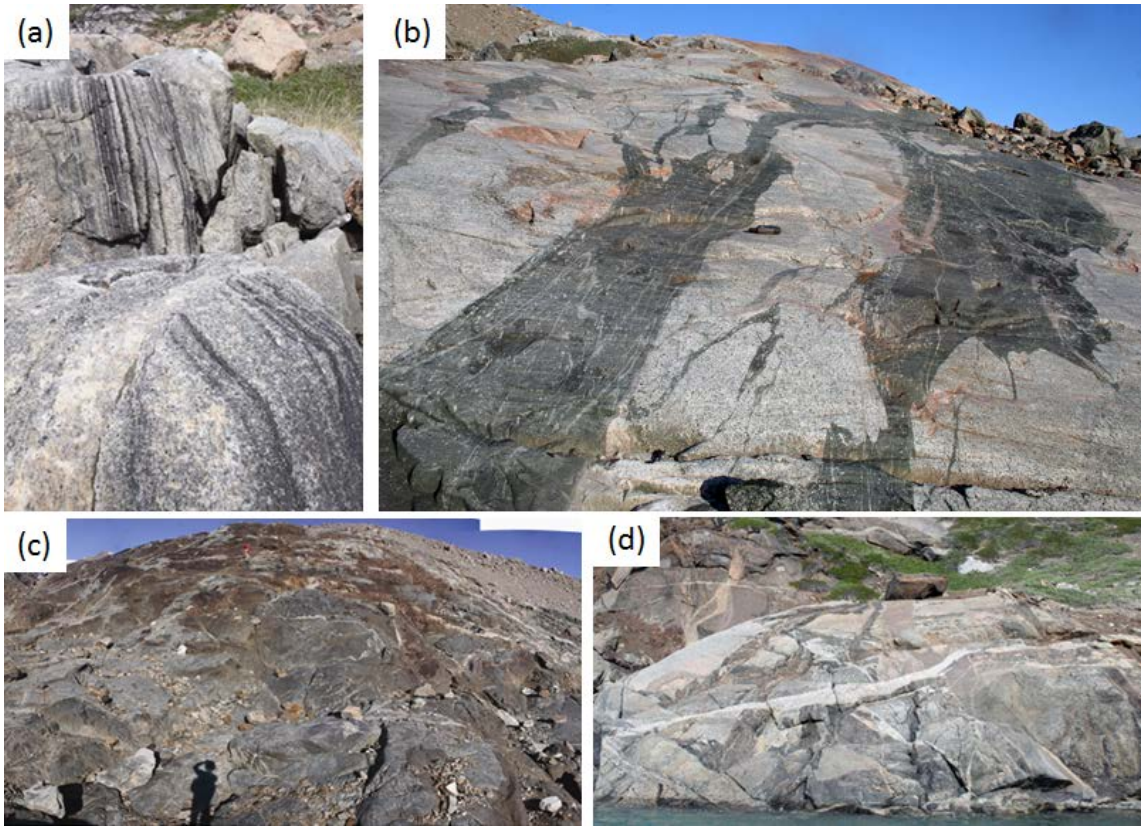

Figure 4.2 *Lithologies of the Ruinnæsset Intrusion.* ***A.*** *Modal layering in gabbro.* ***B.*** *Irregular intrusions of syenite into host (mushy?) syenite or monzonite.* ***C.*** *Large xenolithic block of ultramafic rocks (cumulates?) in the north-eastern part of the intrusion.* ***D.*** *Multiple cross-cutting dykes and sheets of felsic composition.*

Nelsonites, constituting mainly magnetite and apatite, are found at more places in the Ruinnæsset Intrusion as irregular veins and pods cutting the host gabbro/monzonite of the intrusion (Fig. 4.3). The formation of these nelsonitic veins is enigmatic, but one theory based on experimental petrological work suggests that they might form by liquid immiscibility processes, producing Fe-P-rich liquids at a late stage of magmatic differentiation (Philpotts 1967). Such liquids are then segregated into interstitial pore spaces and injected as irregular veins and pods. Bulk chemical analysis of a nelsonite sample (509376; Fig. 4.3) yielded 5.99 wt% P_2O_5, 41.43 wt% $Fe_2O_3^{tot}$ and 5.05 wt% TiO_2.

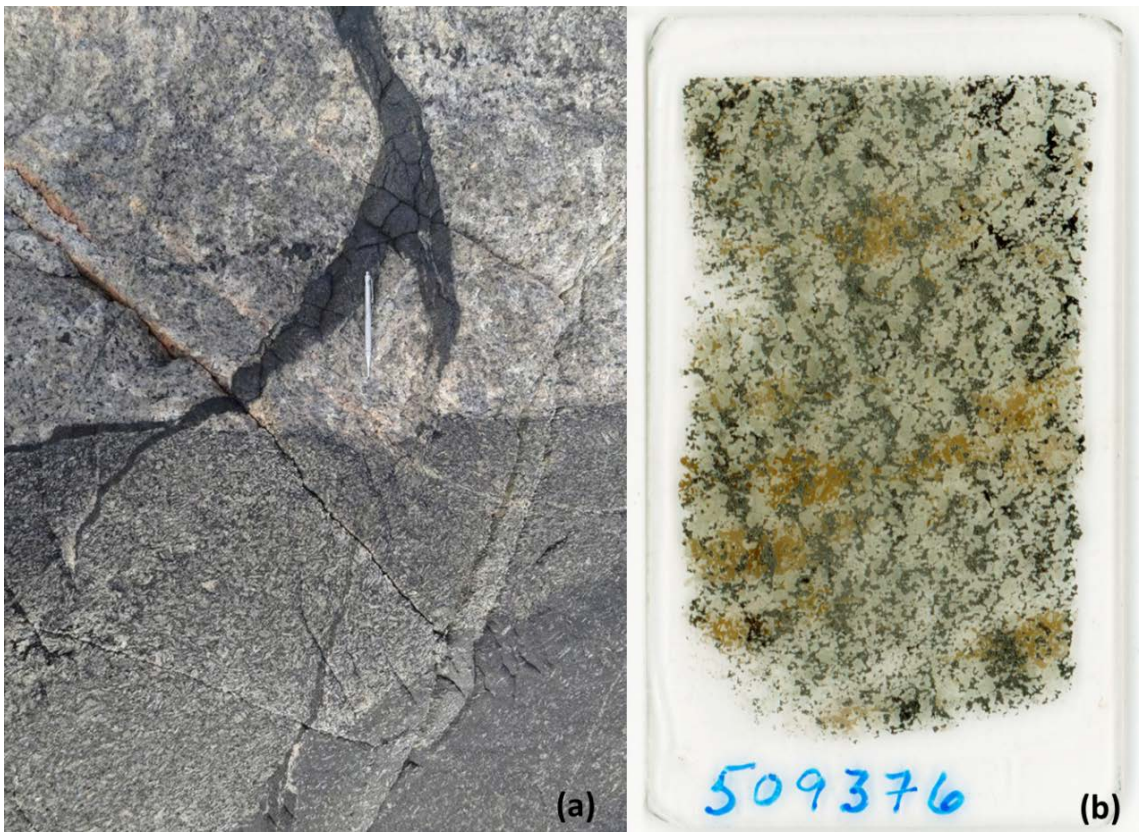

Figure 4.3 *Nelsonites of the Ruinnæsset.* ***A.*** *Field photo showing nelsonite as late discordant veins cutting across a contact between two monzosyenite units (pen for scale).* ***B.*** *Petrographic thin section of a nelsonite vein containing greenish grey apatite and interstitially placed Fe-Ti-oxides, ilmenite and magnetite (scale: 4.5 x 2.5 cm). Bulk chemical analysis for sample 509376 yields 5.99 wt% P_2O_5, 41.43 wt% $Fe_2O_3^{tot}$ and 5.05 wt% TiO_2.*

The new sample set consisting of ~ 200 rock samples from the Ruinnæsset Intrusion covers the different parts of the intrusion and were collected along several profiles. On-going work on these rocks aim at a detailed petrological, mineral chemical and geochemical description, which will help to constrain petrogenetic models for the intrusion, as well as an evaluation of the economic potential of the nelsonites.

Geochemically, the Ruinnæsset rocks define an alkaline evolutionary trend towards enrichment in K_2O with increasing SiO_2 that likely reflects crystal fractionation processes. The silicate bulk samples show moderate to strong LREE enrichments (typically ~ 100-200 x chondrite) relative to the HREE (~ 10 x chondrite). The magnetite-rich samples are high in

FeOt and generally enriched in REE's and P_2O_5, presumably reflecting variable modal abundance of apatite in these mafic layers.

4.3.2 Vend Om Intrusion

The Vend Om Intrusion is a small mafic intrusion situated in the south-eastern part of the SAP. Together with two other mafic intrusions at Iglermiut Island and at Njords Gletscher in the SE part of the Skjoldungen area, Vend Om Intrusion exemplifies a late, undeformed mafic SAP intrusion. The intrusion was indirectly dated to 2690 ± 4 Ma based on a U-Pb zircon age for a felsic pegmatite that has been interpreted as a back-vein from the remobilized host rock into the gabbros of the Marginal Zone (Kokfelt *et al.* 2016c). The late emplacement age of Vend Om Intrusion in relation to the main SAP stage is consistent with the lack of deformation of the intrusion.

The Vend Om Intrusion is ovoid in map view measuring ~ 250 × 450 m and with a concentric architecture defined by layering in the hornblende-bearing gabbro. The outer zone, or marginal zone, is 30-70 m wide and consists of very coarse-grained hornblende-rich melagabbro, often with only a faint layering. The marginal zone surrounds a central sequence of gabbroic rocks with pronounced and steeply inclined magmatic layering (Fig. 4.4).

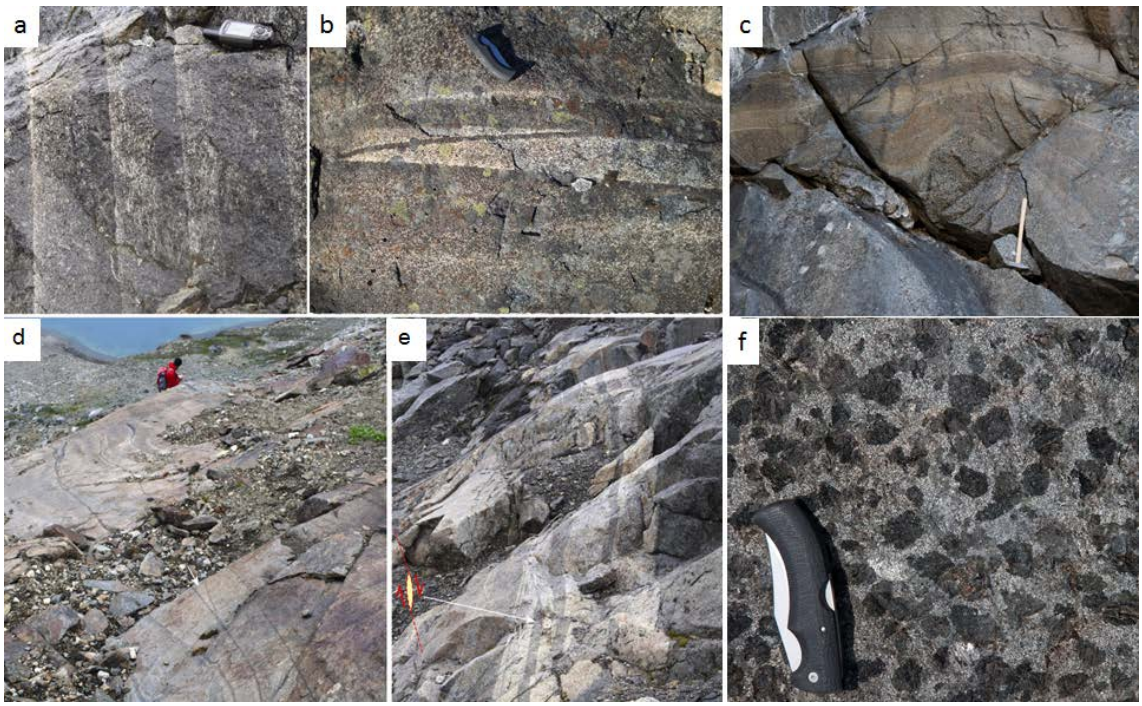

Figure 4.4 *Lithologies of the Vend Om Intrusion.* ***A.–E.*** *Rocks from the internal Layered Series showing various examples of magmatic layering, including modal layering, rhythmic layering, graded layers and bifurcating layers.* ***F.*** *Hornblende-poikilitic gabbro of the Marginal Zone.*

A conspicuous feature of the Vend Om Intrusion is the occurrence of oxide-rich, concordant layers within the Layered Series (Fig. 4.5). At places these bands are very-well developed and may reach up to 1.5 m in thickness, but are usually < 20 cm.

An Honours thesis (Grobbelaar 2012) was followed by a more extensive MSc thesis on the petrology of Vend Om Intrusion (Maarupgaard 2015). The thesis focuses on a petrographic and mineral chemical characterisation of the intrusion and presents new major and trace element bulk rock chemistry compositions 93 samples and mineral chemistry data on 51 samples. The main conclusions in the thesis include that at least two batches of magma are required to explain the variation in mineralogy and mineral chemistry: (1) an early injection of relatively dry magma that crystallized orthopyroxene and clinopyroxene, and (2) a relatively wet magma which caused a reaction of earlier formed pyroxenes to stabilize hornblende. An inwards reversal in the An-content in plagioclase and rather stable Mg# in hornblende are consistent with an open system behaviour in which the second batch of magma replenished the magma chamber, and mixed with the resident magma to produce the Layered Series (Maarupgaard 2015).

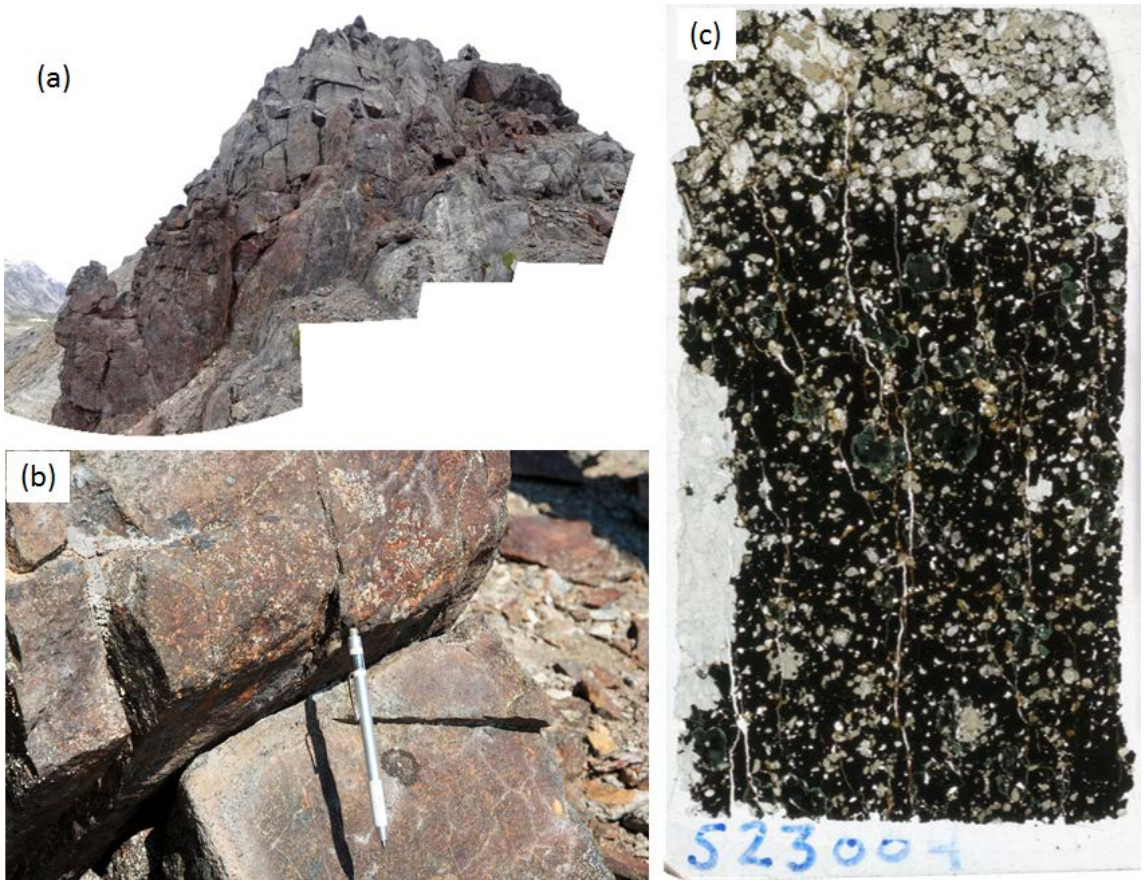

Figure 4.5 *Magnetite-rich band in Vend Om Intrusion.* ***A.*** *In the central part of the intrusion an up to 1.5 m thick wide, concordant oxide-rich band can be followed for c. 50 m pinching out.* ***B.*** *Close-up of the oxide band with a magnetic pen for scale.* ***C.*** *Thin section (2.5 x 4.5 cm) of part of the oxide-rich layer with a mineralogy constituted by magnetite, hercynite, hornblende, plagioclase + minor sulphides.*

4.3.3 The Sfinksen area

The Sfinksen area is situated in the northern part of Skjoldungen Island and exposes several fairly well confined ovoid intrusions ranging from mafic to felsic compositions, including

the Sfinksen Diorite, the Sfinksen Syenite Complex, and the Sfinksen Granite (Nielsen and Rosing 1990). The Sfinksen Syenite Complex is the largest of the intrusions with an outline of ~ 3 km across. Due to erosion of the central parts, it is only exposed along the margins where it constitutes steep-sided mountain crests (Fig. 4.6). Hydrothermal alteration has occurred along the western contact zone to the wall rock gneiss (Fig. 4.6). The south-eastern part of the Syenite Complex appears to be cut by the Sfinksen Diorite, whereas the relationship to the Sfinksen granite, which is hardly reachable to study in situ, is uncertain. New zircon U-Pb age dates on the Sfinksen Syenite Complex indicate it to be 2.73-2.74 Ga, placing it relatively early in the magmatic development of the province. Leucocratic pegmatites cutting the Sfinksen diorite are dated to 2.70 Ga (Kokfelt *et al.* 2016c).

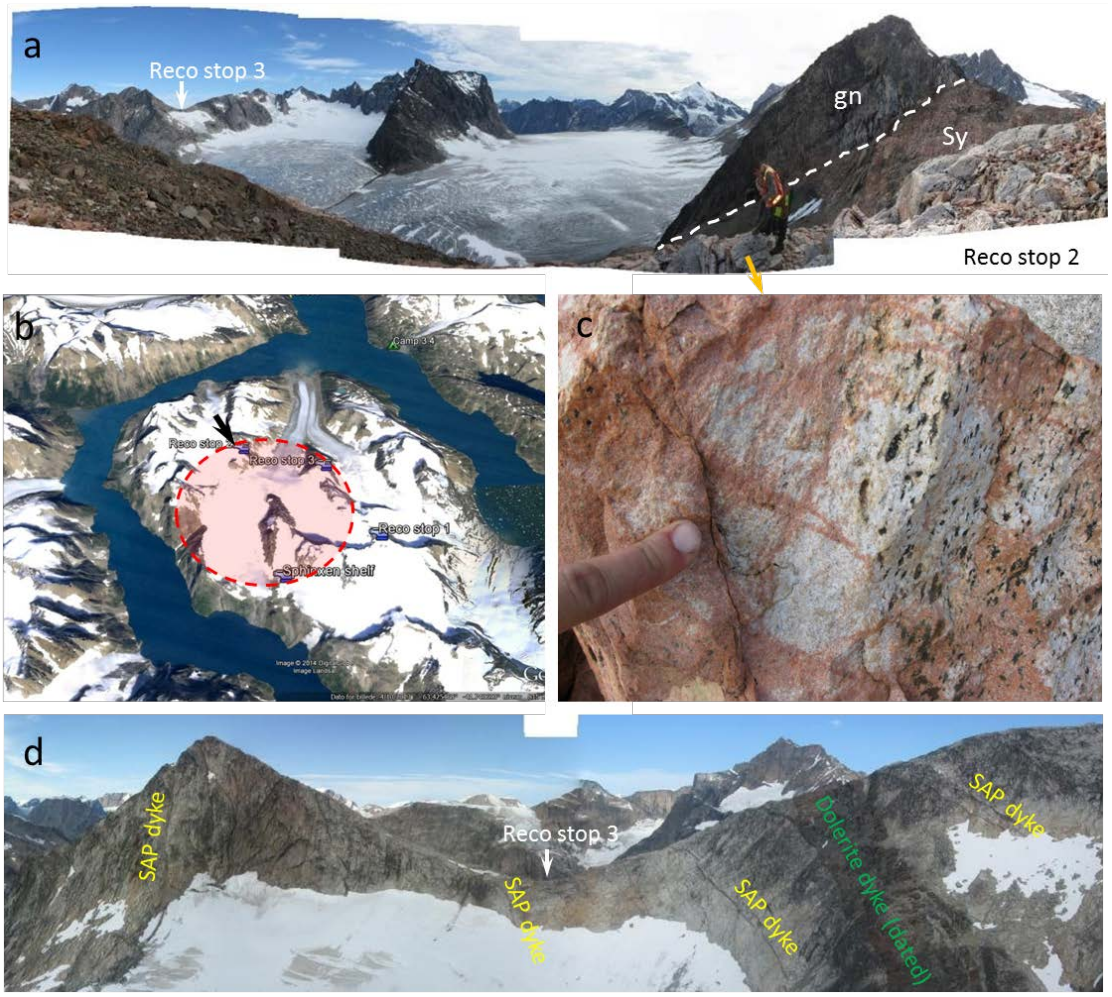

Figure 4.6 *The Sfinksen Syenite Complex is situated in the north-western part of Skjoldungen Island in a semi-alpine terrain.* ***A.*** *View towards southeast and the north-western sharp contact to the surrounding gneiss basement (white stippled line).* ***B.*** *Google Earth map view showing the presumed outline of Sfinksen Syenite Complex. Black arrow indicates direction of view in D.* ***C.*** *Hydrothermally altered syenite close to the north-western contact.* ***D.*** *The intrusion is cross-cut by multiple younger dykes, including so-called 'deformed SAP dykes' up to 1-2 m thick and of intermediate to mafic in composition.*

4.3.4 'Meta-dykes' in Skjoldungen Island area

Mafic to intermediate dykes, usually up to 1 m wide, occur throughout the larger Skjoldungen area, all the way from Halvdans Fjord to the Thrymheim area. Many dykes are more regionally NW-SE-striking, sub-parallel to the longest axis of the Skjoldungen Island, whereas others are more randomly orientated sheets restricted to within close proximity of individual complexes. The dykes owe their name 'meta-dykes' (or 'deformed dykes') from their characteristic blurred contacts to the host rock (Fig. 4.7). The field relations indicate that these dykes intruded syn-tectonically into the NE-SW compressional stress field characterising the initial SAP stage. During the fieldwork in 2011 and 2012, the dykes were targeted for geochemical sampling as they are likely good candidates for representing parental melts of the SAP magmatism – particularly those that are least evolved. An early petrological study of these dykes was undertaken by an Honours student at Stellenbosch University, South Africa (Greeff 2012). Whole rock geochemistry data show that the dykes are invariably alkaline with the characteristic SAP-signature of LIL-enrichment and HFSE-depletion. Compositions vary a great deal from basic to intermediate, indicating that many dykes are fed from magmas differentiated at deeper level. This is supported by some SAP intrusions – like Kokkefars Hat (Geldenhuys 2015) – presenting a more direct correlation between intrusive sheets emanating from compositionally different zones within the exposed intrusion. A more extensive compilation of field relationships, petrography and geochemistry of all dykes and sheets within the province is in progress.

4.3.5 Singertât Complex

The Singertât Complex is situated in the inner parts of Kassortoq fjord, in the southern part of the Skjoldungen Alkaline Province. The alkaline complex is intruded into fenitized gneisses and is estimated to cover an area of ~ 8 km^2 of which less than ~ 1 km^2 is exposed (Nielsen and Rosing 1990). The complex is composed of massive nepheline bearing mafic to leucocratic plutonic rocks covering a range from melteigites and ijolites, cut by a suite of related nephelinitic to urtitic and carbonatite sheets and dykes (Nielsen *et al.* 1988). The only age of the complex derived from a single zircon grain from the carbonate centre of the intrusion. B.T. Hansen dated the zircon and obtained age of 2664 +4/-2 Ma (reported in Blichert-Toft *et al.* 1995). Studies of the Singertât complex are carried out by Sebastian Tappe (University of Johannesburg, South Africa) in collaboration with GEUS.

4.4 Scientific goals for future work

The large set of sample from the SAP (> 500), many of which have been analysed provides the basis for a number of projects at BSc, MSc or PhD levels. The scientific challenges related to the SAP, as initially set out for the SEG project have in part been addressed in reports by Klausen and Kokfelt (2014), BSc and MSc theses by Árting (2013), Geldenhuys (2015), Greeff (2012), Grobbelaar (2012), and Maarupgaard (2015) and international research papers by Berger *et al.* (2014) and Kolb *et al.* (2013). In the future research will aim at: (1) the characterising the parental melt compositions to the SAP magmas on the basis of geochemical modeling in accordance with experimental petrology, (2) the details of the magmatic evolution of well-sampled ansd well-characterised SAP intrusions (e.g. Ru-

innæsset, Sfinksen Syenite Complex, Iglermiut), (3) Identification of the characteristics of the source(s) for the mafic SAP magmas in terms of their whole rock elemental and Hf isotopic compositions, and (4) establish the potential importance of reworking of older crust in the genesis of SAP melts based on Hf isotopes in zircon.

New whole rock Lu-Hf isotopic data have been obtained by Tomas Næraa in collaboration with Axel Gerdes in Frankfurt. Six samples with zircon crystallization ages between 2.75 and 2.70 Ga have been characterised in terms of their Hf isotope ratios. The results of this work were presented by Næraa *et al.* (2014), and further aspects by Kokfelt *et al.* (2016a) (see Chapter 5 for a summary).

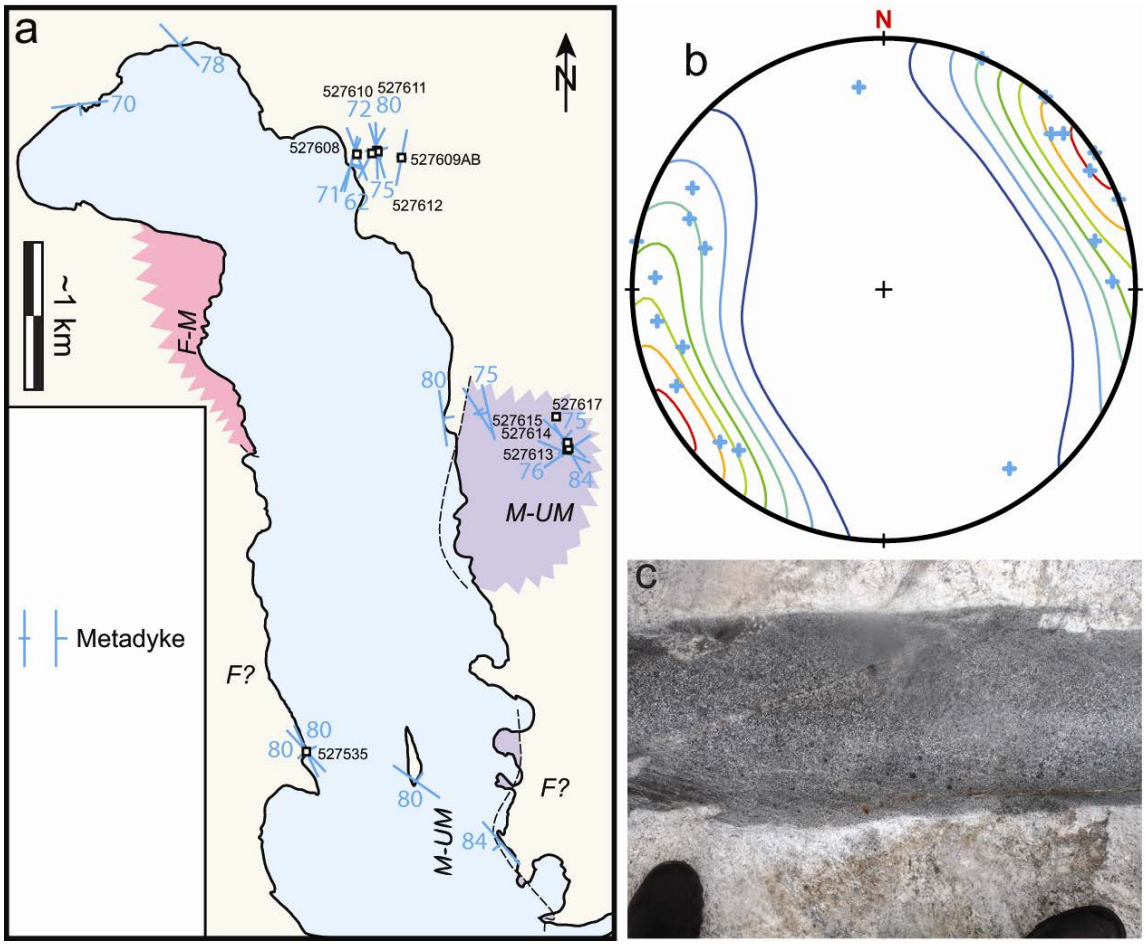

Figure 4.7 *The so-called 'meta-dykes' or 'deformed dykes' that are ubiquitously found in the Skjoldungen Island region.* ***A.*** *Map from the Halvdans Fjord area showing in* ***B.*** *structural measurements of the dykes (poles to planes plotted), indicating a NW-SE orientation of the dykes.* ***C.*** *Field example of a ~ 25 cm thick 'meta-dyke' intruding the agmatitic gneiss. Note the blurred contacts and broken bridges that suggest dextral displaced along the dyke plane.*

5 Geochronology of Archaean rocks

Thomas Find Kokfelt, Kristine Thrane & Tomas Næraa

Zircons from 127 samples of Archaean orthogneisses, migmatites, granitic rocks and pegmatites were analysed during this project. The results are presented in several articles and reports including Kolb *et al.* (2013), Bagas *et al.* (2013), Bagas *et al.* (2016), Kokfelt *et al.* (2016a), Kokfelt *et al.* (2016b), Kokfelt *et al.* (2016c) and Næraa *et al.* (2016). A summary of the results is presented below.

5.1 Analytical methods

The U-Pb zircon analyses were acquired at several different laboratories employing different instrumentation, namely by (1) laser ablation system coupled to a Thermo Finnigan Element2 single collector-magnetic sector field-inductively coupled plasma-mass spectrometer (LA-SF-ISP-MS), at the Department of Petrology and Economic Geology, Geological Survey of Denmark and Greenland (GEUS), Denmark, (2) Photon laser coupled to a Bruker Elite Quadrupole at Lund University, Sweden, (3) Secondary ion mass spectrometry (SIMS), Cameca IMS1280 at the Swedish Museum of Natural History, and (4) Sensitive High Resolution Ion Microprobe II (SHRIMP II) at the John de Laeter Centre of Isotope Research (JDLC), Curtin Technical University, Perth, Western Australia. For details see references above.

5.2 North Atlantic Craton (NAC)

The North Atlantic Craton of South-East Greenland has recently been described by Kolb *et al.* (2013) and Bagas *et al.* (2013) as part of the SEGMENT project. Bagas *et al.* (2013) define the Archaean Thrym Complex as extending from Odin Land in the North to the Ketilidian Province border in the south. Two Archaean orogenic events have been suggested defined within the Thrym Complex; the Timmiarmiut Orogeny (> 2790 Ma) and the Skjoldungen Orogeny (2790-2700 Ma). The Skjoldungen Orogeny is followed by the Singertât stage (2680-2650 Ma) of the Skjoldungen Alkaline Province (Blichert-Toft *et al.* 1995, Kolb *et al.* 2013). The Singertât Stage is characterised by regional extension and strongly alkaline magmatism. These tectonic events are constrained by U-Pb zircon data (Bagas *et al.* 2013, Kolb *et al.* 2013).

New results presented in Kokfelt *et al.* (2016a), Kokfelt *et al.* (2016b), Kokfelt *et al.* (2016c) and Næraa *et al.* (2016) define gneiss protolith ages for the Thrym Complex and for gneisses north of the Thrym Complex in the Gyldenløve Fjord area (Fig. 5.1). The orthogneisses within the Thrym Complex yield protolith ages ranging from *c.* 3045 to 2800 Ma, with a single older sample (523961) collected in the Timmiarmiut area yielding an age of 3231 Ma. Several of the samples also yield younger metamorphic ages between 2760 and 2701 Ma that are attributed to the Skjoldungen Orogeny (Fig. 5.1).

The orthogneisses further to the north in the area around Gyldenløve Fjord yield ages of 2750-2690 Ma that is clearly younger than the Thrym Complex. These orthogneisses formed during the Skjoldungen Orogeny (Fig. 5.1).

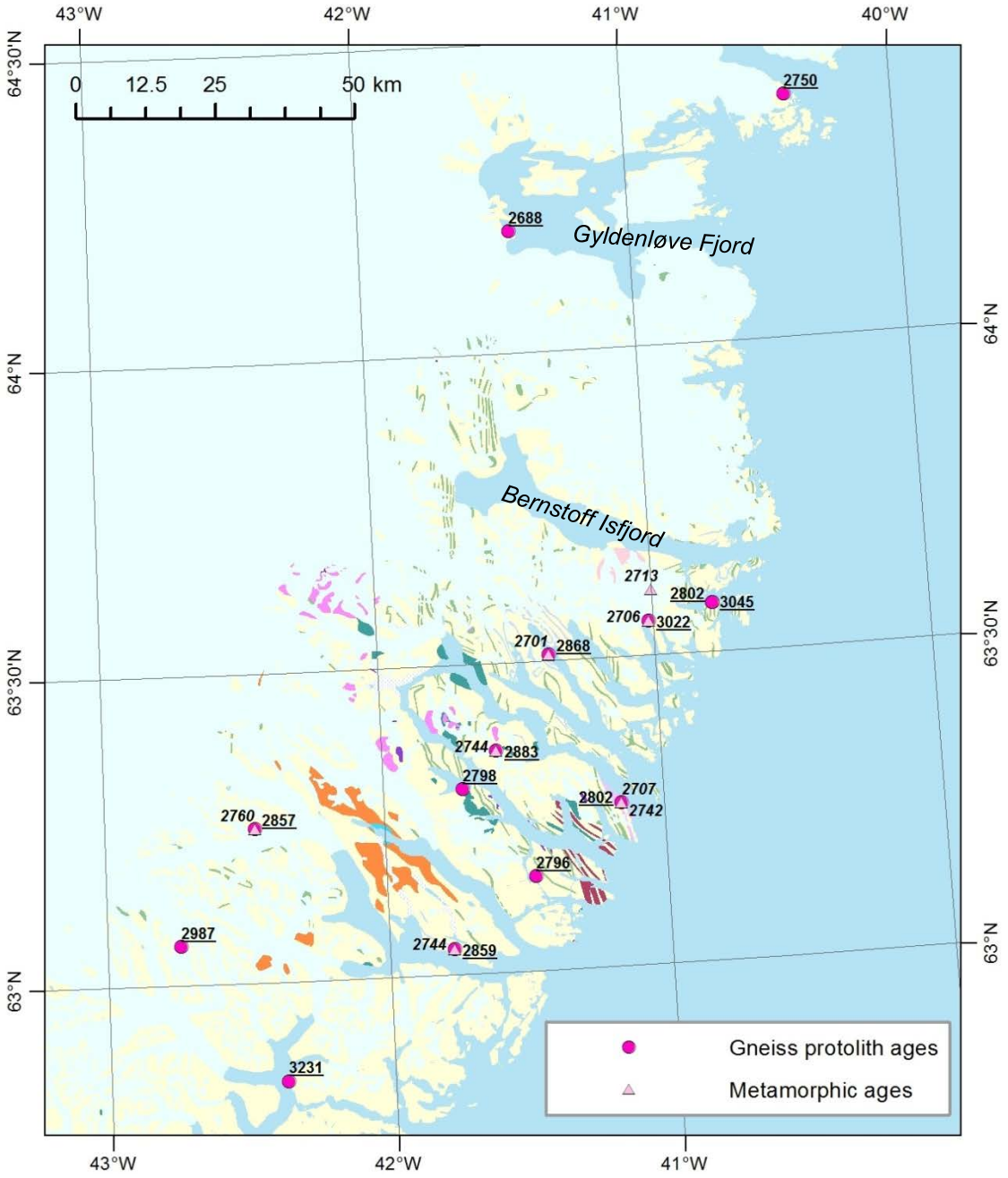

Figure 5.1 *Geological map of the North Atlantic Craton showing the location of samples yielding Archaean protolith ages (n = 14; labels in underlined), as well as Archaean metamorphic ages (n = 7; labels in italic).*

The age map for Archaean intrusions is shown in Fig. 5.2 and represents 97 ages interpreted as intrusion ages. These ages are derived from granite sheets, dykes and plutons that are clearly recognizable in the field as intrusive units, i.e. distinct from the basement rocks. Such rock units are abundant in the area between Mogens Heinesen Fjord in the south (~62°30'N) and Bernstorff Isfjord in the north (~64°30'N), but have not been regis-

tered in the Gyldenløve Fjord area, possibly reflecting a sampling bias (only two samples have been dated from this area). The age range found is largely confined between 2760 and 2670 Ma, with only two samples in the northern part of the area being younger. The majority of the samples comes from the area around Skjoldungen Island and belongs to the 2750-2690 Ma Skjoldungen Alkaline Province (SAP). Despite this sampling bias, it is clear that similar ages to those found within the SAP are recorded throughout the entire area. Subtle systematic differences do however exist, as older ages of 2760-2730 Ma mainly occur in the southern part, whereas these ages are lacking north of Langenæs (the peninsula situated just north of Skjoldungen Island; Fig. 5.2). Particularly the area around Kong Dan Halvø contains intrusions of this older age range. The northern area around Thor Land is dominated by younger ages of 2730-2700 Ma.

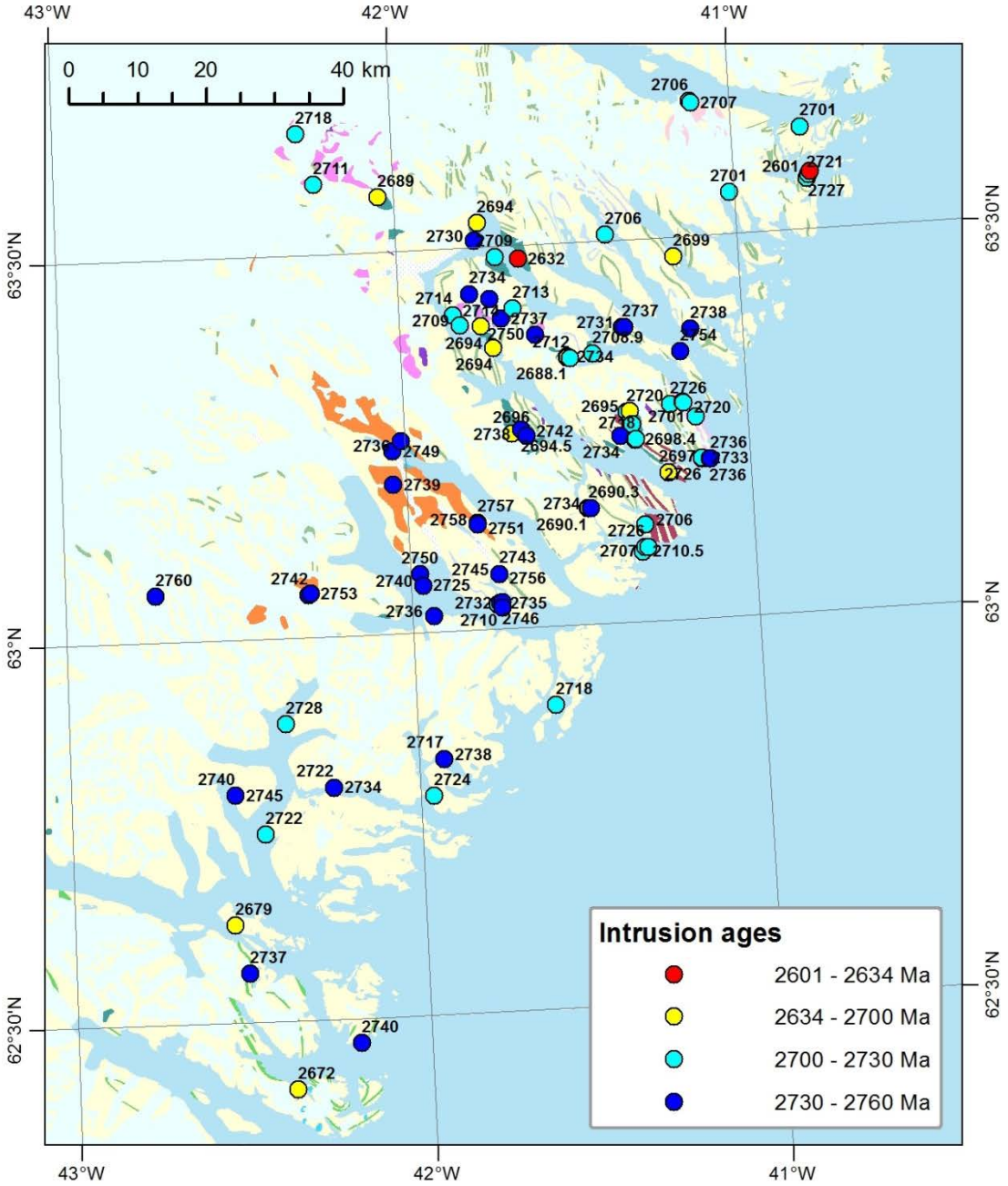

Figure 5.2 *Geological map of the Skjoldungen region showing the ages of the Archaean intrusions (n = 97).*

Figure 5.3 shows the range of inherited ages found in Archaean gneisses and granites. As for the intrusion ages presented above, the oldest inherited ages occur in the more inland part of the southern area with ages ranging from 2950 to 3885 Ma, but with most ages being around 3000 to 3250 Ma. In comparison, further eastwards and northwards, until Skjoldungen Island, younger ages in the typical range between 2800 and 2900 Ma occur. Skjoldungen Island and its surrounding area contain a variety of inherited ages from 2730 to 3350 Ma. Thor Land in the north contains inherited ages from *c.* 2850 to 3000 Ma.

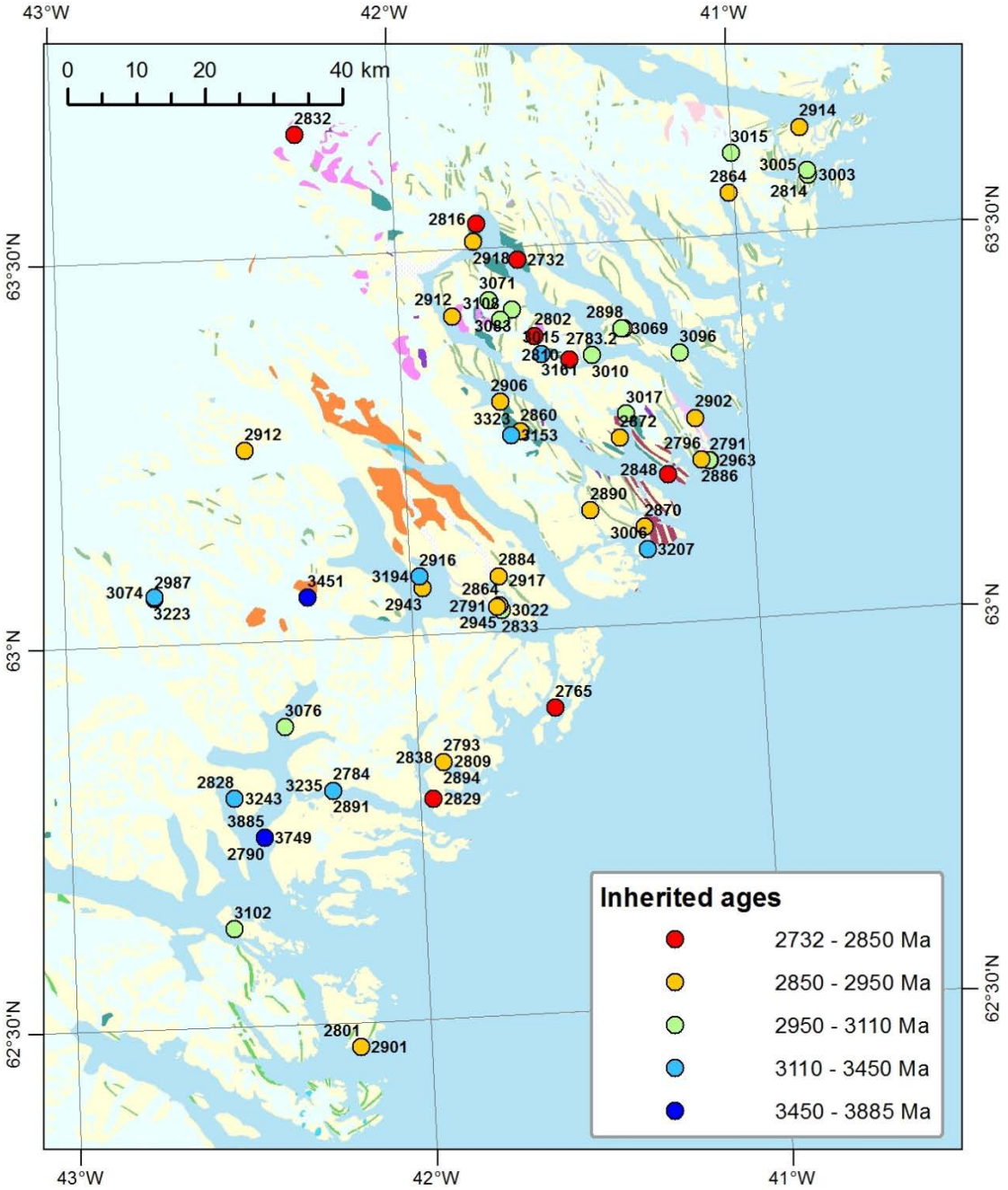

Figure 5.3 *Geological map of the North Atlantic Craton showing the range of inherited ages in Archaean gneisses and granites.*

Overall, the U-Pb dataset generated within the project provides new constraints on the development of the South-East Greenland part of the North Atlantic Craton. The main findings are that some distinctive differences exist between the northern and southern areas, with respect to the intrusion ages (Fig. 5.2).

Further characterisation of the crustal sources for the region has been addressed by recent complementary Hf isotope data on a subset of the samples, and the combined U-Pb-Hf isotope dataset is discussed in Kokfelt *et al.* (2016b). The main outcome of this study of selected samples is that Hf isotope data from the northern and southern areas are distinctly different, indicating that the dominant lithologies were sourced from different crustal reservoirs that they were extracted from the mantle at very different time periods of Earth's evolution. The study shows that the southern area contains source components older than *c.* 3200 Ma (up to *c.* 4000 Ma), whereas the northern area is dominated by sources younger than *c.* 3100 Ma. These systematics might either be explained by the existence of two distinct crustal terranes that were amalgamated at *c.* 2800 Ma, or alternatively as single terrane formed by progressive south to north accretion between *c.* 3100 and 2800 Ma (Kokfelt *et al.* 2016b).

5.2.1 Skjoldungen Alkaline Province

Out of the total of 119 samples that have been dated, 54 samples were sampled from lithologies of the Skjoldungen Alkaline Province. The large number of age determinations allows the establishment of the temporal evolution of the province. The dated samples include intrusive granites, syenites and monzonites, some of which are pegmatitic and aplitic veins. The intrusive ages for the Skjoldungen Alkaline Province rocks are shown on a geological map in Fig. 5.4. Figure 5.5 depicts the density distribution and latitude variation of ages. The 54 samples encompass seven samples published by Kolb et al. (2013) and 47 samples reported more recently by Kokfelt et al. (2016c). The same data are also presented in a more regional context above, but are here discussed in more detail.

Figure 5.4 depicts the areal distribution of intrusion ages in the Skjoldungen Alkaline Province. It shows that magmatism within the province defines an overall younging trend from south to north, with the oldest intrusion ages of 2760-2742 Ma (dark blue) represented by the syenitic gneisses in Skirner Bjerge and around Kong Dan Halvø and three outliers on Skjoldungen Ø and Langenæs. The younger age groups are 2742-2720 Ma (light blue), 2720-2700 Ma (yellow) and 2700-2632 Ma (red) all occur without any distinct geographical systematics along the NW-SE axis from the Thrymheim 'nunatak' along Skjoldungen Ø, and aling the NE shores of Kong Skjold Halvø. This can also be seen in Fig. 5.5B that shows broadly decreasing age with increasing latitude. Thus the earliest phase of SAP magmatism started in the south whereas the subsequent phases shifted their focus towards NE along the central NW-SE axis through Skjoldungen Ø.

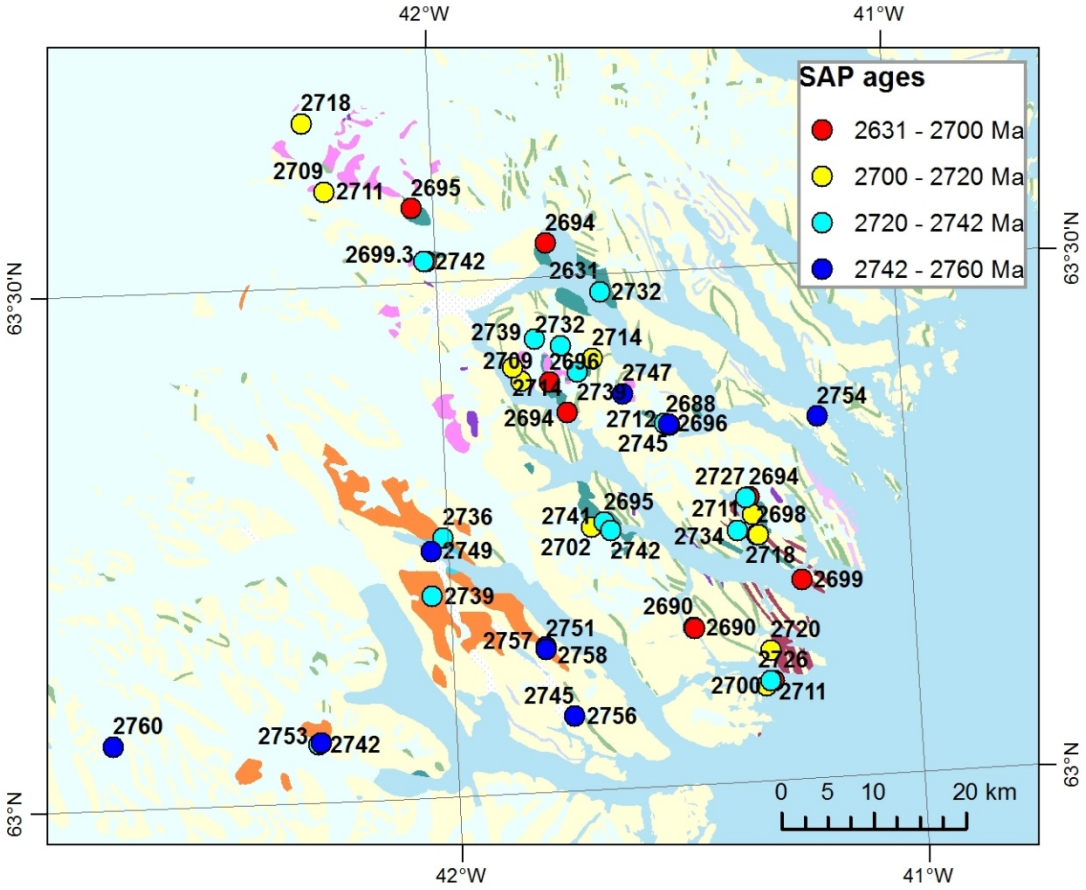

Figure 5.4 *Geological map of the Skjoldungen Alkaline Province showing the new age data as four distinct groups based on age interval. The distribution is broadly systematic with a temporal migration of magmatism from the south to the north from* c. *2750 to 2740 Ma. Subsequent magmatism from 2740 to 2690 Ma is aligned along the NW-SE axis defined by Skjoldungen Island.*

In Fig. 5.5, the SAP intrusions are seen to cover a time period of *c.* 60 Ma from *c.* 2750 to *c.* 2690 Ma (disregarding one younger sample of a 'purple pegmatite' Blichert-Toft *et al.* (1995) at 2632 Ma). Within this time span, four distinct age peaks can be identified at 2752 Ma, 2740 Ma, 2711 Ma, and at 2695 Ma suggesting that magmatism probably at least four overlapping phases.

As seen from Fig. 5.3, the SAP samples also contain inherited zircon cores with ages ranging from *c.* 2800-3450 Ma. These older ages indicate that zircons from the gneissic basement were incorporated into the SAP magmas during emplacement, and witness of crustal contamination processes in the generation of the intermediate to felsic SAP magmas (see also Kokfelt *et al.* 2016c).

In the context of the tectono-metamorphic model proposed for the Skjoldungen area by Kolb *et al.* (2013), the earliest SAP rocks in the Skirner Bjerge could reflect a juvenile mantle melt input related to subduction processes correlating with the convergent Skjoldungen Orogeny. In terms of P-T conditions, this stage would correspond to peak granulite facies metamorphic conditions as recorded in metasedimentary rocks from Helge Halvø (Berger

et al. 2014). The following stage(s) in the evolution of the region was synchronous with the emplacement of the bulk part of the alkaline intrusive rocks forming the SAP in a syn- to late orogenic setting between 2740 and 2700 Ma. This period was characterised by fast uplift of the region, accompanied by retrograde metamorphism under amphibolite facies and greenschist facies conditions and regional scale folding (Berger *et al.* 2014, Kolb *et al.* 2013).

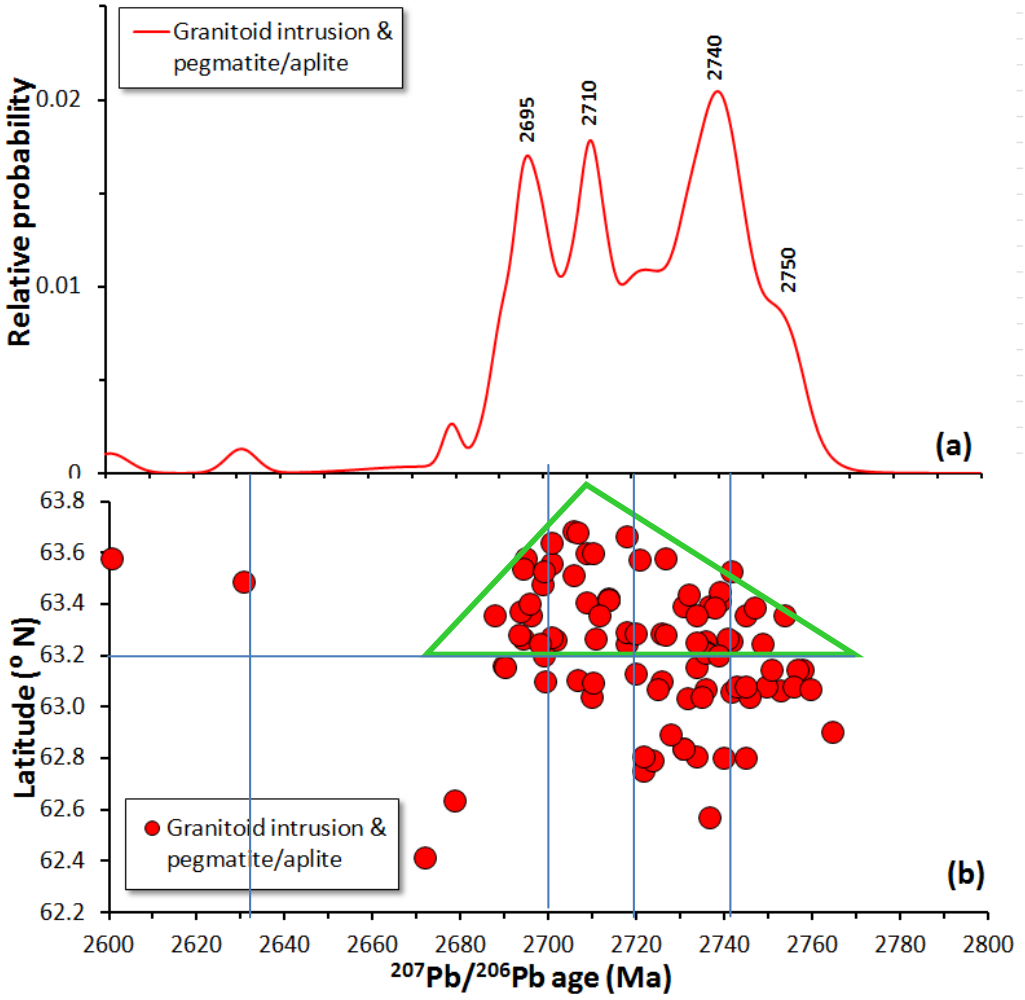

Figure 5.5 *U-Pb ages summarised for 54 U-Pb dated samples from the Skjoldungen Alkaline Province including seven samples from Kolb* et al. *(2013) and 47 samples from Kokfelt* et al. *(2016c).* ***A.*** *Age distribution diagram showing four distinct age peaks at 2695, 2710, 2740 and 2750 Ma (the latter being less distinctly defined).* ***B.*** *The same age data as in A. plotted vs. degree northern latitude, and show a focusing of the magmatisme along the Thrymheim, Skjoldungen Ø and Kong Dan Halvø axis. Data points below 63.2ºN represent intrusive lithologies that may relate to the SAP magmatism.*

5.3 Tasiilaq region or East Greenland Archaean (EGA)

Ten samples of the Archaean orthogneiss basement north of Ammassalik Intrusive Center have been dated (Fig. 5.6). The oldest age obtained from this region originate from banded

gneiss collected on the West side of the Ammassalik Fjord (sample 525233). The sample contains two age populations, the oldest interpreted as the protolith age at 3076 ± 14 Ma, whereas the younger population yields an age of 2681 ± 16 Ma. The younger age is interpreted to reflect a later event of magmatic and metamorphic activity in the area. This sample is the only one investigated from this region yielding such an old age, which is slightly older than the previously known oldest age from in situ samples of the region that is dated at 3034 ± 14 Ma (Blokken Gneiss, Nutman *et al.* 2008a).

A similar distribution of ages is demonstrated by zircon grains from of stream sediment samples (Thrane 2014). Inherited cores have ages up to 3250 Ma and populations of grains at 3000-3100 Ma, around 2800 Ma and 2700 Ma followed by a small population of grains with ages around 1850 Ma.

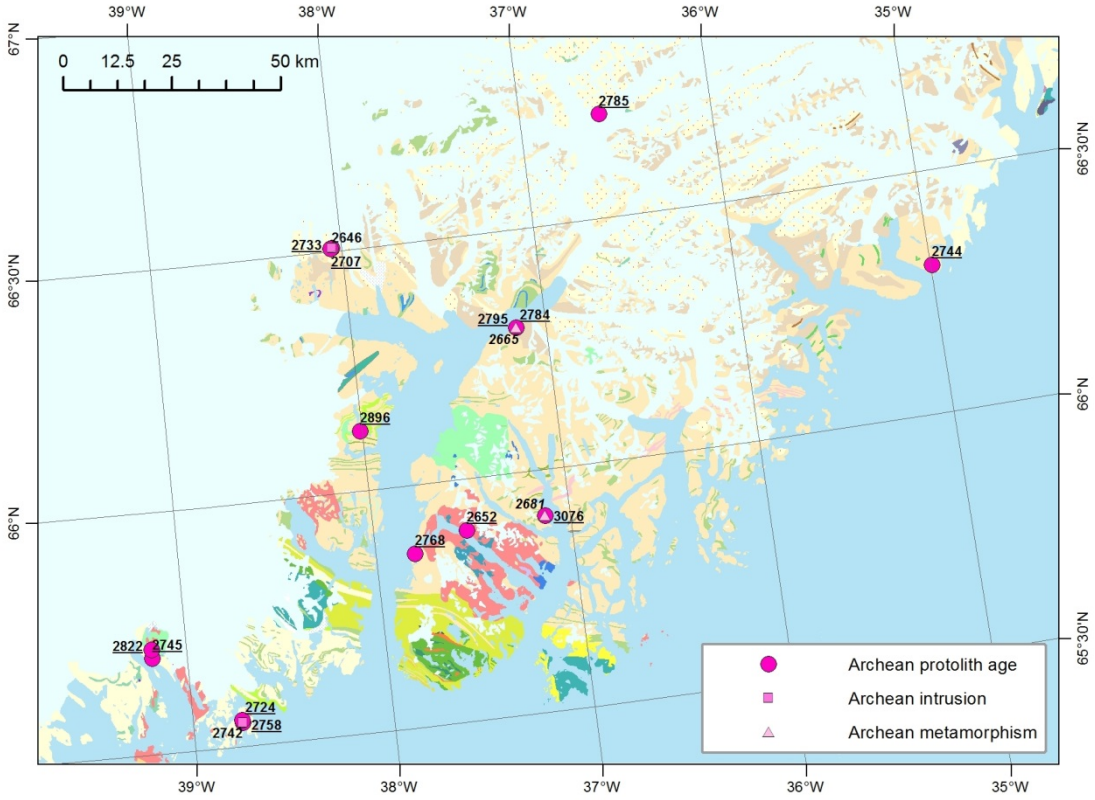

Figure 5.6 *Geological map of the Tasiilaq region showing the location of samples yielding Archaean protolith ages, intrusion ages and metamorphic ages.*

A wide range of ages exist for the orthogneiss basement complex from 2795 ± 10 Ma (sample 525243) to 2707 ± 15 Ma (sample 525245). No clear crustal growth direction is defined by the ages and no age distinction exists between the orthogneisses belonging to the Kummiut Terrane and those of the Schweizerland Terrane. A couple of the gneisses contain inherited zircons with ages of *c.* 3000 Ma.

The youngest age obtained from an orthogneiss in this region comes from a banded gneiss (sample 525210) collected within the Ammassalik Batholith, which yields a crystallization age of 2652 ± 11 Ma. However, granitic gneiss (sample 525246) collected at the Niflheim Thrust yields an age of 2646 ± 5 Ma that is the youngest Archaean age obtained during this

study. These younger ages have also been documented in earlier studies (Kalsbeek *et al.* 1993).

South of Ammassalik Intrusive Center, four orthogneisses and one pegmatite vein from the Isortoq area were dated (Fig. 5.6). Two gneisses were collected around the large diorite and granite intrusion, north of Isortoq. The banded gneisses yield ages of 2822 ± 8 Ma (sample 562915) and 2745 ± 15 Ma (sample 562909). The gneisses also yield younger metamorphic ages at *c.* 1875-1845 Ma and at 1675 Ma, corresponding to the Nagssugtoqidian Orogeny and the later heating from the late Palaeoproterozoic diorite and granite intrusions.

On island of Kitak east of Isortoq, undeformed anorthosites were sampled but did not yield any zircons. On the same island, deformed anorthosite gneisses and a deformed pegmatite vein that cross cuts the deformed anorthosite were also collected. The anorthositic gneisses yield ages of 2758 Ma ± 4 Ma (sample 562936) and 2724 ± 4 Ma (sample 562921), and the crosscutting pegmatite vein (sample 562939) yields an age of 2742 ± 6 Ma (sample 562939).

The Archaean basement ages from the Tasiilaq region are very similar to the Thrym Complex with: (1) several protolith ages of *c.* 3100-2900 Ma; (2) a range of ages between 2790-2700 Ma that corresponds to the age range of the Skjoldungen Orogeny (Bagas *et al.* 2013, Kolb *et al.* 2013); and (3) metamorphic ages associated with intrusions at 2680-2640 Ma corresponding to the Singertât stage (Bagas *et al.* 2013, Kolb *et al.* 2013). These results suggest that the whole region from 62°N to 67°N could belong to the North Atlantic Craton.

6 Archaean tectono-metamorphic evolution

Jochen Kolb & Leon Bagas

The regional structural grain was studied by drawing foliation trajectories on the 1:500 000 Skjoldungen map sheet (Fig. 6.1). Data are scarce between Bernstorff Isfjord and Isortoq, and structures in the Archaean rocks are progressively overprinted by younger deformation.

The regional structural pattern shows that the study area forms a structural unity that is characterised by a complex fold interference pattern (Fig. 6.1). A large-scale early fold closure is observed in the Timmiarmiut area, and evidence for early synforms and antiforms is present in the Bernstorff Isfjord area (Fig. 6.1). Foliation and early folds are refolded into regional-scale folds with shallow west-plunging fold hinge zones in the north and east-plunging fold hinge zones in the south. The area north of Graah Fjord is dominated by a strong, locally mylonitic northwest-southeast trending foliation (Kolb *et al.* 2013).

The earliest (> 2790 Ma; D_T Timmiarmiut Orogeny) deformation fabric is a foliation preserved in mafic and ultramafic rocks and the early- to syn-tectonic orthogneiss (Kolb *et al.* 2013, Lally 2013). The S_T foliation is broadly northwest-southeast trending and is only preserved at outcrop-scale in the other areas. Locally, a down-dip mineral stretching lineation (L_T) is observed.

The S_T foliation is folded into regional-scale upright to reclined isoclinal folds during the Skjoldungen Orogeny (D_S; 2790-2650 Ma). The F_{S1} fold axes plunge gently southwards in the Timmiarmiut area, whereas northwest plunges are recorded in the Skjoldungen area (Fig. 6.1). The axial planar S_{S1} foliation is the penetrative, northwest-southeast trending fabric. It dips mainly moderately to steeply to the southwest, with only local dips to the northeast. The L_{S1} mineral stretching lineation plunges (1) to the west in the western part, (2) south in the central area, and (3) southeast in the east such as on Helge Halvø (Kolb *et al.* 2013). Together with abundant S-C, S-C' and mica-fish fabrics, this indicates deformation to the northeast (Kolb *et al.* 2013). Some rocks of the SAP have a magmatic foliation parallel to S_{S1}. In the Timmiarmiut area, the S_{S1} foliation is near vertical, trending northeast-southwest. Transposition fabrics and L_{S1} down-dip mineral stretching lineation suggest local normal southeast-vergent deformation (Kolb *et al.* 2013, Lally, 2013). The narrow dismembered bands of mafic and ultramafic rocks preserve the early (S_T) and the later (S_{S1}) foliations throughout the region. This strongly suggests that the region structurally represents an integral unit since at least the D_T stage (Kolb *et al.* 2013).

The penetrative foliation is folded into regional-scale open to close folds (F_{S2}), yielding "mushroom" shaped fold interference patterns (Fig. 6.1). Three types of D_{S2} shear zones are (Kolb *et al.* 2013): (1) several tens of meter wide reverse shear zones that sheared off fold limbs; (2) discrete cm-m wide, northeast-southwest trending, near-vertical, sinistral shear zones; and (3) < 20 cm wide, east-west trending, near-vertical, dextral shear zones. The near-vertical shear zones form a conjugate set together with syn-tectonic pegmatite dikes. They are common features that are particularly found associated with intrusions of the SAP (Kolb *et al.* 2013). The acute angle in a northerly orientation and north-south trend-

ing extension veins suggest north-south compression and east-west extension during D_{S2} (Kolb *et al.* 2013).

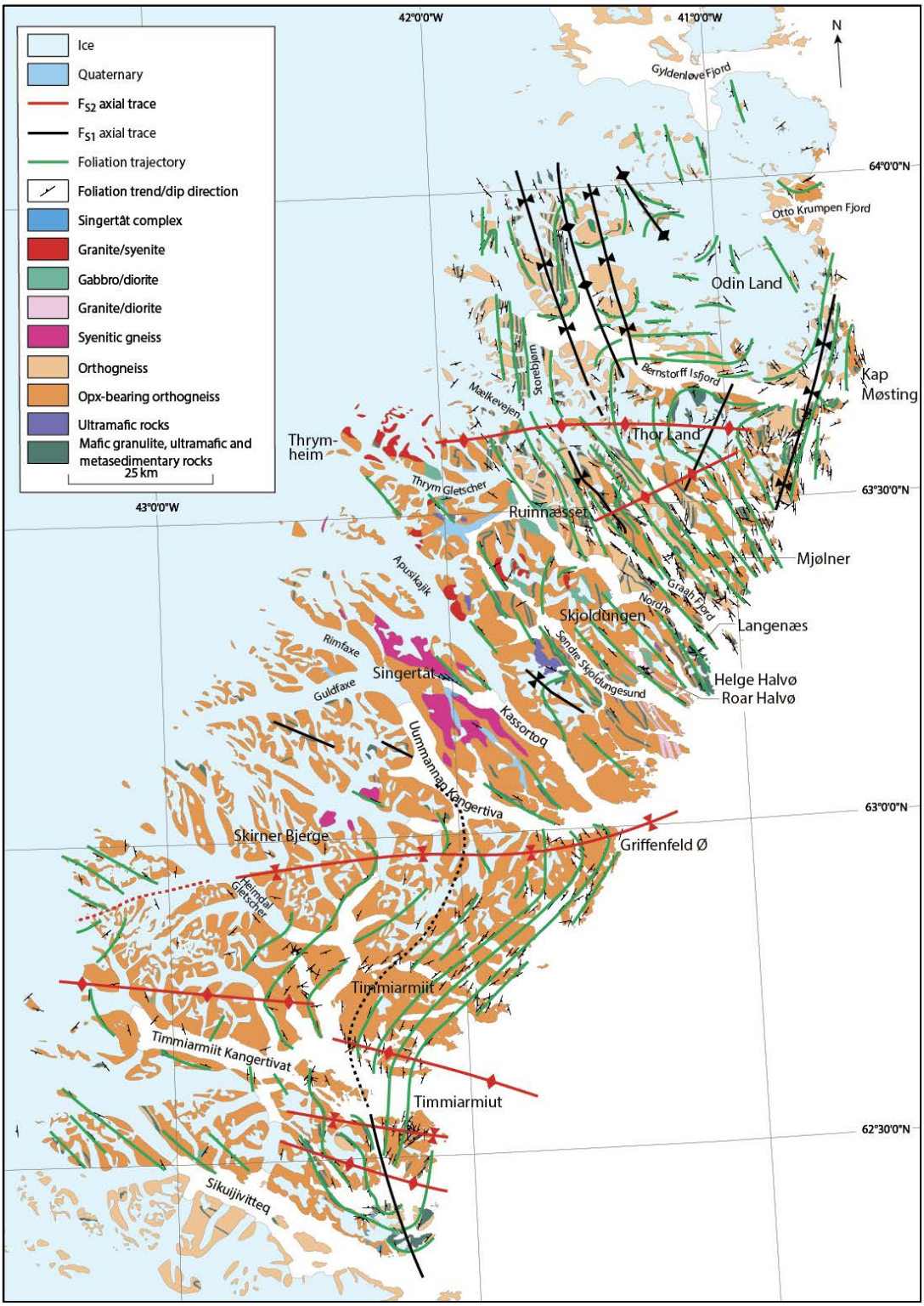

Figure 6.1 *Geological map of the Skjoldungen-Timmiarmiut area with foliation trajectories and fold axial traces outlined, indicating a complex fold interference pattern and general structural uniformity in the Thrym Complex (Kolb* et al. *2013).*

A conjugate set of up to 1 m wide, near-vertical, sinistral southeast- and dextral northeast-trending shear zones (D_R 2680-2650 Ma) are present in the approx. 3 km wide Singertât Complex (Kolb *et al.* 2013). The greenschist facies shear zones can be followed over several 100s of meters. The orientation of these shear zones is indicative of north-south extension and east-west compression (Kolb *et al.* 2013).

The interpreted intrusion age of the oldest orthogneiss in the Thrym Complex is ~ 2850 Ma, which intruded mafic to ultramafic rocks of unknown age (Kolb *et al.* 2013). One mafic granulite sample yielded and U-Pb zircon age of 2859 ± 6 Ma (Bagas *et al.* 2016). Inherited zircons range between 3100 and 2800 Ma, with older inherited grains of 3880-3100 Ma restricted to the Timmiarmiut area, indicating a largely hidden MesoArchaean and even earlier history for the NAC (Fig. 6.2) (Kokfelt *et al.* 2016c, Kolb *et al.* 2013). Many of the NAC rocks preserved granulite facies assemblages and metamorphic zircon ages cluster around 2800-2780 Ma (Kolb *et al.* 2013). This high metamorphic grade overprint obliterated earlier (Timmiarmiut Orogeny) information, with only relics preserved. The protoliths of the orthogneiss that intruded between *c.* 2800 and 2760 Ma are TTG and biotite monzogranite (Kolb *et al.* 2013). The emplacement of these intrusive rocks was at least partly related to melting of the crust during granulite facies metamorphism and possible early extension. Both orthogneiss relicts in migmatite and the matrix of the migmatites define a tectono-metamorphic-magmatic stage at 2760-2740 Ma (Fig. 6.2), suggesting that high-grade metamorphic conditions prevailed until at least *c.* 2740 Ma (Kolb *et al.* 2013). These orthogneisses are mainly granodiorite and were pervasively foliated during the onset of the Skjoldungen Orogeny at granulite facies conditions at a temperature of approx. 760°C and a pressure of 8 kbar (Bagas *et al.* 2013, Berger *et al.* 2014, Kolb *et al.* 2013). Flysh-type metasedimentary rocks contain *c.* 2800 Ma detrital zircons with younger metamorphic overgrowths and were incorporated in the Skjoldungen Orogen (Berger *et al.* 2014). Our data has no U-Pb zircon ages between *c.* 2785 Ma and 2755 Ma and suggests a *c.* 40 m.y. lack of magmatic activity, which in Kolb et al. (2013) is explained by the prevailing conditions in a middle to lower crustal compressional setting (Fig. 6.2).

The emplacement of *c.* 2740 Ma intrusions into wall rocks at amphibolite facies grades indicates that the Thrym Complex was on its retrograde path, which could be related to regional northwest-southeast transpression associated with the Skjoldungen Orogeny (Fig. 6.2). This coincides with the start of alkaline magmatism in the SAP (Berger *et al.* 2014, Kolb *et al.* 2013). Metamorphic zircon ages of *c.* 2720-2700 Ma mark the onset of folding and metamorphism assigned to the second D_{S2} stage of the Skjoldungen Orogeny in a stress field oriented northnorthwest-southsoutheast (Kolb *et al.* 2013). The exhumation of the Thrym Complex occurred relatively fast between *c.* 2755 Ma and 2700 Ma at rates of approx. 0.4 km/m.y., which is similar to exhumation rates related to erosion-driven processes in modern orogens (Berger *et al.* 2014, Kolb *et al.* 2013). The *c.* 2664 Ma Singertât Complex (Blichert-Toft *et al.* 1995) marks the Singertat Stage as defined in Kolb et al. (2013), which caused retrogression at greenschist facies conditions in the D_R deformation zones. This stage is related to relaxation of the stress field at *c.* 2680-2650 Ma, which lead to orogen-normal extension during the post-collisional evolution concluding the Archaean history of the Thrym Complex (Fig. 6.2, Kolb *et al.* 2013).

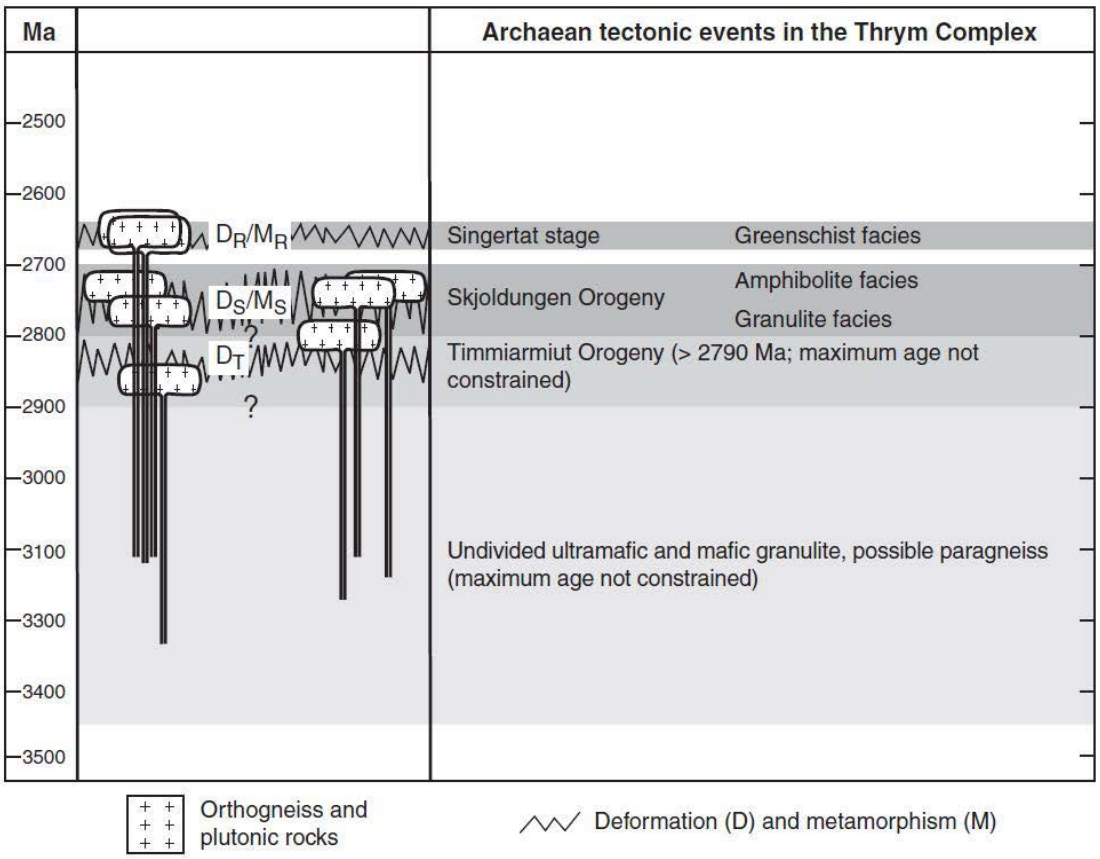

Figure 6.2 *Schematic sketch of the tectono-metamorphic and magmatic evolution of the Thrym Complex in the NAC (simplified after: Kolb* et al. *2013).*

7 Palaeoproterozoic dykes

Martin Bromann Klausen, Mimmi Nilsson & Riaan Bothma

Consistent with the chronological structuring of this report, this chapter only addresses pre-orogenic intrusions, whereas post-orogenic Late Palaeoproterozoic is included in Chapter 12. During the SEGMENT 2011, 2012 and 2014 expeditions, Palaeoproterozoic tabular intrusions (primarily original dykes) were sampled from areas in and around Umivik, Graahs Fjord, Skjoldungen, and Timmiarmiut, as well as four key localities across the region between Jens Munk Ø and Isortoq (the region that suggested as being the foreland of the Nagssugtoqidian Orogen in South-East Greenland (Kolb 2014)).

The field work has resulted in a wealth of data including nearly 200 whole rock geochemical analyses and U-Pb ages on extracted baddeleyites, which has been reported in various thesis works on either Honours- (Bothma 2013, Snyman 2013), MSc- (Bothma, ongoing) or PhD-levels (Nilsson 2016). The following review describes preliminary results on Palaeoproterozoic intrusions within three distinct regions: (1) the core of the North Atlantic Craton (NAC), (2) the Umivik transition zone, and (3) the Nagssugtoqidian deformation front.

In the field, pre-orogenic Palaeoproterozoic dykes are often distinguished from younger dykes on the basis of their degree of either deformation and/or metamorphism, and the term 'meta-dykes' is often appropriate as used in southwestern Greenland (Kalsbeek and Taylor 1985, Nilsson *et al.* 2013). The extent of overprint by the Nagssugtoqidian and Ketilidian orogenies varies broadly with distance to the northern and southern border zones of the NAC, respectively, suggesting that metamorphism of the Palaeoproterozoic dykes was caused by these two orogenies.

7.1 Dykes across the North Atlantic Craton

As argued for the Palaeoproterozoic dykes of South-West Greenland (Nilsson *et al.* 2013), the degree of metamorphism varies across the more protected NAC core, and it can sometimes be difficult to recognize Palaeoproterozoic dykes when metamorphosed and to distinguish these from younger intrusions. However, more detailed petrographical studies typically reveal that pyroxenes generally are not preserved and as a minimum uralitized, that plagioclases saussuritized and that olivines, when originally present, typically are serpentinized. Yet, the degree of metamorphism is fortunately limited and allowed the preservation of igneous baddeleyites, used for precise U-Pb TIMS dating of extracted baddeleyites (Nilsson 2016).

Palaeoproterozoic dykes are typically ~ E-W to ENE-WSW trending and across South-East Greenland easily distinguishable from cross-cutting, distinctly more brown weathered and northerly trending ~ 1630 Ma dykes (M. Nilsson, unpublished data, Section 12.3) and more coast-parallel presumed Tertiary dykes (Section 13.1). Across the southernmost part of the NAC (Timmiarmiut area), however, there are fewer cross-cutting relationships to help distinguishing between ENE-WSW trending Palaeoproterozoic dykes and a sub-parallel swarm of ~ 1270 Ma Mesoproterozoic dykes belonging to the Gardar Province (Bartels *et*

al. 2015, Section 12.3), but relative cross-cutting relationships with N trending ~ 1630 Ma dykes assist field discriminations together with additional petrographical differences.

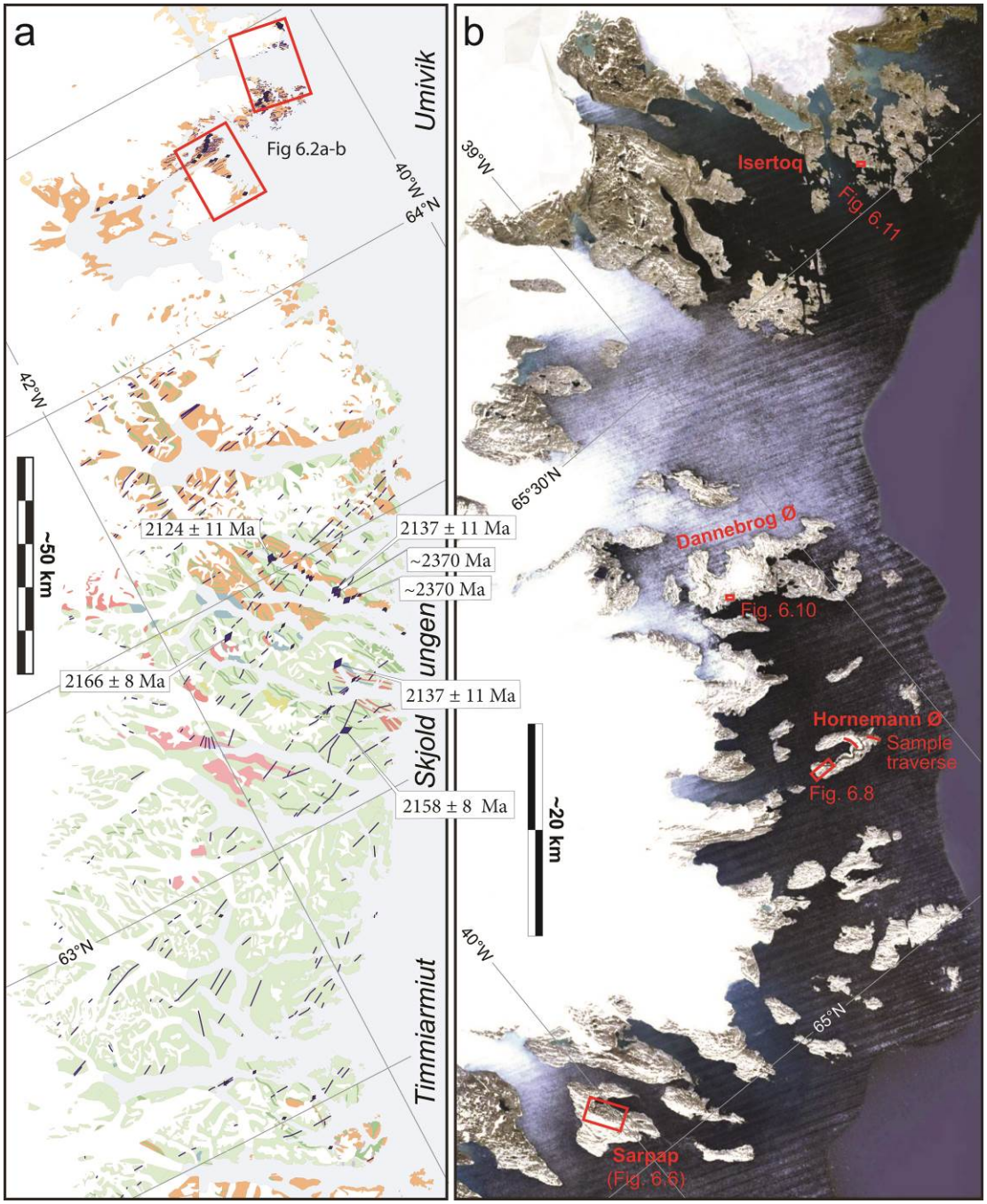

Figure 7.1 ***A.*** *Geological map of the North Atlantic Craton, as exposed along the southeast coast of Greenland. Purple lines: presumed pre-orogenic Palaeoproterozoic dykes with sample sites located by purple diamonds. Larger diamonds: baddeleyite U-Pb TIMS ages for seven Palaeoproterozoic dykes (Nilsson 2016). A more detailed map of the Umivik swarm is shown in Fig. 7.2.* ***B.*** *Google earth image of coast line covering much of the Nagssugtoqidian deformation front, where amphibolites are highly deformed. Four case study areas are indicated with reference to detailed maps in the text.*

The 2375-2365 Ma Grædefjord dykes of South-West Greenland have been speculated to be contiguous under the inland ice (Nilsson *et al.* 2013). This is corroborated by preliminary U–Pb baddeleyite data of two ENE-NE trending dykes in the Gråhavn area north of Skjoldungen, which yield preliminary ages of ~2370 Ma (Fig. 7.1A) (M. Nilsson, preliminary data). These dykes are indistinguishable in trend from co-existing 2140–2125 Ma dykes, termed Ruinnæsset dykes. In South-West Greenland, an E-W trending dyke just south of Nuuk yields an age of 2125 Ma, statistically indistinguishable from the Ruinnæsset dykes. A slightly older set of E-W trending dykes, termed Skjoldungen dykes, yield *c.* 2165-2160 Ma (Fig. 7.1A, Nilsson 2016). No U-Pb ages of coeval dykes are published from South-West Greenland, although the older Iggavik suite in the Paamiut area might be correlative based on a 2180 ± 100 Ma Rb-Sr age (Kalsbeek and Taylor 1985).

The 2045-2020 Ma Kangâmiut dykes across South-West Greenland have also been suggested to extend to SE Greenland, based on trends and a 2015 ± 15 Ma U-Pb zircon age of a dyke in the Ammasalik area (Nutman *et al.* 2008b).

Most Palaeoproterozoic dykes have more or less evolved tholeiitic compositions, with MgO concentration between 3-8 wt% and are geochemically indistinguishable from each other, as well as from Palaeoproterozoic dykes across South-West Greenland. They all have negative Nb-anomalies and are relatively LILE/HFSE-enriched, suggesting that they were all derived from a roughly similar source, presumed to be the metasomatized sub-continental lithospheric mantle (SCLM). It is also possible for asthenospheric melts to acquire similar signatures through assimilation of continental crust, but there are no convincing AFC-trends to support such an interpretation.

7.2 The Umivik Dyke Swarm

Special emphasis is put on predominantly E-W to ESE-WNW trending and variably metamorphosed mafic dykes that cut across the Umivik area, not only because of their dense distribution compared to more widely distributed Palaeoproterozoic dykes across the NAC but also because the Umivik swarm reputedly straddles the southernmost extent of the Nagssugtoqidian deformation front (Bridgwater *et al.* 1973). As observed for the Kangâmiut dyke swarm in western Greenland, the Umivik dykes also become progressively more deformed and metamorphosed towards the Nagssugtoqidian Orogen and thereby hint to a possible link between these two swarms. Rather than a direct correlation to the Kangâmiut swarm, however, it seems more logical to assume that most Umivik dykes are members of the sub-parallel Paleoproterizoic swarms described in Section 7.1. Unfortunately, no baddeleyites have so far been extracted fpr absolute U-Pb age dating from any of these more metamorphosed Umivik dykes.

As for pre-orogenic Paleoproterzoic dykes across the NAC (Section 7.1), post-orogenic Proterozoic and presumed Tertiary dykes, obliquely cross-cut the Umivik swarm as distinctly more brown-weathered intrusions. Although most Umivik dykes classify as metamorphosed Palaeoproterozoic dykes, we also observe six localities where a less altered ‘dolerite’ cuts a much more metamorphosed ‘amphibolite’ dyke (cf., “young” in Fig. 7.2A-B). The E-W to ESE-WNW trending Umivik swarm must therefore incorporate at least one minor

sub-swarm of less metamorphosed (post-orogenic?) dykes, which unfortunately cannot be distinguished from other Umivik dykes on the basis of either their trends or geochemical signatures.

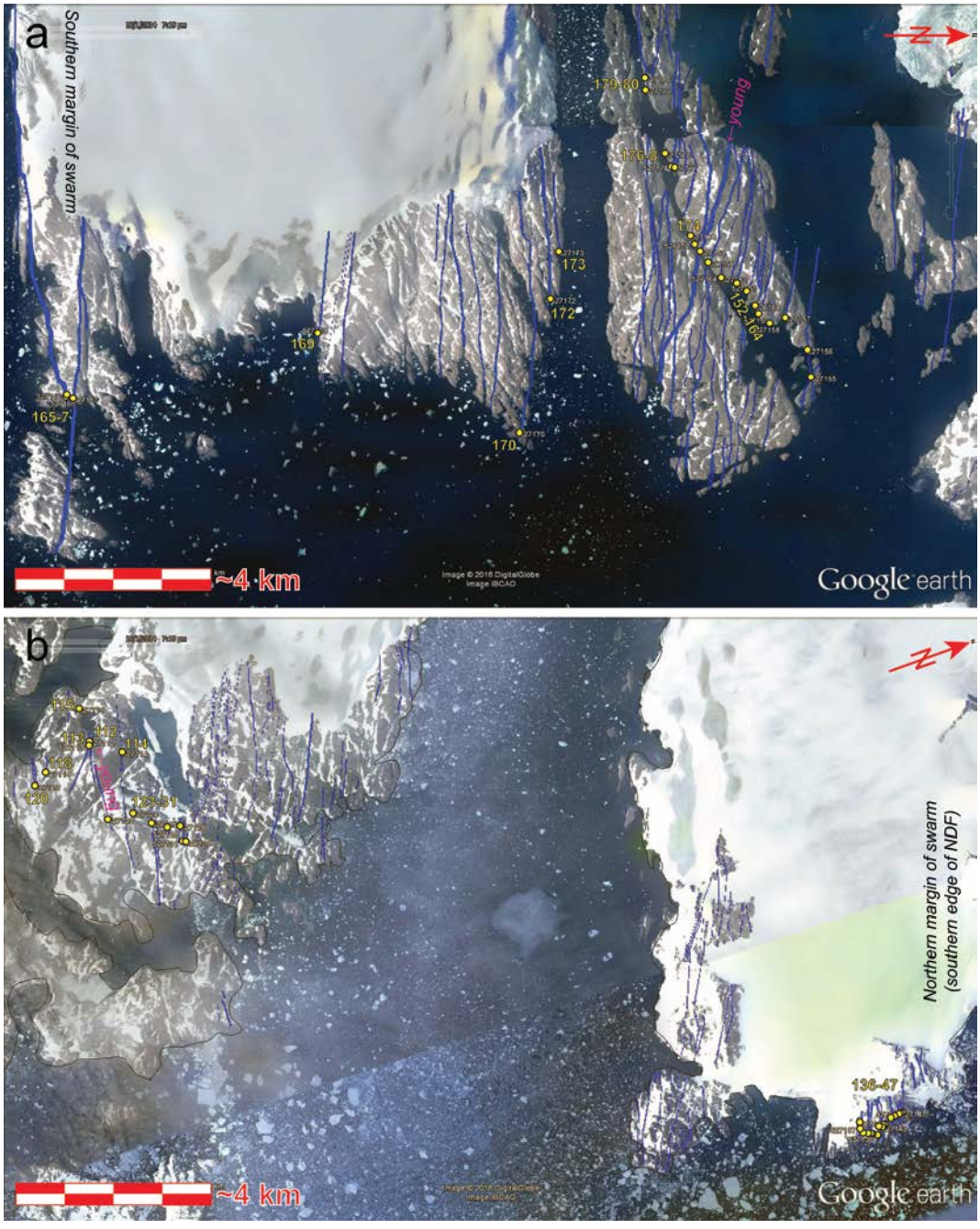

Figure 7.2 *Umivik dykes traced from Google earth.* ***A.*** *Southern profile section of the swarm mapped and sampled across Upernatitivik and "Zebra Island".* ***B.*** *Northern profile section mapped and sampled across the Umivik peninsular and southern part of Jens Munk Ø (including Lynæs and Kap Løvenørn). Sample localities indicated by yellow dots and numbers should be prefixed by GGU527- for full GEUS sample identification. Two cross-cutting and relatively fresh dykes (labelled young) are highlighted to illustrate that sub-group's inconsistent trend.*

From the Umivik swarm's southern margin along Gyldenløve Fjord (64˚12'N) and up to Lynæs (64˚27'N), dykes remain relatively regular and vertical, but begin to dip more gently northwards across its most northerly exposed margin at Kap Løvenørn (64˚28'N). This apparent tilting is tentatively interpreted to record the southernmost effect of significant Nagssugtoqidian top-to-S deformation. Across the same ~40 km long dyke swarm section (Fig. 7.2A–B), the moving average thickness of Umivik dykes decreases from the swarm's S-margin and correlates inversely with an increased density of dykes towards Kap Løvenørn (average thicknesses from 15.0 m to 5.4 m and dyke densities from ~2% to ~15%, respectively); a structural pattern recorded across margins of other rift-related swarms (Klausen 2006). Thus, the Umivik dykes could have been emplaced within a more focused paleo-rift rather than being members of a more widely distributed giant (radiating) swarm. Even if dykes could have become tectonically thinned towards the southernmost extent of significant Nagssugtoqidian deformation, it is difficult to see how this deformation could also have increased dyke density, and the Umivik swarm is therefore likely to have been emplaced within a more focused paleo-rift; the northern part of which is likely to have been obliterated by the deformation.

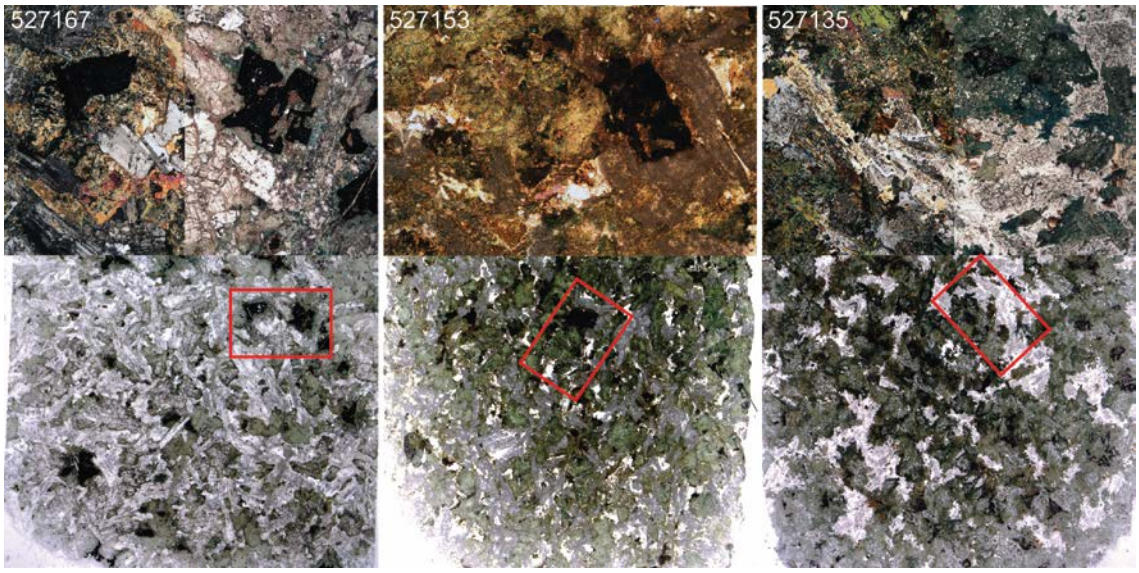

Figure 7.3 *Different grades of metamorphism of proto-doleritic dykes across the Umivik Dyke Swarm exhibited by thin section 527167 (from southernmost part of Upernattavik), 527153 (from the central "Zebra Island"), and 527135 (from Kap Løvenørn). For each sample, the lower part represents a flatbed scanned image (width of view ~ 20 mm), upon which the upper microscope photograph is located (left half under crossed and right half under plane polarized light, and entire width of view ~ 5 mm). Note how the semi-pristine sub-ophitic texture in 527167 is pervasively uralitized and saussuritized in 527153 and eventually even pseudomorphic textures are obliterated in 527135. Also note how the opaque (Fe,Ti)-oxides progressively break down. All samples numbers should be prefixed by GGU-.*

Thin sections of 60 Umivik dykes document an apparent change from weakly uralitized (± serpentinized) and saussuritized dykes along the southernmost part of the swarm (e.g. 527167 in Fig. 7.3), through more pervasively uralitized and saussuritized pseudomorph textures (e.g. 527153 in Fig. 7.3) to pseudomorphic textures becoming obliterated by metamorphic amphiboles and plagioclase (e.g. 527135 in Fig. 7.3). The observed systematic

petrographical change across the Umivik Dyke Swarm is consistent with it straddling the southernmost extent of the Nagssugtoqidian deformational front, as proposed by Bridgwater *et al.* (1973). This is supported by the mentioned onset of deformation at Kap Løvenørn, rapidly increasing in intensity to the north.

Geochemically, most of the Palaeoproterozoic dykes sampled across the Umivik Dyke Swarm exhibit similar incompatible element patterns, with distinct positive Pb and negative Nb-Ta anomalies, which signifies a lithospheric component in their petrogenesis (Fig. 7.4 left). The more elevated, sub-parallel, patterns can be related to more evolved magmas with lower MgO and higher TiO_2 (Fig. 7.4 right). These patterns also resemble most other Palaeoproterozoic dykes across the NAC – both southwestern and southeastern Greenland – and are thereby consistent with the Umivik Dyke Swarm being part of the same regional swarm(s), or at least derived from a similar metasomatized SCLM. However, more rigorous geochemical comparisons may yet reveal subtle differences.

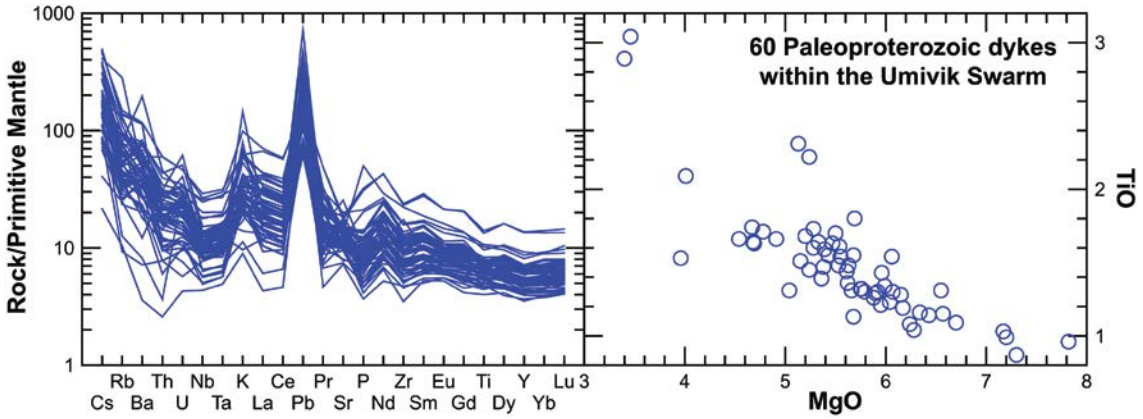

Figure 7.4 *Selected geochemical plots for 60 Palaeoproterozoic dykes sampled across the Umivik Dyke Swarm shown by (left) a primitive mantle normalized spider diagram (Sun and McDonough 1989) and (right) MgO versus TiO_2.*

7.3 Intrusions across the Nagssugtoqidian Deformation Front

Four case study areas into the Nagssugtoqidian Deformation Front (NDF) were selected for petrographic and geochemical investigations. From south to north they include: (1) the Sarpap Island (65°04'N), (2) Hornemann Ø (65°10'N), (3) Dannebrog Ø (65°19'20''N, and (4) the Isertôq archipelago (65°32'N). These study areas provide insights into both pre-orogenic emplacement of Palaeoproterozoic mafic intrusions and the degree of deformation/metamorphism across the NDF (Myers 1987). Overall, a first-order geochemical subdivision can be made between a 'tholeiitic' suite that resembles other Palaeoproterozoic dykes (including the Umivik swarm) and a relatively SiO_2-rich and TiO_2-(and FeO-)poor suite, shown in blue and red, respectively (Fig. 7.5). The relatively SiO_2-rich suite includes a number of MgO-rich samples that straddle the boninite fields of (Le Maitre 2002). Thus, the NDF may include a substantial swarm of so-called 'boninitic norite' intrusions, recognized across South-West Greenland (Hall and Hughes 1987) and arguably belonging to a special global group of ~2.0 to ~2.7 Ga continental intrusions (Hall *et al.* 1989b, Srivastava 2008). Most 'boninitic' intrusions across the NDF do not, however, share similar steep REE

patterns as this global group and it may be speculated whether metasomatic processes selectively added SiO_2 and leached out TiO_2 and FeO.

7.3.1 Sarpap

The most southerly study area in the NDF on Sarpap Island represents a uniquely well preserved ~ 2 x 1 km large ellipsoidal 'enclave', surrounded by more intensely sheared rocks (Fig. 7.6). This 'window' into near pristine configurations of mafic intrusions reveals several cross-cutting sets of intrusions with distinctly different orientations (dykes, sills and sheets). Seventeen out of 25 samples belong to the 'boninitc' suite, identified in Fig. 7.5 (including most of its high-MgO samples), whereas only 6 are 'tholeiitic' and 2 are granophyres. Many of the thicker dykes and sills are relatively pristine brown-weathered rocks of primarily 'boninitic' meta-norites, including some potential orthopyroxenitic cumulates (Fig. 7.7) to explain MgO-contents up to 22 wt% (Fig. 7.6), which collectively suggests that the 'bonintic' signatures are primary.

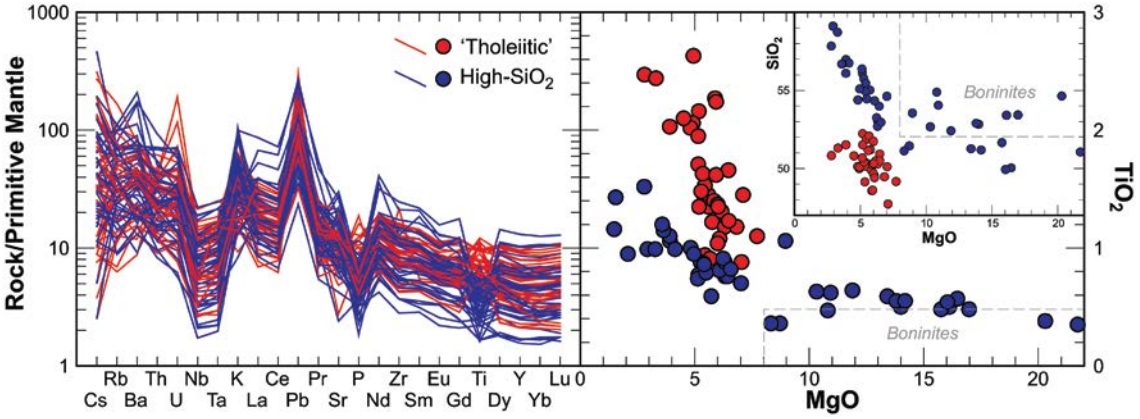

Figure 7.5 *Geochemistry of 80 mafic intrusions across the Nagssugtoqidian Deformation Front, plotted as in Fig. 7.4, but including a MgO versus SiO_2 diagram (right insert). Samples are subdivided into a typical 'tholeiitic' suite (blue) and a more SiO_2-rich 'boninitic' suite, the latter of which includes some exceptionally MgO-rich intrusions (primarily from Sarpap). The three most MgO-poor granophyric samples have SiO_2 > 60 wt%. Boninite fields are from Le Maitre (2002). See text for more details.*

Figure 7.6 shows two thick NW-SE trending and 'tholeiitic' meta-dolerite dykes, which appear to be the oldest intrusions within the Sarpap 'enclave' and may be part of the same folded dyke. No field evidence was found of the northernmost 'tholeiite' cutting through the meta-dolerite sill, even though two of its segments could be correlated across it. A subparallel, 'boninitic' and NW-SE trending norite dyke also intersects the sill, but their cross-cutting relationship was not studied. The eastern part of the 'enclave' is made up of a chaotically boudinaged assemblage of both thick 'boninitic' and 'tholeiitic' intrusions, which may well link up to any of the three more regular NW-SE trending dykes. Only the outer margins of thicker intrusions may be significantly sheared and recrystallized into fine-grained black amphibolite. A group of thinner dykes and sheets were not preserved and are more pervasively sheared amphibolites, even though these consistently cut the thicker NW-SE trending dykes as well as the sill (Fig. 7.6). Only thick dikes preserved their primary textures and

minerals. The widths, foliations and degree of metamorphism of the thin amphibolite sheets may be due to Nagssugtoqidian top-to-S deformation preferentially affecting moderately NW-dipping sheets.

The noritic sill constitutes the most distinguishable feature of Sarpap. Its thickness is difficult to estimate precisely, but it appears to have been able to partially melt the underlying host rock to form granophyric back-veins into the sill, which may even have accumulated into a larger sill-like intrusion that could be mistaken for a differentiated 'Sandwich Horizon' (yellow in Fig. 7.6). There is also no layering within the sill, to support such an interpretation. As mentioned it was impossible to determine cross-cutting relationships between the sill and two of the NW-SE trending dykes, which clearly extend from both sides of the sill, but it seems unlikely, however, for the 'tholeiitic' dyke to have fed the 'boninitic' norite sill.

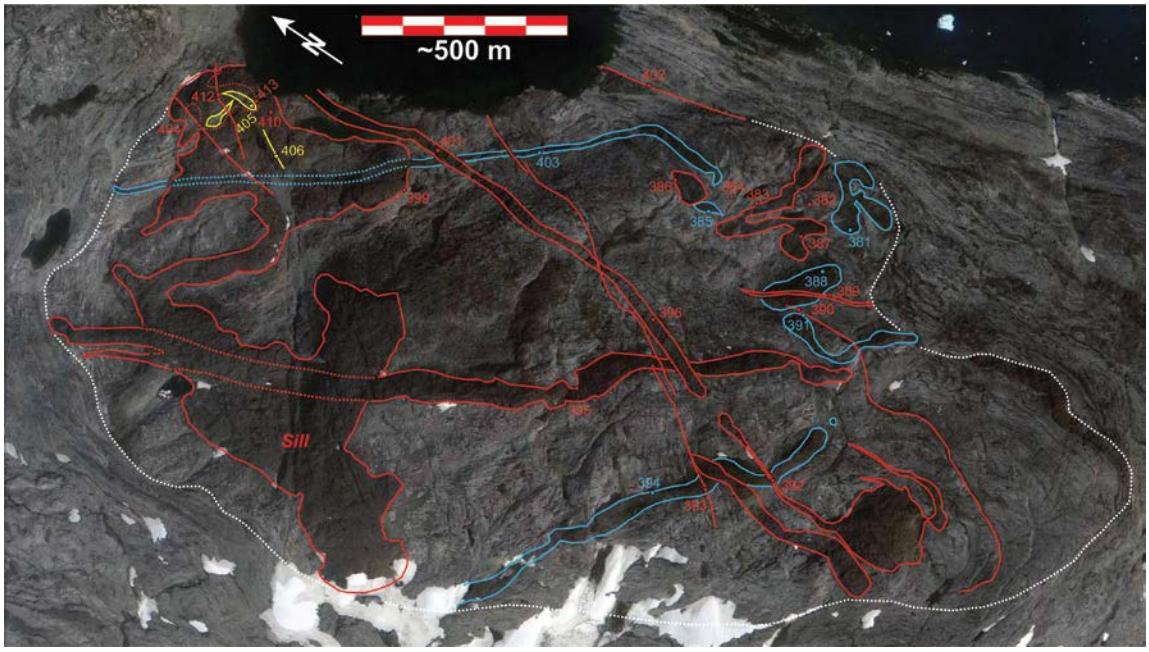

Figure 7.6 *In the central parts of the Sarpap Island in the southern NDF, a well preserved large 'enclave' (outlined by dotted white line) is surrounded by intensely sheared rocks and provides a window into near-pristine configurations of intrusions, distinguished by colours as belonging to (1) a tholeiitic blue suite, (2) a 'boninitic' red suite, and (3) yellow granophyres (probably contact melted host rocks at base of sill), identified in Fig. 7.5. On the basis of orientations, these are furthermore subdivided into (1) a large meta-noritic sill (red outline on left side of image); (2) at least three ~NW-SE trending thick brown-weathered dykes; two of which are 'tholeiitic' (blue) and another that is 'boninitic' (red) and potential feeder to the sill; (3) a complex cluster of irregular intrusions across the eastern part of the enclave, which may represent folded/boudinaged extensions of both 'tholeiitic' and 'boninitic' intrusions, and (4) one thick ~N-S trending meta-noritic dyke (red) that cuts all other intrusions, except for perhaps a group of similar striking but moderately W-dipping thin amphibolite sheets that are often foliated yet cut most other intrusions. Prefix GGU563- needs to be added to acquire a complete GEUS sample number.*

A single N-S trending and sub-vertical 'boninitic' norite dyke cross-cuts the NW-SE trending dykes, and its fresh petrography (Fig. 7.7 left) suggests that it represents the youngest in-

trusive event recorded at Sarpap. It is also oblique to the generally more moderately NW-dipping amphibolite sheets but their cross-cutting relationships were never determined in the field. Unlike a nearby N-S trending presumed Tertiary dyke, the N-S trending norite is truncated at both ends by the pervasive Nagssugtoqidian deformation that surrounds the Sarpap 'enclave' and is therefore obviously also Palaeoproterozoic.

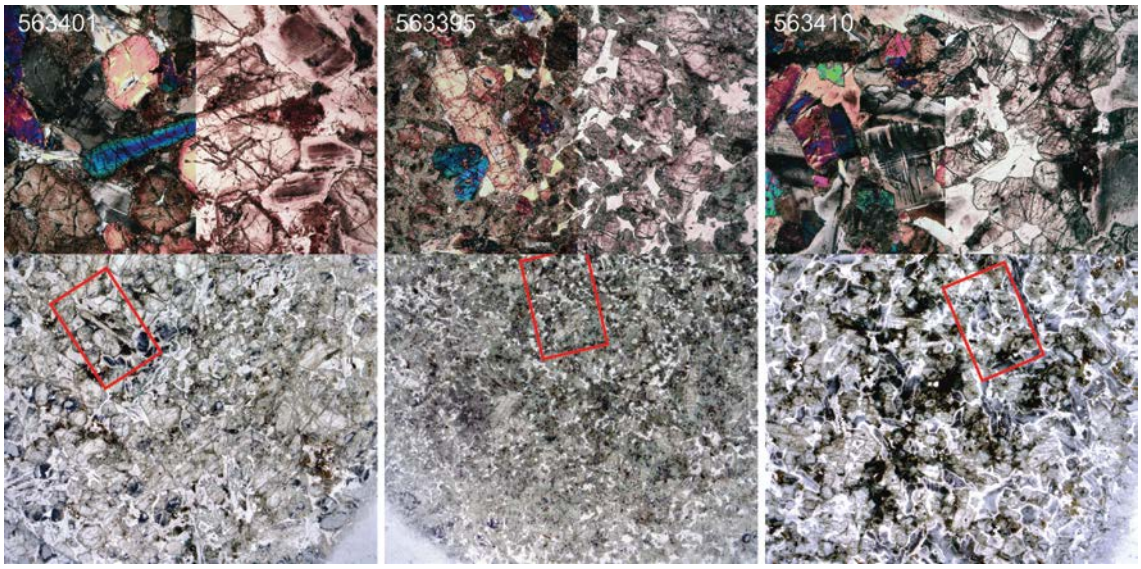

Figure 7.7 *Petrography of 'boninitic' norite intrusions from Sarpap. Left: Fresh N-S trending dyke; sample 563401. Centre: Partly altered NW-SE trending dyke; sample 563395. Right: Weakly altered sill; sample 563410. All samples originally crystallized euhedral orthopyroxenes and interstitial plagioclase. For each sample, the lower part represents a flatbed scanned image (width of view ~ 20 mm), upon which the upper microscope photograph is located by a red rectangle. Left half of microphotograph under crossed and right half under plane polarized light (entire width of view is ~ 5 mm). See Fig. 7.6 for sample locations. All sample numbers should be prefixed by GGU-.*

7.3.2 Hornemann Ø

At Hornemann Ø there is an intense swarm of sub-parallel, E-W trending, moderately N-dipping, predominantly top-to-S sheared and locally garnet-bearing amphibolites, with local tight folds (Fig. 7.8). Similar parasitic folding is even observed for a < 1 m thick felsic dyke inside a thicker amphibolite dyke, testifying to intense shortening, which is significantly greater than observed at Sarpap. It is likely that Hornemann Ø coincides with a major N-dipping thrust zone, consistent with Nagssugtoqidian top-to-S deformation. The intense ~ N-S directed shortening has an associated orthogonal ~ E-W directed stretching component, recorded by parallel lineation as well as locally boudinaged amphibolites. This orthogonal stretching also accounts for an apparent greater number of thinner amphibolite bands, which must then have had more similar rheological properties as their felsic host rocks in order to not having become boudinaged.

With the exception of the protected interiors of thicker boudinaged segments (e.g., sample 563472 in Fig. 7.9 lower right), most deformed Palaeoproterozoic intrusions across the NDF are foliated amphibolites, as illustrated by representative micro-photos in Fig. 7.9 for

both ‘boninitic’ (top row) and ‘tholeiitic’ (bottom row) samples. More rigorous determinations of metamorphic grades remain to be done on these polished thin sections, which often include garnets. However, a first-order petrographical distinction can be made between the more Fe-Ti-rich ‘tholeiitic’ samples having more biotite than ‘boninitic’ samples.

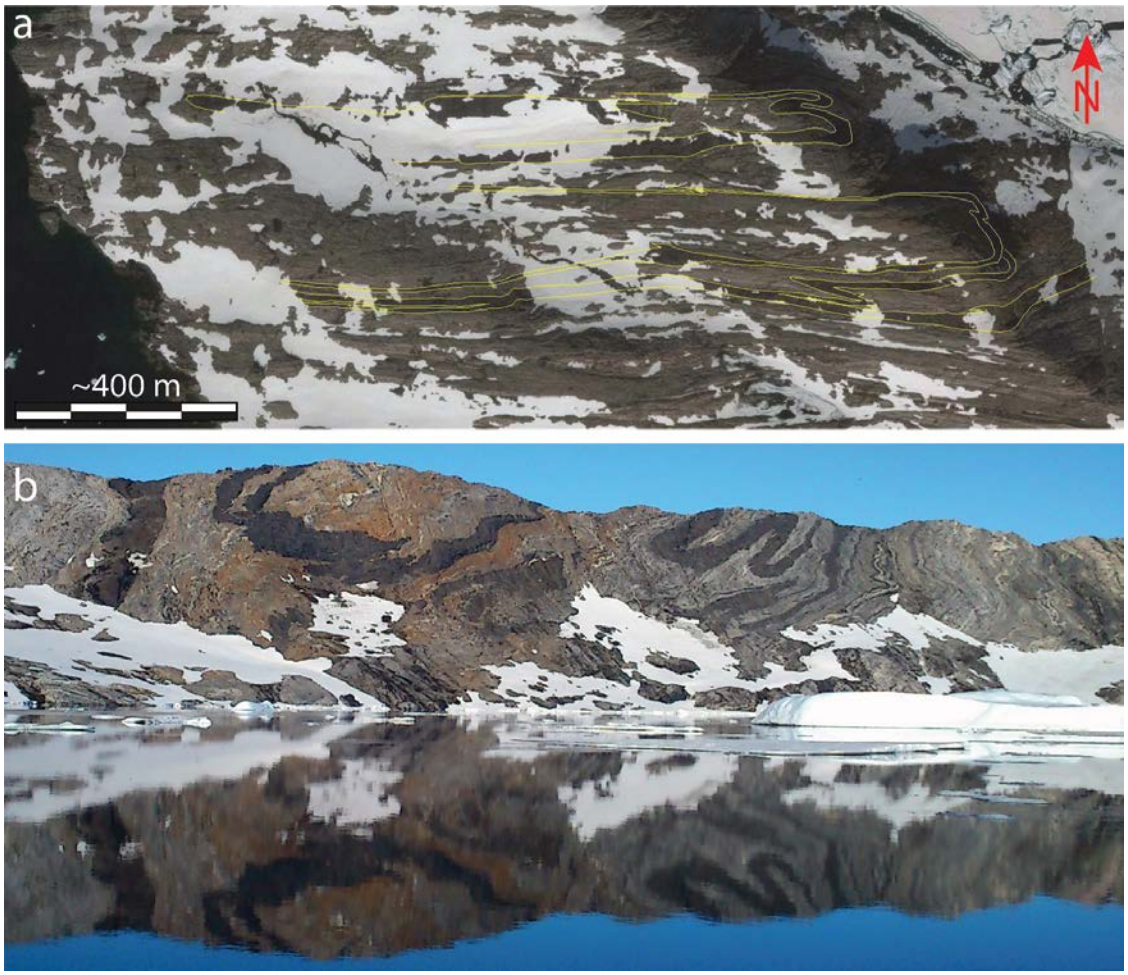

Figure 7.8 *Folded amphibolites across the western limb of the horse-shoe shaped Hornemann Ø (around 65°9’44”N; 39°44’46”W).* ***A.*** *Google earth map upon which amphibolite margins have been traced by yellow lines.* ***B.*** *Cross-section (looking west) of the eastern side of the island limb in A., showing synforms in a vertical section.*

A third of the 32 amphibolite samples from a > 2 km long N-S section across the southern part of Hornemann Ø area appear to belong to a more SiO_2-rich and correspondingly TiO_2-(and FeO-)poor ‘boninitic’ suite, whereas the remainder are ‘tholeiitic’ (Fig. 7.6 right). Only one sample from a relatively old and deformed amphibolite have MgO > 9 wt% (14 wt%) and that irregular intrusion is clearly trending more obliquely WSW-ENE (and possibly less inclined) across predominantly foliation-parallel, E-W trending and tightly folded amphibolites.

7.3.3 Dannebrog Ø

A number of relatively regular N-S trending and thick mafic dykes cut across Dannebrog Ø and these are on closer inspection locally sheared 'tholeiitic' amphibolites. At one locality (Fig. 7.10) more obscure, foliation-parallel and thin sheets of 'boninitic' character are clearly cross-cut by these N-S trending 'tholeiites'. Nevertheless, the N-S trending 'tholeiites' are also apparently displaced ~100 m along a foliation-parallel and shallow NNE-dipping thrust, as evidenced by two drag-folded dykes in Fig. 7.10. Both the orientation of and displacement along this thrust is consistent with top-to-S shearing during the Nagssugtoqidian Orogeny, and this thrusting appears to have been focused along a pre-existing, foliation-parallel and 'boninitic' intrusion.

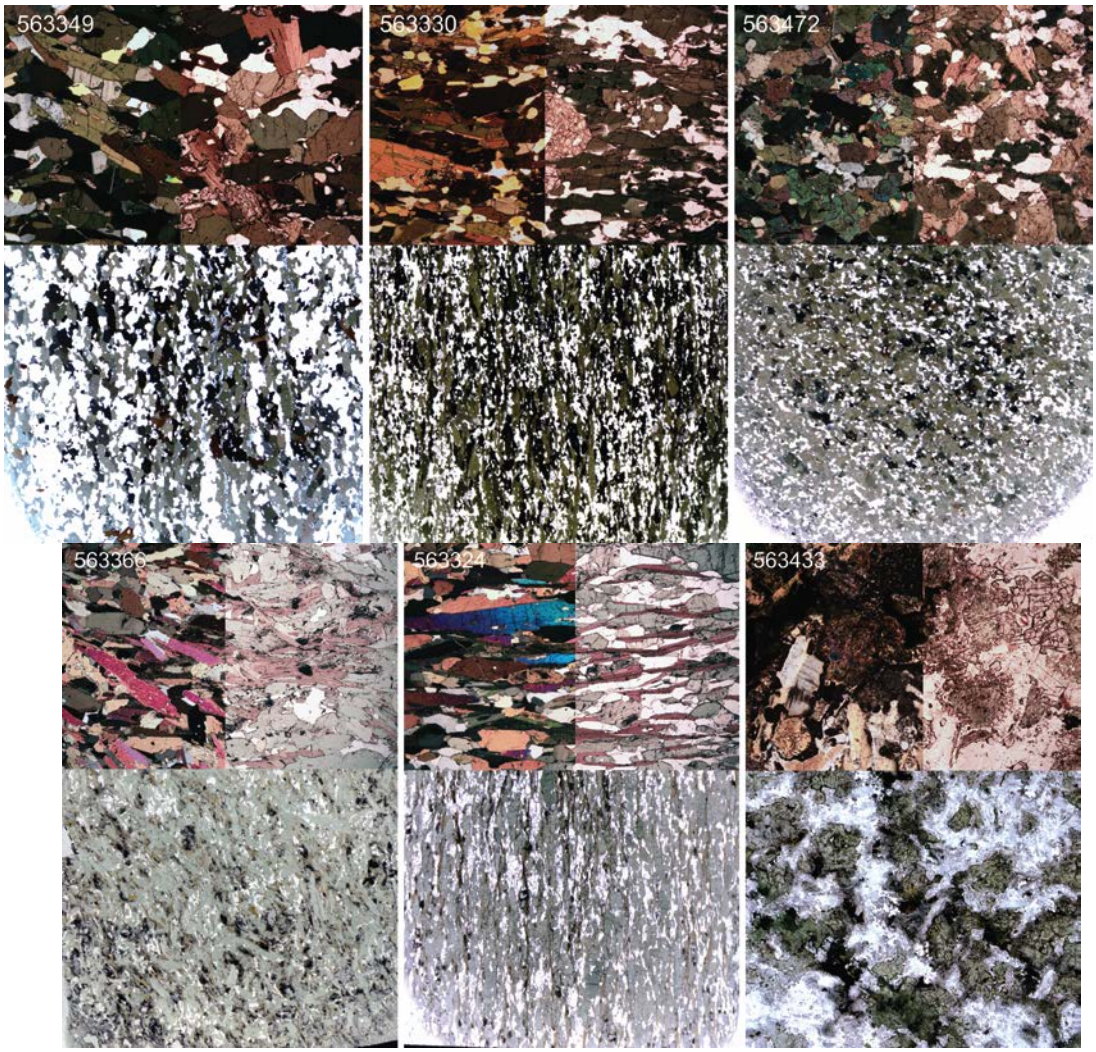

Figure 7.9 *Petrography of 'boninitic' (top row) and 'tholeiitic' (bottom row) amphibolites from (left) Hornemann Ø, (centre) Dannebrog Ø, and (right) Isortoq; progressively closer to the Nagssugtoqidian suture. Relatively higher Fe and Ti in the 'tholeiitic' samples gives rise to a higher abundance of biotite, compared to 'boninitic' amphibolites from the same three localities. For each sample, the lower part represents a flatbed scanned image (width of view ~ 20 mm) and upper part a microscope photograph, where its left half is under crossed and right half under plane polarized light (entire width of view is ~ 5 mm). All sample numbers should be prefixed by GGU-.*

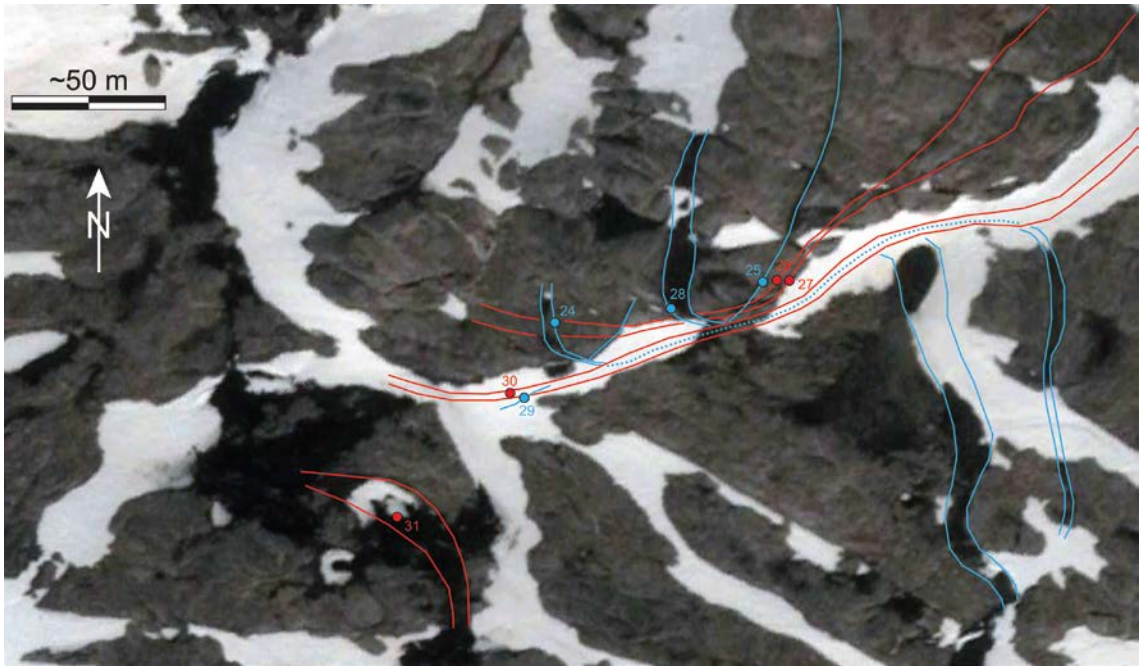

Figure 7.10 *Dannebrog Ø locality (around 65˚19'29''N; 39˚40'46''W) exhibiting an earlier foliation-parallel 'boninitic' suite (red) cross-cut by steeper ~ N-E trending 'tholeiite' dykes (blue), which are Palaeoproterozoic amphibolites and apparently displaced ~ 100 m along a low-angle, foliation-parallel thrust. Note that the 'boninitic' sheet along the same thrust plane is older than the cross-cutting 'tholeiites'; just intensely sheared. Each sample needs to be prefixed by GGU5633- for a full GEUS sample number.*

7.3.4 Isortoq

The Palaeoproterozoic intrusions are heavily deformed at Isortoq (often flat-lying, tightly folded and/or boudinaged) as well as obscured by syn-orogenic felsic intrusions. The sampled locality in Fig. 7.11 reveals two generations of both thin and thick, cross-cutting Palaeoproterozoic intrusions, which are (1) older foliation-parallel and moderately NNW- dipping 'boninitic' sheets, that are consistently cross-cut by (2) younger N-S trending 'tholeiitic' dykes. This is similar to what is observed at Dannebrog Ø, suggesting that this is a regionally extensive relationship. The younger dykes are metamorphosed (cf., sample 563433 in Fig. 7.9, which, even if it is not sheared, contains garnet), cut by late-kinematic felsic pegmatites and maybe related to late-orogenic Nagssugtoqidian mafic intrusions further north.

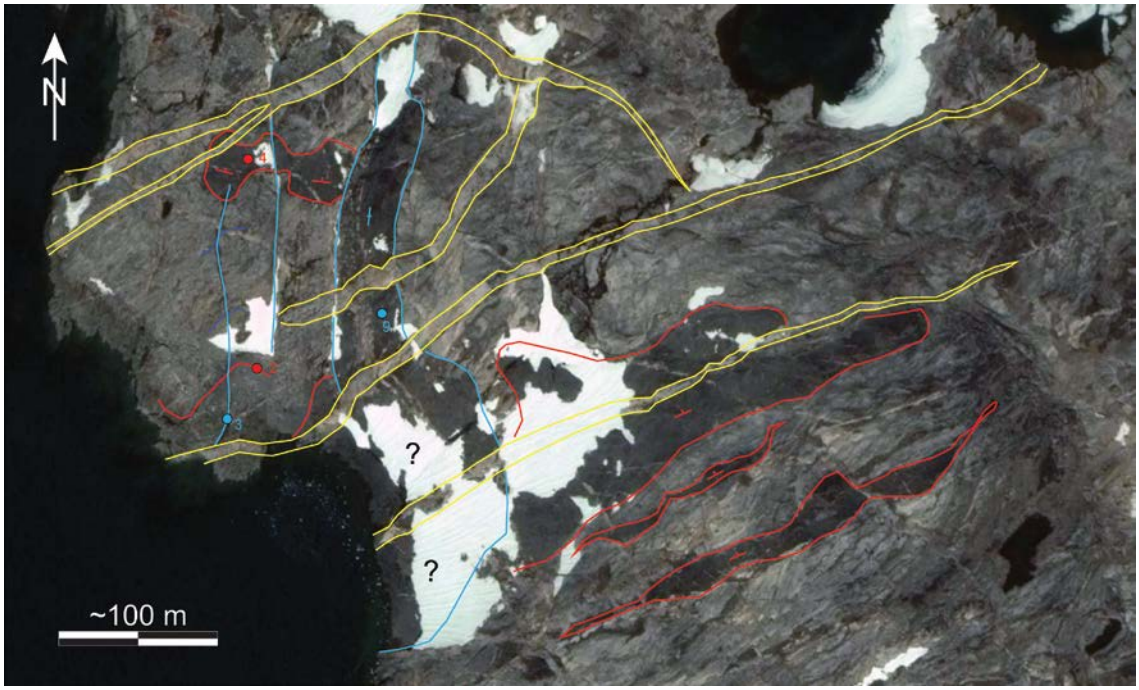

Figure 7.11 *Isortoq locality (around 65˚32'55''N; W38˚54'45''W) exhibiting an earlier foliation parallel 'boninitic' suite (red) cross-cut by steeply N-E trending 'tholeiites' (blue), which are Palaeoproterozoic amphibolites and cut by late-kinematic felsic pegmatites (yellow). Each sample needs to be prefixed by GGU56343- for a full GEUS sample number.*

8 Palaeoproterozoic supracrustal rocks

Jochen Kolb, Leon Bagas, Vincent van Hinsberg & Nanna Rosing-Schow

Palaeoproterozoic supracrustal rocks have been summarized as Síportôq Supracrustal Association (Kalsbeek 1989) until field work and literature review recognized more geologically and geochronologically different units (Kolb 2014). The lithostratigraphy of the Palaeoproterozoic supracrustal rocks has not been investigated in detail in the SEGMENT project and only a brief description of the different units from south to north is given here.

Between Jens Munk Ø and Isortoq poorly investigated, probably Palaeoproterozoic rocks consist of mylonites interpreted as meta-greywacke overlain by different meta-sedimentary rocks and amphibolites. The rocks are metamorphosed in the greenschist to lower amphibolite facies and are thrust sheets on top of or interleaved with Archaean orthogneiss.

The < 1910 Ma Kap Tycho Brahe unit of meta-sedimentary rocks and amphibolite forms doubly folded belts in the Isertoq Terrane (Kolb 2014). The lithostratigraphic sequence consists of three lower amphibolite horizons that are separated by ultramafic and calc-silicate rocks including possible marble (Wright *et al.* 1973) and migmatitic paragneiss. Polymict, pyroclastic breccia contains 0.3 to 1 m wide meta-sedimentary, meta-gabbro and amphibolite fragments in a plagioclase-hornblende matrix (Hall *et al.* 1989a). Ultramafic rocks consist of olivine, tremolite, amphibole, anthophyllite, chlorite and talc, with locally large (up to 2 cm diameter) orthopyroxene porphyroblasts. These ultramafic rocks dominantly occur as boudins and represent sills or dykes. The amphibolite and meta-gabbro contain hornblende, plagioclase, garnet and, locally, corundum, kyanite and tremolite (Hall *et al.* 1989a). These rocks are overlain by quartzite and quartz-mica gneiss with small feldspar augen and locally preserved cross-bedding, containing garnet, kyanite, sillimanite and graphite in places (Hall *et al.* 1989a, Wright *et al.* 1973). Locally, thin < 0.5 m thick amphibolite dykes crosscut the meta-sedimentary rocks (Wright *et al.* 1973). The metamorphic mineral assemblage of the quartz-mica gneiss is indicative of amphibolite facies conditions in the temperature range of 500-700°C and pressures of 4-8 kbar.

Paragneiss, quartzite and biotite schist of the Kuummiut unit are the dominant Palaeoproterozoic, < 2200-2100 Ma rocks north of Tasiilaq and east of Sermilik (Kolb 2014), which consist of quartz, biotite, feldspar, and variable amounts of muscovite, garnet, kyanite, sillimanite and graphite (Hall *et al.* 1989a). Aluminous horizons dominated by up to cm-sized garnet and kyanite are locally developped (e.g. north of Johan Petersen Fjord). The metamorphic mineral assemblage is characteristic of upper-amphibolite facies conditions. Narrow layers of grey graphitic marble and associated calc-silicate rocks, and grunerite-gneiss are locally present (Hall *et al.* 1989a). Amphibolite, containing plagioclase, hornblende, biotite, garnet and minor quartz, forms 0.3 to 100 m thick horizons parallel with the lithological layering in the meta-sedimentary rocks (Hall *et al.* 1989a).

The Helheim unit to the north and west of Sermilik, and exposed on a series of nunataks north of Fenrisglacier, is characterised by meta-diorite, amphibolite, marble, calc-silicate rocks, quartzite, kyanite/sillimanite-garnet schist, ultramafic rocks and garnet-biotite gneiss in several doubly folded belts (Hall *et al.* 1989a, Kolb 2014). The meta-sedimentary rocks

consist of quartz, biotite, garnet, kyanite, sillimanite and locally graphite, and the meta-diorite and amphibolite contain hornblende, plagioclase, quartz and garnet (Hall *et al.* 1989a). The metamorphic conditions were estimated at ~ 640°C and ~ 5.3 kbar (Baden 2016). Kyanite appears to be the characteristic regional alumino-silicate phase, with sillimanite replacing it where thermal gradients were locally elevated, mainly in proximity to intrusions.

9 Palaeoproterozoic intrusions

Thomas Find Kokfelt, Kristine Thrane, Anne Brandt Johannesen, Trygvi Bech Árting, Sam Weatherley, Jakob Kløve Keiding, Jochen Kolb, Vincent van Hinsberg & Tomas Næraa

9.1 The Ammassalik Intrusive Complex

The Ammassalik Intrusive Complex (AIC) consists of three ovoid, *c.* 20 km long and 10-15 km wide, mafic to felsic intrusions. From west to eat the intrusions are named Johan Petersen (formally the Hobbs) Intrusive Centre, Tasiilaq (formally the Ammassalik) Intrusive Centre and Kulusuk Intrusive Centre. The intrusions are surrounded by banded biotite-garnet gneiss. The elliptical bodies are arranged *en echelon* about 35 km apart with a WNW-ESE trending axis (Kolb 2014). Conjugate sets of near-vertical dykes between the intrusions trend predominantly NW-SE and N-S (Friend and Nutman 1989). The intrusive centres exhibit a near-vertical, SE-trending magmatic foliation that becomes stronger towards contacts (Friend and Nutman 1989, Kolb 2014).

The igneous rocks consist predominantly of medium- to coarse-grained diorite, norite and melanogabbro along with minor lenses of pyroxenite and subordinate orthopyroxene-bearing granite (Andersen *et al.* 1989, Friend and Nutman 1989, Wright *et al.* 1973). The cores of the intrusions are usually homogeneous, medium- to coarse-grained diorite generally without wall rock xenoliths. Towards the outer rims, the intrusions become progressively more heterogeneous with increasing amount of autoliths and xenoliths. Magma mixing and mingling resulted in a variety of heterogeneous intermediate rocks.

Thin vertical mafic dykes cut both mafic and felsic intrusive rocks and are themselves cut by three generations of pegmatite dykes (Wright *et al.* 1973). The two early sets of pegmatite are orthopyroxene-bearing and the later set is biotite-bearing. They are separated by thin orthopyroxenite dykes (Wright *et al.* 1973).

Up to 1 km thick sheets of well-foliated Kfs-phyric monzogranite with local orthopyroxene occurs on Kulusuk Island and at the southern margin of the Tasiilaq intrusion (Andersen *et al.* 1989, Friend and Nutman 1989, Wright *et al.* 1973). Zoned, pink Kfs-pegmatite is the youngest igneous rock, and is common near the margins (Wright *et al.* 1973).

The magma temperature of the AIC was estimated at approx. 1100°C (Andersen *et al.* 1989). Thermobaromety on diorite yields temperatures of 830-850°C and pressures of *c.* 7.5 kbar (Friend and Nutman 1989). Fluid inclusion microthermometry yields pressures of 6-8 kbar and retrograde overprint at 550°C and 2-3 kbar (Andersen *et al.* 1989).

9.1.1 The Johan Petersen Intrusive Centre

The Johan Petersen (formally Hoobs) Intrusive Centre consists of younger gabbronorite, leucogabbronorite and Qtz-gabbro, which cut diorite, tonalite, granodiorite and granite (Fig. 9.1). A large mingling zone divides the two groups of igneous rocks, with minor mingling

zones being ubiquitous. The mingling zones are typically parallel to the penetrative regional foliation trend. Diorite and granodiorite are greenish to lighter greyish-white containing orthopyroxene, clinopyroxene, plagioclase, quartz, biotite, hornblende, magnetite and K-feldspar. Granodiorite is richer in quartz, K-feldspar and biotite. Orthopyroxene is replaced by hornblende and biotite. Coarse-grained grey Hbl-gabbro, gabbro, gabbronorite, minor dark grey to black melanogabbronorite and pyroxenite, and local light grey Qtz-microgabbro are characterised by mingling zones separating gabbro and gabbronorite. The rocks mainly consist of orthopyroxene, clinopyroxene, hornblende, biotite, plagioclase and variable amounts of quartz. Fine-grained gabbro dykes and anastomosing pyroxenite to melanogabbro and -norite stringers cross cut the igneous rocks. Kfs-phyric monzogranite is the youngest intrusion and mingled with the mafic-ultramafic stringers in the centre of the intrusion. It consists generally of K-feldspar, quartz, plagioclase, biotite and hornblende.

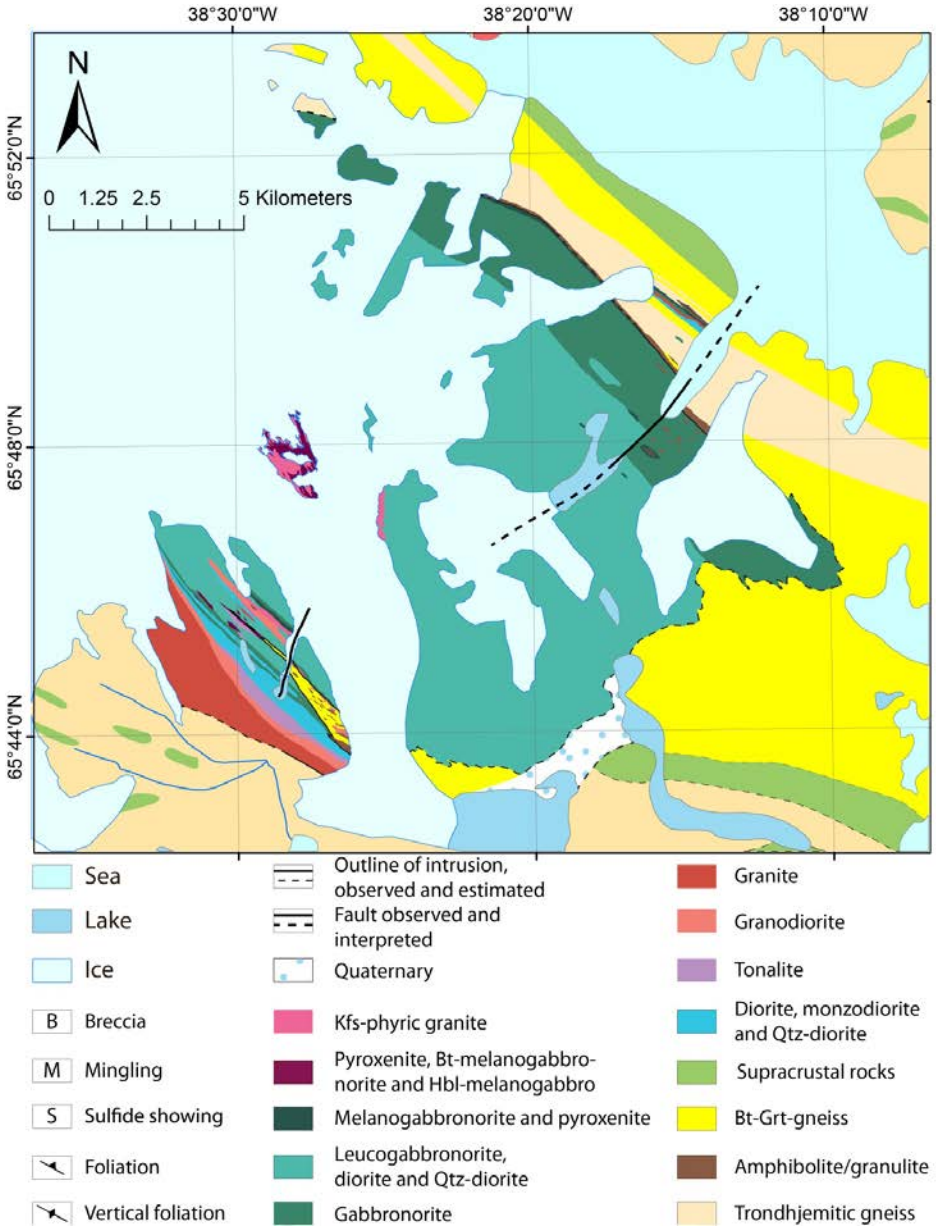

Figure 9.1 *New detailed map of the Johan Petersen Intrusive Centre based on new mapping in 2014. The centre was previously referred to as the Hobbs centre.*

9.1.2 The Tasiilaq Intrusive Centre

The Tasiilaq (Ammassalik) Intrusive Centre was first mapped out by a group from University of Birmingham in the late 1960's and early 1970's. Further investigations were conducted by GGU in the 1980's, resulting in a revised map of the intrusion that also provided the basis for the compiled 1:500 000 map sheet of Escher (1990). The Tasiilaq Intrusive Centre comprises mainly leucocratic gabbronorite that cross-cuts a less abundant melanocratic gabbro. These gabbroic rocks form in places distinct mingling zones, suggesting that these magmas were intruded close in time and coexisted in a semi-liquid state (Fig. 9.2 and Fig. 9.3A). The gabbroic rocks are at places cut by late veins and dykes of anorthosite and leucocratic pegmatites, as well as orthopyroxene veins (Fig. 9.3A). The intrusion was emplaced into wall rock consisting of quartzofeldspathic garnet gneiss, which has granulite facies assemblages close to the contact, and has been mobilized and mixed with the intrusive rock. The intrusion was dated to 1886 ± 2 Ma by zircon U-Pb TIMS dating, an age interpreted to represent the intrusion age of the complex (Hansen and Kalsbeek 1989). This age was later confirmed by Nutman *et al.* (2008b), but with a relatively large analytical error.

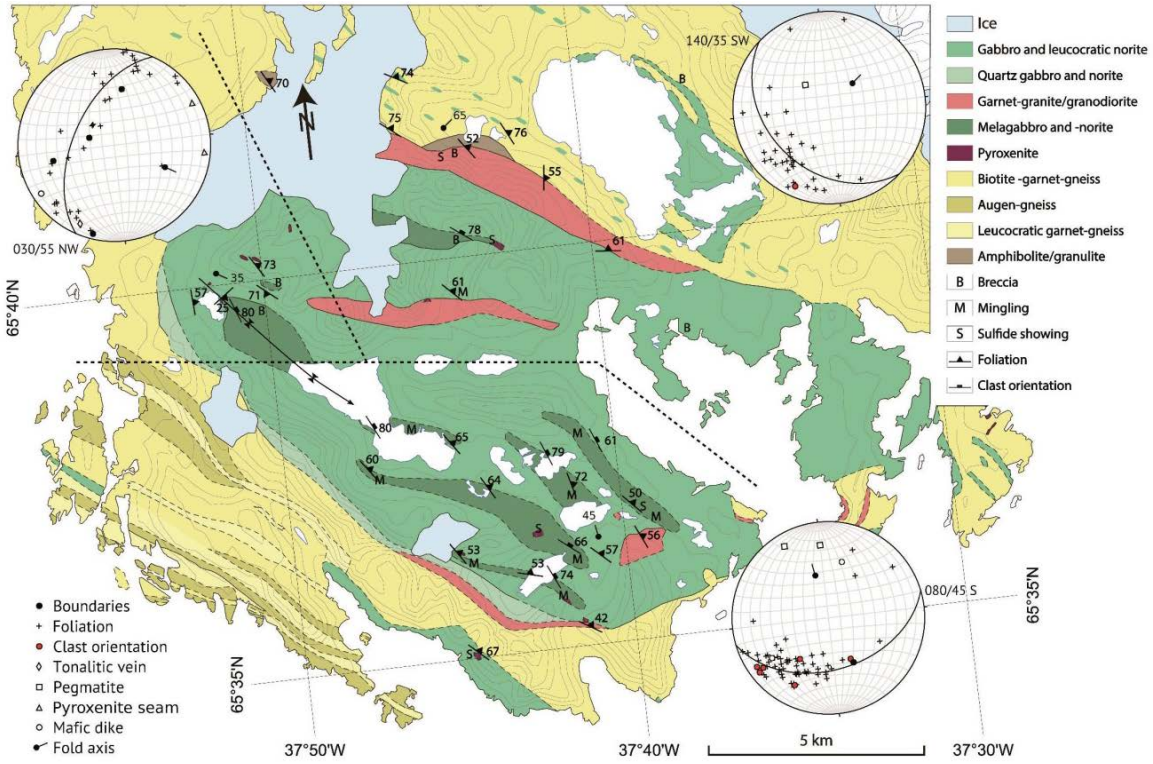

Figure 9.2 *New detailed map of the Tasiilaq Intrusive Centre based on mapping carried out within the SEGMENT project in 2014. Note that mingling zones are marked by "M" on the map. A summary of the structural measurements is shown for three different sectors of the intrusion plotting poles to planes (Árting 2016). The centre was previously referred to as the Ammassalik centre.*

During the SEGMENT project, the Tasiilaq Intrusive Centre was studied over a period of six weeks from eight different field camps placed in the central and western part of the intrusion. The work is summarised in a MSc thesis that was defended at University of Copen-

hagen in May 2016 (Árting 2016). The thesis work includes a revised version of the existing geological map (Fig. 9.2), a description of this map, as well as new whole rock geochemical data for *c.* 70 samples and new zircon U-Pb ages by SHRIMP on six samples from the intrusion.

One of the main conclusions of the work of Árting (2016) regards the temporal evolution of the intrusion, addressed through the new U-Pb zircon age dates. These new ages expand the known range for active magmatism in the centre to nearly 50 million years, from 1911 ± 6 Ma to 1864 ± 9 Ma. A systematic spatial distribution of the ages were found as the gabbroic rocks in the northern part of the intrusion are older than in the southern part, suggesting that magmatism probably migrated southwards over this time period (Árting 2016).

Another result of the thesis work is a detailed petrogenetic model that is based on the distribution of rare earth elements in the most primitive rocks of the Tasiilaq Intrusive Centre. This model indicates that it is possible to account for the signatures in the near primary Tasiilaq magmas by mixing 20% melt of a basaltic oceanic plate with depleted mantle, and then melting this mixture to an amount of *c.* 20% within the spinel lherzolite field. In general terms, the conclusion of the geochemical modelling was that a metasomatized mantle source region is required to explain the Tasiilaq magmas. This is found to be consistent with the idea of ongoing subduction of oceanic plate leading up to the time of continent-continent collision that formed the Nagssugtoqidian orogenic belt.

9.1.3 The Kulusuk Intrusive Centre

The Kulusuk Intrusive Centre was studied on Kulusuk Island proper during one week of field work in August 2015, and prior to this, in 2012 (while waiting for transport to Skjoldungen) for half a day. The 2015 fieldwork was planned as a framework for a petrological and geochemical student project, for which reason the student took part in the fieldwork. The student project officially starts in September 2016 and is planned as a MSc thesis at the University of Copenhagen and to be terminated in the summer 2017. The principal aims of the fieldwork and the MSc project were to reinvestigate the lithological variation occurring on Kulusuk Island by comparing with previous detailed mapping by the University of Birmingham group (see above), and to carry out sampling for further analytical work. The main focus for the sampling was on the gabbroic rocks of the intrusive centre, but also the host gneisses were studied, including the contact zone where wall rock interaction processes were studied. The potential for mineralisation of Ni sulphides is well known within the AIC (see Chapter 16), and due attention was paid the search for areas favorable for sulphide mineralisation.

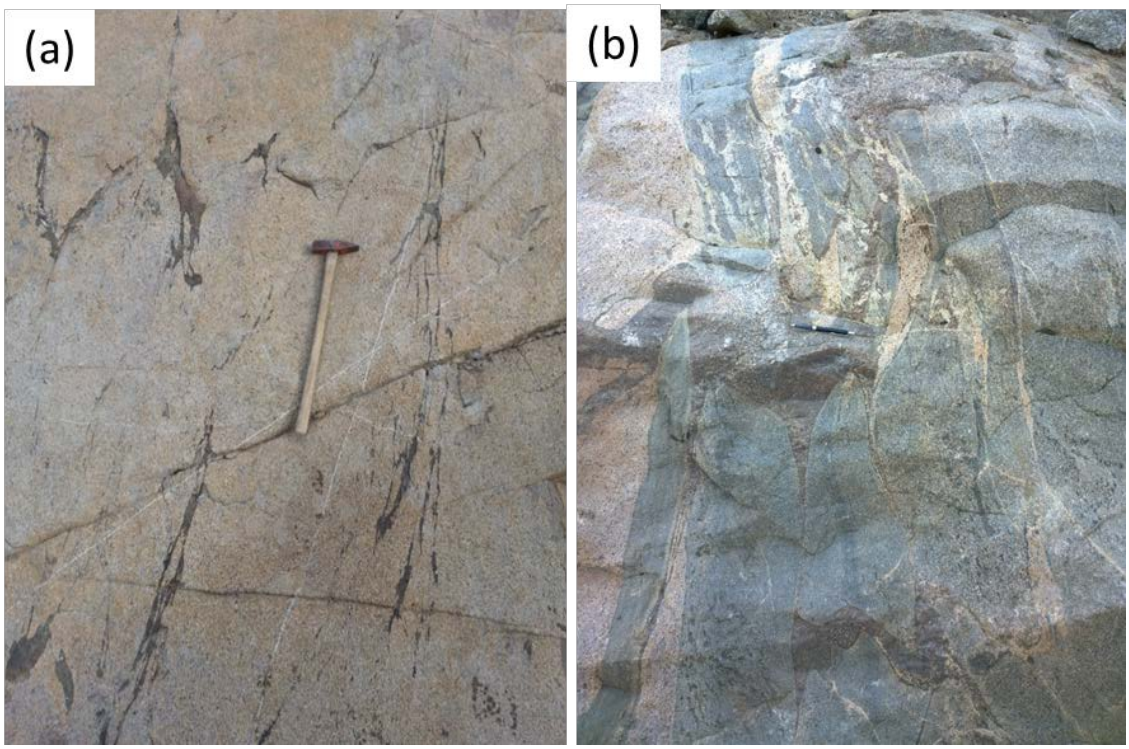

Figure 9.3 ***A.*** *Mesocratic gabbronorite cut by stringers of orthopyroxenite (locality 14TBA186).* ***B.*** *Mingling zone exposing mesocratic gabbronorite in contact to melanocratic gabbro, and with dark brown pyroxenite veins placed along the cuspate boundaries (locality 14TBA256).*

Thirty-one samples were collected from Kulusuk Island (Fig. 9.4), sectioned and analysed for major and trace elements. The MSc thesis work will providepetrographic descriptions and interpretations and whole rock geochemical study as basis for petrogenetic modelling and comparison to the neighbouring Tasiilaq Intrusive centre (Árting 2016). Representative rock types of the Kulusuk Intrusive Centre are illustrated in Fig. 9.5.

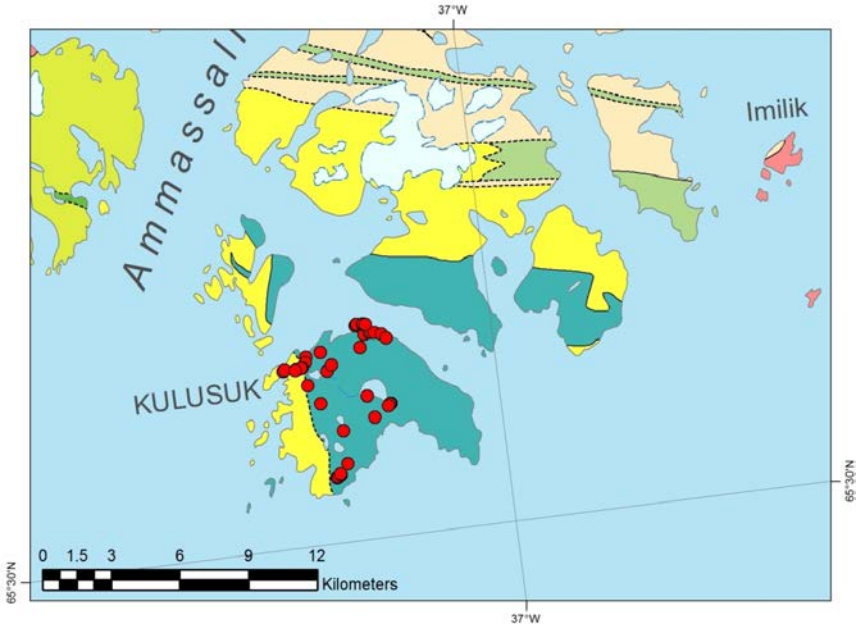

Figure 9.4 *Sample map of the Kulusuk Centre on Kulusuk Island, with sampling locations indicated by red circles.*

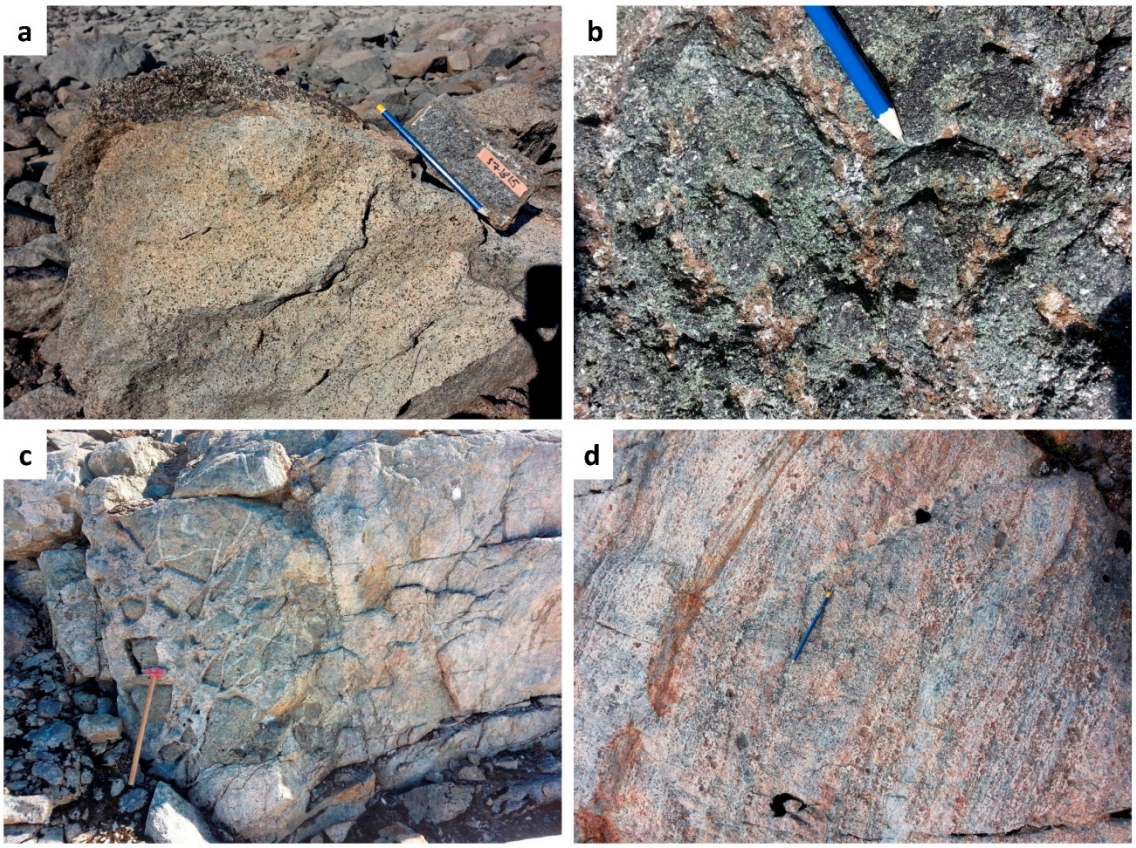

Figure 9.5 *Examples of rock types and contact relations at the Kulusuk Intrusive Centre, Kulusuk Island.* ***A.*** *Leucocratic gabbronorites.* ***B.*** *Phlogopite-bearing poikilitic pyroxenite.* ***C.*** *Intrusive breccia of leucocratic gabbronorite intruding melanocratic gabbronorites.* ***D.*** *Garnet-bearing gneiss wall rock at contact zone.*

9.2 The Ammassalik Batholith

The Ammassalik Batholith is situated 10-40 km north of Tasiilaq town, where it occupies the northern part of Ammassalik Ø and the region immediately north of Ikaasartivaq Fjord (Fig. 9.6). The fjord dissects the central part of the batholith in a NW-SE direction And provide a phenomenal cross section of the batholith. The batholith measures roughly 32 x 25 km in outer dimensions and is dominated by granitic and dioritic rocks. Granitic rocks dominate the western and southernmost parts. A separate granite intrusion, the Aria granite, is identified at the western end of the Ikaasartivaq Fjord (65°54'N, 37°38'W) and was previously prospected for as ornamental stone, but has remained unexploited. Smaller units of gabbroic to dioritic rock are also present, particularly in the eastern part of the batholith where the Tasilartik gabbro has been mapped out as a separate unit measuring ~6 x 3 km in outcrop. The central part of the batholith is constituted by mafic (dioritic) sills and sheets intruded into, or interfingering with, felsic (granitic or granodioritic) lithologies, as can be observed in the upper reaches of the fjord walls.

Previous investigations of the Tasiilaq area included detailed mapping of the Ammassalik Batholith by the University of Birmingham group from 1967 to 1970. Wright *et al.* (1973) describe the intrusive complex as a late- to post- orogenic calc-alkaline suite. They note sharp contacts, widespread evidence of stooping and negligible contact or retrograde metamorphism and consequentially suggest the batholith was intruded at a relatively high crustal level. The geological complexity found within the intrusive complex by the Birmingham group was not transferred onto the official 1:500 000 scale map of Escher (1990) that only included intermediate to felsic (diorite, granodiorites and granites) and gabbroic rock types.

The batholith was dated to 1680 -8/+10 Ma by (Kalsbeek *et al.* 1993) and the more recent zircon U-Pb ages on granites and diorites confirm this age, but also indicate the existence of younger ages within the intrusive complex down to *c.* 1550 Ma in the latest granites (see Chapter 10). This age span places the intrusive complex some 200-350 million years after the Ammassalik Intrusive Complex and confirms it to be of postorogenic nature, and unrelated to the earlier intrusions in the area.

The recent fieldwork in the area confirmed the complexity of the batholith as it was originally depicted on the field maps from the Birmingham group. The complex is composed of multiple intrusions of mainly granite and diorite, in addition to previously recorded gabbroic and ultramafic rock units. The batholith contains widespread examples of magmatic mingling relations indicating the co-existence of magmas of contrasting composition and properties (Fig. 9.7). A detailed account of the field relations found within the Ammassalik Batholith was reported by Kokfelt *et al.* (2015a).

9.3 Johan Petersen Fjord Granite

Granites were studied at the Johan Petersen fjord on the western side of Sermilik (Fig. 9.6). The granite here defines a separate body ~6 km in diameter intruded into the gneiss basement that contains supracrustal rocks. The intrusion is unnamed in the GMOM database at GEUS, but was referred to as Johan Petersen Fjord Granite in the field report (Kokfelt *et al.*

2015a). The precise relationship of the granite with the Ammassalik Batholith is unclear as the granite remains undated (note: two samples processed for U-Pb dating failed to produce an age due to massive common Pb in the separated zircons). However, it is considered likely to be part of the Ammassalik Batholith, constituting a satellite intrusion. The intrusion is dominated by pinkish granite, composed of alkali feldspar, quartz, plagioclase and minor mafic minerals of biotite and/or hornblende. The granite is homogeneous and is lacking enclaves commonly observed elsewhere in the Ammassalik Batholith (Kokfelt *et al.* 2015a).

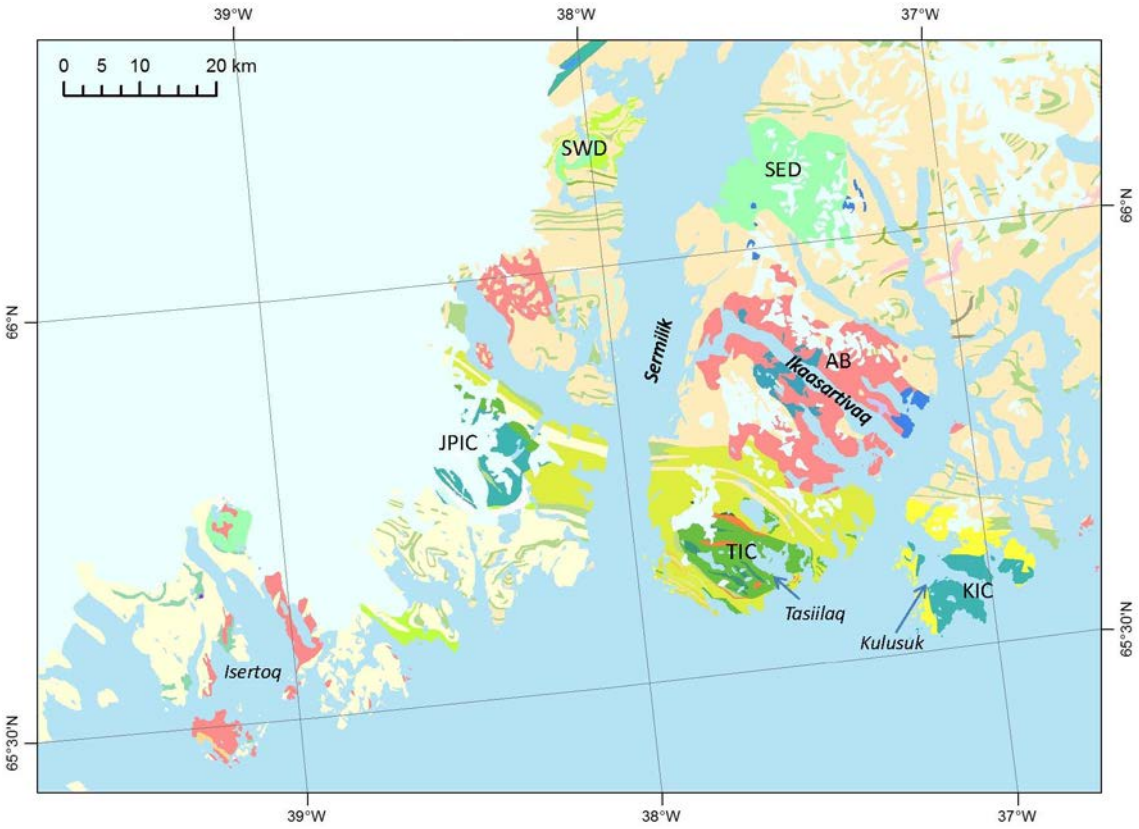

Figure 9.6 *The geological map of the Tasiilaq area as from the 1:500 000 scale map. The* c. *1.68 Ga Ammassalik batholith is situated between the Sermilik and the Ammassalik Fjords north of the 1.89 Ga Ammassalik Intrusive Complex. The Ammassalik batholith has a roughly rounded outline and is constituted by granite, granodiorite and diorite with minor gabbroic and ultramafic rocks. The Johan Petersen Fjord granite, west of Sermilik, resembles the granites from the Ammassalik batholith and is presumed to be related to this.*

9.4 The Sermilik East Diorite (Imersivaq Intrusion)

The Sermilik East Diorite intrusion (10 x 10 km) is exposed on the eastern shore of the Sermilik Fjord centred ~ 20 km north of the northernmost part of Ammassalik Batholith (Fig. 9.6). The official name from the GMOM database is the 'Sermilik East Diorite' but for simplicity is referred to as the Imersivaq Intrusion named after a lake a little southeast of the intrusion. The intrusion received relative little attention and remains poorly studied. Previous reconnaissance work suggested that the intrusion was emplaced early in the Proterozoic evolution of the Tasiilaq region (cf. Chadwick and Vasudev 1989), in possible agree-

ment with a Sm-Nd model age of 2200 Ma by Kalsbeek *et al.* (1993). The outline of the intrusion coincides broadly with (though slightly displaced from) a large prominent positive magnetic anomaly (Fig. 9.8), suggesting that the Imersivaq Intrusion probably extends at depth.

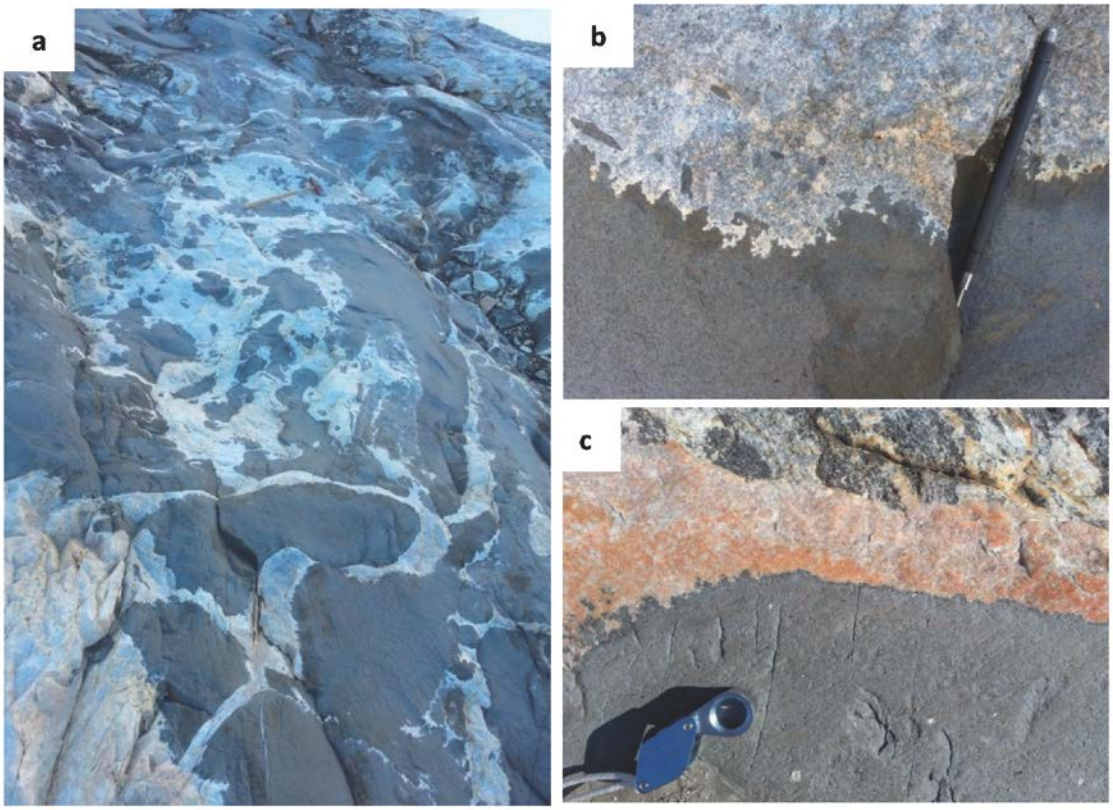

Figure 9.7 *Spectacular examples of magma mingling in a 2-5 m wide dyke in the Ikaasartivaq Fjord area.* ***A.*** *Along strike view of dyke with mafic (dioritic) and felsic (granitic) magmas mingling at various scales.* ***B.*** *and* ***C.*** *Examples of crenulated interfaces between mafic and felsic melts (rocks). See also Kokfelt* et al. *2015a.*

The new fieldwork related to this project (Kokfelt *et al.* 2015a, Kokfelt *et al.* 2015b) clearly documents that the rocks of the intrusion expose pristine magmatic textures, including a diorite-granodiorite-granite association very similar to that found in the Ammassalik Batholith. Several examples of mafic-felsic magma mingling complexes have been observed within the intrusion (Fig. 9.9), which in essence is similar to those found within the Ammassalik Baholith.

A further, and robust argument for a genetic link between Imersivaq and the Ammassalik Batholith, comes from a recent U-Pb zircon age of a diorite sample from the Imersivaq Intrusion giving an age of 1670 ± 5 Ma, thus agreeing closely with the age of the Ammassalik Batholith (see Chapter 10). It is therefore concluded that the Imersivaq Intrusion represents a northern satellite centre of the Ammassalik Batholith, thus expanding the size of the batholith considerably compared to what was previously thought.

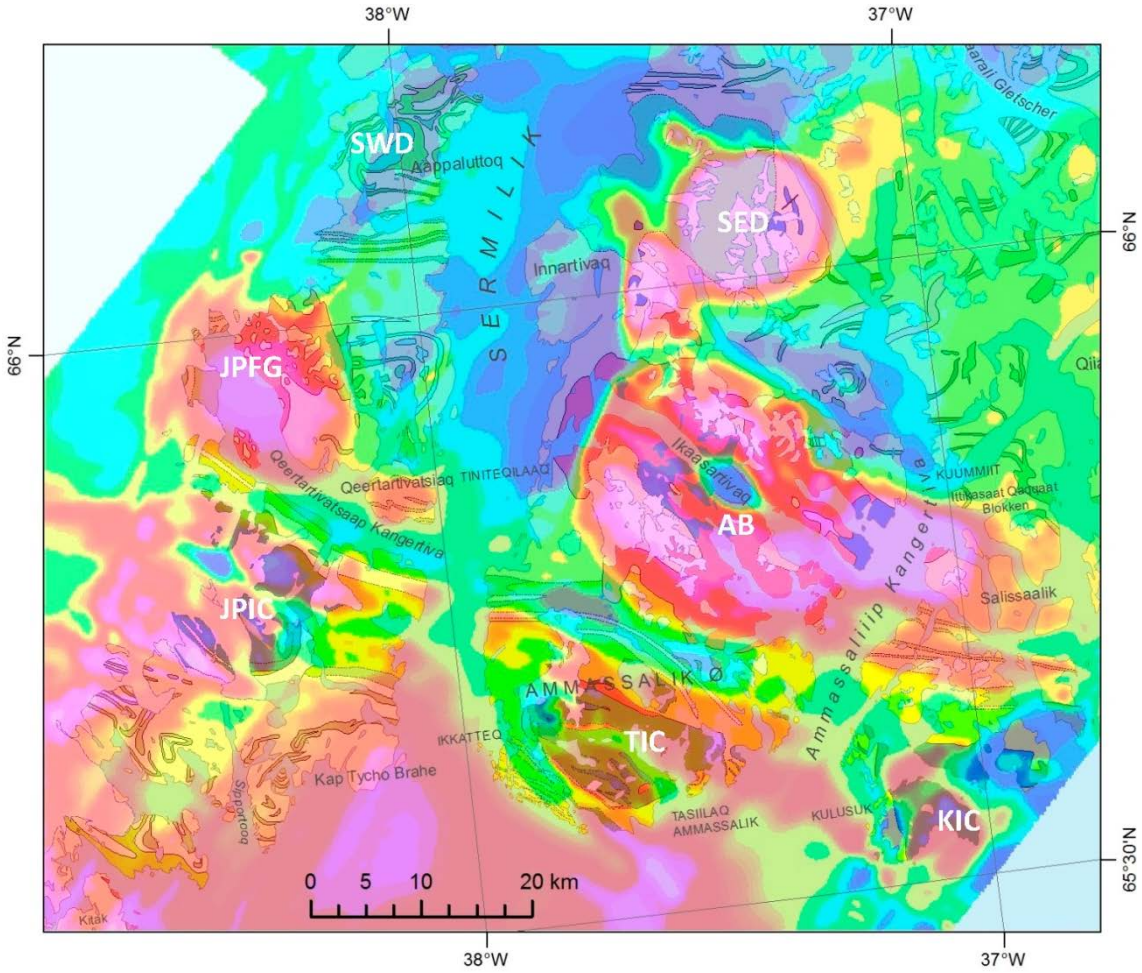

Figure 9.8 *Aeromagnetic data (flown in 2012-2013) overlain on top of the 1:500 000 scale geological map of the Tasiilaq region. The main Palaeoproterozoic intrusions in the area are labelled; JPIC = Johan Petersen Intrusive Centre, TIC = Tasiilaq Intrusive Centre, KIC = Kulusuk Intrusive Centre, AB = Ammassalik Batholith, JPFG = Johan Petersen Fjord Granite, SWD = Sermilik West Diorite, SED = Sermilik East Diorite. Several of the intrusions are characterised by magnetic anomalies, with clear bulls-eye patterns for Sermilik East Diorite (note some displacement relative to the geological boundary occurs), the Ammassalik Batholith and Johan Petersen Fjord Granite.*

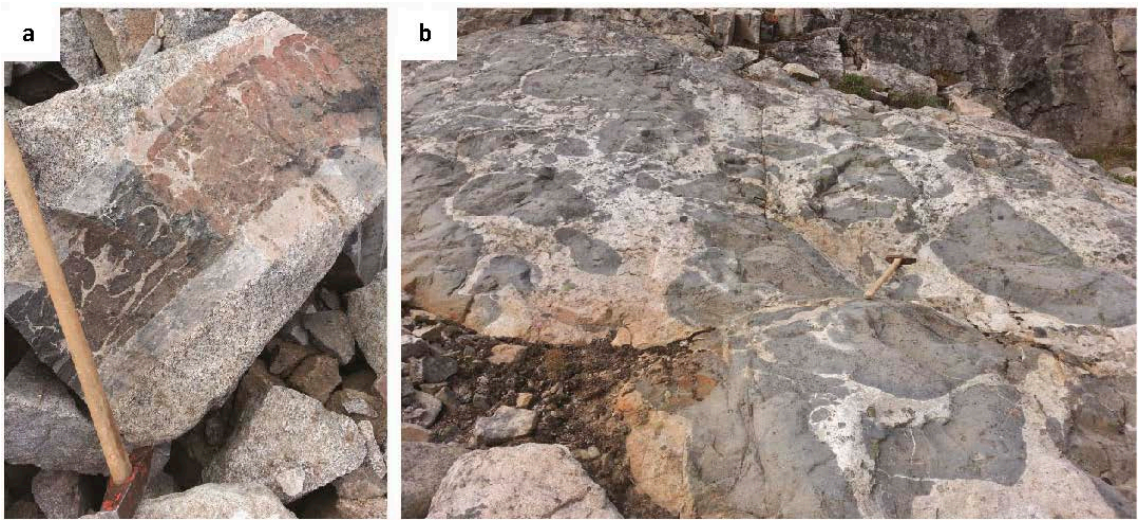

Figure 9.9 ***A.*** *Composite dyke in diorite consisting of an outer felsic member and an inner mafic-felsic mingled member locally having flow textures.* ***B.*** *Mafic-felsic pillow complex from the Imersivaq Intrusion showing mafic diorites in a felsic matrix.*

9.5 The Sermilik West Diorite

On the west side of Sermilik, a smaller body of meta-diorite and meta-tonalite intruded the Archaean basement (Fig. 9.6). The intrusion is poorly studied and the boundaries to the surrounding basement are not well defined. The basement at the southwestern contact consists of orthogneiss and a meta-sedimentary package that includes calc-silicate rocks and garnet-kyanite gneiss. The diorite has a well-developed gneissic banding defined by lenses of quartz and plagioclase in a matrix of amphibole, garnet and minor biotite, and is locally intruded by tonalite. It was previously believed that it was of similar age and origin as the Imersivaq intrusion, however, a sample of meta-tonalite was dated by U-Pb zircon to be 1901 ± 9 Ma by Nutman *et al.* (2008b), interpreted as the crystallization age. Few grains with lower Th/U ratios from the same sample yield an age of 1840 ± 56 Ma indicating that the zircons in the rock were recrystallized during a later high-grade metamorphic event. The results indicate that Sermilik West Diorite represents the early part of the orogeny and is contemporaneous with the Ammassalik Intrusive Complex.

9.6 Isortoq granites and diorites

The area surrounding Isortoq is dominated by a large domain of only slightly deformed granite (Fig. 9.6). To the east of this massive granite, the area shows large-scale net-veining crosscutting the basement (Fig. 9.10). In the northern part of the area towards the ice cap, the granite forms a dome-structure, which underlies and intruded into older diorite. Both, the diorite and the granite are largely undeformed, although local shear zones, post-dating emplacement, are present. Roof pendants of basement are common in the granite and the diorite and these locally develop reaction rims dominated by biotite. The basement

is composed of orthogneiss, amphibolite and calc-silicate rocks locally enclosing boudins of serpentinized ultramafic rocks, and is part of the Kap Tycho Brahe unit.

Mingling textures involving different dioritic compositions show the coexistence of several magma pulses. The differences are mainly shown by grain-size distribution with only minimal compositional differences between the different types of diorites. The granite also varies in appearance in different parts of the complex, having an equi-granular texture almost devoid of ferromagnesian minerals in exposures close to its southern contact, versus mm-sized phenocrysts of pink K-feldspar in a fine-grained matrix in the complex' interior. Unfortunately no direct contacts between granite types were observed in the field. Cross-cutting field-relations clearly demonstrate that the granite is younger than the diorite, as opposed to the Ammassalik Batholith where the field-relations suggest melts to be contemporaneous. Later pegmatites crosscut both the granite and the diorite.

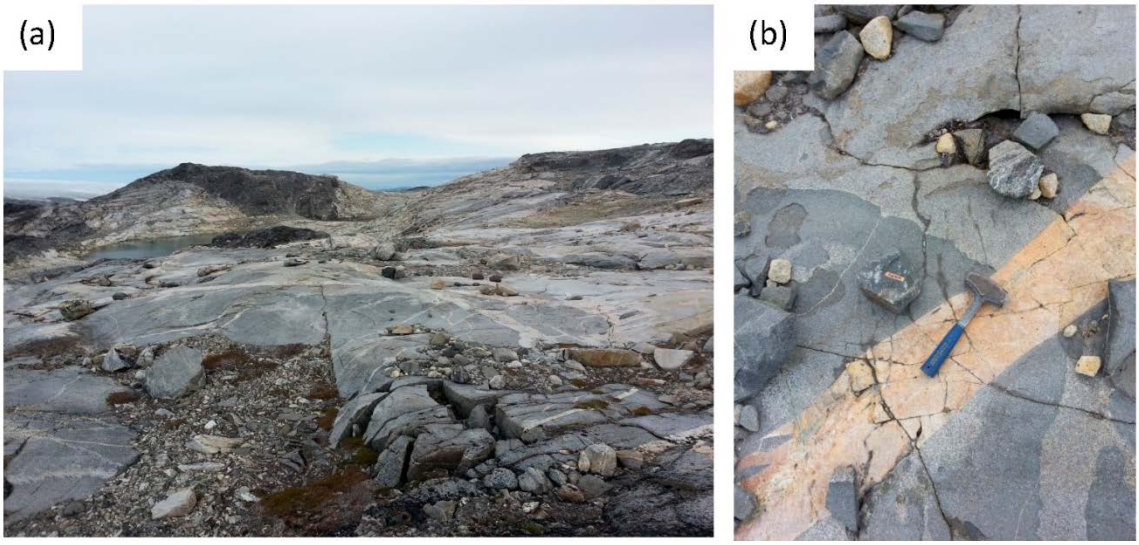

Figure 9.10 ***A.*** *Granite intruded the diorite as veins in the foreground. In the background the large granite dome is sitting underneath the dark diorite.* ***B.*** *Two phases of diorite mingled and are intruded by granite vein.*

10 Geochronology of Palaeoproterozoic rocks

Kristine Thrane, Thomas F. Kokfelt, Tomas Næraa, Trygvi B. Árting & Erwann Lebrun

Zircons from 45 samples of Palaeoproterozoic gneisses, granites, diorites, gabbros and leucocratic pegmatites were analysed during this part of the SEGMENT project. The results are presented in a separate report by Kokfelt *et al.* (2016b), and in a MSc thesis by Árting (2016) that was defended at the University of Copenhagen in May 2016. A summary of the obtained ages is shown in Fig. 10.1 and given below.

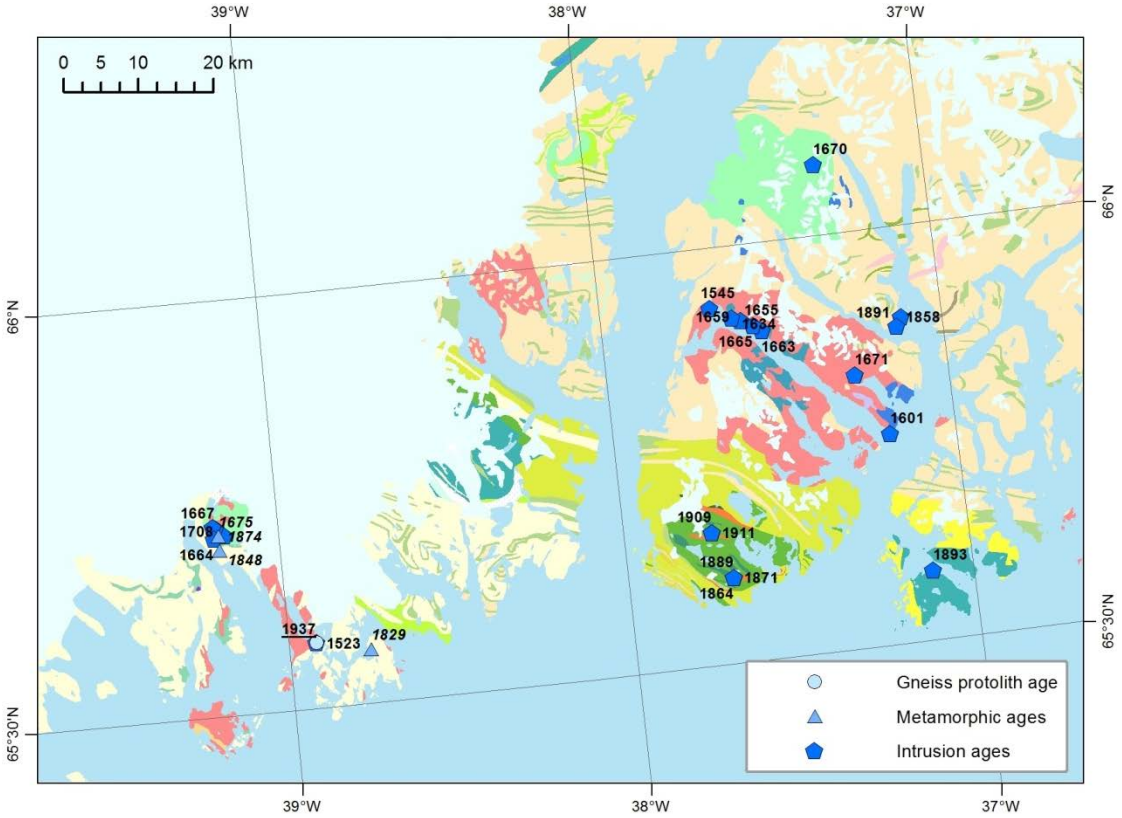

Figure 10.1 *Geological map of the Tasiilaq region showing the location of the Palaeoproterozoic samples yielding ages for the gneiss protoliths (labels bold, underlined), metamorphism (bold, italic), and intrusions (bold).*

10.1 Analytical methods

The majority of the analyses were acquired by the laser ablation system coupled to a Thermo Finnigan Element2 single collector-magnetic sector field-inductively coupled plasma-mass spectrometer (LA-SF-ISP-MS) at the Department of Petrology and Economic Geology, Geological Survey of Denmark and Greenland (GEUS), Denmark. In addition, several samples were analysed by the Sensitive High Resolution Ion Microprobe II (SHRIMP II) at the John de Laeter Centre of Isotope Research (JDLC), Curtin Technical University, Perth, Western Australia. For details see the references listed above.

10.2 Gneisses

Based on previous studies and earlier work of this project, the orthogneiss basement of the region from 62°N to 67°N was thought to be exclusively of Archaean age. Therefore, it was surprising to find a grey, banded orthogneiss (sample 525259) in the Isortoq area that is Palaeoproterozoic, yielding an age of 1937 ± 7 Ma. The sample has several inherited Archaean zircons, but the vast majority of the ages fall in a relatively tight cluster around this relatively young age. This age has not been recorded in this area previously, and its significance is unclear.

A garnet-bearing gneiss (sample 525231), assumed to be paragneiss, was sampled on the west side of the Angmagsalik Fjord. This sample also contains a relatively tight cluster of ages with a weighted mean average of 1891 ± 7 Ma. Although it is uncommon to obtain such a tight cluster of zircon ages for a supracrustal rock, there are several possible sources with comparable ages nearby, namely the Ammassalik Intrusive Complex and the meta-tonalite West of Sermilik (Árting 2016, Hansen and Kalsbeek 1989, Nutman *et al.* 2008b).

Other paragneisses were also analysed, of which two samples have a mineralogy and a general appearance that leaves little doubt as to their sedimentary origin. One sample (525260) from the belt north of Kitak has a detrital age pattern dominated by a large 2050-1900 Ma peak and a significant peak at 2150 Ma. The Archaean population is minor and the oldest grain is *c.* 2850 Ma. This meta-sedimentary rock is interpreted to be Palaeoproterozoic, deposited and deformed during the Nagssugtoqidian Orogeny.

The Blokken meta-sedimentary rock (525252) containing both garnet and sillimanite, yields a very different age pattern than the previous sample. It has two distinct peaks with one Archaean peak dominated by 2800-2650 Ma ages and one peak dominated by *c.* 1900 Ma ages. Two analyses yield ages of *c.* 1680-1660 Ma. This meta-sedimentary rock is also interpreted as Palaeoproterozoic, and likewise deposited and deformed during the Nagssugtoqidian Orogeny after the intrusion of the Ammassalik Intrusive Complex. The 1680-1660 Ma ages are believed to reflect the later events related to the emplacement of large diorite and granite intrusions related to the Ammassalik Batholith, which may have heated and metamorphosed the surrounding basement rocks. The Ammassalik Batholith is in Fig. 9.8 suggested to underlie at least part of the Blokken area.

Palaeoproterozoic metamorphic ages are obtained from several of the Archaean orthogneisses, especially in the Isortoq area. The ages range from 1874-1829 Ma and correspond to deformation and collision event following the Ammassalik Intrusive Complex.

10.3 Pegmatites

There are no records of Palaeoproterozoic pegmatites south of 65°30'N and only a few pegmatites from areas further N were dated. One pegmatite (sample 525229) that cross-cuts the paragneiss on the west side of Ammassalik Fjord yields an age of 1858 ± 7 Ma.

Another pegmatite cross cutting the Archaean orthogneiss collected within the Ammassalik batholith yields an age of 1663 ± 9 Ma, similar to the age to the batholith.

10.4 The Ammassalik Intrusive Complex (AIC)

The Ammassalik Intrusive Complex comprises three intrusions: The Kulusuk Intrusive Centre, the Tasiilaq (formerly Ammassalik) Intrusive Centre and the Johan Petersen Fjord (formerly Hobbs) Intrusive Centre. The Tasiilaq Intrusive Centre was previously dated at 1886 ± 2 Ma by zircon U-Pb TIMS dating (Hansen and Kalsbeek 1989). The age was interpreted to represent the intrusion age of the complex. New samples from the units of the centre increase the age span of the magmatism to 1911-1864 Ma, including the samples dated by T.B. Árting and presented in his MSc thesis (Árting 2016). A single sample was analyzed from the Kulusuk Intrusive Centre, yielding an age of 1893 ± 8 Ma, thus overlapping the age range found in the Tasiilaq Intrusive Centre. No samples from the Johan Petersen Fjord Intrusive Centre have been analyzed at the time of writing.

10.5 Ammassalik Batholith

The large Ammassalik Batholith north of the Ammassalik Intrusive Complex comprise granites, granodiorites, diorites, collectively shown as intermediate and felsic rocks and gabbros on the 1:500 000 map sheet of Escher (1990) . It would seem to be a rather uniform body, but is shown in early mapping campaigns composed of many intrusive units, therefor name ‘batholith’. The Ammassalik Batholith is composed of several different types of granitic, dioritic and gabbroic rocks that have intruded as plutons, plugs, sills and sheets, that often show mingling of magmas and so-called “pillowd dykes” (Kokfelt *et al.* 2015a, Kokfelt *et al.* 2015b, Chapter 9). The batholith was dated by Kalsbeek *et al.* (1993) to be 1680 -8/+10 Ma (U-Pb zircon).

Several samples of diorite and granite were collected and dated during this project. The diorites yield ages from 1671-1634 Ma and the granites yield ages from 1665-1659 Ma. The ages of the diorites and granites are overlapping, which is consistent with the field evidence for magma mingling and co-existence of more magma types. A felsic aplite that cuts across the contact between a pillowed dyke and the granitic host yields an age of 1601 ± 3 Ma, thus suggesting that the magmatism in the region extended for at least 70 million years.

A distinct granite body in the batholith, the Aria granite (Kalsbeek *et al.* 1993) is exposed around the northwest end of Ikaasartivaq Fjord. It was originally assumed to be part of the Ammassalik Batholith but new results yield an age of 1545 ± 15 Ma, showing that it is significantly younger than the main batholith or that it at least represents a very late pulse.

10.6 Isortoq

A large intrusion composed of both diorite and granite is exposed north of Isortoq (Fig. 10.1). It includes several types of the diorite, two of which are dated. A fine-grained diorite and a coarser-grained quartz-diorite yield ages of 1667 ± 4 Ma (sample 562902) and 1664 ± 4 Ma (sample 562910), respectively. These ages are contemporaneous with the ages of the diorites in the Ammassalik Batholith. The granite in the same area forms a large dome that is underlying and intruding the diorite. Several samples of the granite from this dome were collected and analysed but no reliable ages were obtained due to massive amounts of common Pb in zircon. The common Pb corrected ages are around 1700 Ma despite the fact that field observations dictate that the granite should be younger than the diorite, and the1700 Ma age is considered unreliable. The Isortoq, granite also outcrops south of the diorite-granite dome.. The granites form in this area a large net-veining structure intrusive into the Palaeoproterozoic gneiss of the region. A sample of this granite yielded an age of 1523 ± 12 Ma, an age rather similar to the Aria granite from the west corner of the Ammassalik Batholith. It is an open question whether the granite from the large dome structure is of the same age or older than the granites of the Ammassalik Batholith.

10.7 Sermilik East Diorite (Imersivaq)

Prior to this study, the only age reported for the diorite was a Sm-Nd model age yielding 2200 Ma (Kalsbeek *et al.* 1993). According to the printed 1:500 000 map sheet, the diorite is interpreted to be of similar age as the diorite intrusion on the west side of Sermilik, which has later been redefined as a meta-tonalite and dated by U-Pb zircon to be 1901 ± 9 Ma (Nutman *et al.* 2008b). During this study several attempts were made to date the diorite, but several samples did not yield any zircons. However, we finally succeeded and obtained an age of 1670 ± 5 Ma. The age demonstrates that the Sermilik East Diorite is contemporaneous with the Ammassalik Batholith rather than the meta-tonalite west of Sermilik. As a consequence of this finding, the Imersivaq Intrusion seems to define a separate northern satellite intrusion related to the Ammassalik Batholith, thereby expanding considerably the volume and area of the Ammassalik Batholith magmatism.

11 Palaeoproterozoic tectono-metamorphic evolution

Jochen Kolb, Annika Dziggel, Sascha Müller & Leon Bagas

The NAC and the EGA or Rae Craton have Palaeoproterozoic orogens at their margins, the Nagssugtoqidian Orogen in the north of the NAC in the Tasiilaq area, separating it from the EGA or Rae Craton and the Ketilidian Orogen in the south (Garde *et al.* 1999, Garde *et al.* 2002, Kolb 2014, Nutman *et al.* 2008a, Nutman *et al.* 2008b). The area between Timmiarmiut and Jens Munk Ø remained a relatively unaffected shield area of the NAC (Bridgwater *et al.* 1973, Bridgwater and Gormsen 1969, Kolb *et al.* 2013, Wright *et al.* 1973).

11.1 Palaeoproterozoic evolution of the NAC

The Thrym Complex between Timmiarmiut and Jens Munk Ø is intruded by various sets of dykes in the Palaeoproterozoic and cross cut by brittle faults of various geometry (Kolb *et al.* 2013). The dykes commonly have chilled margins, and the faults show ubiquitous development of pseudotachylites, indicating relatively cold conditions resulting from the near complete exhumation of the Thrym Complex in the NeoArchaean. Three Palaeoproterozoic mafic dyke swarms are distinguished: (1) *c.* 2135 Ma WSW-trending dykes (Umîvik dykes) (Bridgwater *et al.* 1990, Lassen *et al.* 2004); (2) *c.* 1750 Ma W-trending appinite dykes in the south; and (3) the *c.* 1630 Ma N-trending Melville Bugt Dyke Swarm. Pseudotachylite in NE-trending faults yields *c.* 2000 Ma Ar-Ar ages. On Ikermit Island and the mainland further to the west fine-grained greenschist facies greywacke with centimetre-scale fragments has a folded contact with the orthogneiss of the Thrym Complex. Detrital zircons yield NeoArchaean to MesoArchaean ages, indicating deposition in the Palaeoproterozoic. This data indicates that the NAC was variably overprinted in the Palaeoproterozoic, probably with initial rifting or extension at *c.* 2135-2000 Ma, followed by *c.* 1900-1750 Ma Palaeoproterozoic orogeny and again a late extensional stage.

11.2 The Nagssugtoqidian Orogen of South-East Greenland

Archaean and Palaeoproterozoic rocks of the Tasiilaq area were earlier interpreted as a long-lived (~ 700 million years) mobile belt (Bridgwater and Myers 1979, Chadwick *et al.* 1989, Myers 1984, 1987b). Modern geochronological techniques help advanc our understanding of the geological evolution and helped to correlate the orogen in South-East Greenland with orogens in central West and North-West Greenland, Canada and Scotland (Friend and Kinny 2001, Kalsbeek *et al.* 1993, Kolb 2014, Nutman *et al.* 2008b, St-Onge *et al.* 2009).

The oldest Palaeoproterozoic rocks are *c.* 2400 and 2050 Ma mafic dykes (Kalsbeek *et al.* 1993, Nutman *et al.* 2008b). They are followed by Palaeoproterozoic supracrustal rocks consisting of metamorphosed psammitic and semipelitic rocks, marl, carbonates and mafic rocks that structurally overlay Archaean orthogneiss, amphibolite and mafic granulite. These rock types characterise the Helheim unit in the north (Kolb 2014). The < *c.* 2200-

2100 Ma eastern Kuummiut unit is composed of metamorphosed psammitic and pelitic rocks, local carbonates, mafic sheets of probable basaltic composition and ultramafic lenses. The siliciclastic rocks have an Archaean provenance (Kalsbeek *et al.* 1993, Nutman *et al.* 2008b). An ultramafic layered intrusion in the Ivnartivaq Complex was emplaced at *c.* 1955 Ma and a tonalite intruded at *c.* 1900 Ma (Brooks and Stenstrop 1989, Nutman *et al.* 2008b). The sedimentation predates the AIC and tonalite emplacement (*c.* 1910-1880 Ma), but postdates the mafic dykes and the Ivnartivaq Complex. Intrusions and the siliciclastic and carbonate rocks may indicate passive continental margin setting and Palaeoproterozoic spreading (Kolb 2014).

The Kap Tycho Brahe supracrustals south of the AIC tectonically overlays Archaean rocks and consist of metamorphosed bimodal volcanic rocks with lenses of ultramafic rocks (Kolb 2014). These are covered by pelitic and psammitic siliciclastic rocks with a *c.* 1950-1910 Ma provenance (Kalsbeek *et al.* 1993, Nutman *et al.* 2008b), which compare to AIC (Kolb 2014). The meta-sedimentary rocks are interpreted as flysch deposits sourced from the erosion of a developing volcanic-arc, and the bimodal nature of the meta-volcanic rocks suggested to a volcanic-arc setting (Kolb 2014). The *c.* 1910-1880 Ma AIC intruded into Archaean and Palaeoproterozoic rocks in a continental arc setting and pre-dates regional metamorphism by some 15 million years (Hansen and Kalsbeek 1989, Kolb 2014, Nutman *et al.* 2008b).

The metamorphism and pressure-temperature-time (PTt) evolution has seen only few investigations, but Palaeoproterozoic structures and metamorphic conditions apparently vary considerably between the terranes north and south of the AIC (Kolb 2014). The AIC and the area to the south are structurally relatively simple and record peak metamorphic conditions of 600°C and 7 kbar at *c.* 1910-1885 Ma, contemporaneous with NW-SE compression and nappe transport to the southeast in the Isertoq Terrane (Kolb 2014, Nutman *et al.* 2008b).

In the Kuummiut Terrane are frequently found structures related to at least four deformation stages, and relics of and pseudomorphs after high-pressure mineral assemblages in garnet pyroxenite and retrogressed eclogite (Kolb 2014, Müller *et al.* 2016, Nutman *et al.* 2008b). Conventional geothermobarometry combined with pseudosection modelling suggest conditions of 750-815°C and 15.8-18.2 kbar (Müller *et al.* 2016). The eclogite facies mineral assemblages became unstable during decompression at high-pressure amphibolite facies conditions of 632-725°C and 10.7-12.5 kbar (Müller *et al.* 2016). Retrograde decompression between *c.* 1870 Ma and 1820 Ma occurred during thrust imbrication to the east-northeast in an ENE-WSW compressional stress field (Kolb 2014, Müller *et al.* 2016). D_2 structures, folds, reverse-oblique-slip and normal shear zones, formed during NE-SW compression in all terranes at amphibolite facies conditions, except the northernmost Schweizerland Terrane (Kolbs 2014).

The Niflheim Thrust juxtaposed the Schweizerland Terrane and the Kuummiut Terrane during NW-SE compression at lower amphibolite facies conditions, forming a set of shear zones in the hanging wall of the thrust and fold structures in the Kuummiut Terrane (Kolb 2014). This caused further retrogression in the rocks of the Kuummiut Terrane late in the metamorphic evolution, either at *c.* 1820 Ma or *c.* 1740 Ma. No D_3 structures have been

observed south of the Kuummiut Terrane. The *c.* 1670 Ma granites were emplaced during D_4 orogen-normal NE-SW, representing the last Palaeoproterozoic stage observed in the Tasiilaq area (Kolb 2014).

11.3 The Ketilidian Orogen of South-East Greenland

The area between Napasorsuaq Fjord and Timmiarmiut is mainly underlain by rocks of the Thrym Complex (Bagas *et al.* 2013, Escher and Nielsen 1983, Garde *et al.* 1999, Kolb *et al.* 2013, Lally 2013). In nunataks on the main land in the west, the Archaean orthogneiss is unconformably overlain by conglomerate (Escher and Nielsen 1983). The matrix is fine-grained and consists of quartz, feldspar and clay minerals. Minor angular clasts are K-feldspar, clinopyroxene, quartz, titano-magnetite, ilmenite and quartz sandstone. Rounded clasts are recrystallized, metamorphic quartz, medium-grained clinopyroxene-quartz-plagioclase igneous rock, fine-grained biotite-plagioclase-quartz volcaniclastic rock with angular very fine-grained rock and quartz, medium-grained biotite-plagioclase-quartz rock, sandstone with quartz-feldspar matrix, very fine-grained rocks, orthogneiss and fine-grained volcanic hornblende-rich rock. In general sedimentary and volcanoclastic rock clasts predominate. Greenschist facies metamorphism is indicated by replacement of several minerals by epidote, sericite and prehnite. Detrital zircons are older than 1920 Ma, yielding a maximum age of deposition. On the islands of Ikermit and Otto Rud, however the Archaean rocks are intruded by *c.* 1800 Ma monzogranite, granodiorite, diorite, gabbro, porphyritic aplite and pegmatite that commonly form sheets and sill-like bodies and less commonly up to 50 m wide plutons. The monzogranite is locally cordierite-bearing. A green biotite-epidote-calcite mineral assemblage and undulose extinction and subgrain formation in quartz indicate metamorphism in the greenschist facies. The southern margin of the NAC evolved with initial unconformable clastic sedimentation and was subsequently intruded by a suite of igneous rocks at *c.* 1800 Ma. The intrusive suite has a within-plate geochemical signature and is interpreted as magmatism cause by Palaeoproterozoic underplating. Subsequently, Archaean and Palaeoproterozoic rocks were affected by weak tectono-metamorphic overprint late in the Ketilidian Orogeny.

12 Post-orogenic Proterozoic dyke swarms

Martin Bromann Klausen, Mimmi Nilsson & Alexander Bartels

Across the south-eastern coast of Greenland, three Proterozoic swarms of tabular intrusions can be distinguished from metamorphosed and deformed pre-orogenic Palaeoproterozoic dykes (Section 12.1). They are primarily distinguished on the basis of their greater freshness.

Late- to post-orogenic appinite intrusions (Section 12.1) straddle the boundary between the Ketilidian Orogen and the southern margin of the North Atlantic Craton, and consistently cut pre-orogenic dykes (green sill in Fig. 12.1). The Melville Bugt Dyke Swarm (Section 12.2) is more extensive and, furthermore, has a distinctly different N(NW)-S(SE) regional trend that cuts orthogonally across Palaeoproterozoic dykes across the entire SEGMENT area north to Tasiilaq (orange dykes in Fig. 12.1).

Dykes of the Gardar Province (Section 12.3, Bartels et al. 2016) are like the appinities restricted to an area inside and just north of the Ketilidian Orogen, but trend sub-parallel to Palaeoproterozoic dykes and are thereby less obvious in the field (red dyke in Fig. 12.1).

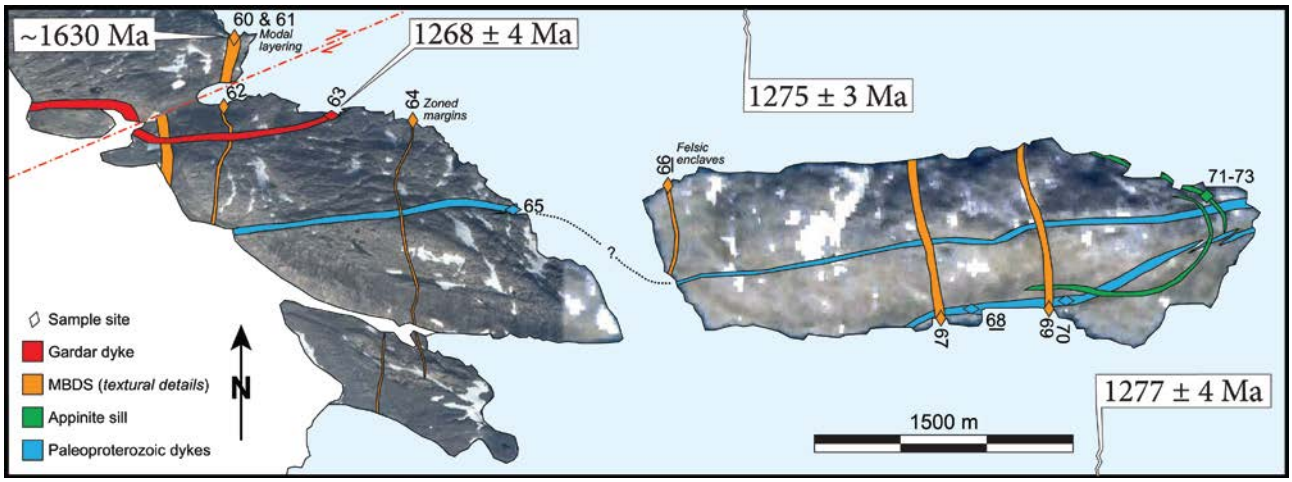

Figure 12.1 *Tabular intrusions and faults superimposed upon a Google Earth map of the inner Timmiarmiut area (around 62°37'36"N; 42°41'38"W). Type locality illustrates cross-cutting relationships between four magmatic events: (1) a pair of E-W trending Palaeoproterozoic dykes (Section 6.1); (2) a late-Ketilidian appinite sill (Section 12.1); (3) six N-S trending ~1.63 Ga dykes of the Melville Bugt Dyke Swarm (MBDS); and (4) an E-W trending ~1.27 Ga dyke of the Gardar Province. The latter dyke appears to be less dextrally offset than the most westerly located and thicker Melville Bugt dyke (exhibiting nearly 500 m of lateral displacement), yet possibly drag-folded, by a WSW-ENE trending shear zone. Labelled sample localities are indicated by colour coded diamonds. All sample numbers should be prefixed by GGU-.*

12.1 Appinite intrusions

Andrews *et al.* (1971) first reported the presence of appinitic (hornblende-rich) intrusions within the Timmiarmiut area. These, predominantly tabular, but also plug-like intrusions of variable orientations were emplaced during the latter stages of the Ketilidian Orogeny, extending across the southern border of the eastern NAC of Greenland. They are generally thinner (average of 5 m) than other mafic Palaeoproterozoic and Mesoproterozoic dykes that cross-cut the same area, with the exception of a thick sill (Fig. 12.1 and Fig. 12.2A–B) and associated plugs. The modal layering in the appinitic sill (Fig. 12.2B) indicates relatively low magma viscosities. Tabular appinites appear to have quite variable orientations (cf., inserted stereo-graphical diagram in Fig. 12.2), but there may be a clustering of steeply-dipping dykes that appear to be either N(NW)-S(SE) or W(SW)-E(NE) trending. Intrusions are often autolith-rich (Fig. 12.2C) – especially within or close to plugs – and indicative of relatively violent and rapid magma emplacement. Rarer carbonatite veins (Fig. 12.2D) are tentatively associated with the appinites.

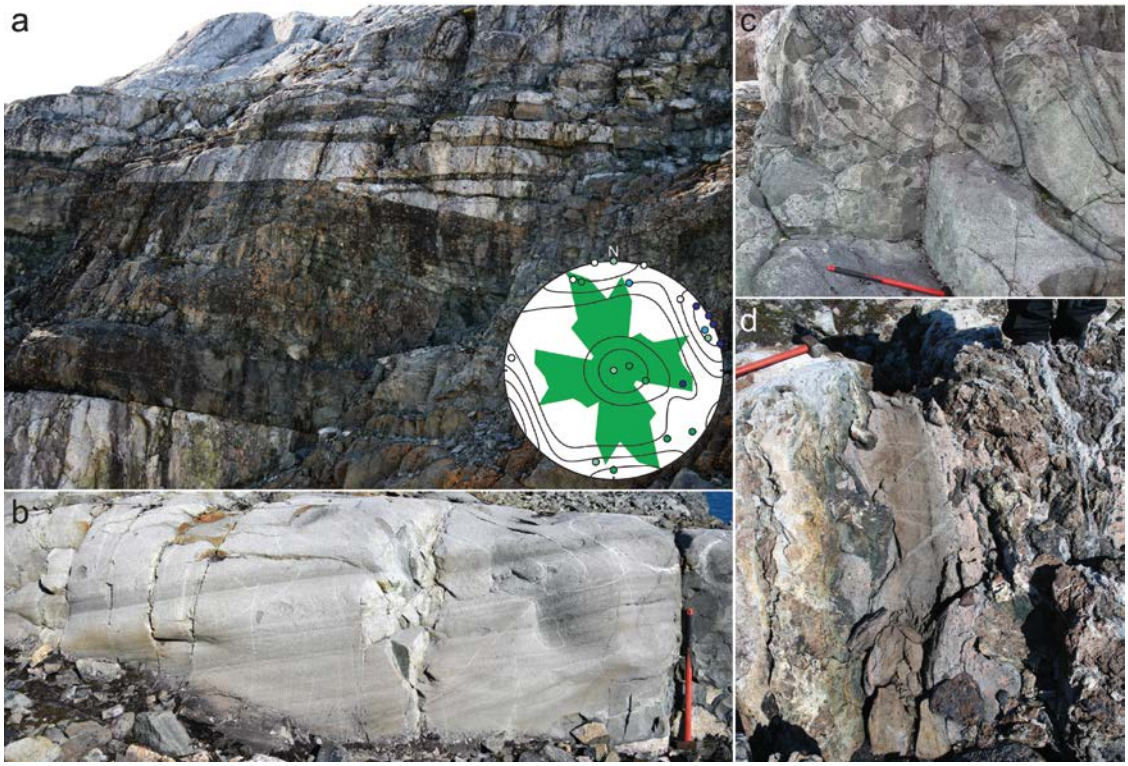

Figure 12.2 *Selected field photos of appinite and associated carbonatite intrusions.* ***A.*** *An ~ 8-10 m thick appinite sill (sample GGU541371-3 in Fig. 12.1) with several roof splays, cross-cut by an E-W trending ~1270 Ma dyke (Gardar Province) across the lower left of the photograph.* ***B.*** *Detail of lower part of the sill in A., exhibiting modal layering, including some cross-bedding in the lowermost part of this outcrop.* ***C.*** *An autolith-rich centre of an appinite dyke, from which sample GGU527199X was sampled.* ***D.*** *Carbonatite vein with euhedral zircon, ilmenite and possibly other exotic phenocrysts. Sledge hammer shaft is ~ 1.2 m long. Inserted equal area stereographical plot, shows a bi-directional moving average rose diagram, as well as the contoured distribution of poles to 22 measured planes of tabular appinite intrusions. These are geochemically subdivided into predominantly Cr-rich (purple poles), 'spessartitic' (dark green poles) and 'more evolved 'vogesitic' subtypes (pale green poles), including two dykes with cumulate autoliths (pale blue poles).*

The compositions of these appinites are equally variable, ranging from ultramafic cumulates (Fig. 12.3 left) to felsic differentiates (Fig. 12.4 right), but are all dominated by primary igneous amphiboles (Fig. 12.3) – as opposed to secondary metamorphic minerals found within other Palaeoproterozoic dykes. These unifying characteristics of appinites reflect magmas with relatively high P_{H2O}, which is in turn consistent with their petrogenesis and emplacement within a late-orogenic setting (Murphy 2013). If it was not for the occasional absence of amphibole phenocrysts, many of the appinites could equally well be classified as calc-alkaline lamprophyres, and more specifically as amphibole-dominated spessartites and vogesites (Le Maitre 2002).

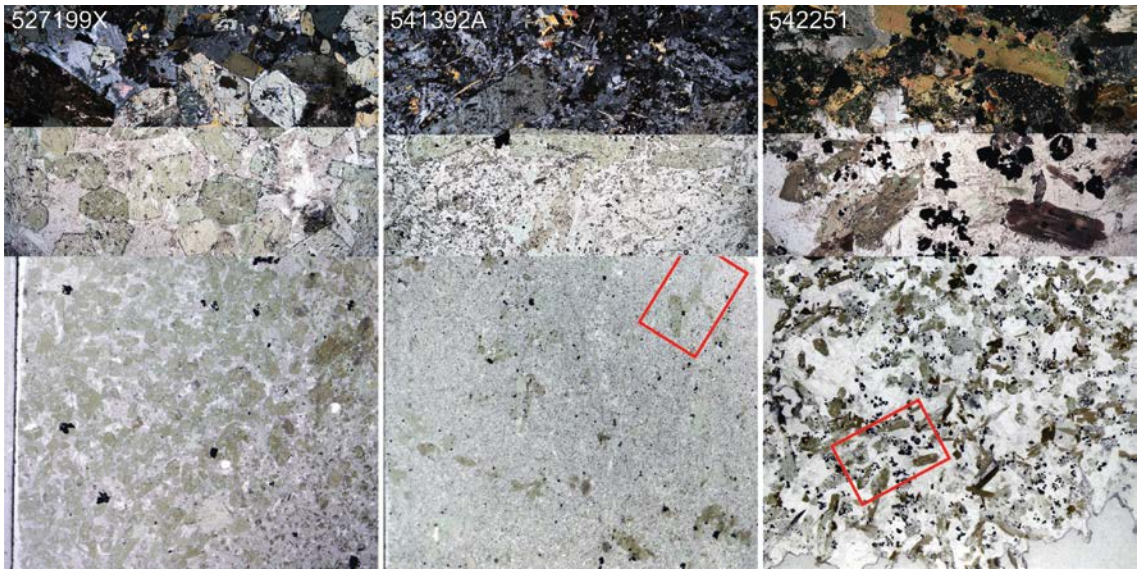

Figure 12.3 *Thin section petrography of three selected appinites, with flat-bed scanned images along the bottom (width of view ~ 20 mm) and microscope photographs along the top (crossed polarized light on top of plane polarized light, with total width of view ~5 mm). Sample 527199X shows a portion of a crystal-supported cumulate autolith with euhedral hornblende cumulates, primarily surrounded by intercumulus plagioclase. Sample 541392A shows the fine-grained and hornblende-phyric texture of a more evolved ('vogesitic') appinite sheet. Sample 542251 shows a particularly Cr-rich appinite, with large abundance of cumulate(?), opaque and euhedral chromite grains, as well as a greater abundance of biotite than observed in many other appinites (i.e., 'kersanitic'). All sample numbers should be prefixed by GGU-.*

The high P_{H2O} is also reflected by lower Fe (i.e., more calc-alkaline) differentiation trend, including an early onset of TiO_2-depletion (Fig. 12.4), which may also be related to relatively early (Fe,Ti)-oxide fractionation. A lack of Al- and Sr-depletion (not shown) is, furthermore, consistent with amphibole fractionation, followed much later by plagioclase fractionation from such hydrous magmas. Resulting trends and rock types thereby differ distinctly from all other Palaeoproterozoic dyke swarms across South-East Greenland (as well as Mesozoic and presumed Tertiary dykes discussed below), and can be related to differentiation of magmas with relatively high P_{H2O}, presumably derived from a SCLM that was highly metasomatized during the Ketilidian Orogeny (Murphy 2013). Associated carbonatite veins (Fig. 12.2D) also offer evidence for relatively high P_{CO2}.

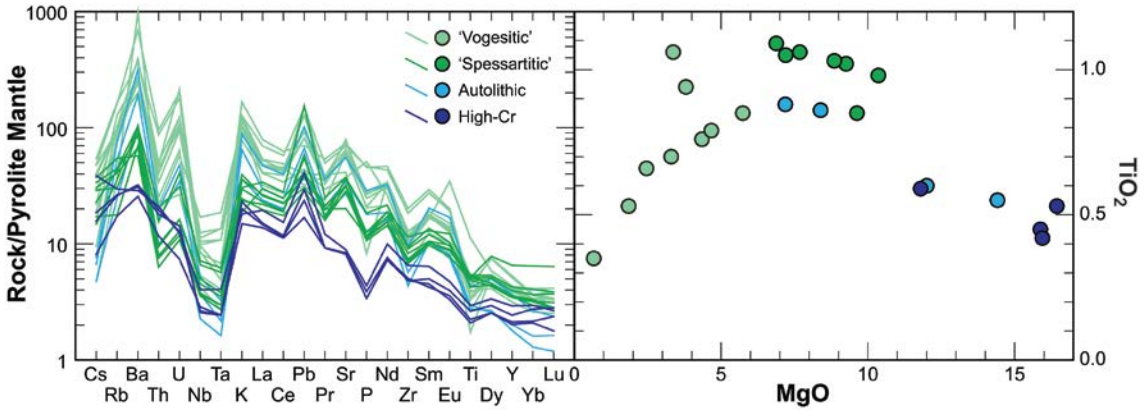

Figure 12.4 *Selected geochemical plots for 25 appinite intrusions sampled across the Timmiarmiut area plotted as in Fig. 7.4.*

12.2 Melville Bugt Dyke Swarm

A distinct swarm of N(NW)-S(SE) trending dykes cuts across most of the south-eastern coast of Greenland. Halls *et al.* (2011) proposed that these represent the continuation of North-West Greenland's Melville Bugt Dyke Swarm (Kalsbeek and Taylor 1986, Nielsen 1990), based on parallel structural trends on either side of Greenland's central ice cap, and thereby extended it into a > 2000 km long trans-Greenlandic structure. Klausen *et al.* (2014) supported this correlation through a geochemical match between dyke core samples, and it is in this context important to note that dyke margin samples appear to be severely contaminated by the host rock (e.g. Kalsbeek and Taylor 1986). A U-Pb age on extracted baddeleyites from North-West Greenland's Melville Bugt Dyke Swarm suggests that the dykes were emplaced at ~ 1630 Ma (Halls *et al.* 2011), and this is corroborated by a similar unpublished preliminary age by M. Nilsson (cf., ~ 1630 Ma in Fig. 12.1).

In the field, the Melville Bugt dykes stand out as being paler orange-brown weathered (Fig. 12.5) and always contain at least one or two plagioclase megacrysts (Fig. 12.6.a). It is not uncommon for these dykes to be dextrally offset by oblique transverse faults (e.g., Fig. 12.1), which may have formed through northward propagation during the opening of the Atlantic Ocean. Otherwise, Melville Bugt dykes are relatively undeformed. Dyke widths occasionally swell (Fig. 12.5A), in a manner that is inconsistent with normal brittle fracture mechanics and is better explained by local thermal erosion of host rocks. Evidence for partial melting of the host rock is provided by centimetre wide fine-grained felsic margins, related felsic back-veins and rounded blebs inside the dykes (Fig. 12.6B–C). Contact melting can be explained by (1) either the host rock and/or magma being very hot; (2) prolonged magma flow (through-put); and/or (3) exceptionally thick dykes (average ~ 11.8 m). Prolonged magma flow is supported by locally well-developed rhythmic modal layering as well as common 'zoned' margins (Fig. 12.5B–C).

There are also indications of excessive fluid interaction along parts of Melville Bugt dykes, expressed by intense reddish alteration of host rock gneisses. Judging from the lack of discolouration in between the two parallel dykes in Fig. 12.5B, however, it is assumed that this alteration involves externally derived crustal fluids.

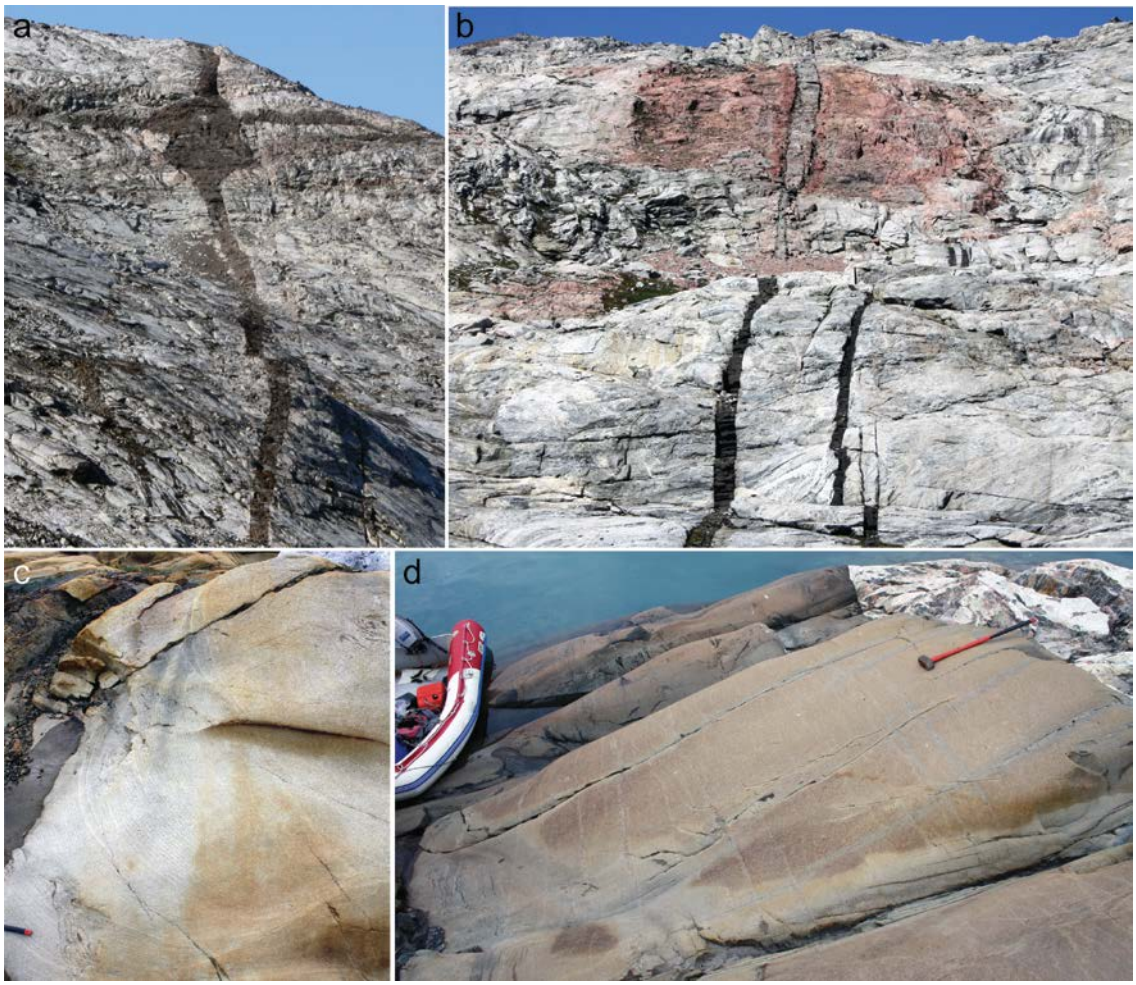

Figure 12.5 *Melville Bugt dyke field relationships.* ***A.*** *Conspicuous dyke width swelling close to where the dyke cross-cuts a Palaeoproterozoic dyke in the Umivik area.* ***B.*** *Two parallel and ~1 m thick dykes, around which there is a conspicuous local red-colouring of feldspars in the gneissic host rock. The discolouration appears to be more intense along the outer margins of the two dykes, whereas the internal block is less altered.* ***C.*** *Trough-like rhythmic modal layering, close to where GGU541360-1 was sampled (Fig. 12.1). End of hammer shaft provides a scale.* ***D.*** *Thin margin-parallel coarser-grained zones in dyke sampled by GGU541365 (Fig. 12.1). These zones can often be matched into symmetrical sets inward from both dyke margins, and may reflect several magma pulses and/or in situ crystallization fronts during fluctuating* P_{H2O}*. Hammer shaft is ~80 cm long.*

The fresh and remarkably homogenous petrography of Melville Bugt dykes is summarized by Fig. 12.7, where the rounded internal outline of a feldspar megacryst suggests that these were initially in disequilibrium with the melt and subsequent albite twinned plagioclase (plg) overgrowth is presumably of similar composition as matrix plagioclase laths. Subhedral olivines (ol) have partial inclusions of small plagioclase laths, suggesting that the matrix initially crystallized on the plagioclase-olivine cotectic. Subhedral opaque phases are most likely (Fe-Ti)-oxides (ox), which appear to have started crystallizing slightly later, but before the co-crystallization of interstitial augite (cpx). If the feldspar megacrysts crystallized from the melt, the resulting crystallization sequence could be plg → ol+plg → ol+plg+ox → ol+plg+ox+cpx, which is more typical for tholeiites than alkali basalts.

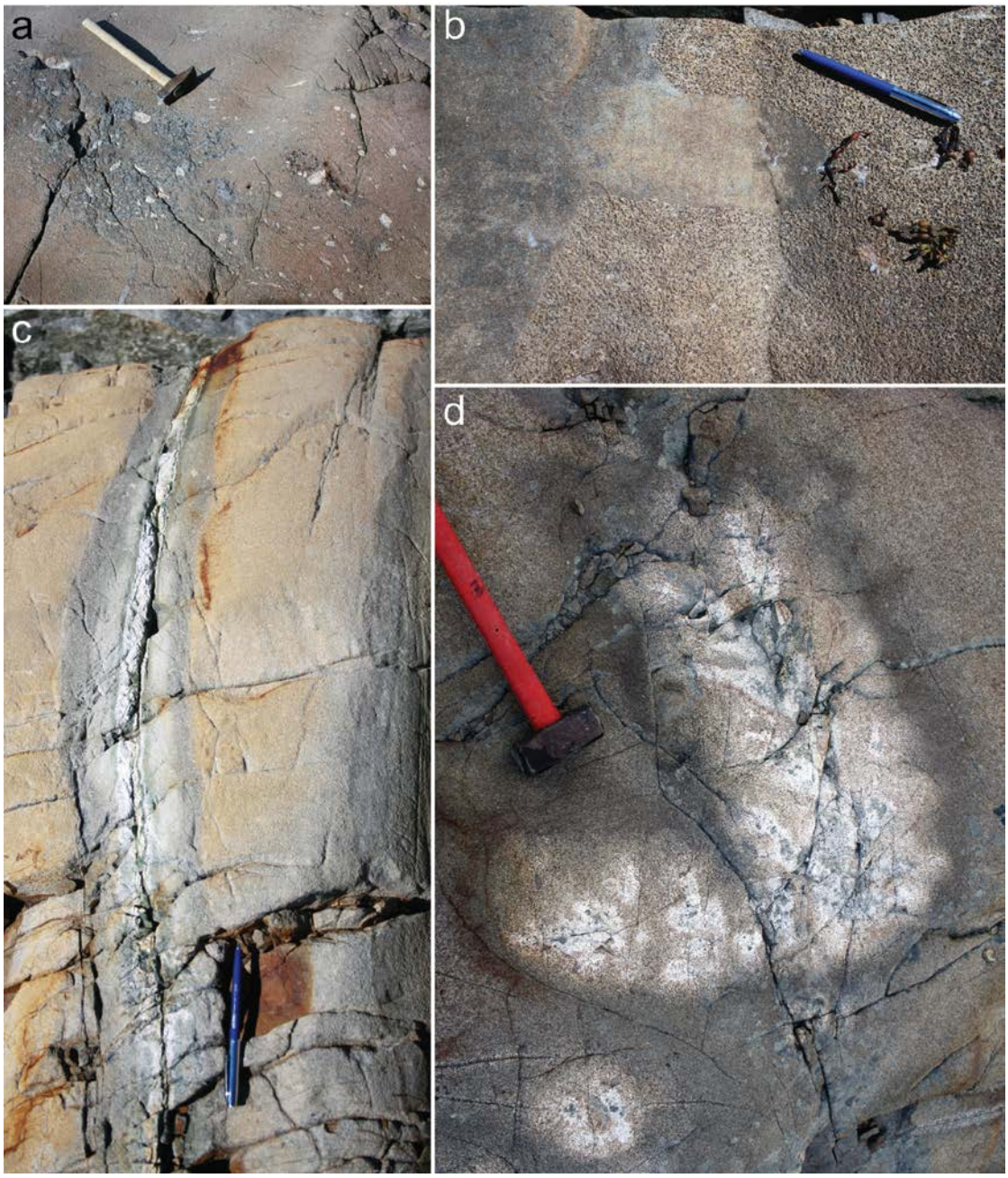

Figure 12.6 *Internal features of Melville Bugt dykes.* ***A.*** *Local cluster of diagnostic feldspar megacrysts, which are otherwise more scattered but always present (hammer shaft is ~60 cm long).* ***B.*** *Less than 2 cm wide felsic vein injected orthogonally into a Melville Bugt dyke from its margins (i.e., confined to the dyke and never cross-cutting the host rock). It is interpreted as a back-vein of host rock contact melts, which furthermore altered 5-6 cm into the solidified host dyke. Pen is ~13 cm long.* ***C.*** *Numerous centimetre large felsic enclaves, surrounded by haloes of altered host dyke, could be either partly dissolved host rock xenoliths or blebs of host rock contact melts. Hammer head is ~16 cm long.* ***D.*** *Fine-grained enclave within a coarse-grained dyke interior, with a more mafic composition, yet similar geochemical signature, as its host*

Geochemically, most Melville Bugt dykes share remarkably similar incompatible element signatures with distinct positive Pb and negative Nb-Ta (Fig. 12.8 left), typical for a lithospheric component. Their resemblance to ~200 million years older (late-orogenic) and less

evolved appinites (‘spessartites’, Fig. 12.4) led Klausen *et al.* (2014) to propose a common metasomatized sub-continental lithospheric mantle source for both swarms, even if Melville Bugt dyke magmas were distinctly drier. The geochemical homogeneity both along and across the Melville Bugt Dyke Swarm of relatively evolved magmas (having experienced primarily plagioclase and olivine fractionation), together with the large volumes incorporated into a ~ 2000 km long swarm, argues for a single correspondingly large magma reservoir, which according to normative nepheline-diopside-olivine-hypersthene-quartz plots by Thompson (1982) resided at ~ 30 km’s depth. Finally, geochemical analyses of a rounded fine-grained enclave and its host dyke (Fig. 12.6D) indicate that this enclave has a more primitive parental composition, yet similar geochemical signature. The enclave could be interpreted as a chilled margin autolith.

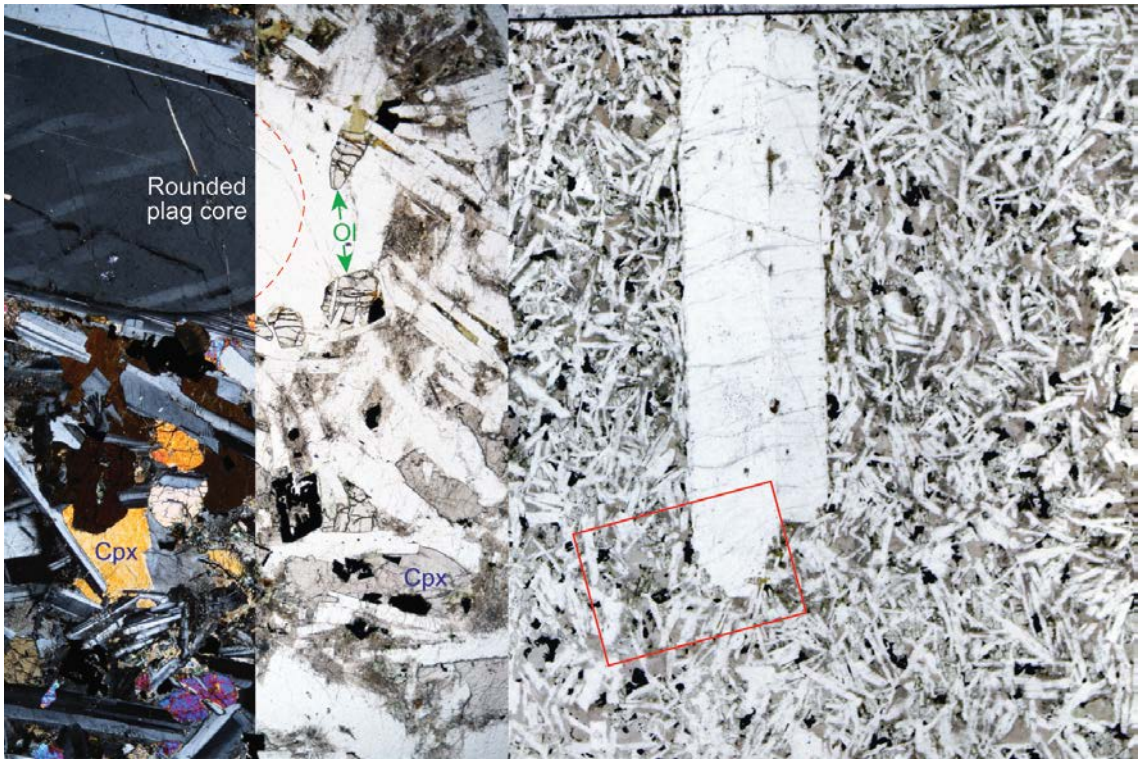

Figure 12.7 *Thin section of sample GGU541367. Right half shows a flat-bed scanned image of a feldspar megacryst in a sub-ophitic matrix. To the left, a microscope photograph (crossed polarized left half and plane polarized right half) shows rounded internal outline of the feldspar megacryst overgrown by albite twinned plagioclase. The matrix is made up of plagioclase laths, subhedral olivines (ol) and opaques, as well as interstitial augite (cpx).*

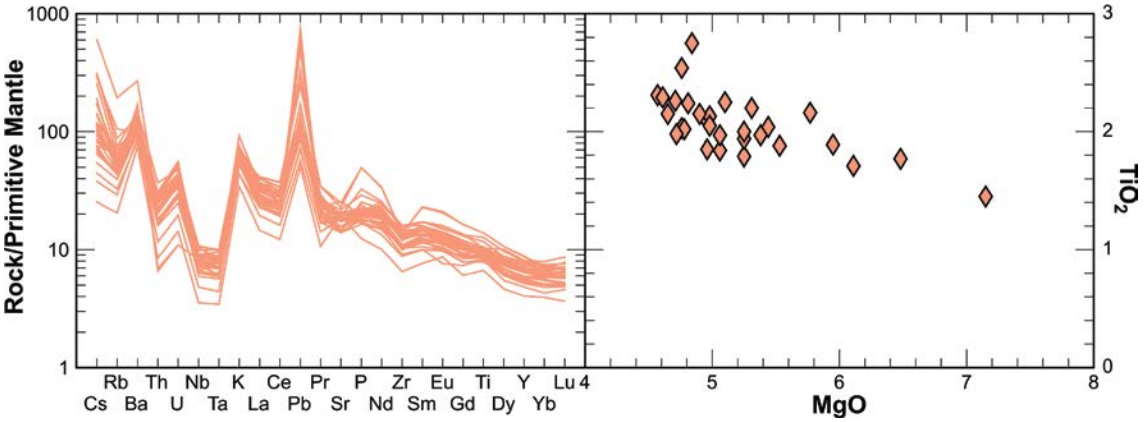

Figure 12.8 *Thirty geochemical samples from the Melville Bugt Dyke Swarm across South-East Greenland as in Fig. 7.4. Left: Spider diagram showing parallel patterns with distinct positive Pb and negative Nb-Ta, as well as notably high Ba. Right: Variation diagrm showing moderate TiO_2 concentrations of ~2 wt% and a clustering of samples at ~5 wt% MgO.*

The many unusual aspects of the Melville Bugt Dyke Swarm advocates for unusual petrogenetic diversification and emplacement processes, within an equally unusual tectonic setting. Slightly differing *c.* 1630 Ma plate reconstructions (e.g. Evans and Mitchell 2011, Johansson 2013, Pesonen *et al.* 2012) all point to a Nuna/Columbia supercontinent with an particularly long-lived 'outboard Andean margin', which experienced several island arc accretion events, leading to the formation of extensive Palaeoproterozoic orogens across Labrador, southern Greenland (Ketilidian), central Greenland (Nagssugtoqidian) and the Baltic Shield (Sveconorvegian). These orogenic belts also host some exceptional post-orogenic anorthosite-mangerite-charnockite complexes and rapakivi granites, many of which formed around the same time as the Melville Bugt Dyke Swarm. A central magma source for the Melville Bugt Dyke Swarm beneath the Ketilidian Orogen must have injected up to 2000 km long dykes laterally across Greenland and at a high angle to Nuna/Columbia's active margin. It is debatable whether the same or another similar large magma reservoir fed a coeval diabase dyke swarm across the Baltic shield (e.g. Rämö 1991) but its setting, late-orogenic lamprohyres (e.g. Andersson *et al.* 2007, Rutanen *et al.* 2011) and coeval rapakivi granites replicate southern Greenland. One can only speculate on what triggered the generation of such large volumes of dry magmas at *c.* 1.63 Ma (slab break-up during ridge subduction?), whether such a large basaltic magma reservoir formed roughly coeval rapakivi granites through lower crustal melting, and how the Melville Bugt Dyke Swarm's conspicuous large feldspar megacrysts may relate to roughly coeval anorthosites.

12.3 Dykes of the Gardar Province

Although difficult to distinguish from roughly parallel Palaeoproterozoic dykes, WSW-ENE trending dykes were recognized in the Timmiarmiut area from cross-cutting relationships (Bridgwater *et al.* 1973). Three recent U-Pb baddeleyite ages of 1268 to 1277 Ma (Fig. 12.1) confirm this notion and provide a more precise age for the earliest magmatic event within the rest of the Gardar Province (Bartels *et al.* 2016). Field relationships, petrography and geochemistry of the few Gardar dykes that cut across the Timmiarmiut area are ade-

quately described and interpreted in Bartels *et al.* (2016). In summary, Bartels *et al.* (2015) and Bartels *et al.* (2016) describe geochemical 'fingerprints' that are consistent with a sub-continental lithospheric mantle source and only little crustal assimilation. They, furthermore, propose a correlation between the Gardar Province in Greenland and coeval Harp dykes across Newfoundland, and suggest that these were emplaced within a continental back arc setting, linking up with roughly coeval Sudbury and Central Scandinavian dyke swarms.

13 Late Cretaceous to Palaeogene rocks

Samuel Weatherley, Jakob Kløve Keiding, Martin B. Klausen, Thomas Kokfelt, Charles Lesher, Christian Tegner & Thomas Ulrich

The geology of South-East Greenland includes the southernmost section of the East Greenland rifted volcanic margin, an assemblage of Palaeogene igneous complexes, dykes and volcanic products that relate to the birth of the Atlantic Ocean (see review by Brooks, 2011). Compositions of the Palaeogene rock types are variable, encompassing mafic, felsic, quartz-saturated and quartz-undersaturated lithologies. During the SEGMENT project, field efforts were focused on dolerite dykes south of 66°30'N (Isortoq), the Kap Gustav Holm Plutonic Centre (66°34'N, 34°22'W), the Sulugssut Intrusive Complex (66°32'N, 34°46'W), and the Kialineq Plutonic Centre (66°56'N, 34°57'W). Petrological, geochemical and geochronological work on samples collected during the most recent field seasons is currently in progress.

13.1 Dykes

Between 57-54 Ma, continental breakup led to the emplacement of the extensive "Coast-parallel swarm of East Greenland (Wager and Deer 1938) (hereafter, the coastal dyke swarm) in what is now the eastern coast of Greenland (Klausen & Larsen 2002, Lenoir *et al.* 2003, Myers 1980, Nielsen 1975, Nielsen 1978, Nielsen and Brooks 1981, Wager and Deer 1938). Dykes are exposed for over 350 km along the coast between Kap Wandel (66°18'N, 34°53'W) and Nansen Fjord (68°18'N, 29°53'W) (Myers 1980), and persist for a total distance of ~ 780 km between 63°N and 69°45'N, if offshore extensions revealed by aeromagnetic surveys are included (Larsen 1978). The structure of the coastal dyke swarm is well studied, particularly in the region north of Kap Gustav Holm and Kangerlussuaq where the structure of the swarm reveals a domino-block marginal crustal flexure along a narrow volcanic rifted margin (Klausen and Larsen 2002, Nielsen and Brooks 1981). Along the onshore section of the coastal dyke swarm, basic dykes comprise more than 50% of the outcrop area (Myers 1980) and can in extreme cases comprise almost 90% of the exposed terrain (Brooks 2011, Nielsen 1978).

Most of the Palaeogene dykes are medium to coarse-grained dolerites with ubiquitous plagioclase, clinopyroxene, ±olivine, oxides, as well as low temperature chlorite-rich alteration assemblages. Nielsen (1978), Gill *et al.* (1988), Klausen and Larsen (2002) and Hanghøj *et al.* (2003) classified the dykes into different groups on the basis of their geochemistry and relative age, and suggested that the differences can be explained in terms of source parameters such as mantle heterogeneity, and the depth and extent of melting.

In the re-investigated northernmost section of the SEGMENT area between Kap Gustav Holm and Kialineq, the coastal dyke swarm intruded the Archaean basement (Fig. 13.1). The dykes are characteristically brown in colour, strike parallel to the coast and reach thicknesses of up to several tens of metres. South of Kap Gustav Holm the main coastal dyke swarm lies offshore. However, some scarce but still prominent dykes of suspected Palaeogene age (age dating pending) are found onshore. In the central portion of the

SEGMENT area between 65°N and 66°N, the suspected onshore Palaeogene dykes can be recognized as two sub-swarms, labelled S and N in Fig. 13.2. The northern sub-swarm, corresponding to *N* in Fig. 13.2, is defined by at least six dykes that strike approximately E-W. The southern sub-swarm, corresponding to *S* in Fig. 13.2, located between Tasiilaq and Umivik (64°15'N, 40°30'W), comprises twelve sub-parallel and slightly curved dykes that trend in a NE-SW to N-S direction.

Figure 13.1 *South-Westward view of the coastal dyke swarm intruding Archaean gneisses at the peninsula immediately to the west of Kap Gustav Holm.*

The dykes in the southern sub-swarm coincide with distinct aeromagnetic anomalies. In the southern onshore sub-swarms, dykes vary in thickness from 5 to 76 m and are generally thicker than those of the main coastal dyke swarm, which have average thicknesses of 3-6 m (Klausen and Larsen 2002). A particularly thick example of one of the suspected Palaeogene dykes outcropping at Kap Tycho Brahe (65°38'N, 38°15'W) is shown in Fig. 13.3A. These 'southern' dykes have steep, sharp and sinuous contacts with the host rock, are undeformed and surface weather into characteristic brown colour. They exhibit a gradation in grain size from sub-mm near the contacts to up to 5 mm in their doleritic to gabbroic interiors. Steeply dipping, contact parallel centimetre-scale modal layering is commonly observed (Fig. 13.3B). One dyke was observed exhibiting an internal contact within inward protruding dendritic pyroxene (Fig. 13.4).

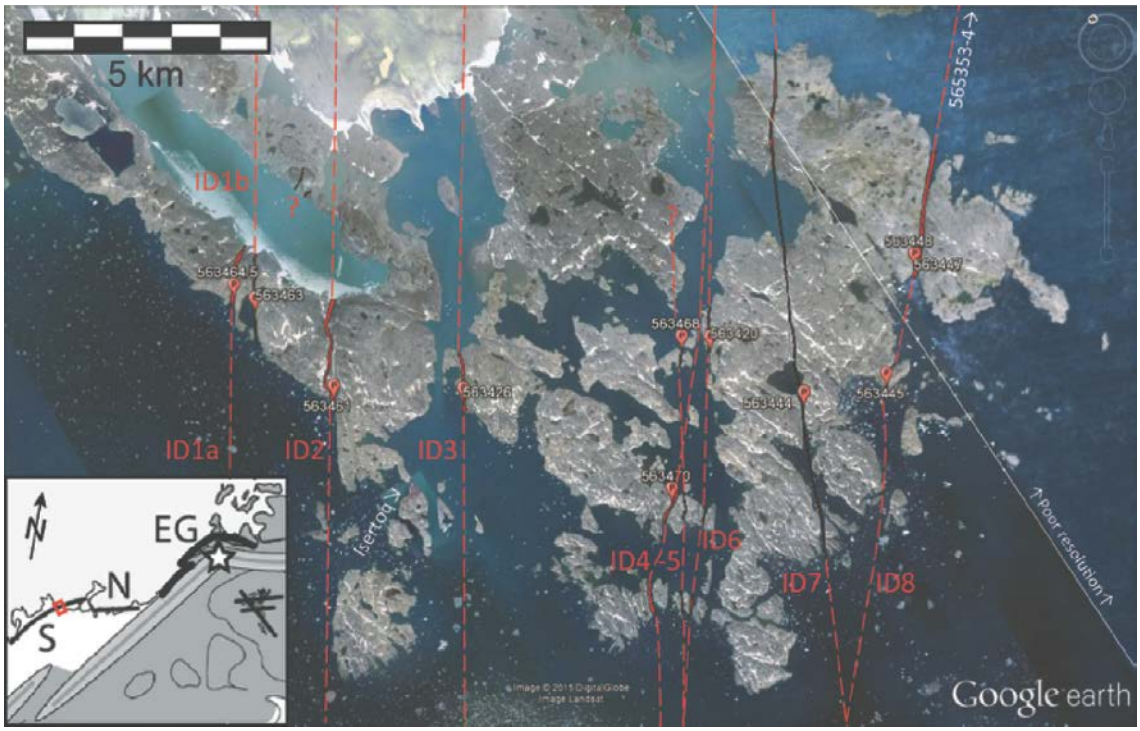

Figure 13.2 *Main figure: Google Earth image showing eight presumed Palaeogene dykes (dashed red lines) and sample locations in the region surrounding Isortoq. Insert map: Schematic indication of the major dyke swarms along the southeast and southern east coast of Greenland and the Faroe Islands (modified by Klausen and Larsen 2002). Red box indicates the region shown by the Google Earth image. EG – main coastal dyke swarm, N – northern sub-swarm, S – southern sub-swarm.*

Whilst presently there are no geochronological constraints on the age of the dykes across the central portion of the SEGMENT area, we conjecture on the basis of the sharp contacts, well developed chilled margins containing amygdoidals and lack of penetrative deformation that they are Palaeogene in age. Furthermore, the dykes bear close compositional resemblances to tholeiitic members of the coast-parallel dyke swarm, for which Loreti (2015) and Klausen and Loreti (2016) described Ocean Island Basalt (OIB) like incompatible element patterns and suggested they may be linked to a Proto-Icelandic mantle plume source.

13.2 Kap Gustav Holm

The Kap Gustav Holm Plutonic Centre, located at 66°36'N, 34°15'W is exposed on the narrow headland of Kap Gustav Holm and the adjacent island of Nanertalik (Fig. 13.5). Topographically, the peninsula comprises two peaks reaching over 1000 m in height that are separated by a saddle located approximately 250 m above sea level. The plutonic centre was initially described by Wager (1934) and was later mapped by GGU in 1978 (Myers *et al.* 1979a). Subsequent studies focused on the petrogenesis of the intrusive suite (Myers *et al.* 1993) and the hydrothermal alteration history (Kleckner 1997).

Figure 13.3 ***A.*** *Candidate Palaeogene dolerite dyke, striking NE-SW, intruding into gneiss at Kap Tycho Brahe.* ***B.*** *Modal layering in the central portion of the Palaeogene dolerite dykes at Kap Tycho Brahe.*

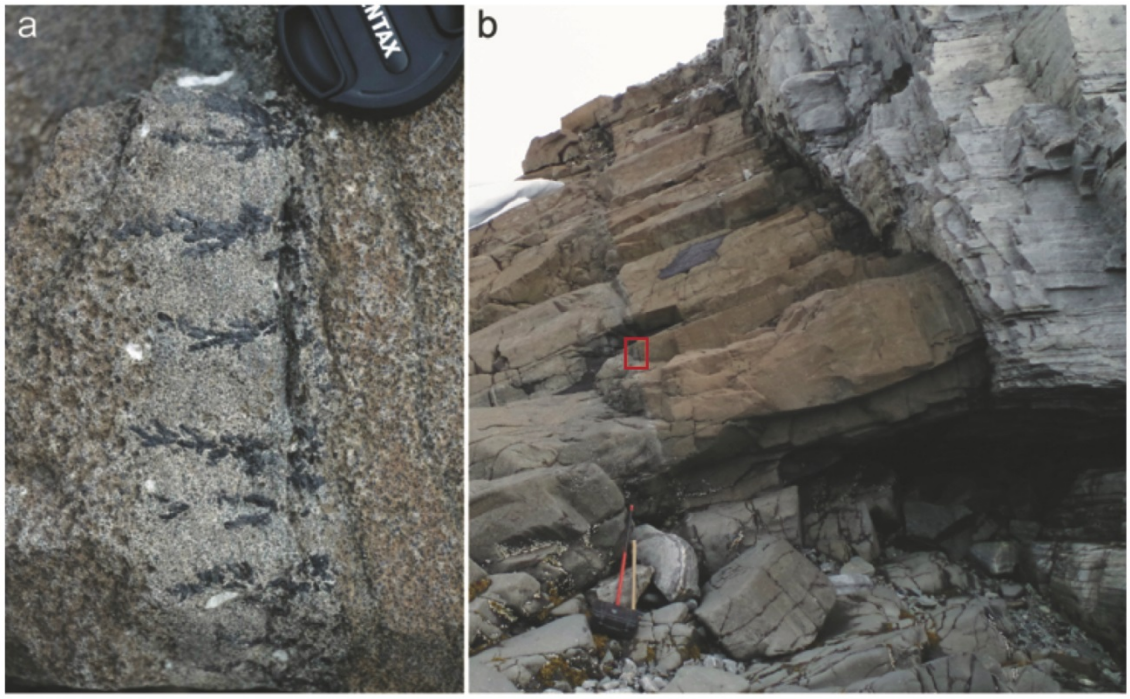

Figure 13.4 *A candidate Palaeogene dyke from north of Køge Bugt* (c. *65°N) showing an internal contact.* ***A.*** *Close-up of the internal contact showing inwards-growing dendritic pyroxene crystals.* ***B.*** *Outcrop-scale view of the dyke showing a* c. *2 m thick chilled marginal zone. Red box shows the location of photo A.*

The plutonic centre at Kap Gustav Holm includes early gabbroic units and later plutons, sheets and ring dykes of monzonite, syenite and granite. These units intruded into amphibolite facies Archaean gneisses and an overlying sequence of sedimentary rocks and basaltic lavas. Volcanic lithologies are preserved above the intrusive rocks at both the southern and main Kap Gustav Holm peaks. Prior to emplacement of the intermediate and evolved lithologies, the gabbro was cut by gabbroic pegmatite and then tilted towards the east during flexure of the crust. Dip measurements made on the volcanic units indicate that the amount of tilting is around 45°. Myers *et al.* (1993) identified the sedimentary rocks and lavas as late Cretaceous to early Palaeogene in age on the basis of fossilized lamellibranchs and are noted that the rock units are broadly equivalent to the Kangerdlugssuaq Group sediments and Lower Basalts (Nielsen *et al.* 1981).

Field relationships reveal that the gabbros are the oldest of the plutonic units. Although no direct radiometric dates have yet been obtained from the gabbros, Myers *et al.* (1993) observed that the gabbros were tilted during flexure of the crust, which is thought to have developed during flexure of the crust. Lenoir *et al.* (2003) dated tilted dykes to 55-54 Ma and vertical dykes to *c.* 51 Ma, and on the basis of this showed that flexure developed rapidly within a 2.9 Myr interval between 55 Ma and 51 Ma. The later intermediate and felsic intrusions were dated using Rb-Sr and K-Ar methods, which yield imprecise but overlapping intrusions ages between 53 ± 5 Ma to 49 ± 3 Ma (Myers *et al.*, 1993). Taken together, these constraints indicate that emplacement and crystallization of the Kap Gustav Holm Plutonic Centre occurred approximately within the period of 55-50 Ma.

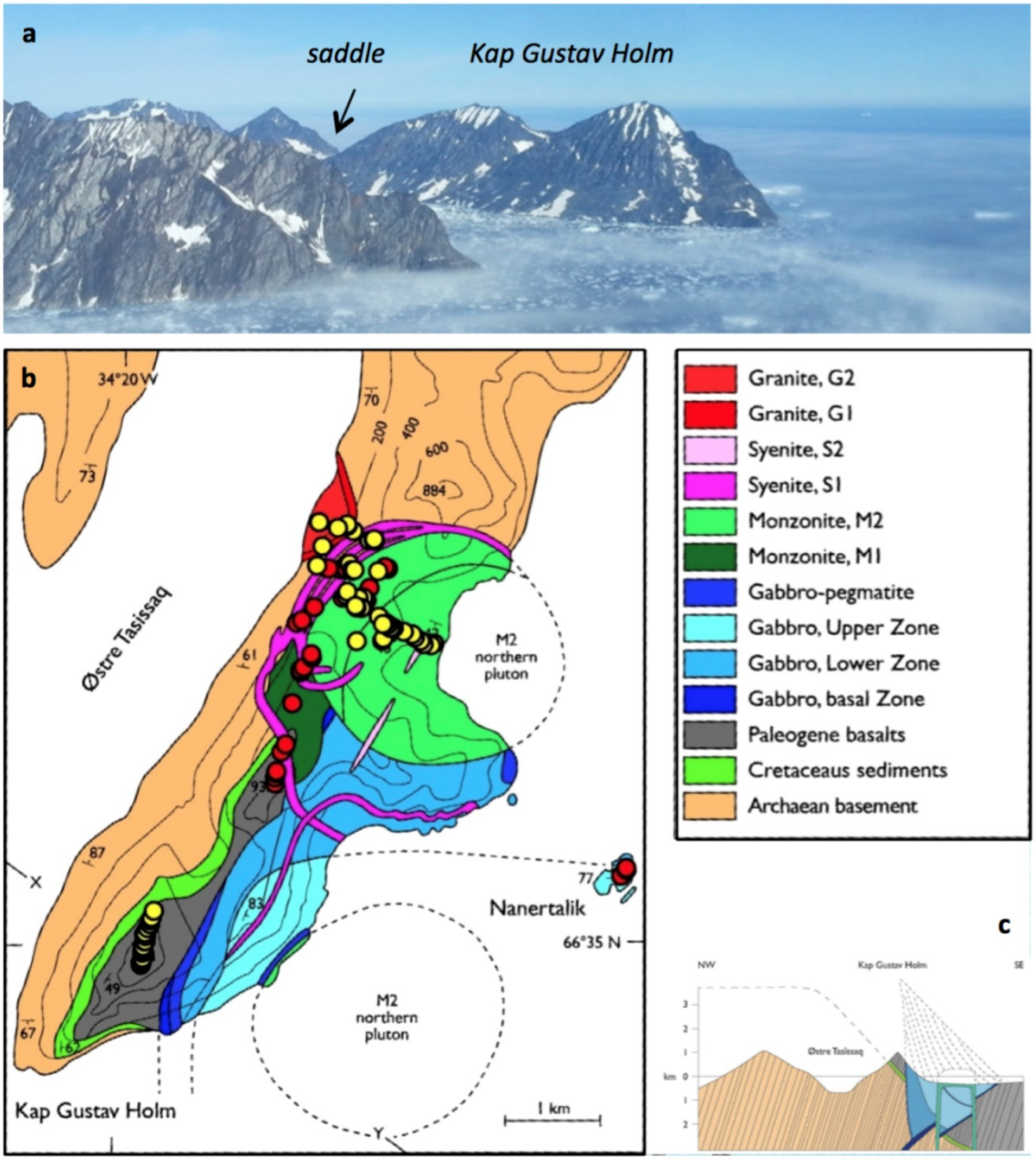

Figure 13.5 ***A.*** *View of Kap Gustav Holm from the SW. The foreground in the left of the image shows Archaean rocks (pale buff colour) intruded by the main coastal dyke swarm.* ***B.*** *Geological map of Kap Gustav Holm showing sample localities from the 2104 field season.* ***C.*** *Schematic cross-section through the southern part of the intrusion along the line X-Y in B.. B. and C. are after Myers* et al. *(1993).*

13.3 Late Mesozoic sedimentary rocks and basalts

On the current geological map of Kap Gustav Holm (Myers *et al.* 1993) (Fig. 13.5B), late Mesozoic to Paleozoic sedimentary rocks are shown to occur as a continuous unit between the Archaean rocks and overlying basaltic lava flows. However, during fieldwork in 2014, only xenoliths and blocks of sedimentary rocks were found, perhaps indicating that sedimentary rocks are overrepresented on the current geological map.

Basalts were observed to form a continuous outcrop along the ridge in the southern part of the Kap Gustav Holm peninsula (Fig. 13.6A). In general, the basalts dip at approx. 45° to the southeast, and include identifiable textures including vesicles (Fig. 13.6D) that are now filled with suspected zeolite phases (Fig. 13.6B) and pillow-like structures (Fig. 13.6C). Individual flows were only partly recognized in the field due to metamorphism and deformation in the coast parallel flexure and dyke swarm; usually a change in phenocryst content or a vesicular texture could be interpreted as a flow top.

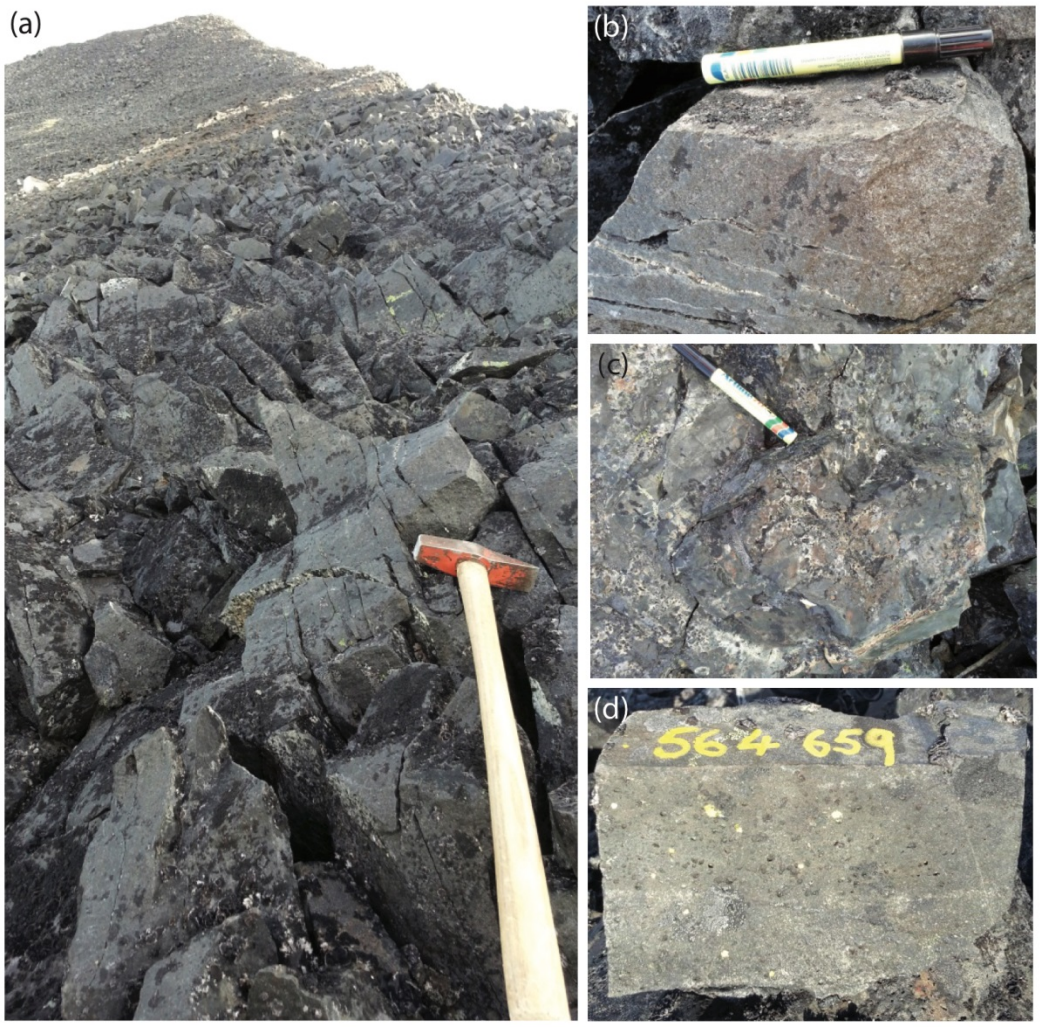

Figure 13.6 ***A.*** *View south along the northern crest, showing basalts that are tilted ~40° towards the SE. The white patch in the middle distance is a syenitic dyke intrusion that hosts angular blocks of diorite (Kokfelt* et al. *2015a).* ***B.*** *Plagioclase-bearing basaltic lava with vesicles partly filled by zeolites.* ***C.*** *Pillow-like structure within the basalts.* ***D.*** *Sample of vesicular basaltic lava.*

13.4 Gabbro

The Kap Gustav Holm gabbro comprises a sequence of layered gabbros that contain plagioclase, pyroxene, olivine and magnetite. Myers *et al.* (1993) described the body in detail

and, on the basis of changes in texture and mineralogy, divided the gabbro into a Basal Contact Zone, Lower Zone and Upper Zone. Where visible, the magmatic layering can be seen to dip steeply towards the southeast, suggesting that the intrusion was tilted following crystallization. The Basal Zone comprises heterogeneously deformed, fine- to medium-grained, foliated gabbro up to 100 m thick. The Lower Zone is 250-1500 m thick and comprises medium-grained olivine gabbro that exhibits notable igneous lamination of plagioclase. The rocks exhibit poorly defined layering that is recognized on the basis of variations in the relative proportions of mafic and felsic minerals and by the intensity of plagioclase lamination. Towards the base of the unit, amphibole- and chlorite-bearing assemblages indicate that the gabbros were modified by late-stage reactions. The Upper Zone is composed of medium-grained gabbro that exhibits well-developed, planar layering of great lateral extent. The upper portion of the unit has been removed by erosion; thus the minimum thickness is estimated at 500 m and 700 m. Myers *et al.* (1993) noted that the mineralogy of the Upper Zone is similar to that of the Lower Zone, except that the late-stage reactions are less advanced. They also suggested that the abrupt reversals in cryptic and phase layering reflect injections of new magma.

13.5 Gabbro pegmatite

The gabbro hosts several sheets of gabbro pegmatite, up to 150 m thick that are concordant with the igneous layering. The pegmatite is heterogeneous, exhibiting leucocratic and melanocratic patches, and vugs that contain magnetite, plagioclase, amphibole, epidote, actinolite, quartz, prehnite and chlorite. Myers *et al.* (1993) reported that the mineral compositions of typical gabbro-pegmatite samples fall within the range of those from the layered gabbros.

13.6 Monzonite, granite, syenite

The Kap Gustav Holm monzonite, granite and syenite units occur as plutons and ring dykes. These bodies intruded and cut the Kap Gustav Holm gabbros, and display little evidence of tilting, indicating that they post-date the main flexure event. On the main Kap Gustav Holm peninsula, monzonite mainly occurs in two discrete centres that have slightly differing mineralogy (Myers *et al.* 1993). However, only the better exposed and more accessible northern pluton (M2, Fig. 13.5B), measuring some 2.5 km in diameter, was visited during the SEGMENT project.

In general, this monzonite is coarse-grained and its mineralogy is dominated by olivine, poikilitic hornblende, plagioclase, alkali feldspar, clinopyroxene, orthopyroxene and magnetite. It possesses well developed modal layering, load-casts, erosional channels and cross bedding, and numerous xenoliths of gneiss, metasedimentary rocks and sheet-like metabasalts. Igneous layering and trains of metavolcanic inclusions dip towards the centre of the pluton, defining an internal saucer-shaped structure. Metabasalt xenoliths vary in size from tens of centimetres to hundreds of metres, and have hornfels textures, amphibole and/or pyroxene porphyroblasts and thin veins of undetermined mineralogy. In places, the metabasalts contain relict amygdaloidal textures and are often cut by monzonite veins con-

taining miarolitic cavities with quartz and epidote. In the north-western part of the intrusion, the xenoliths appear to be dominated by gneiss and sedimentary clasts, whereas in the central and south-eastern part of the intrusion, the xenoliths are dominantly metabasalt. Some of the xenoliths are composite, comprising both metabasalt and gneiss and probably represent the original depositional contact of basalt flows onto the basement. Myers *et al.* (1993) noted that metavolcanic xenoliths account for approximately 50 vol% of the rock towards the base of the monzonite, but decrease in abundance with stratigraphic height.

Two types of syenite (S1 and S2, Fig. 13.5B), identified earlier by Myers *et al.* (1993) occur as vertical to subvertical ring dykes (Fig. 13.7), which cut and encircle the northern M2 pluton. These syenites are uniform and coarse-grained, and exhibit miarolitic cavities, suggesting crystallization occurred at shallow depths. The interiors of the syenite bodies are typically free of xenoliths, although locally, they can contain angular xenoliths of gneiss, metabasalt or monzonite. However, close to and along the contact with the monzonite, submetre sized inclusions of angular to rounded, pillow-shaped clasts of basalt provide evidence for magma mingling (Fig. 13.8), paralleling observations made in the Kialineq district (see below). Additionally, close to the top of the northern peak, a previously unreported, syenitic breccia containing clasts of basalt, tuff, and more rounded blobs of gabbroic material intrudes as an irregular, 10 m wide dyke into the surrounding basalts.

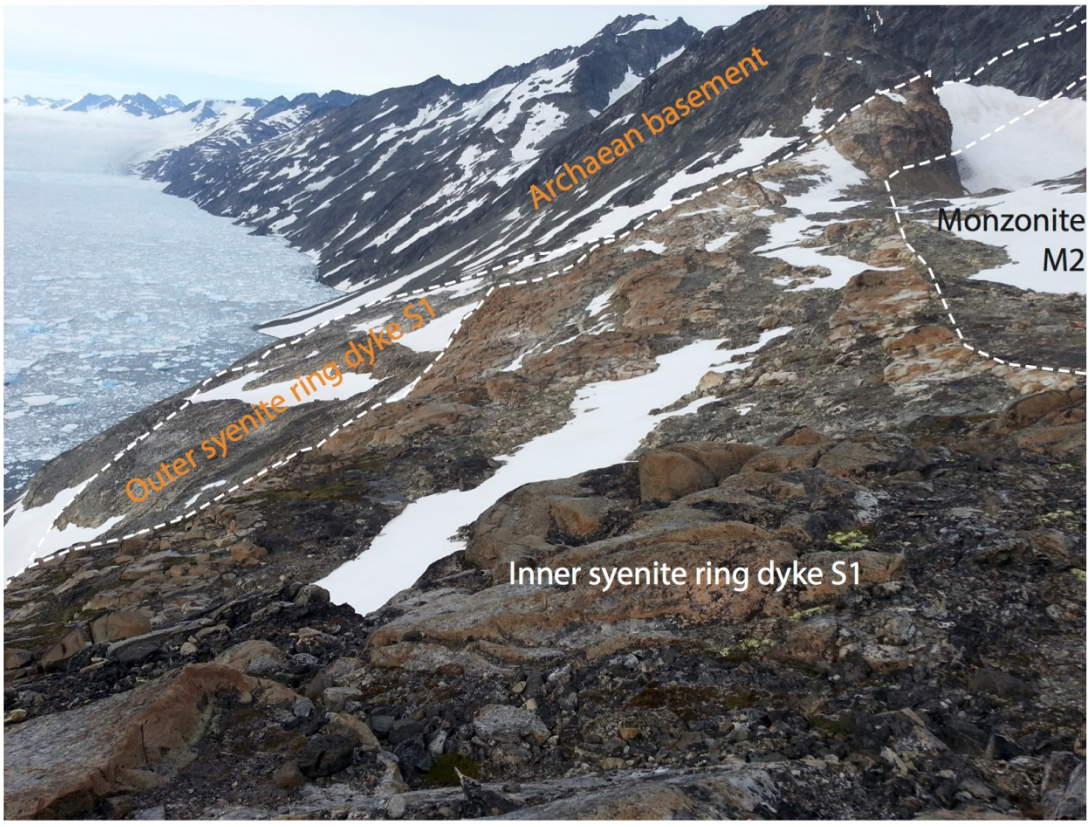

Figure 13.7 *View north showing the western part of the northern M2 monzonite surrounded by two generations of S1 syenitic ring dykes (inner and outer).*

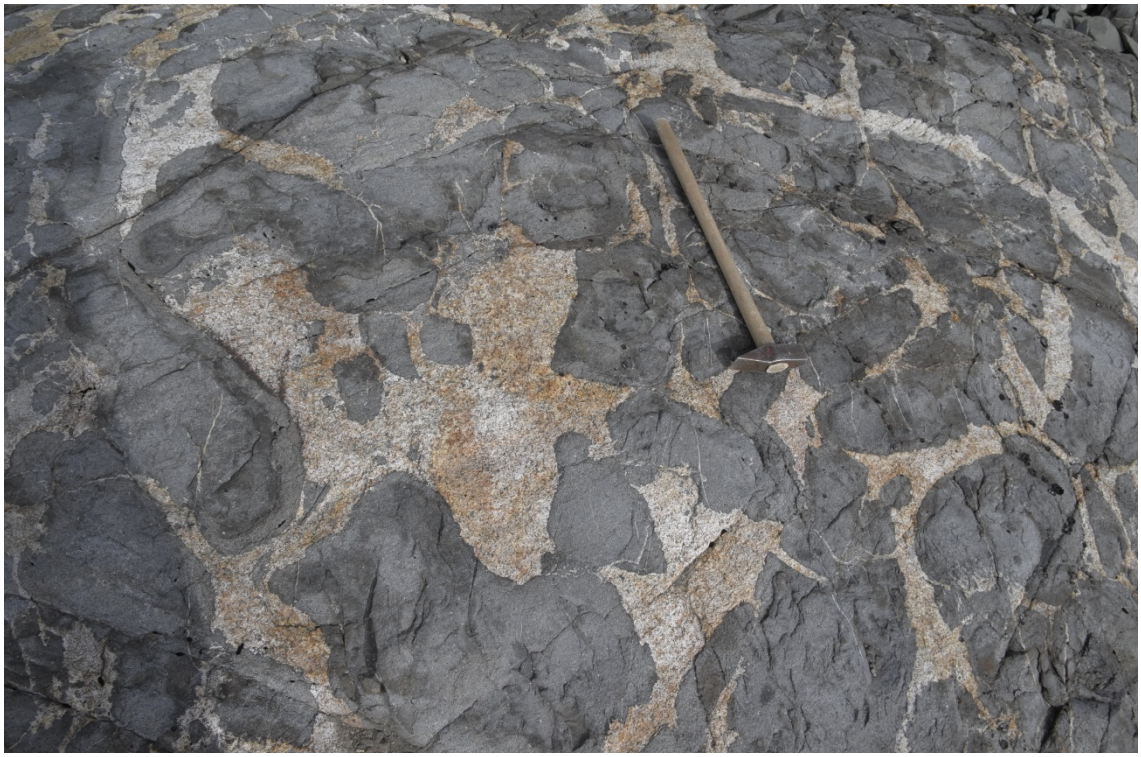

Figure 13.8 *Mafic-felsic pillow complex from close to the northern M2 monzonite pluton, Kap Gustav Holm.*

Granitic lithologies occur predominantly in the north-western part of the Kap Gustav Holm centre (Fig. 13.5B) as a composite pluton and associated ring dyke complex. Additionally Myers *et al.* (1993) reported the presence of numerous granitic sheets and ring dykes around the southern M2 monzonite pluton and up to Kap Bucholz app. 10 km to the north. The granite is generally fine-grained and hosts miarolitic cavities and patches of coarse pegmatite. Vuggy alteration and weathered sulphides are found close to the pegmatitic patches. Myers *et al.* (1993) noted that the contact between the two dominant granitic units, G1 and G2 (Fig. 13.5B) varies from sharp to cuspate, suggesting that both magmas existed in an unconsolidated state.

13.7 Kialineq Plutonic Centre

The Kialineq Plutonic Centre (Fig. 13.9), situated at 67°N, is a plutonic system of mafic, intermediate, felsic and net-veined rocks that document protracted and episodic stages of magma mixing, mingling, replenishment and emplacement. The area is poorly known due to its remoteness and extremely rugged, alpine topography, extensive ice-cover and intricate coastline (Fig. 13.10). Previous investigations in the Kialineq area have reported on the general geology and the petrology, geochemistry and geochronology of selected intrusions (Bernstein and Bird 2000, Brooks 1977, Brooks 2011, Brown and Becker 1986, Brown *et al.* 1977, Deer 1976, Gleadow and Brooks 1979, Kokfelt *et al.* 2015a, Nielsen 2002, Tegner *et al.* 2008), and portions of the plutonic centre were revisited in 2014 to improve the baseline knowledge of the area.

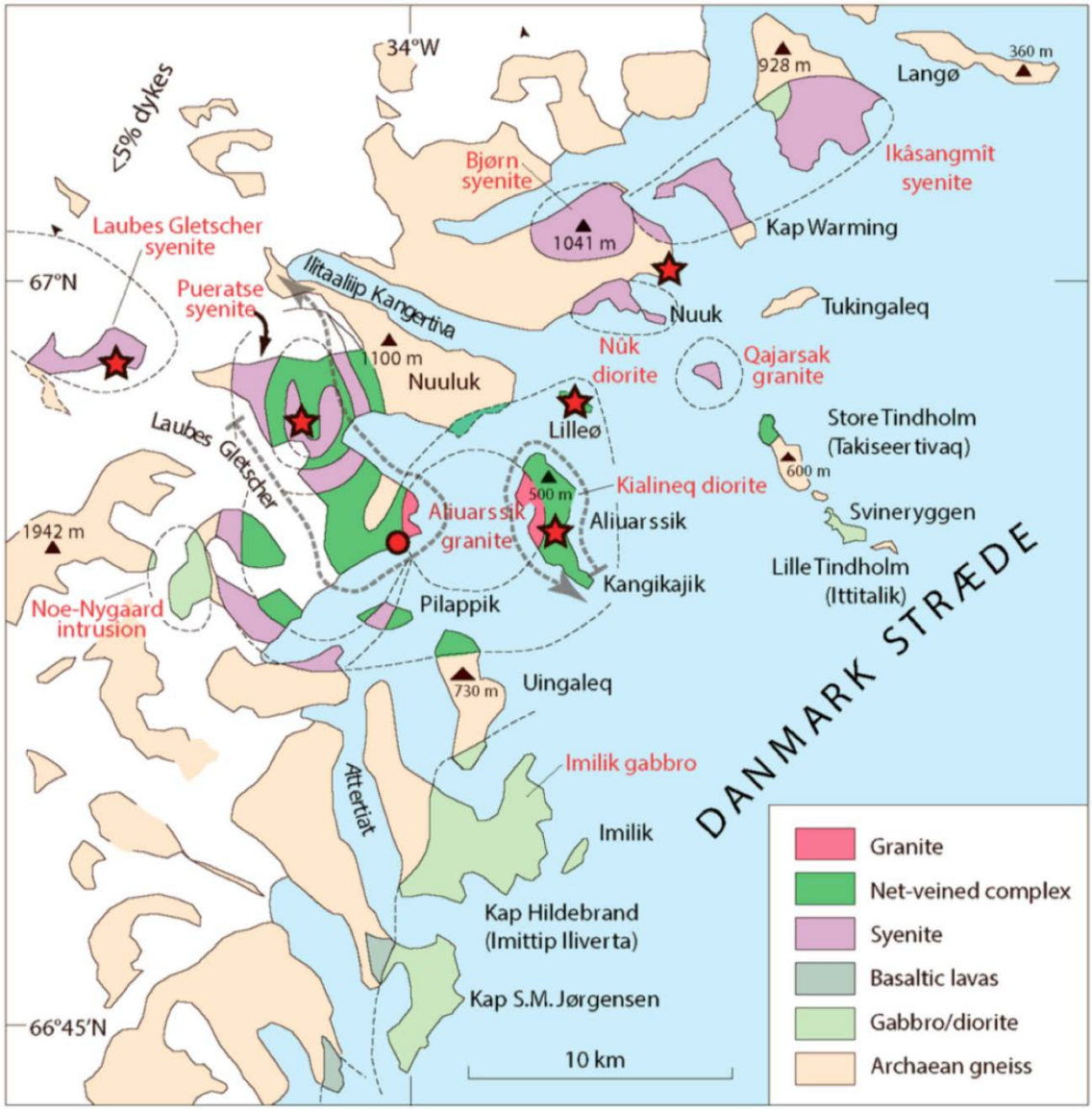

Figure 13.9 *Geological map of the Kialineq area. Geological localities are labelled in red text; corresponding geographical names are labelled in black text. Grey stippled lines indicate the suggested outlines of plutons. Thick grey dashed arrow indicates the flight path along which oblique photos were taken in 2014. Map is from Brooks (2011), after Bernstein and Bird (2000), and based on an unpublished map by D. Rex (pers. comm. 1985).*

The plutons within the Kialineq district are dominated by gabbroic, dioritic, syenitic and granitic rocks. Current mapping efforts (Fig. 13.9) suggest that individual plutons are roughly ellipsoidal in shape and up to 10 km in diameter. However, the Imilik gabbro in the south of the Kialineq district outcrops over a similar area, but is thought to be considerably larger (Brooks 2011). The plutonic rocks are often cut by aplite dykes, intrusion breccias, and are closely associated with a mafic-felsic pillow complex that is an important unit in the area (Fig. 13.11). The pillow complex generally consists of aphanitic basaltic to andesitic pillows with cuspate to crenulated, cauliflower-like margins that are surrounded by fine- to medium-grained felsic rock (Fig. 13.12A-C). Within this unit, pillows are typically elongate to irregular ellipsoidal in shape and tend to be aligned with their long axes parallel. This lithology

typically occurs as sheet-like bodies within diorite or syenite that can reach several hundred metres in thickness. In some cases, the host rock displays evidence for magmatic hybridisation by the presence of ghost-like or 'faded' blobs of slightly more mafic composition (Fig. 13.12D)(Kokfelt *et al.* 2015b). Sheets of mingled mafic-felsic material are often separated from the country rock by a thin layer of felsic material; the contact between the felsic and country rock is variable, sometimes changing from angular to cuspate over a short distance. In some places, larger bodies of felsic material intruded the country rock and contain miarolitic cavities, suggesting crystallization at relatively shallow depths. On-going work includes mineral barometry to obtain an estimate on the depth of intrusions in the Kialineq district.

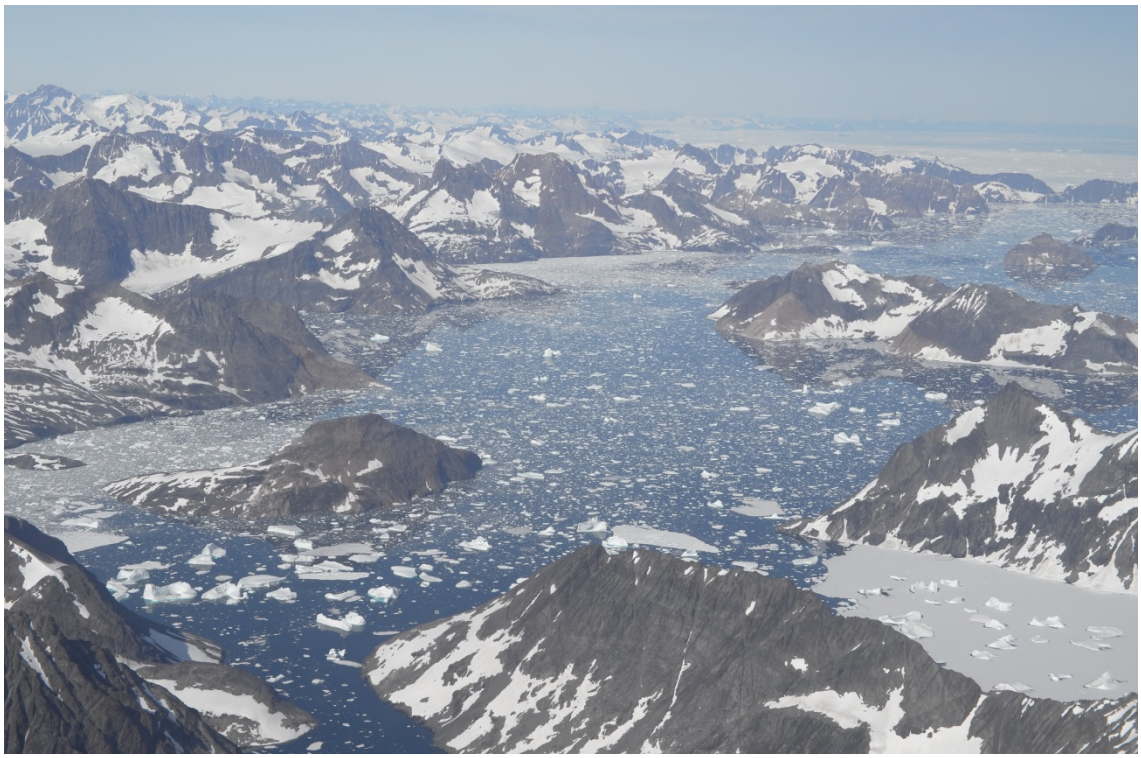

Figure 13.10 *Aerial view of the Kialineq district, looking northwest.*

Additional evidence for shallow processes is provided by a package of volcanic rocks exposed just north of Nuuk that are described by Brown and Becker (1986). The package is of uncertain thickness, but extends for several hundred metres along the coast (Fig. 13.13A). These rocks include a green, heterolitic tuff (agglomerate) that hosts a variety of centimetre-sized, rounded to angular lithic fragments that appear to be of volcanic and plutonic origin (Fig. 13.13B). Minor sulphide mineralisation is associated with this unit, although a more prominent, 20 m wide x 200 m long hydrothermal alteration zone close by contains sulphide blebs of pyrite-chalcopyrite-(arsenopyrite). Whole rock analysis of two mineralised and altered samples returned Cu values in the range 210-290 ppm, Zn values up to 6300 ppm, and Au concentrations up to 10 ppb (Poulsen 2016). The alteration mineralogy consists of sericite, chlorite, and minor epidote and is typical of phyllic and propylitic alteration assemblages found in magmatic-hydrothermal systems. It is speculated that the alteration zone represents a fluid conduit related to degassing of the intrusions and formation of some of the breccia bodies in the area.

Figure 13.11 *The mafic-felsic pillow complex at Aliuarssik.*

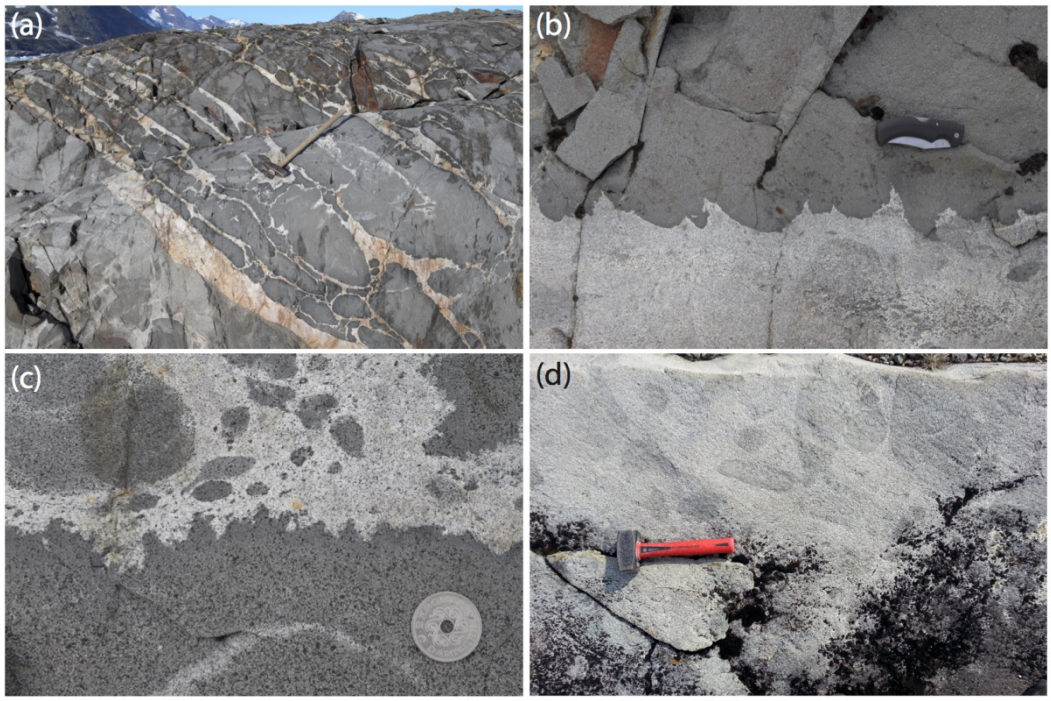

Figure 13.12 ***A.*** *Diorite sheets and pillows (dark grey) in a felsic matrix (light-coloured), Pilappik Island.* ***B.*** *Crenulated base of a diorite sheet (dark grey) in a felsic matrix (light-coloured), N of Laubes Gletscher.* ***C.*** *Crenulated contacts between diorite pillows (dark grey) and felsic matrix (light-coloured), N of Laubes Gletscher.* ***D.*** *Rounded, dioritic blobs (dark grey) in a slightly more felsic host diorite (lighter grey), Lille Ø.*

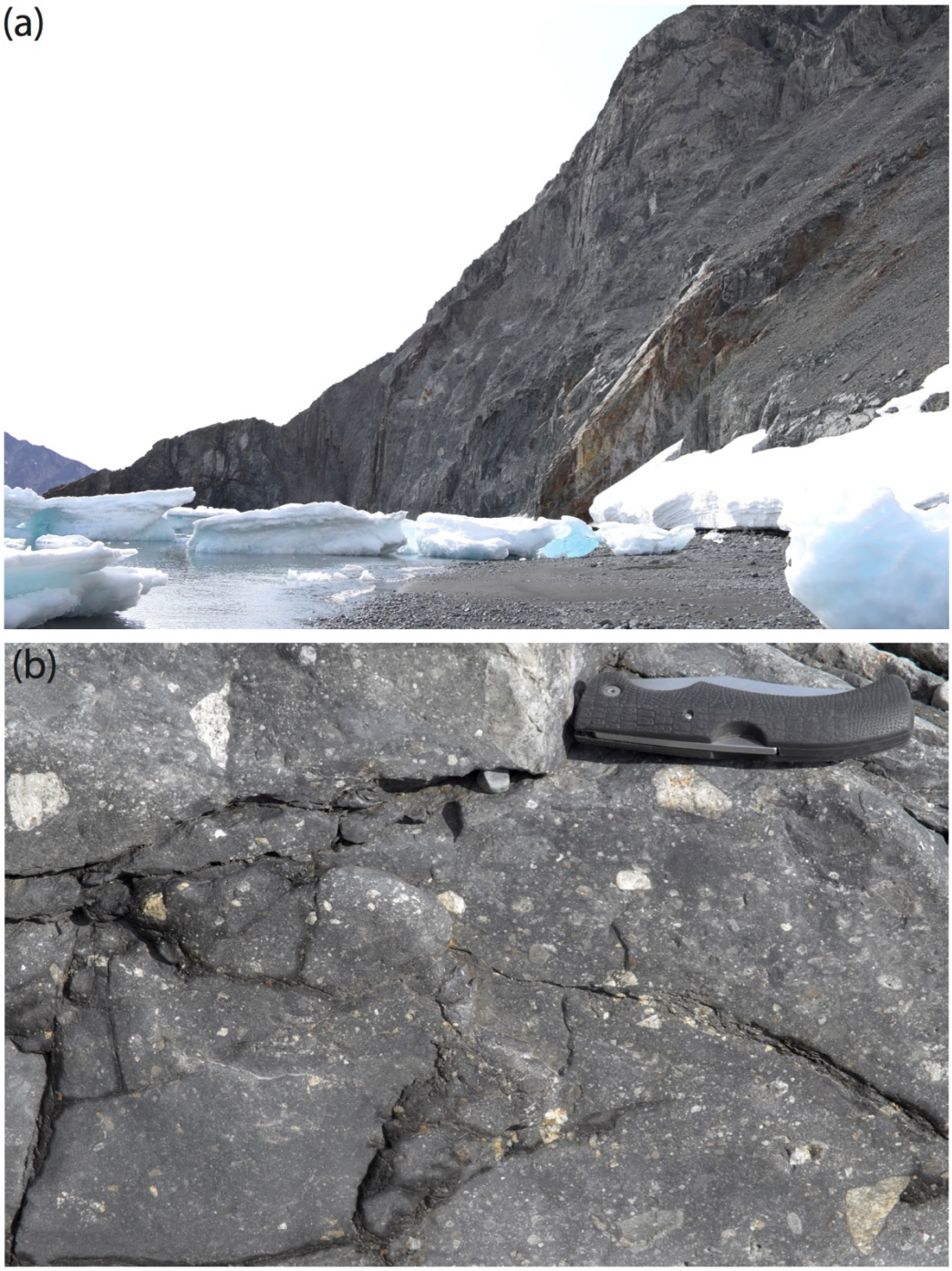

Figure 13.13 ***A.*** *Volcanic rocks at the headland NE of the old Nuuk settlement.* ***B.*** *Heterolithic tuff (volcanic agglomerate) showing a variety of rounded and angular lithic fragments that appear to be of volcanic origin. Headland of the peninsula north of the old Nuuk settlement.*

Previous geochronological work by Beckinsale *et al.* (1970), Brown *et al.* (1977), Gleadow and Brooks (1979), Tegner *et al.* (2008), and additional unpublished Rb-Sr isochrons, K-Ar and $^{40}Ar/^{39}Ar$ dates from D.C. Rex (summarised in Brooks 2011) reveal that the rocks of the Kialineq Plutonic Centre crystallized approx. in the interval of 37-35 Ma, with the youngest dates originating in the southern part of the district. Samples collected during the 2014 field season are currently being analysed to build on and test the present understanding of the

geochronology of Kialineq. New results from U-Pb dating of zircons include an age for the syenitic rocks at Laubes Gletscher of 35.30 ± 0.32 Ma, at Pueratse Fjord of 33.22 ± 0.21 Ma and a syenite clast in the volcanic rocks of 35.55 ± 0.18 Ma.

13.8 Sulugssut Intrusive Complex

Sulugssut is the southernmost known Palaeogene intrusive complex in East Greenland (Fig. 13.14). The complex, which was discovered by GGU in 1986, is little known due to its relatively inaccessible location in a glaciated alpine region close to the coast, and because of its limited exposure across a few narrow ridges that are separated by snowfields and glaciers. The Sulugssut complex measures approx. 5 km in diameter and consists of a silica-undersaturated plutonic core that, although variable in composition, is dominated tinguaites and ijolites. The complex hosts numerous associated dykes and sheets that are also silica-undersaturated.

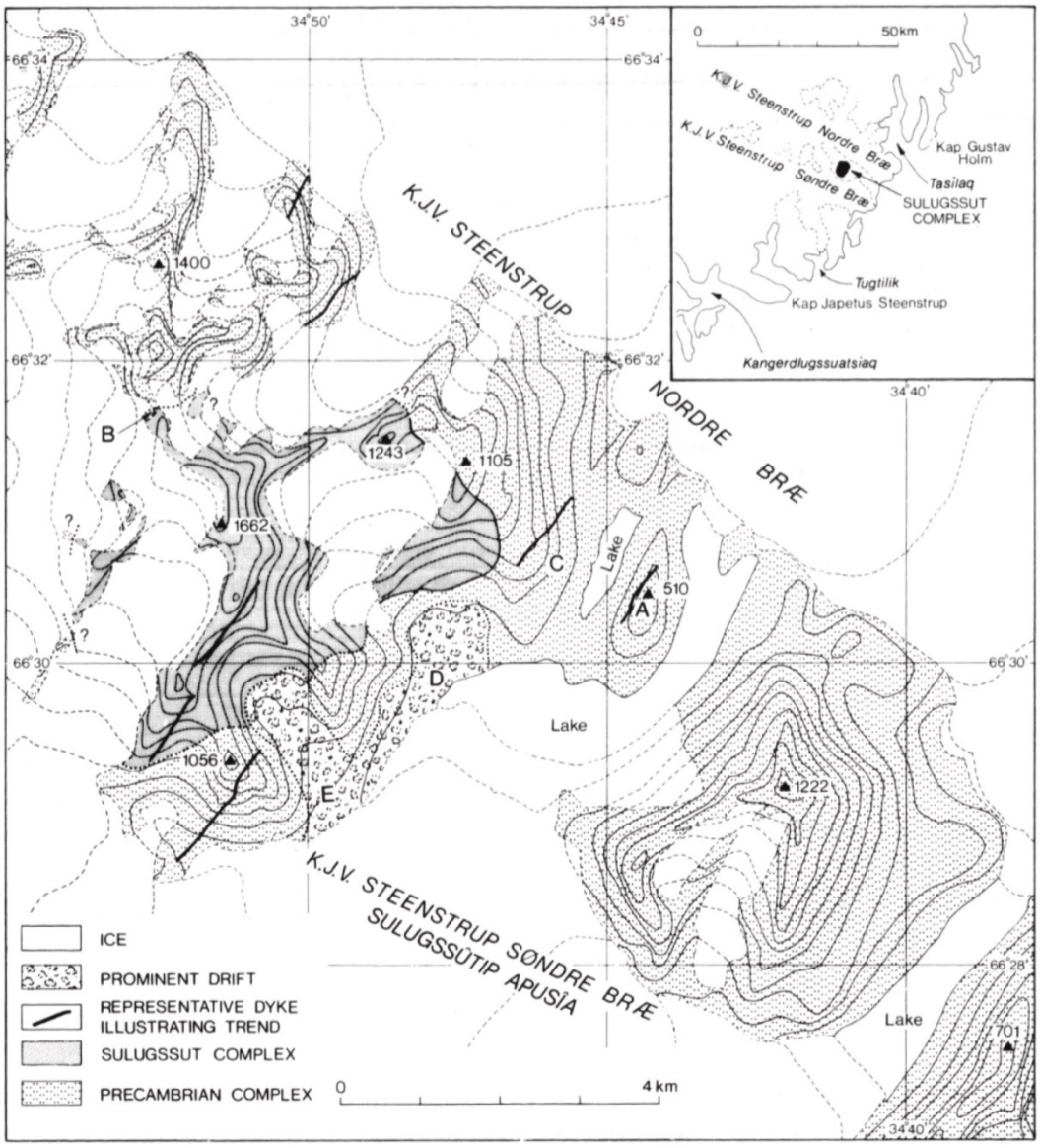

Figure 13.14 *Map of the Sulugssut intrusive complex from Brooks (1989). A-E indicate the localities visited in 1986. Contours are spaced at 100 m intervals.*

Brooks (1989) described three distinct types of dykes, all < 1 m wide within different areas of the complex: (1) grey porphyritic dykes with alkali feldspar and nepheline in the groundmass, (2) greenish, fine-grained trachytic to phonolitic dykes (tinguaites) and (3) rusty-brown weathering, dark coloured porphyritic dykes. Palaeogene alkaline dykes have also been described by Rucklidge *et al.* (1980) at Tugtilik, approx. 25 km SW of Sulugssut, and may possibly be related to the complex. The Sulugssut dykes trend NE-SE, cut the plutonic centre, and are hosted in highly strained, locally mylonitic, mid-grey granitic gneiss. The gneiss hosts metre thick sheets and enclaves of leucogabbro that comprises centimetre-sized plagioclase megacrysts set in a finer-grained groundmass of biotite and amphibole (Fig. 13.15A). Tholeiitic brown dykes belonging to the regional coast parallel dyke swarm also occur in the area but the crosscutting relationships with the Sulugssut dykes remain unclear. Ar/Ar dating of biotite from two dykes gives ages of 58.3 ± 0.9 Ma for the dyke swarm (Storey *et al.* 2007); thus the Sulugssut complex represents the earliest plutonic magmatism recorded from the East Greenland volcanic rifted margin.

Figure 13.15 ***A.*** *A 60 cm thick sheet of leucogabbro (spotted lithology) hosted in highly strained to mylonitic gneiss (blue-grey colour).* ***B.*** *A grey nepheline(?) porphyritic dyke, c. 80 cm wide that is distinct to the dykes studied by Brooks (1989).* ***C.*** *Close-up of the dyke in B. showing how the grey dyke is locally infiltrated by dark-coloured rocks with voids, possibly from dissolved carbonate.* ***D.*** *Lamprophyre dyke, hosted in basement gneiss, cut by sheets of carbonatite.*

During fieldwork in 2014, several additional dyke types were identified (Kokfelt *et al.* 2015a). Collectively, the Sulugssut dyke swarm includes nephelinites, foidites and phono-

lites that are locally cut by carbonatitic veinlets (Fig. 13.15B–D). Preliminary results from the new sample suite show large variability in bulk-rock composition and petrography even within separate dyke groups. Geochemically, Sulugssut shows similarities to the alkaline Gardiner Complex at the Kangerlussuaq Fjord, but is generally more evolved and does not contain any olivine. Electron microprobe analyses of augites in nephelinites and foidites show compositional gaps and changes in their fractionation trends. Together with Fe-Mg disequilibrium observed between phenocrysts and liquid compositions (estimated from bulk rock compositions), this points towards a highly dynamic system with several plumbing events (Lenskjold 2015).

14 Regional geochemical data

Bo Møller Stensgaard

14.1 Regional geochemical stream sediment surveys

A regional sampling for stream sediment geochemistry as well as surface/stream water hydrochemistry and glacial overburden till sampling for indicator mineral studies was carried out in 2009 and 2010 in preparation of the SEGMENT project (Fig. 14.1, Stensgaard 2014; Stensgaard *et al.* 2009, 2015). The data have been made public available via the online 'Greenland Mineral Resource Portal' (www.greenmin.gl). Only a brief summary of the some of the results of the regional geochemistry with focus on the mineral potential are included here. The stream sediment data together with the hydrochemistry and indicator mineral datasets and available geochemical company data should be analysed in greater details than the summary provided here.

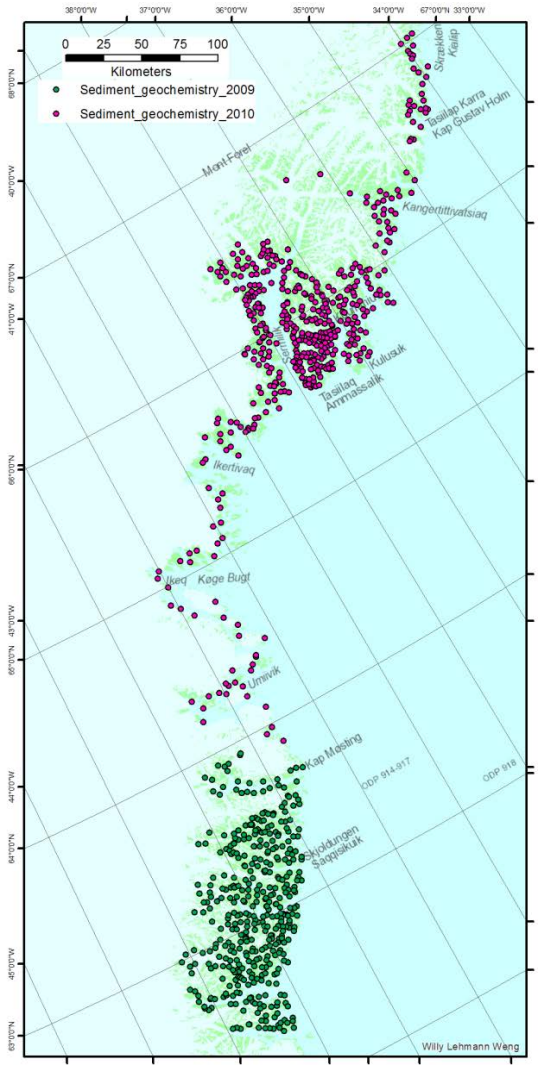

Figure 14.1 *Distribution of stream sediment localities in South-East Greenland from the regional sampling programs that were carried out in 2009 and 2010 prior to the SEGMENT project.*

14.1.1 Nickel, chromium, copper, platinum group elements potential

As also noted by Steenfelt (2013) elevated nickel, chromium, copper and titanium-dioxide within the Archaean and Palaeoproterozoic in western and South-East Greenland generally outlines areas with known belts of mafic metavolcanics (amphibolites and mafic granulites).

As illustrated in Fig. 14.2, the entire Thrym Complex, part of the North Atlantic Craton in the Skjoldungen region in South-East Greenland, forms the most persistent and most homogenous elevated chromium region within the Palaeoproterozoic and Archaean parts of Greenland and resembles, although a bit more diffuse, the chromium responses, found in the area south of Frederikshåb Isblink and in the area between Godthåbfjord and Maniitsoq in southern West Greenland. The combined nickel, chromium, copper and titanium-dioxide responses found in the Palaeoproterozoic Nagssugtoqidian parts of South-East Greenland in the Tasiilaq region resembles those that are found in the western-most area between Sukkertoppen Iskappe and Nordre Strømfjord in central West Greenland, an area which corresponds to the foreland and parts of the central zone of the Nagssugtoqidian orogen in West Greenland. This area is also characterised by amphibolite and granulite facies conditions, intense deformation, high amount of mafic and supracrustal units and intrusion of the Sisimiut Charnockite Suite that are thought to be related to the collisional orogenic event in the Nagssugtoqidian orogeny in central West Greenland. It is notable that the eastern-most part of the Nagssugtoqidian orogen, including part of the central core zone and the northern zone of the orogen in central West Greenland is low in all four illustrated geochemical elements in Fig. 14.2.

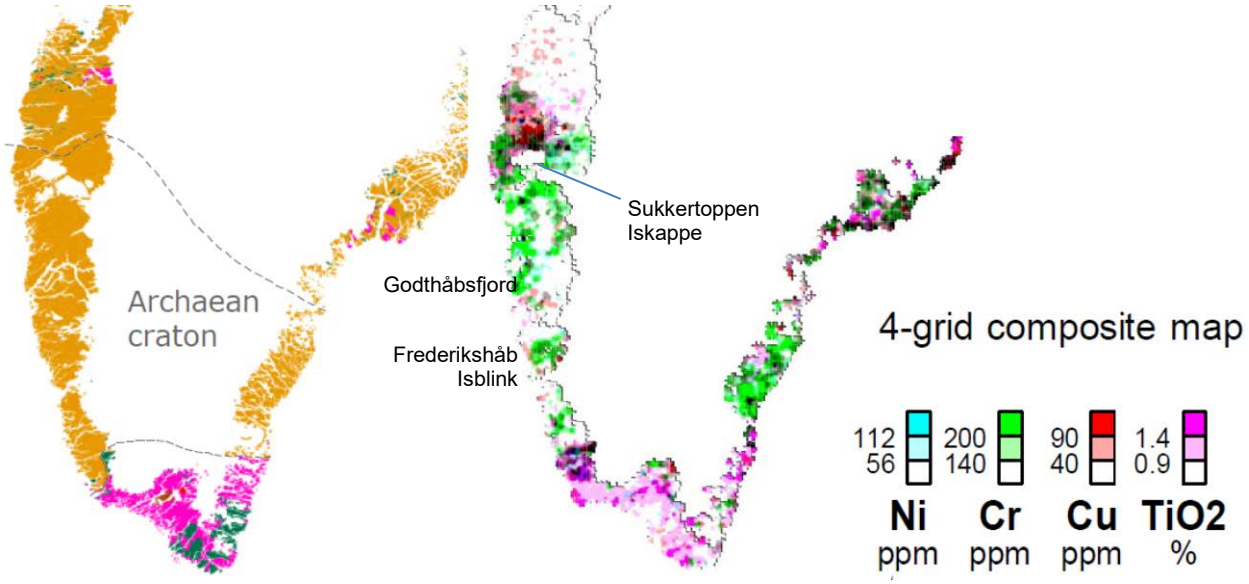

Figure 14.2 *Geochemical signature nickel, chromium, copper and titanium from regional stream sediment data within the Palaeoproterozoic and Archaean parts of West, South and South-East Greenland. From Steenfelt (2013).*

In the Palaeoproterozoic Nagssugtoqidian area and the northern part of the North Atlantic Craton area (Fig. 14.3) in South-East Greenland especially high chromium, copper and nickel in the stream sediments are reflecting areas with higher amounts of mafic supracrus-

tals/granulites/amphibolites units within the basement. The Ammassalik Intrusive Complex (1.89 Ga) and the Sermilik East Diorite (Imersivaq Intrusion, 1670 ± 5 Ma) is clearly reflected by high vanadium content in the stream sediment geochemistry. The mafic parts of the Ammassalik Batholith, which the Sermilik East Diorite (Imersivaq Intrusion) is suggested to be linked to, is also reflected by high vanadium whereas the more felsic part are low in vanadium. The Palaeogene igneous province is clearly mimicked by combined high vanadium, copper, chromium and nickel.

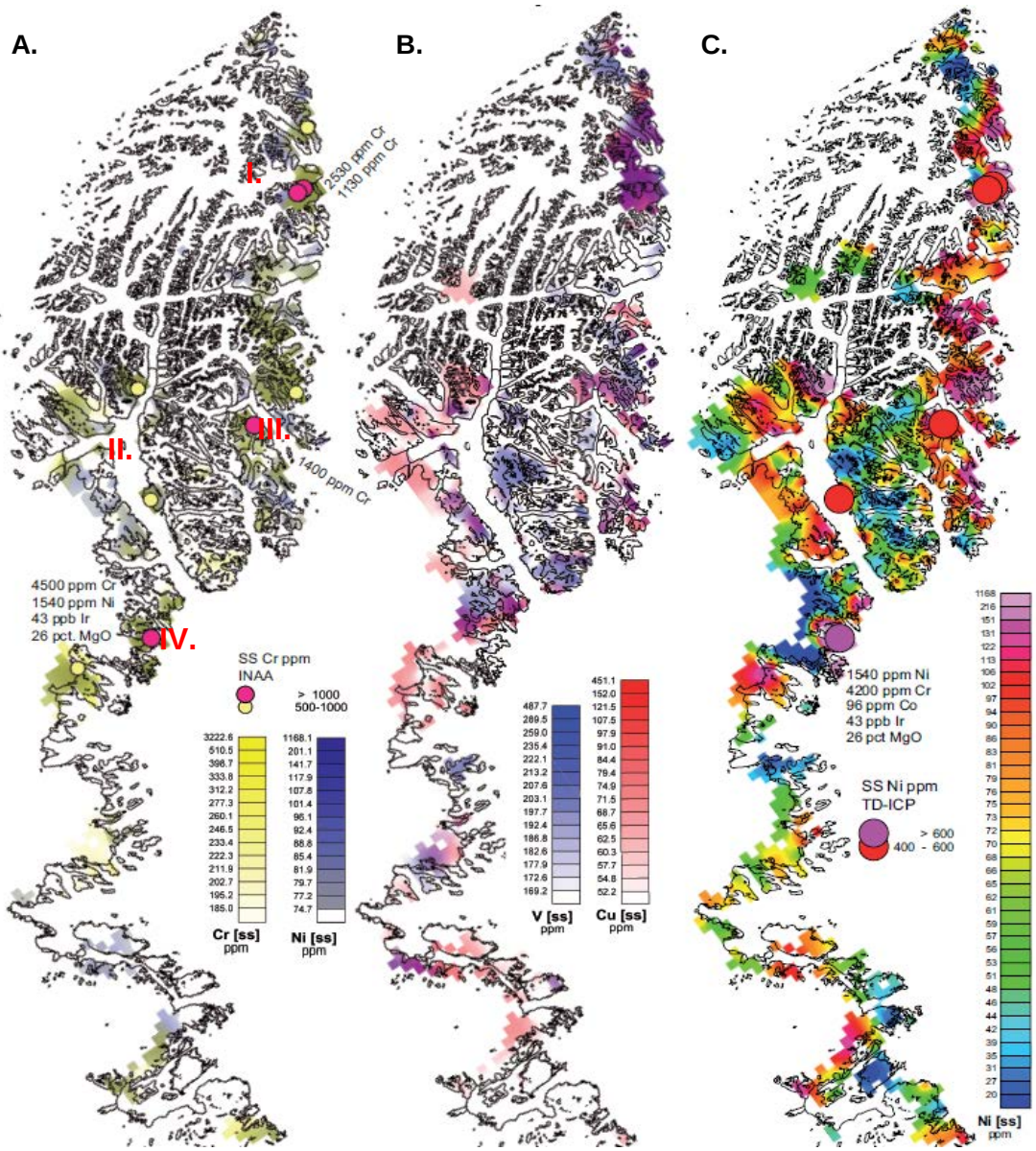

Figure 14.3 ***A.*** *Combined visualization of chromium and nickel grids,* ***B.*** *vanadium and copper grids and* ***C.*** *nickel grid separately. The grids are based on regional fine-fraction (< 0.1 mm) sediment geochemistry (mainly from stream sediment samples). Highest obtained values in Cr and Ni are indicated by coloured dots in A. and C. The roman numerals in red colour in A. refers to I. K.J.V. Steenstrup Nordre Bræ, II. Sermilik, III. Sermiligaaq and IV. Nattivit Kangertivat; all referred to in the text.*

The highest nickel values obtained are found at Nattivit Kangertivat, east shore in central part of Sermilik Fjord, west shore of inner part of Sermiligaaq Fjord and south of K.J.V. Steenstrup Nordre Bræ. The anomalous nickel values are also followed by some of the highest obtained chromium values. The ones at Nattivit Kangertivat, east shore in central part of Sermilik Fjord, west shore of inner part of Sermiligaaq Fjord (Fig. 14.3) all corresponds to areas with mafic supracrustal units; the area at Nattivit Kangertivat also contains larger ultramatic bodies. The two anomalous samples at K.J.V. Steenstrup Nordre Bræ drains the area that are characterised by Archaean basement (orthogneiss) intruded by the Palaeogene Sulugssut Intrusive Complex (dykes complex) and Palaeogene coast-parallel dyke swarm and could reflect ultramafic or mafic components from the later of the two.

For the southern area of the North Atlantic Craton the mafic granulites of the Thrym complex along the Søndre Skjoldungensund, the inner part Bernstorff Isfjord and the area north of Bernstorff Isfjord is characterised by high copper, nickel, Ni/Mg-ratio and chromium (Fig. 14.4). These areas correspond to the area with known nickel mineralisation within mafic to ultramafic bands (see section 15.1). The Skjoldungen Alkaline Province (SAP) is characterised by general lower copper, nickel and chromium, but relative higher vanadium compared to the area north of SAP. The region south of SAP, between Kassortoq and Timmiarmiut, is characterised by high vanadium, chromium and nickel. This is believed to originate from the high content of mafic enclaves/rafts in the otherwise orthogneiss dominated region.

14.1.2 Gold potential

Several gold-bearing samples from the public hunt for minerals program, Ujarassorit (Fig. 14.5, Petersen and Thomsen 2014), as well as some anomalous gold values in stream sediment sampling campaigns by NunaMinerals A/S in 1996 (Lie 1997) indicates a potential for gold in the Tasiilaq region.

This is also supported by the findings in the new GEUS-MMR stream sediment geochemistry dataset in which both elevated gold and gold-pathfinder elements such as arsenic and caesium also are found (Fig. 14.6).

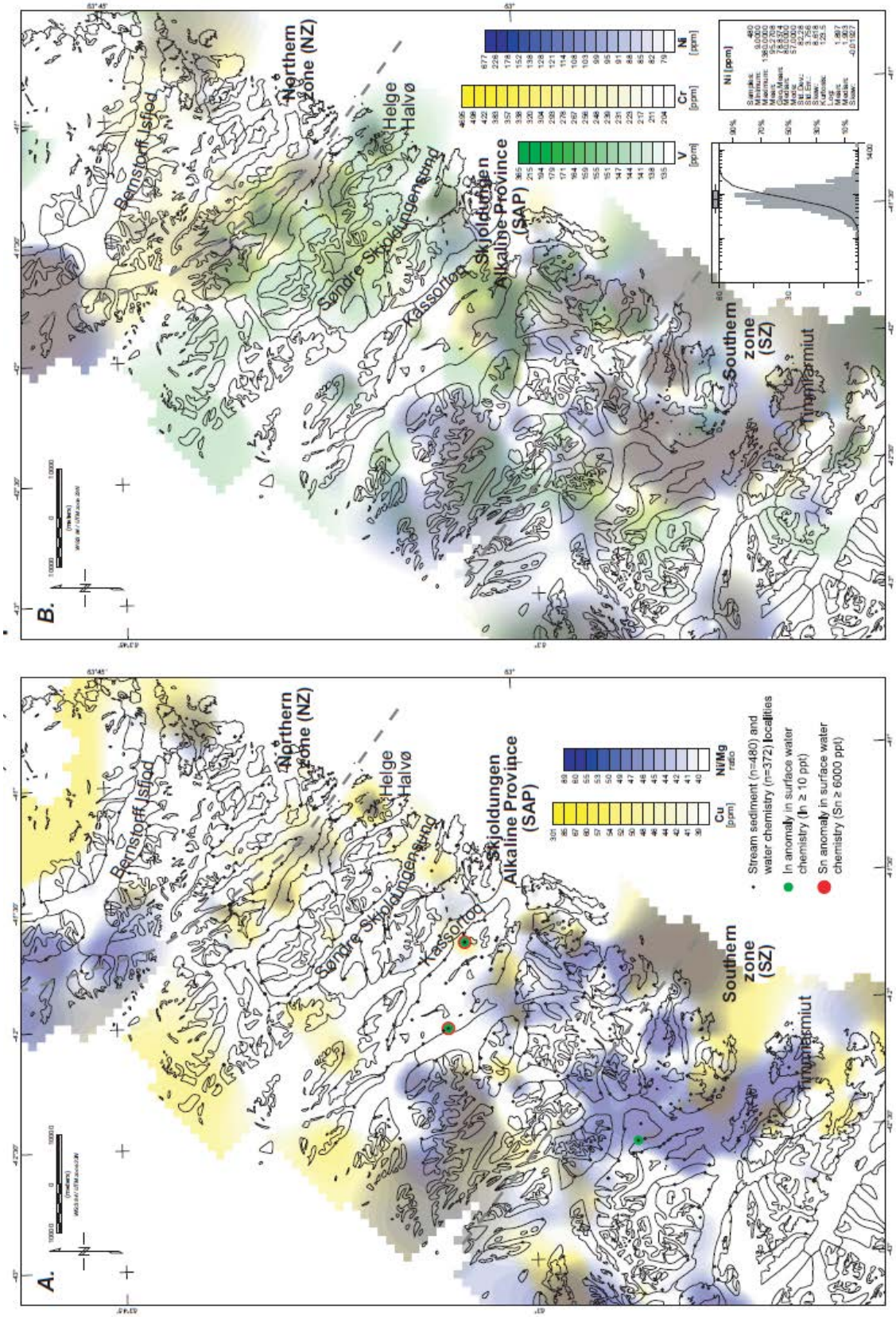

Figure 14.4 ***A.*** *Stream sediment geochemistry plot of copper (yellow) grid with transparent plot of Ni/Mg ratio grid (blue) on top. Sample localities are plotted on top together with anomalous Sn and In from surface water chemistry.* ***B.*** *Stream sediment geochemistry plot of vanadium plotted with transparent chromium (yellow) and nickel (blue) on top.*

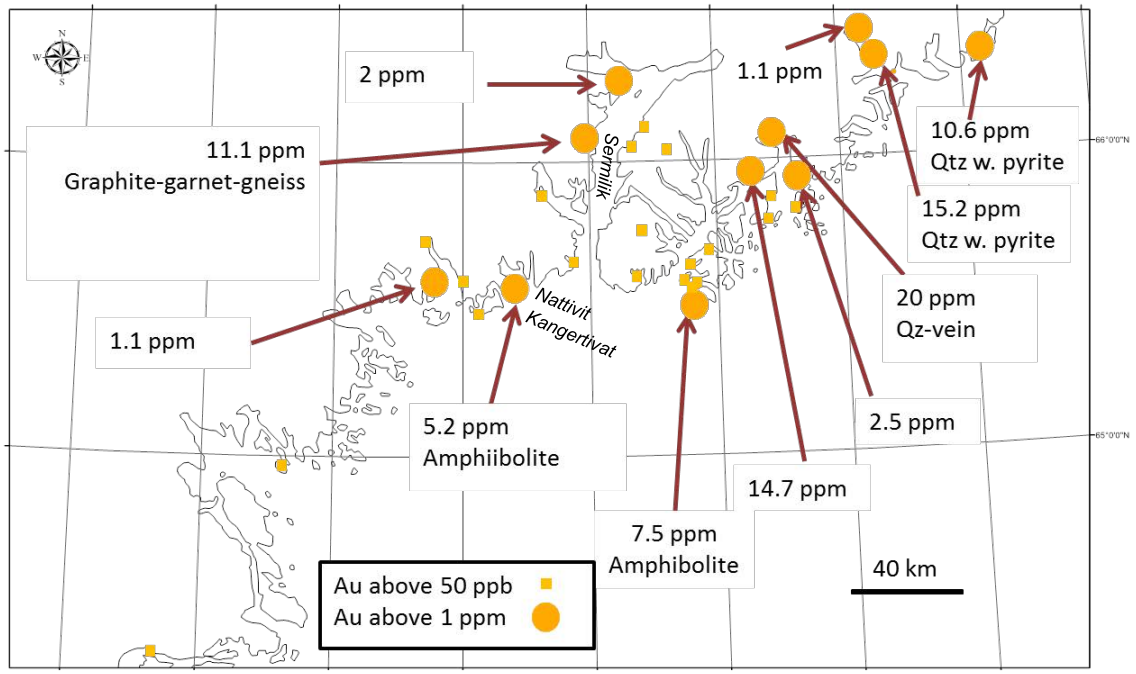

Figure 14.5 *Gold from analysed Ujarassiorit rock sample. The Ujarassiorit samples cover samples from the years 1989-2013. The samples are reported as being both floats and in-situ bedrock samples; due to the nature of the public hunt for minerals program the exact sample localities are often insufficiently recorded. Figure from Petersen and Thomsen (2014).*

Especially the supracrustal dominated and contact affected aureole areas south and north of the Ammassalik Intrusive Complex (AIC) as well as areas at Nattivit Kangertivat and east and west of the central part of Sermilik Fjord is characterised by having clusters of samples with elevated gold (30-190 ppb Au) within areas characterised by also high traditional gold-pathfinders elements such as arsenic and/or caesium. Other elements, that also can be considered as gold-pathfinder elements, such as molybdenum and tungsten (Fig. 14.7), are also found to be elevated in some of the gold-arsenic-caesium elevated areas. The highest encountered gold in a stream sediment sample (190 ppb Au) within the Tasiilaq region is located in the northern-western part of the contact aureole that envelope the Tasiilaq Intrusive Centre; an area that also is characterised by intense shearing. A follow-up field investigation during SEGMENT 2014 fieldwork failed to identify an in-situ gold mineralised setting in this area.

No notable elevated gold or arsenic (highest content being 35 ppb Au, Figs 14.8 and 14.9) have been encountered in the stream sediment geochemistry from Skjoldungen region although there might be a small cluster of samples with elevated elemental values at Timmiarmiut in the southern part of the Skjoldungen region.

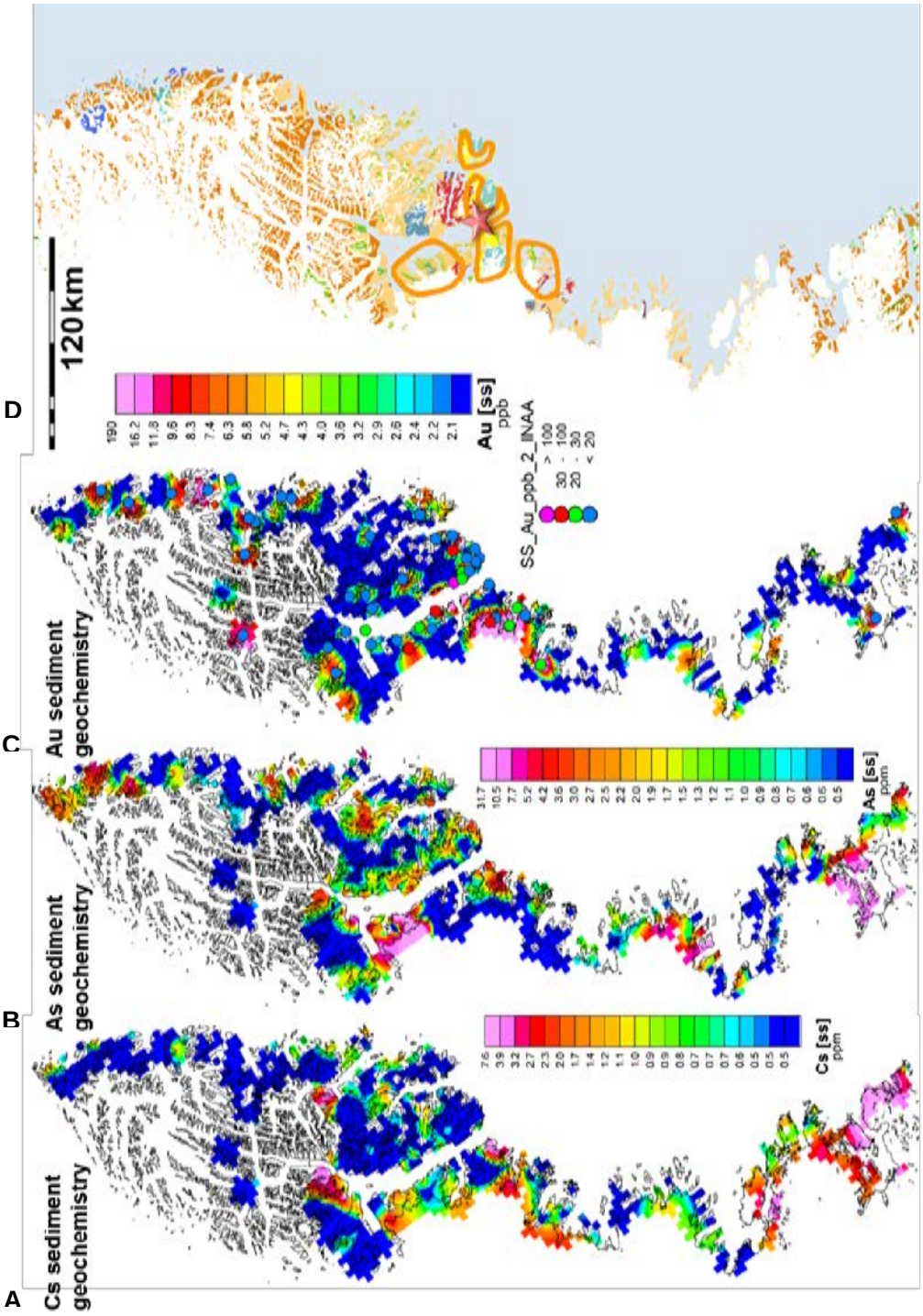

Figure 14.6 *Gridded regional stream sediment geochemistry distribution of **A.** caesium, **B.** arsenic and **C.** gold with indication of highest anomalous gold. **D.** The geological map with indication of areas that according to the three gridded geochemical distributions are judged to be most potential for gold.*

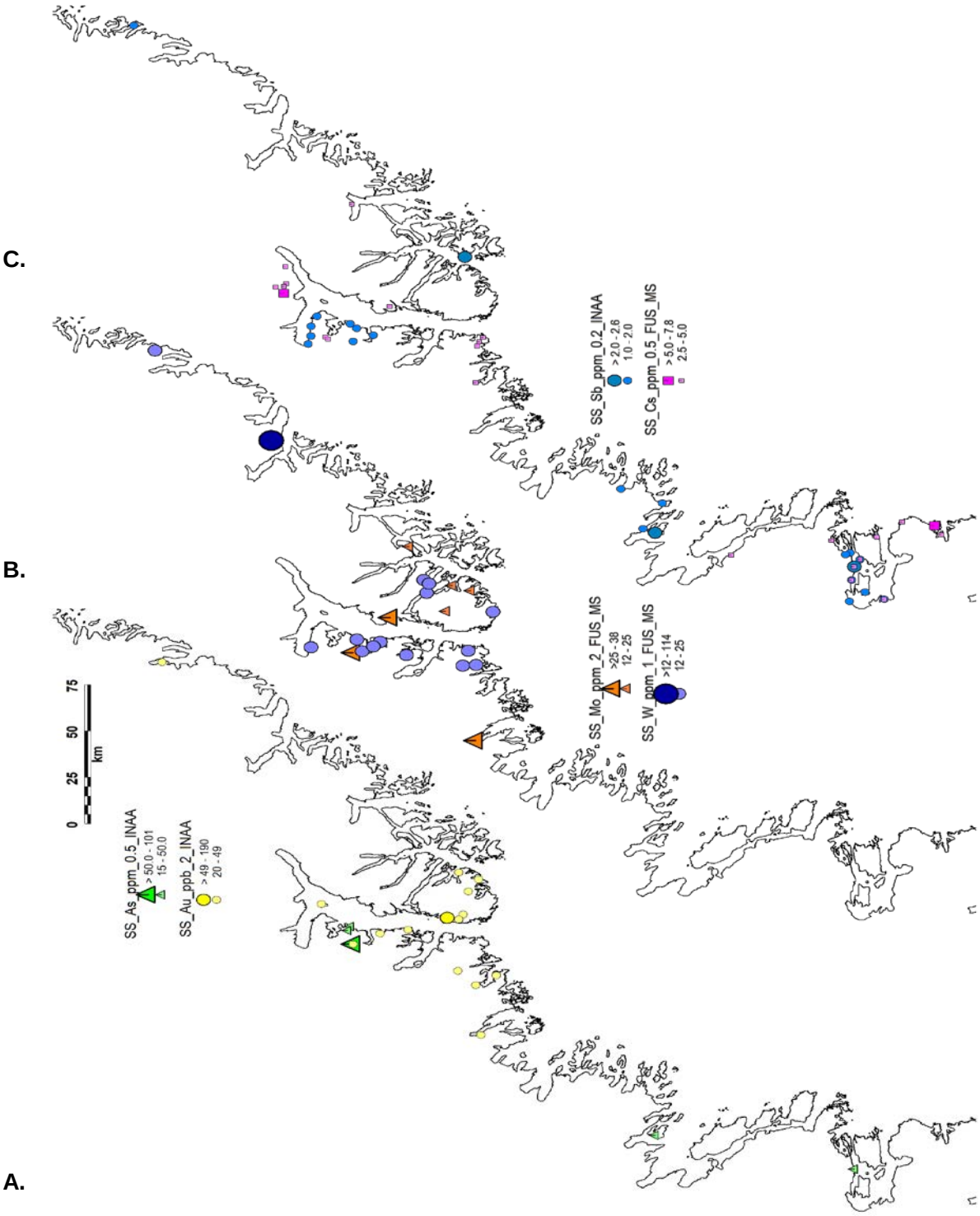

Figure 14.7 *Distribution of individual stream sediment samples that are elevated in **A.** As, Au, **B.** Mo, W, **C.** Sb and Cs. A relationship between samples with high values of these elements is observed in several areas throughout the Tasiilaq region.*

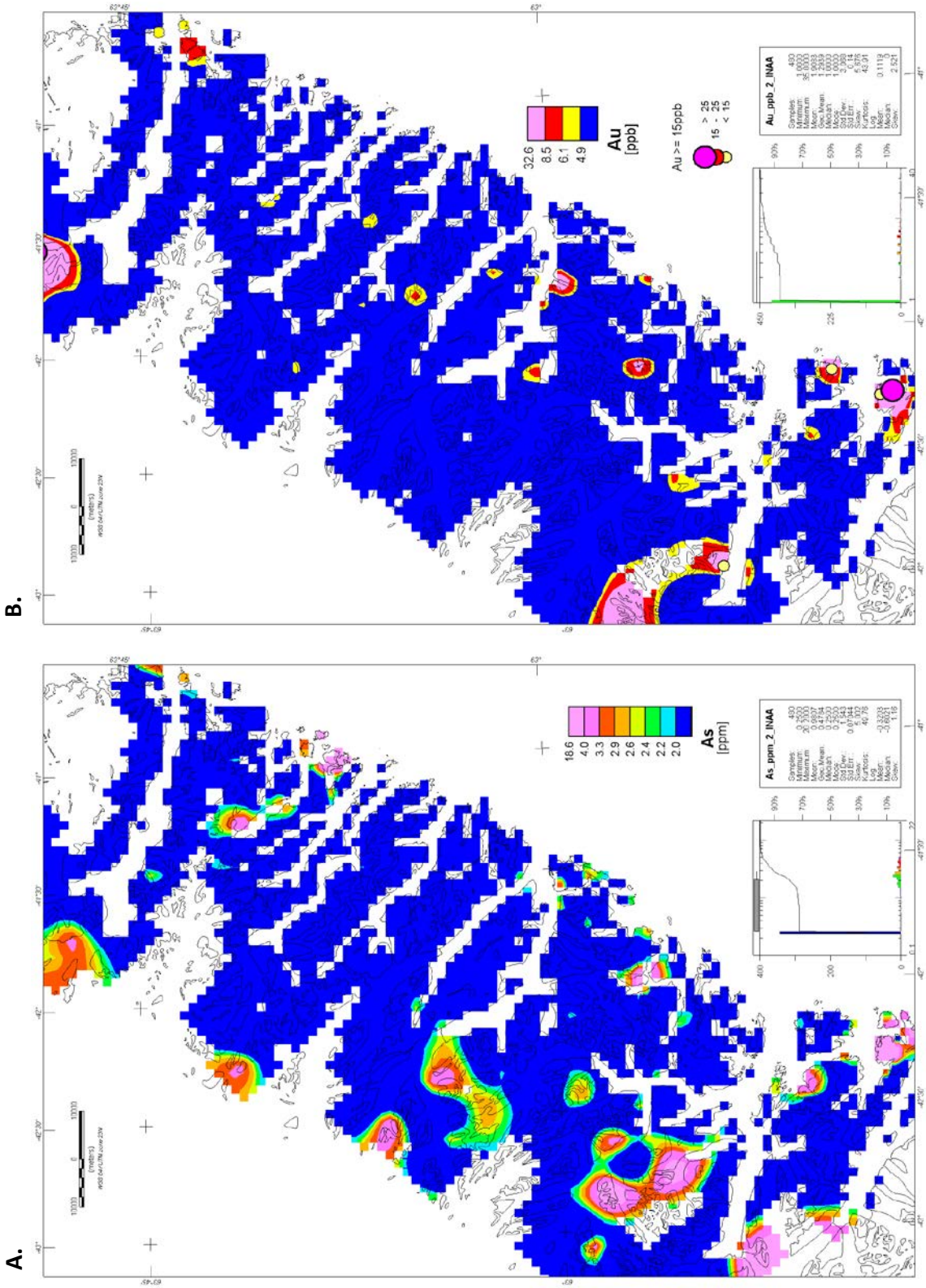

Figure 14.8 *Distribution of **A.** arsenic and **B.** gold in the stream sediment geochemistry data from the Skjoldungen region. No notable highly elevated gold or arsenic is encountered in the region.*

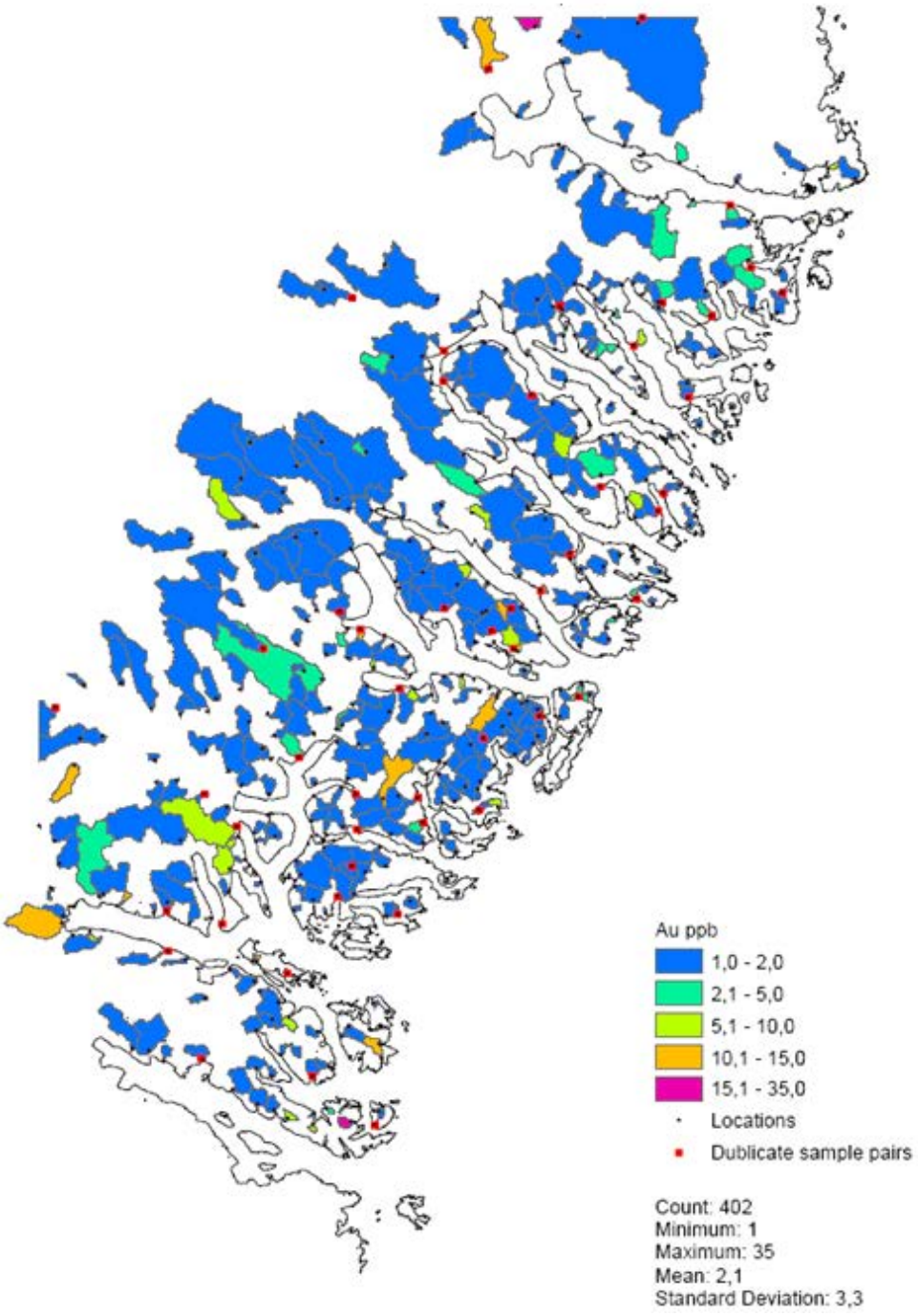

Figure 14.9 *Distribution of gold in stream sediment geochemistry plotted on the basis of water sheds (drainage basins) derived from an analysis of the digital terrain model for the Skjoldungen region.*

14.1.3 Stream sediment geochemistry mapping of intrusive phases

The Ammassalik Intrusive Complex contrast to surrounding gneiss and supracrustal dominated areas. Especially high phosphor (Fig. 14.10) but also europium and to some extend also barium and strontium (Fig. 14.11) reflect the Ammassalik Intrusive Complex (III, IV and V in Fig. 14.10). The region further to the north that hosts the Palaeogene Sulugssut Intru-

sive Complex and the Palaeogene Kialineq Plutonic Centre (I and II in Fig. 14.10) is also characterised by elevated to high phosphor and europium and in addition niobium. The Palaeogene area is in general characterised by high titanium (Fig. 14.11).

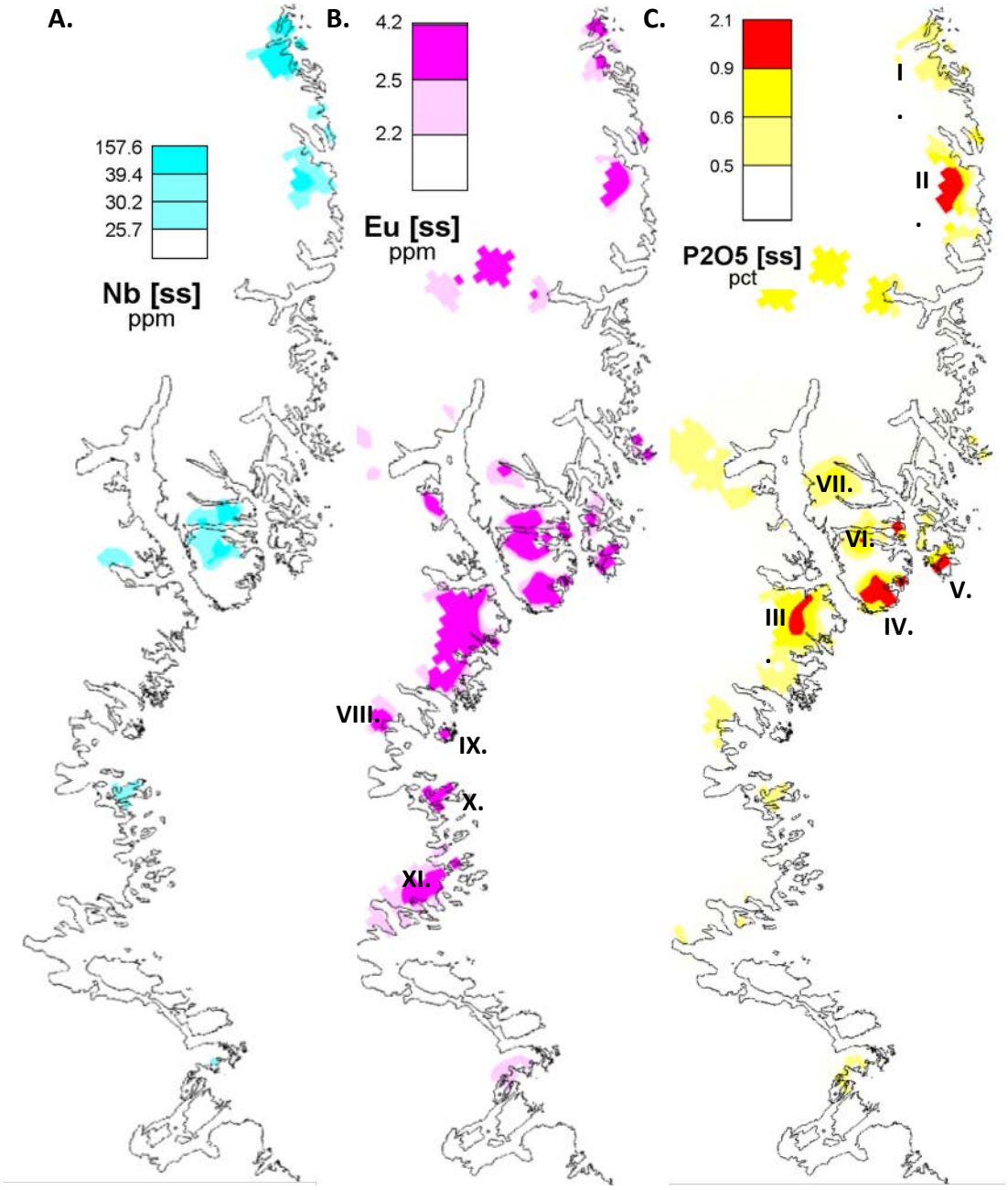

Figure 14.10 ***A.*** *Niobium,* ***B.*** *europium and* ***C.*** *phosphor distribution from region stream sediment geochemistry mimicking areas characterised by intrusive phases and activities. The roman numerals in B. and C. refer to I. Kialineq Intrusive Centre, II. Sulugssut Intrusive Complex, III. The Johan Petersen Intrusive Centre, IV. The Tasiilaq Intrusive Centre, V. The Kulusuk Intrusive Centre (the later three intrusive centres belongs to the Ammassalik Intrusive Complex), VI. The Ammassalik Batholith, VII. The Sermilik East Diorite intrusion (Imersivaq Intrusion; part of the batholith), VIII. + IX. North of Isortoq diorite and granite (contemporaneous with ages of the Ammassalik Batholith), X. + XI. Anomalies that cannot be related to exposed intrusive lithologies.*

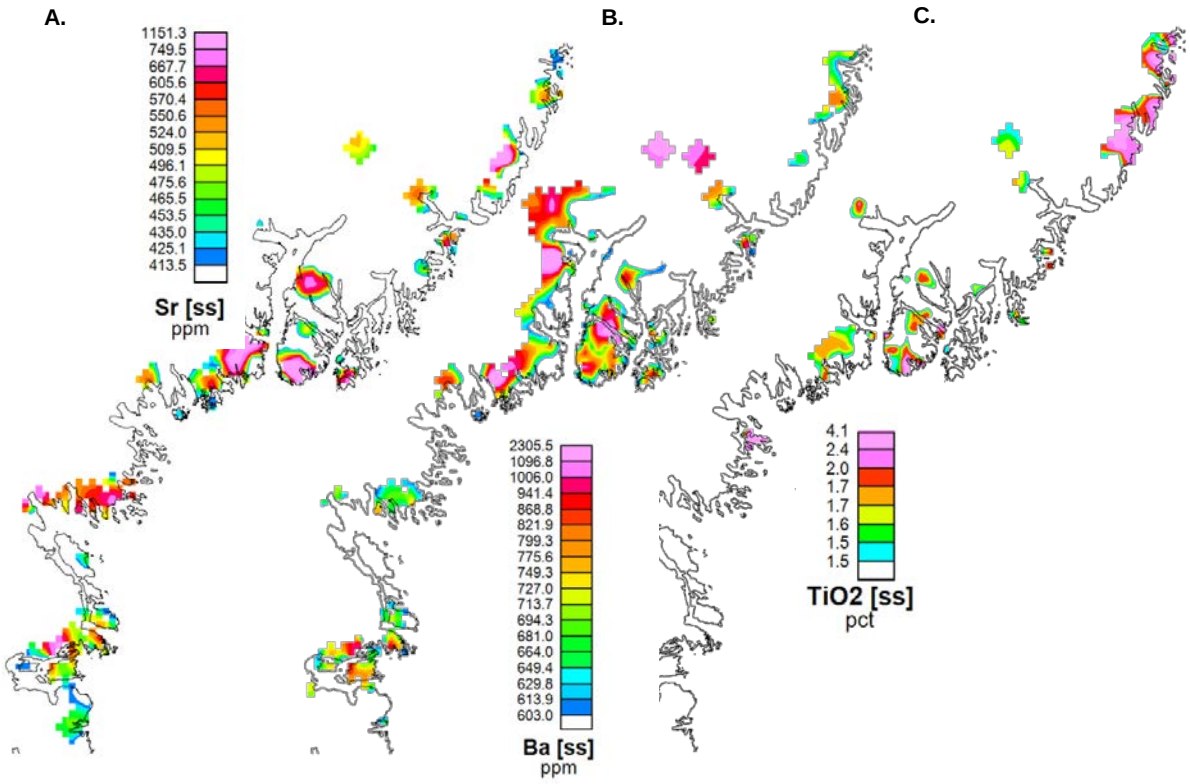

Figure 14.11 *Stream sediment geochemistry distribution of **A.** strontium, **B.** barium and **C.** titanium-dioxide.*

The Ammassalik Batholith centred on the northern part of Ammassalik Island and the fjord Ikaasrtivaq, is also clearly mimicked by the stream sediment geochemistry with areas being high in niobium, europium, but only moderate phosphor (VI in Fig. 14.10). Areas of the batholith is furthermore high in titanium-dioxide (Fig. 14.11.C)

Part of this Ammassalik Batholith is also characterised by high ytterbium, yttrium and lanthanum (Fig. 14.12) although this feature also extend into and characterised the contact aureole that envelopes the intrusive centres of the Ammassalik Intrusive Complex which also yield extremely high yttrium and general high rare earth elements (grids of rare earth elements are not shown). The high ytterbium, yttrium, lanthanum and rare earth elements it thought to be a product of the high garnetization and extensive hydrothermal activity that characterise the contact metamorphosed contact aureole enveloping the Ammassalik Intrusive Complex.

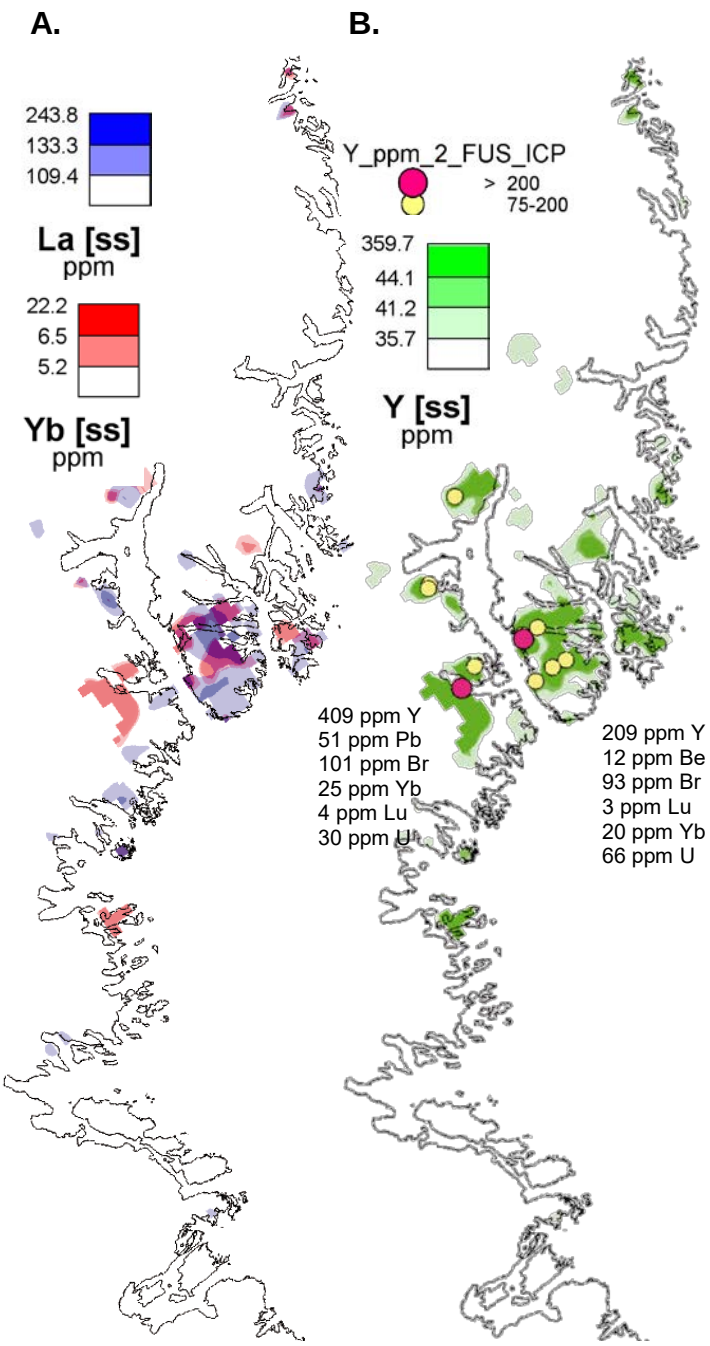

Figure 14.12 *Distribution of **A.** lanthanum, ytterbium and **B.** yttrium with selected geochemical content of the samples that have the highest content of yttrium.*

The Sermilik East Diorite (VII in Fig. 14.10), which is suggested to be the northernmost part of the Ammassalik Batholith, lacks elevated niobium, ytterbium, yttrium and lanthanum (Fig. 14.12) which otherwise characterise lithologies from the Ammassalik Batholith exposed further to the south. Instead, the Sermilik East Diorite shows highly elevated strontium (Fig. 14.11) and in that respect resembles the Ammassalik Intrusive Complex.

At Isortoq, high europium, elevated phosphor (VIII and IX in Fig. 14.10) together with high strontium, barium (Fig. 14.11) and elevated lanthanum, ytterbium and yttrium seem related to diorite and granites that are contemporaneous with the Ammassalik Batholith.

South of Isortoq two other areas X and XI Fig. 14.10 are characterised by elevated to high high niobium, europium, phosphor, strontium and titanium-dioxide; see also Fig. 14.11 and Fig. 14.12). This signature resembles that of the other intrusive lithologies of the region. However, no know sources for these anomalies have been located.

In the Skjoldungen region of the North Atlantic Craton the SAP is mimicked by the stream sediment geochemistry by combined elevated to high content of niobium, tantalum and yttrium (Fig. 14.12). Especially the areas dominated by the late granites, syenites along the Skjoldungen Ø trend of intrusives are clearly mimicked by high content of all three elements. Also the Singertât Complex at Kassortoq and areas south of Kassortoq on Kong Dan Halvø dominated by syentitic gneisses and syenite to syenitic gneiss in the Skirner Bjerge are clearly outlined by the three elements in combination.

A further area that is high in the three elements is a zone from the southern part of the island Timmiarmiit to outer parts of the fjord Sikuijivitteq, centered on the Timmiarmiut Island (Fig. 14.13). Besides smaller tabular and plugs-like Ketilidian intrusions of appinitic (hornblende-rich), gabbroic to dioritic intrusions at the peninsula north of the outer part the fjord Sikuijivitteq this area contains WSW-ENE trending Gardar dykes (Bartels *et al.* 2016) than could explain the elevated elemental abundancies. However, another likely explanation is the occurrence of post-tectonic ultramafic dikes (lamprophyres) and small alkaline diorite-carbonatite dykes or ovoid bodies of the Timmiarmiut Alkaline Province (Kolb *et al.* 2012). Also notable is the reported deformed and metamorphosed up to 40 m wide carbonatite dykes/horizons that are intruded/interleaved with orthogneiss in a 400 m wide N-S trending corridor on Timmiarmiut Island (Tukiainen, 2014).

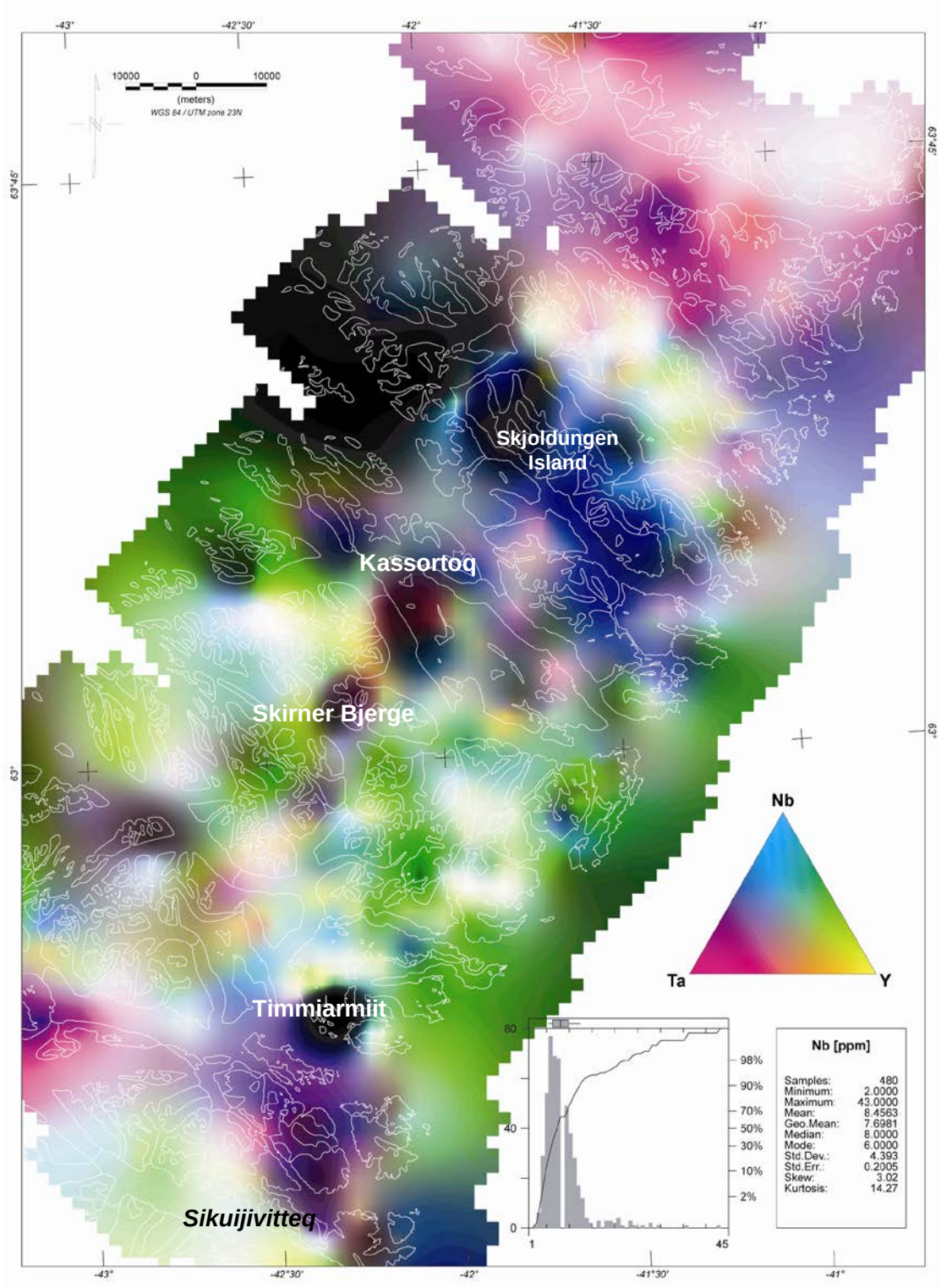

Figure 14.13 *Combined ternary-plot of stream sediment distributions of tantalum, niobium and yttrium. High content in all three elements will be black or blackish while low content in all three elements will be visualized as white or dull colors.*

15 Regional geophysical data

Bjørn H. Heincke

15.1 Data acquisition and data description

In 2012 and 2013 two airborne magnetic surveys were collected for GEUS along the East Coast from Greenland (Rasmussen 2013, Rasmussen *et al.* 2013, Riisager and Rasmussen 2013). These surveys are a continuation the AEROMAG project that started in the early 1990s. Within this project the complete ice-free area of West, South and South-East Greenland were systematically covered by airborne magnetic data with comparable acquisition parameters. This result is a consistent high-quality and high resolution aeromagnetic data compilation from the Svartenhuk Peninsula (72°N) in Western Greenland, down to the southern tip of Greenland (Kap Farvel, ~60°N) and up along the East Coast to 67°30'N.

The two new 2012 and 2013 surveys cover the remote coastal area of East Greenland from Kap Cort Adelaer (61°45'N) in the south to the area around Kap Gustav Holm in the north (67°30'N; see Figs 15.1 and 15.2). EON Geosciences Inc. gathered these data with a fixed wing airplane and made also the subsequent basic processing. The surveys were carried out by flying along a gently draped surface 300 m above the ground. The main flight direction for the 2012 and 2013 survey was oriented NNE-SSW and NE-SW, respectively, and flight separation of the parallel line was 500 m for both surveys. In addition, tie-lines with 5000 m separation were flown in an orthogonal direction. The southern part of the 2013 survey covers in addition to the ice free onshore region, also a significant part of the nearby offshore shelf region.

Quality of the final processed data is excellent and no leveling artefacts are observed even on the higher derivatives. However, particularly the southern part covered by the 2012 survey is characterised by rough topography. Many mainly NW-SE to WSW-ESE running fjords and narrow valleys prevent everywhere constant and small terrain clearance and distances from the ground > 1500 m occur in a number of places (see Fig. 15.3). This is critical for the interpretation, because weakening of magnetic anomalies in these areas is mainly associated with large source distances and less with variations of the magnetization in the ground. Therefore magnetic lineaments in this part often coincide with these topographic lows.

15.2 Discussion of results and Interpretation

In both datasets both elongated narrow lineaments and wider elliptical and massive anomalies are observed. To be able to focus on both types of features, both the total magnetic intensity (Fig. 15.1) and its first vertical derivative (VG) (Fig. 15.2) are presented. VG is suited to better resolve narrow trends having anomalies with high wavenumber.

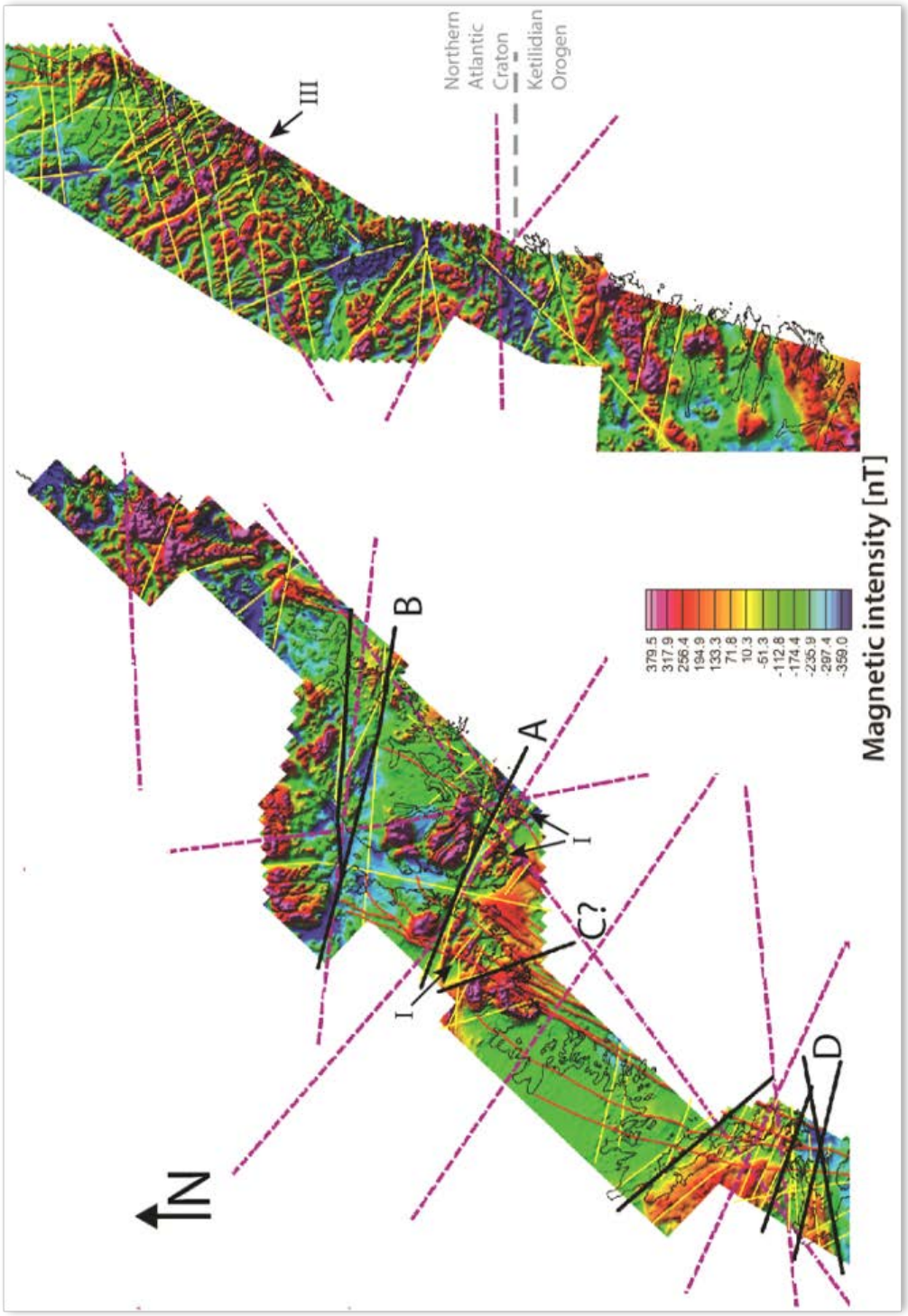

Figure 15.1 *Total magnetic intensities (TMI) from the AEROMAG2012 and the AEROMAG2013 datasets (after reduced-to-pole). The northern and southern parts are shown on the left and on the right, respectively. Thick black lines indicate regional elongated anomalies having low-wavenumber and can be associated as regional trends. Yellow and red lines show narrow elongated anomalies. The red marked anomalies are associated with tertiary dikes, but the yellow marked anomalies likely originate from other type of shallow features like secondary fault zones. Purple dashed lines are regional trends identified in the CAMP-M compilation (Gaina* et al. *2011). The roman number I refers to the noritic and dioritic intrusions of the Ammassilik Intrusive Complex (AIC).*

15.2.1 Pronounced trends

To reliably identify major deep-seated elongated regional trends and first order lineaments, elongated low wavenumber anomalies are identified from the AEROMAG data sets (black lines in Fig. 15.1) and are compared with elongated anomalies present in the Circum-Arctic Mapping Project (CAMP) compilation of regional magnetic data from Gaina *et al.* (2011) (see dashed magenta lines in Fig. 15.1 and Fig. 15.4). A very pronounced WNW-ESE trend is observed in both datasets immediately north of the intrusions of the Ammassalik Igneous Complex (see A in Fig. 15.1). In the AEROMAG data it is characterised with a negative anomaly (Riisager and Rasmussen 2013) and it is striking that this anomaly seemingly continues across the inland ice in the CAMP compilation and in this way build a link between the Nagssugtoqidian orogeny in West Greenland (see Fig. 15.4) and the contemporaneous orogeny in the Tasiilaq region commonly referred to as the Nagssugtoqidian Orogen and the Ammassalik Mobile Belt in Kalsbeck *et al.* (1989). Looking closer to this anomaly in the Tasiilaq region, it consists of a number of smaller lineaments having slightly different directions ranging from E-W to almost WNW-ESE. A direct structural correlation extrapolated and interpreted from the aeromagnetic data between the Nagssugtoqidian Orogen of West Greenland and the orogeny of the Tasiilaq region have to be further investigated before an final decision can be taken.

Another mostly E-W striking anomaly is located further to the north at the northern end of the Sermilik Fjord (see B in Fig. 15.1). This anomaly is less well resolved in the AEROMAG data than A, which is to some extent caused by the large ground clearance due to the topographic low, and also the link to any regional trends across the inland ice is less obvious (Fig. 15.4).

The NNW-SSE oriented trend C (Fig. 15.1) is only determined from the AEROMAG data and it is questionable, if it related to any geological structure. The AEROMAG 2013 survey is rather narrow at this location and the trend may originate more from the alignment of intrusions than from a regional lineament.

In the region around Umivik several regional trends (black lines summarized with the letter D in Fig. 15.1) are present in the AEROMAG data having orientations that vary from NW-SE to WSW-ENE. The most northern one in the southern Køge Bugt and on the Jens Munk Ø is very much covered by ice or located in the sea. Nearby deformation features are observed on the Jens Munk Ø having slightly different strike directions. On the other hand the positive values of these anomalies are more indicative for dykes. In summary the origin of this anomaly is not uniquely identified yet.

The transition zone from the Proterozoic Ketilidian Orogeny in the south to the North Atlantic Craton (~ 62°N) in the north coincides with a zone having negative magnetic values in the AEROMAG data; however an obvious trend is not observable (see Fig. 15.1). This trend is easily “overlooked” due to narrow width of the AEROMAG 2012 survey at this latitude and because it is masked by a pronounced boundary from high positive magnetic values in the South (Ketilidian Orogeny) to lower values in the North (North Atlantic Craton) in the magnetic data CAMP compilation across the Inland Ice.

Further regional trends are observed in the magnetic compilation from Gaina *et al.* (2011) that are not seen in the AEROMAG data (see Fig. 15.1 and Fig. 15.4). A reason is surely that the AEROMAG surveys are too narrow (in E-W direction) that large-scaled features become traceable. This means consideration and incorporation of regional magnetic trends from other compilations (see Fig. 15.1) is important for an interpretation of the magnetic data.

15.2.2 Second order lineaments

Several NNE-SSW trending sub-parallel linear positive anomalies (see red lines in Fig. 15.1 and positive lineaments in Fig. 15.2) are observed in the central and southern part of the AEROMAG 2013 survey. These anomalies extend over distances of more than 150 km and continue to the south in the near coastal offshore region. These anomalies show a clear gradual change in the strike and point to the south at the Kap Møsting, where these anomalies terminate. In the northern part (around the Sermilik Fjord) the orientation of the lineaments is more variable and deviate from sub-parallel behaviour. Here they are also partly obscured by other stronger anomalies associated with Ammassalik Igneous Complex and other Palaeoproterozoic intrusions. Although the positive anomalies are difficult to trace here, it does not seem that they are interrupted by these old structures, which is consistent with the field observations (see section 9.1). The anomalies are particular strong (up to ~ 300 nT) and have dense swarm pattern (separation of 0.5-6 km between individual anomalies) in the region around Isortoq and and Kap Tycho Brahe (around 65°30'N, 38°55'W).

It is very likely that these linear positive anomalies in the southern part of the AEROMAG 2013 survey are associated with large mafic dykes of Palaeogene age. These dykes are linked to the continental breakup responsible for the flood basalt sequences of the East Greenland Tertiary Igneous Province (Nielsen and Brooks 1981, Klausen and Larsen 2002). This interpretation is supported by field observations in the region southwest of Tasiilaq, where steep and fresh NNE-SSW trending dykes with widths of up to several tens of meters are exposed (see also section 13.1 and Fig. 13.2, where this dykes swarm is named S). This is also in agreement with results from an Euler deconvolution (Riisager and Rasmussen 2013) indicating that the top of the associated structures is very shallow (< 400 m) and it is likely that dykes are exposed in the onshore region near the coast. The age of the dykes is not yet determined, but seafloor spreading anomaly C24n (53.4-55.9 Ma) and dykes dated at Kap Gustav Holm are 51 to 55 Ma and it is likely that these dykes have similar ages or possibly slightly older ages due to the northward propagation of the opening of the North Atlantic. It seems that there is a change from a positive to a negative sign for the most eastern lineaments (located east of Kulusuk) hinting to a reversal of the magnetic field at that time.

Several other second order lineaments are observed particularly in the southern part of the area (south of 65°N) (see yellow lines in Fig. 15.1 and elongated features in vertical derivative of the TMI in Fig. 15.2). Although many of them coincides with fjords and narrow valleys, their linear character suggest that very much that they are associated with (pre-)-existing fault zones.

In the area from Ikeq in the North (65°5'N) to the Jens Munk Ø (64°50'N) in the South three narrow negative anomalies are observed having a strike from mostly E-W to WNW-ESE. The two northern ones coincide with mapped sinistral fault zones, but no displacements are observed for the cross-cutting anomalies related to the Palaeogene dykes described before. The southern one is not mapped, but is responsible for a dextral displacement of the same anomalies suggesting that these fault zones are of young age (and possibly still active).

In the area around Umivik (64°10'N to 64°30'N) other of these second order anomalies (with positive values) correlate with the pronounced dykes of the E-W to ESE-WNW trending Palaeoproterozoic Umivik Dyke Swarm (see section 7.2.). As an example, the pronounced dykes on the Upernatitivik and the Umivik peninsular coincide with positive magnetic lineaments (compare Fig. 7.3. with Figs 15.1. and 15.2).

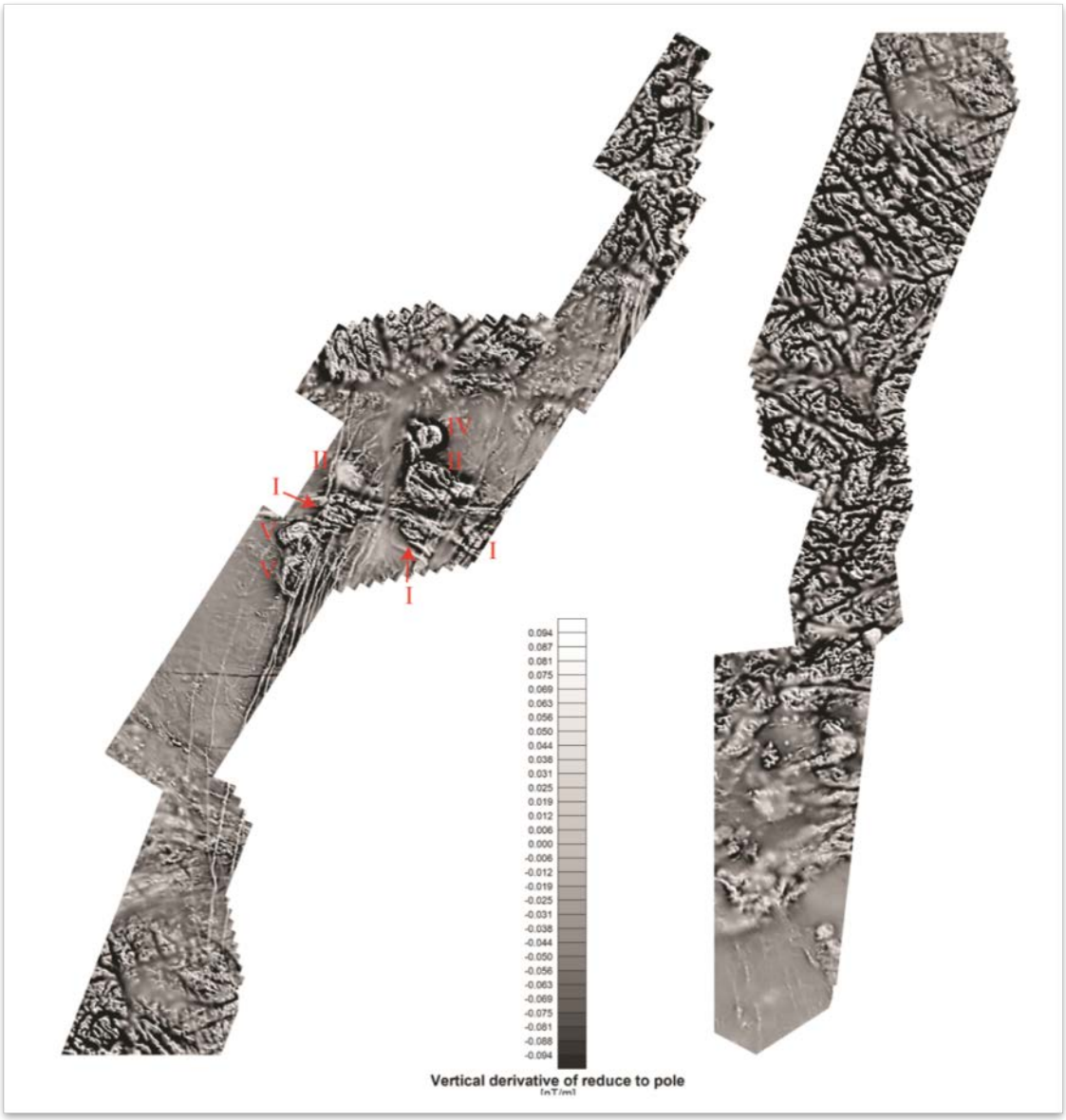

Figure 15.2 *Vertical gradient of the reduced-to-pole image shown in Fig. 15.1 - for geographical location please refer to this figure. Colour shading is applied to this plot; declination and*

inclination of the light source is 45°. The roman letters indicate some of the anomalies associated with the Proterozoic intrusions (see comments in the text).

15.2.3 Anomalies associated with intrusions

The mafic to felsic intrusions of the Ammassilik Intrusive Complex (AIC) are associated with relatively weak positive elliptical magnetic anomalies (up to ~ 450 nT) (see I in Figs 15.1 & Figs 15.2 – and see also Fig. 9.8) that are better identifiable in the 1st vertical derivative of the magnetic field (Fig. 15.2).

In contrast, the granitic to dioritic Ammassalik Batholith and the Johan Petersen Fjord Granite located immediately north of the regional magnetic trend A (see II in Fig. 15.2 and Fig. 9.8) are characterised by stronger magnetic anomalies (maximum values of ~ 500 nT and ~ 1200 nT, respectively) that are partly located within the nearby fjords. An interesting characteristic of the Ammassalik Batholith is that the centre of the anomaly has a lower total magnetic field than along the borders that may indicate a change of the magnetic properties and possibly the lithologies of the batholith from the centre outward.

Immediately east of the Ammassalik Batholith another smaller positive anomaly is present (up to ~ 1400 nT). Outcrops at the along the western shore line of the Ammassalik Fjord suggest that it originates from the Tasilartik Gabbro, although most of the anomaly is located within the fjord area.

An almost circular-shaped and strong positive anomaly (up to ~ 2000 nT) corresponds to the Sermilik East Diorite at the Eastern side of the Sermilik Fjord and ~ 20 km north of the northernmost part of Ammassalik Batholith (see IV in Fig. 15.2).

Two stronger elliptically shaped magnetic anomalies southwest of the AIC close the village of Isortoq are suggested associated with the Isrtoq granites and diorites intrusions (V in see Fig. 15.2). The granite intrusion is exposed on the islands of the archipelago and the geophysical observation link the exposure to one large intrusive body. The diorite intrusion in the same area is in the shown extent under the Inland Ice. In addition, there is a circular anomaly (only the outer circle is characterised by magnetic high-values) structure visible between the two intrusions that may indicate the presence of yet another intrusion. This anomaly, however, is almost completely covered by ice except for its most southern border.)

In the southern part in the area around Skjoldungen and Timmiarmiut, some rock units are not related to obvious anomalies, e.g. metamorphosed mafic, mafic rocks or rocks associated with SAP, although a NW-SE running positive anomaly (III in Fig. 15.1) coincides with an area where rocks from mafic Archaean intrusive rocks (e.g. Stærkodder Vig) are mapped (see Fig. 3.1). Fjords and deep elongated valleys cutting fjords surely make it particularly difficult to assign any anomalies to rock units because low magnetic values typically correlates with large ground clearances (compare Fig. 15.1 and Fig. 15.2 with Fig. 15.3).

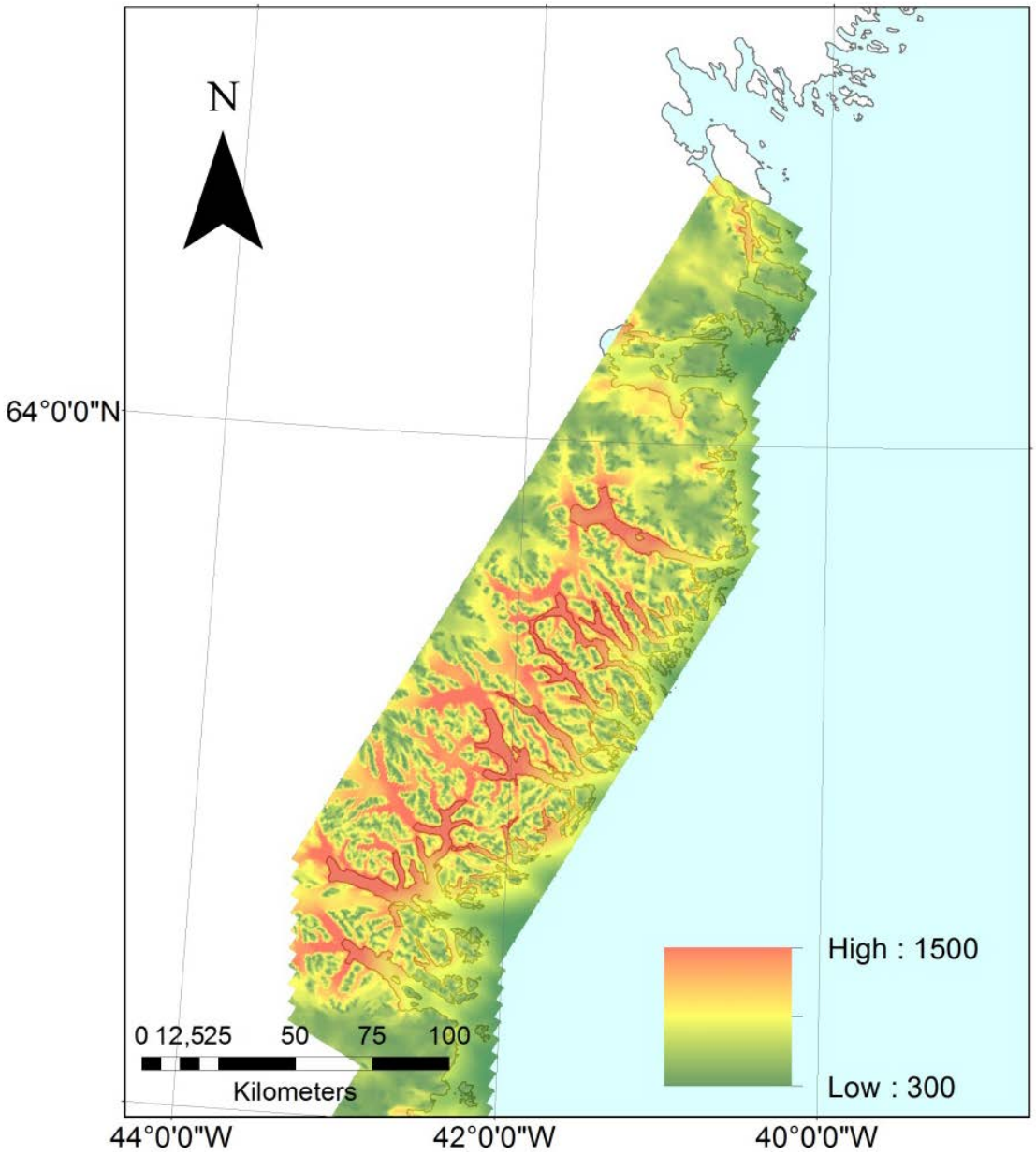

Figure 15.3 *Ground clearances during measurements of the AEROMAG 2012 survey in meter.*

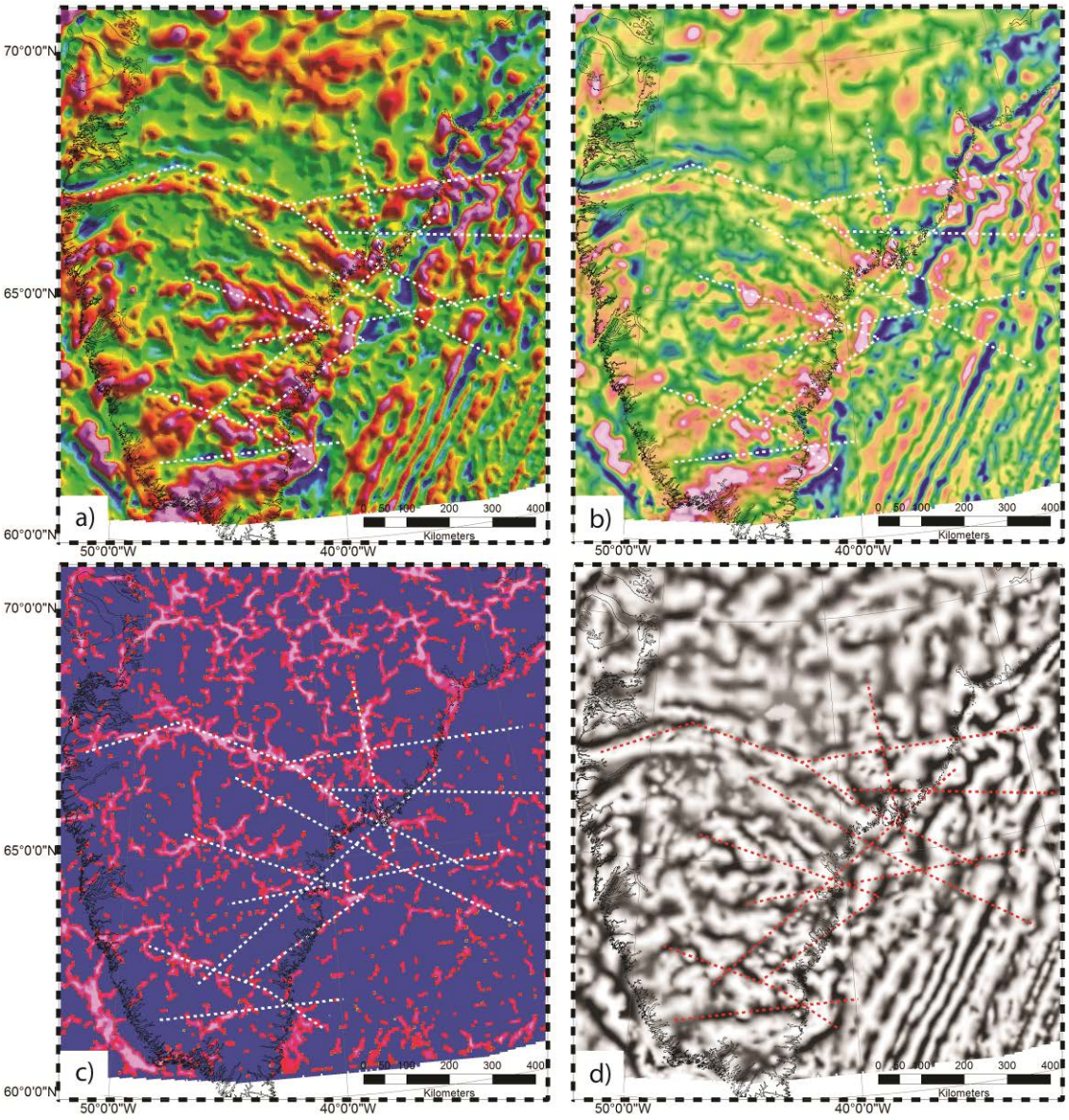

Figure 15.4 *Different maps that are determined from the magnetic field compilation CAMP-M (Gaina* et al. *2011) and used to extract the main magnetic trends (see dashed lines in all figures; trends located apart from the area of interest are not picked). The different maps show:* ***A.*** *Colour shaded map from total magnetic intensity.* ***B.*** *Coloured map of the total magnetic intensity that is overlain by a transparent greyscale image of the tilt derivative.* ***C.*** *Map of the phase symmetry similar to the workflow described in Holden* et al.*, 2008.* ***D.*** *Map after applying a dynamic range compression (see Kovesi (2012)) onto the magnetic field data; here, a cut-off frequency of 64 (1/km) is used for the high-pass filter. Note that magnetic fields used to generate these images are reduced to the pole.*

16 Economic geology

Jochen Kolb, Leon Bagas, Bo Møller Stensgaard, Anne Brandt Johannesen, Nanna Rosing-Schow, Marco L. Fiorentini, Diogo Rosa, Nicolas Thébaud, Majken D. Poulsen, Nynke Keulen, Thomas Find Kokfelt, Vincent van Hinsberg & Martin B. Klausen

The study area in South-East Greenland between 62°N and 67°N is underlain by Meso- to NeoArchaean granite-gneiss complexes of the Thrym Complex (NAC) and the Kuummiut and Schweitzerland terranes (EGA or Rae Craton), and Palaeoproterozoic supracrustal rocks, which are metamorphosed to amphibolite facies grades or higher. Palaeoproterozoic intrusions cluster in the Tasiilaq area. This geological scenario restricts potential mineralisation to (1) systems that not only have an upper crustal expression but may also be preserved in the mid to lower crust; (2) systems that involve high-grade metamorphism in ore genesis; or (3) Palaeoproterozoic igneous systems. Several hitherto unknown mineral occurrences have been discovered during the SEGMENT project and already known occurrences have been studied in more detail. Some latest conceptual advances in mineral system analysis have been applied to further refine the prospectivity of South-East Greenland and lay the foundations for future studies in the area.

16.1 Company activities

The following review of the company-driven mineral exploration activities in South-East Greenland is based on an updated (to June 2016) and slightly modified version of a summary provided by B. Thomassen in Thorning (2009). The available archived and released company reports are referred to as “GRF no. XXXXXX” (GEUS Report File no.). These are downloadable via www.geus.dk/dodex.

Kryolitselskabet Øresund A/S, 1963

- Kryolitselskabet Øresund carried out helicopter reconnaissance between Julianehåb and Kap Japetus Steenstrup (66º15’N), mostly in the form of visual inspection for signs of mineralisation including sampling of promising localities. Unfortunately, the reporting was not completed (GRF no. 21241).

Nordisk Mineselskab A/S, 1971

- Nordisk Mineselskab carried out mineral reconnaissance at Kialineq (66º55’N), but did not obtain any significant results. (GRF no. 20907).

Ujarassiorit Mineral Hunt Programme, 1989-2008

- Several samples anomalous in especially Au-Pt-Pd-Ni-Cu have been submitted from the Ammassalik area. Follow-up work in the Ammassalik area in 1990 showed anomalous Au, As, Se, Ag and base metals.

Nunaoil A/S, 1996-1998

- 1996: Geochemical exploration was carried out in the Ammassalik area. Au and Ni anomalies were registered (GRF no. 21520).
- 1997: Follow-up exploration in the Ammassalik area indicated Ni-Cu-Au-Co mineralisation (GRF no. 21684).
- 1998: Follow-up exploration in the Ammassalik area lead to the discovery of Ni-PGE-Au-Cu-mineralisation in ultramafic rocks (GRF no. 21690).

Major General Resources Ltd., 1999

- Major General Resources Ltd carried out diamond exploration in the Saqqisikuik area. The analytical results have not been reported (GRF no. 21722).

Nunaminerals A/S, 2001-2008

- 2001: Additional follow-up exploration was carried out on Ni-PGE-Au-Cu-mineralisation in the Ammassalik area (GRF no. 21794).
- 2002: Additional reconnaissance and follow-up exploration in the Ammassalik area (GRF no. 21826).
- 2007: Field work was carried out (no released/archived company report available at the time of writing).

Gem Fields Resources Ltd., 2003-04

- 2003: Field work in the Ammassalik area indicated new Au-PGE-Ni-Cu-mineralised localities (GRF no. 21839).
- 2004: Continued exploration for Au-PGE-Ni-Cu in the Ammassalik area (GRF no. 21916).

Inco Ltd., 2005

- Exploration for Ni-Cu in the Ammassalik area with no conclusive results (GRF 21964).

Greenland Minerals and Energy Ltd., 2011

- Exploration for Ni-Cu-PGE in the Skjoldungen area. The decision to take up the license was partly based on the recent data published from the SEGMENT project (no released/archived company report available at the time of writing).

Plymouth Minerals Ltd., 2011

- Exploration for REE in the Timmiarmiut area. The decision to take up the license was partly based on the recent data published from the SEGMENT project. (GRF no. 22609)

21st North ApS, 2012 and 2015

- 2012: 21st North ApS was awarded an exploration license on Au-PGE-Ni-Cu-mineralised localities south of Tasiilaq and just south of Johan Petersen Fjord (no released/archived company report available at the time of writing). A small field work campaign was carried out.
- 2015: 21st North ApS was awarded an exploration licence on graphite at Auppaluttoq (see section 16.6). The decision to take up the license was partly based on the

recent data published from the SEGMENT project. The license is still active at the time of writing.

16.2 Ni-Cu sulphide mineralisation in the Thrym Complex

The Ni-Cu sulphide mineralisation in the Thrym Complex is hosted by the metamorphosed mafic-ultramafic bands and lenses in orthogneiss (Bagas *et al.* 2016, Owen and Kolb 2012, Rennick and Kolb 2012). The mafic-ultramafic bands are dominantly composed of mafic granulite, with a few bands containing elongated and irregular ultramafic bodies. Field relationships of the geochemical discrimination into two types (M1, UM1, M2 and UM2, respectively) are unclear.

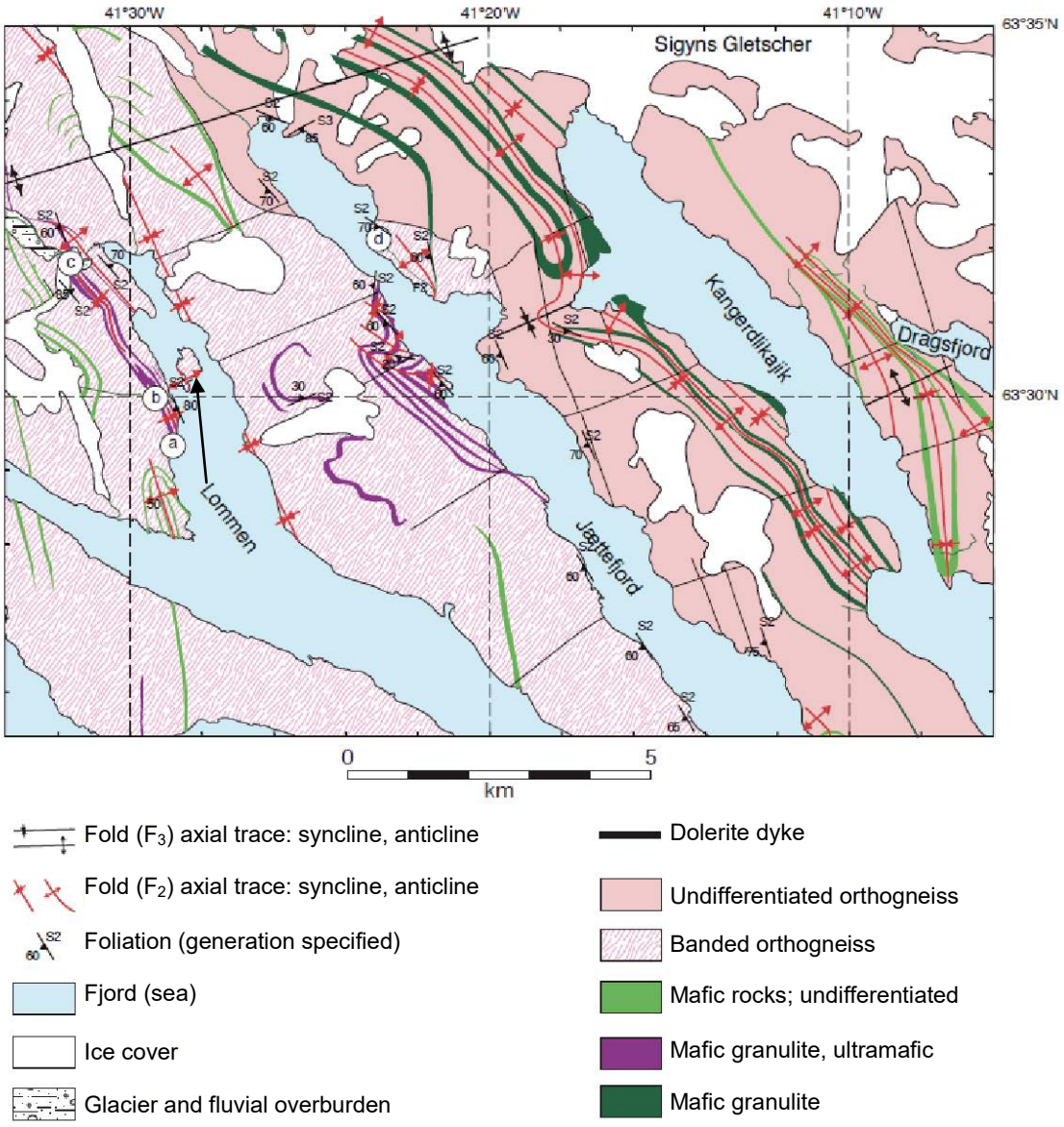

Figure 16.1 *Geological map of the Lommen-Jættefjord area with Ni-Cu-sulphide mineralisation locations (a-d) (Bagas* et al. *2016).*

The mafic-ultramafic band at Lommen is approx. 60 m thick (Locality 'a' in Fig. 16.1). The ultramafic rock close to the centre of the band has irregular shape, is ~15 m thick and dominantly made up of green-grey peridotite with minor black pyroxenite (Fig. 16.2). The pyroxenite intruded along the S_{S1} foliation at the contact with the more massive peridotite (Bagas *et al.* 2016).

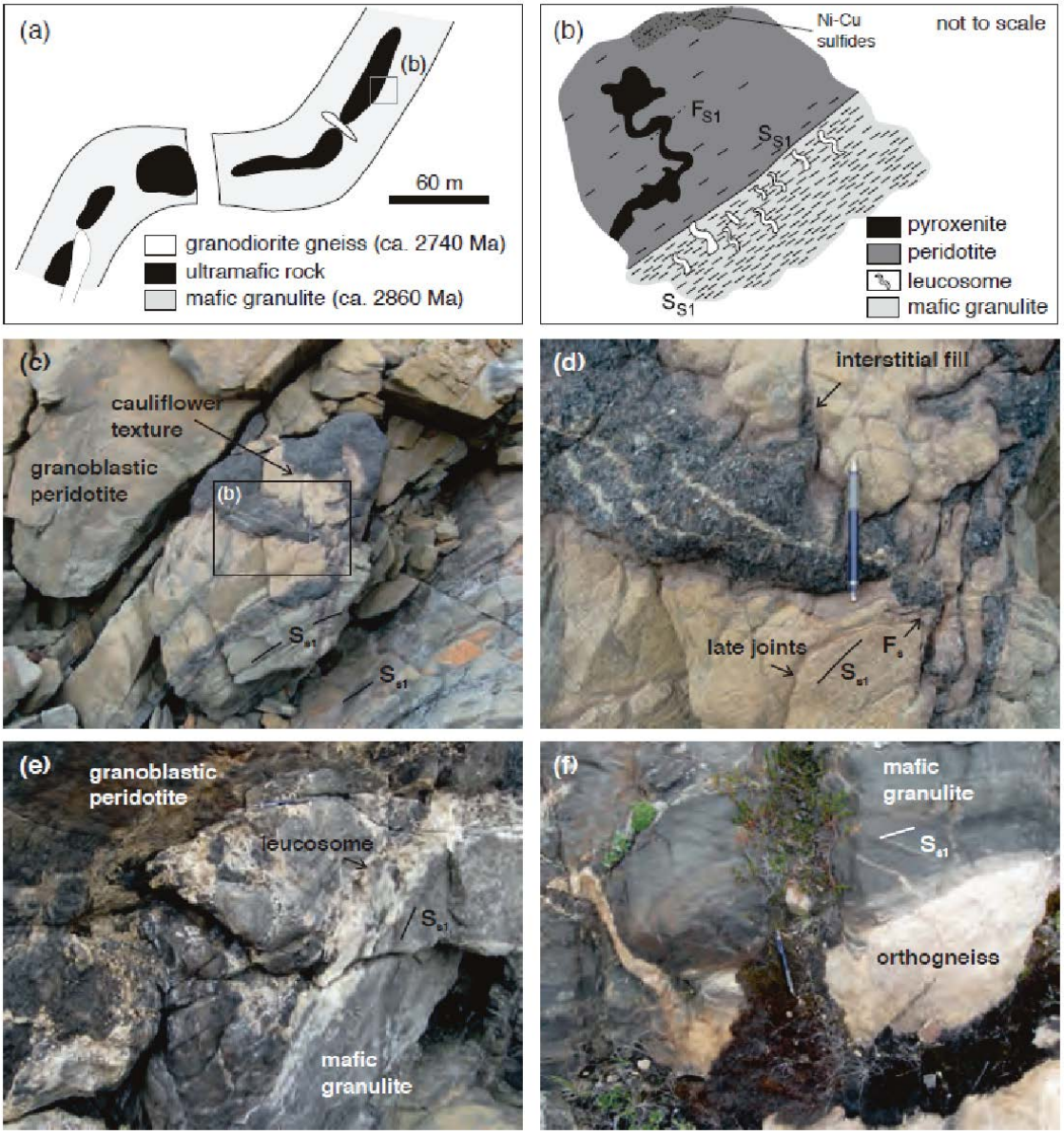

Figure 16.2 *The Lommen Ni-sulphide mineralisation:* ***A.*** *Sketch of a folded band of mafic and ultramafic rocks in granodiorite gneiss matrix. The ultramafic rocks form boudins in the centre of the bands;* ***B.*** *schematic enlargement of the S_{S1}-parallel contact between the mafic granulite and ultramafic rocks. The peridotite is intruded by pyroxenite, which is not foliated but shows open fold structures with the S_{S1} foliation as the axial planar foliation. The leucosomes in the mafic granulite at the contact with the peridotite, the intrusion parallel S_{S1} foliation, and the weak deformation structures in the ultramafic rocks indicate syntectonic intrusion into mafic granulite host during peak metamorphic conditions;* ***C.*** *Green peridotite and black pyroxenite have irregular contact relationship with cauliflower textured parts and interstitial infill of pyroxenite into peridotite, indicating mingling. Note that the black pyroxenite appears to be intruded parallel to the S_{S1} foliation and being folded by F_{S1}, where crosscutting, suggesting early- to syn-tectonic intru-*

sion; ***D.*** *enlargement of C.;* ***E.*** *mafic granulite with abundant leucosomes at the contact with ultramafic rocks; and* ***F.*** *orthogneiss showing intrusion structures into the mafic granulite (Bagas* et al. *2016).*

Sulphide mineralisation (Fig. 16.3) has been identified at Lommen, in Graah Fjord, and Jættefjord (localities 'a', 'b', 'c', and 'd'Fig. 16.1). Two styles are distinguished: (1) interstitial to net-textured sulphide mineralisation (≤ 20 vol.% sulphides; pyrrhotite-chalcopyrite-pentlandite), which is dominantly hosted by the peridotite; and (2) sulphide mineralisation and hydrothermal quartz alteration in two parallel, 0.5 m wide D_{S2} shear zones in retrogressed mafic granulite (Bagas *et al.* 2016). The interstitial to net-textured sulphides yields up to 0.5% Ni, 0.25% Cu, Pt 24 ppb, Pd 162 and Cr 0.5%.

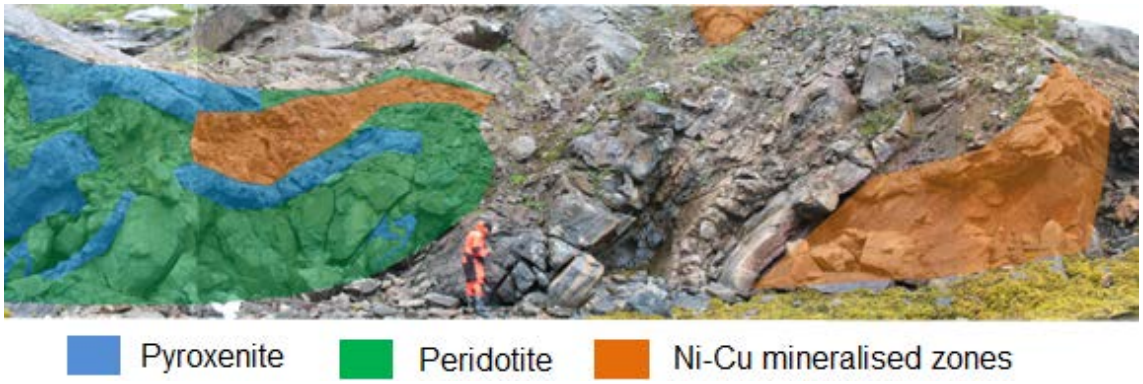

Figure 16.3 *The pyroxenite and peridotite layers in the Lommen area in Graah Fjord with indication of Ni-Cu mineralised zone.*

Interstitial to net-textured sulphide mineralisation is dominantly hosted by peridotite but also forms sulphide-rich (10-15 vol.%) zones at the contact between peridotite and mafic granulite (Bagas *et al.* 2016). The major sulphide mineral is pyrrhotite with minor pyrite, chalcopyrite and pentlandite (Owen and Kolb 2012). Pentlandite commonly forms lamellar exsolutions within pyrrhotite. Pyrrhotite and pentlandite form rounded inclusions in orthopyroxene. Pyrite commonly forms rounded grains edged by chalcopyrite (Owen and Kolb 2012). Different mineralised horizons contain varying proportions of three oxide-sulphide assemblages (Bagas *et al.* 2016, Owen and Kolb 2012): (1) spinel-magnetite-hematite-wüstite; (2) pentlandite-pyrrhotite; and (3) pyrite-chalcopyrite. The best reported values show Ni and Cu contents up to 5180 ppm and 2560 ppm, respectively. Combined PGE-Au contents are modest, with values up to 240 ppb (Bagas *et al.* 2016, Owen and Kolb 2012).

The sulphide mineralisation associated with hydrothermal quartz alteration is hosted in E-trending moderately S-dipping D_{S2} shear zones for example in the Jættefjord area (Fig. 16.1). The mineralised shear zone consists of quartz and plagioclase with sutured grain boundaries and relict grains of plagioclase and pyroxene. Sulphides generally cross-cut the silicate phases through jigsaw-fit fractures. The shear zone-hosted mineralisation is notably depleted in nickel with a maximum assay of 680 ppm Ni, whereas it contains up to 2280 ppm Cu (Bagas *et al.* 2016, Owen and Kolb 2012).

The first style of mineralisation is greatest in volume and is commonly associated with mafic granulite and peridotite with M1 and UM1 affinity. The second style of mineralisation is not spatially associated with either M1-UM1 or M2-UM2 rocks. Sulphides have instead been remobilised, possibly sourced from the first style of mineralisation, and concentrated in the shear zones as vein filling (Bagas *et al.* 2016). On the basis of the geological observations, we put forward the hypothesis that the primary interstitial Ni-Cu sulphide mineralisation formed at lower crustal levels by igneous processes (Bagas *et al.* 2016). A better understanding of geological processes in the deeper crust are required in order to decide, whether the mineralised occurrences could represent a small part of a still undiscovered larger system.

16.3 Mo-W mineralisation in the early SAP

A quartz-wolframite-molybdenite vein with phyllic alteration was identified during the reconnaissance work in the Skjoldungen area on the north-western part of the Thrudvang peninsula, close to the Kangertikajik Fjord (Fig. 16.4)(Rosa and Ulrich, 2015). The approx. 30 cm wide, sub vertical vein is hosted in mafic granulite (Fig. 16.5) yields up to 1.6% W and 263 ppm Mo. Molybdenite yields a Re-Os age of 2749 ± 11 Ma contemporaneous with early intrusions from the SAP, e.g. granite-monzogranite and Skirner Bjerge Syenite (Rosa and Ulrich 2015). Two rusty-weathered horizons in amphibolite (retrogressed mafic granulite) have anomalous W content (up to 0.55% W) due to scheelite mineralisation, but are low in Mo. Both mineralisation styles are closely spatially related and interpreted to having formed contemporaneously by magmatic hydrothermal processes (Rosa and Ulrich 2015). The fluid inclusions in quartz of the vein are sparse and show a one-phase high-density CO_2 composition. Whether this fluid is responsible for the mineralisation or if it is a feature of later re-crystallization cannot be unequivocally be determined.

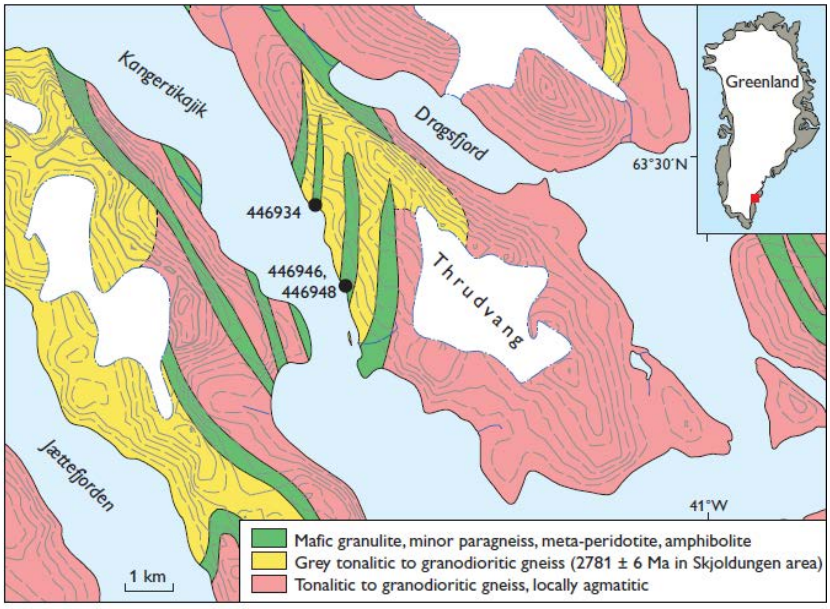

Figure 16.4 *Location of Mo-W mineralisation on Thrudvang peninsula north of Jættefjorden and north of island Skjoldungen indicated by the black dots (labelled with GGU sample numbers).*

Figure 16.5 *The* c. *30 cm wide subvertical quartz-wolframite-molybdenite vein hosted in mafic granulite at the Thrudvang peninsula*

16.4 Magnetite mineralisation in the SAP

Some *c.* 2700 Ma layered intrusions of the SAP host magnetite bands and veins. The Vend Om Intrusion is a small 350 x 450 m elliptical intrusion with ≤2 m wide bands of ≤35 vol.% magnetite and hercynite, hornblende and plagioclase (Fig. 16.6) (Klausen and Kokfelt 2014). Several ≤ 0.2 m wide magnetite, ilmenite and spinel bands are present in the Njords Glacier (Fig. 16.7) (Klausen and Kokfelt 2014). Most notable metal content is vanadium content of up to 1.7 wt% V_2O_5. Narrow veins with magnetite and apatite mineralisation cross cut the magmatic layering of the Ruinnæsset complex (Klausen and Kokfelt 2014). Although the mapped occurrences are small, it shows the mineral potential in the larger region.

16.5 Ni-PGE sulphide mineralisation in the Ammassalik Intrusive Complex (AIC)

The AIC has numerous Ni and Cu anomalies in stream sediment samples, which was the reason for mineral exploration in the area since the mid-1990s. Most recent mineral exploration was concentrated on the southern rim of the Tasiilaq Intrusive Centre, the central complex in the AIC.

In 1997, an approx. 90 long and 1-8 m wide mineralised lens of serpentinized ultramafic rocks was discovered, returning up to 1.0 wt% Ni, 0.5 wt% Cu, 0.4 ppm Au and 615 ppm Co in mineralised samples (Lie 1997). Similar values have been obtained in various mineral exploration projects until 2012. The interstitial network of ore minerals consists of pyrrhotite, pentlandite, chalcopyrite and minor magnetite (Lie 1998). The mineralisation was interpret-

ed to be hosted in ultramafic rocks that occur in the contact aureole of the Tasiilaq Intrusive Centre. Geophysical investigations were, therefore, restricted to the outer contact zones of the AIC (Lie 1998).

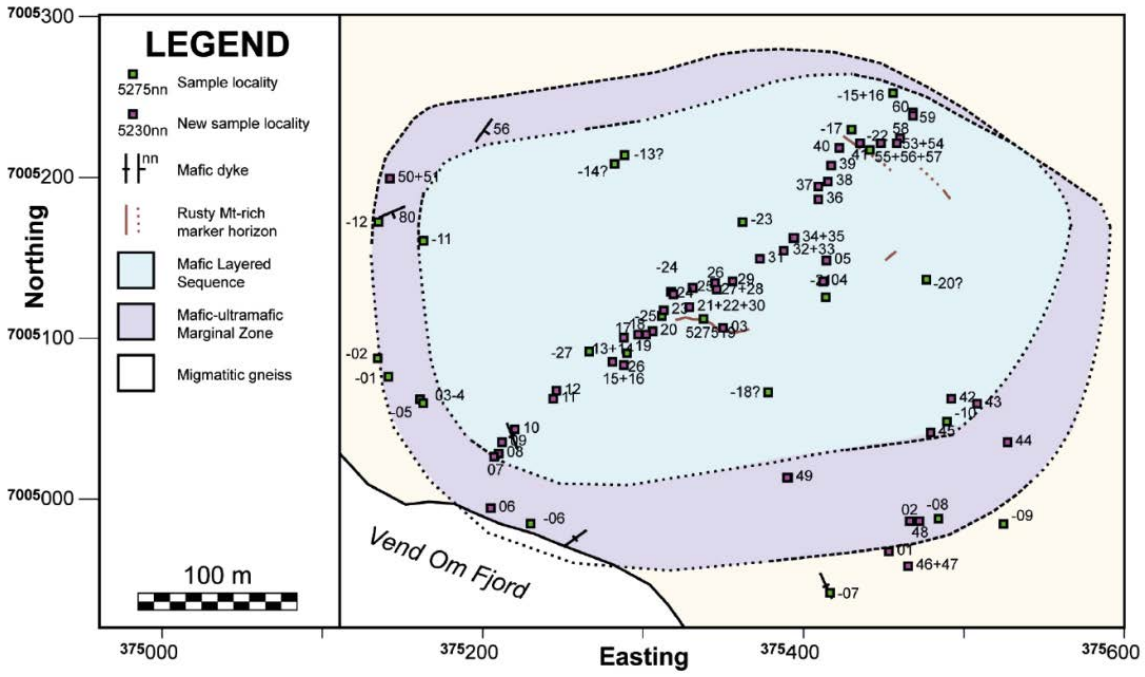

Figure 16.6 *Map of the Vend Om Intrusion with indication of the rusty magnetite rich horizons.*

Figure 16.7 *Magnetite-rich band within the layered gabbro sequence at the Vend Om Intrusion. The layer (here outlined by dashed white lines) is up to 1.5 m thick and can be followed over ca 50 m lateral distance where after it is thinning out.*

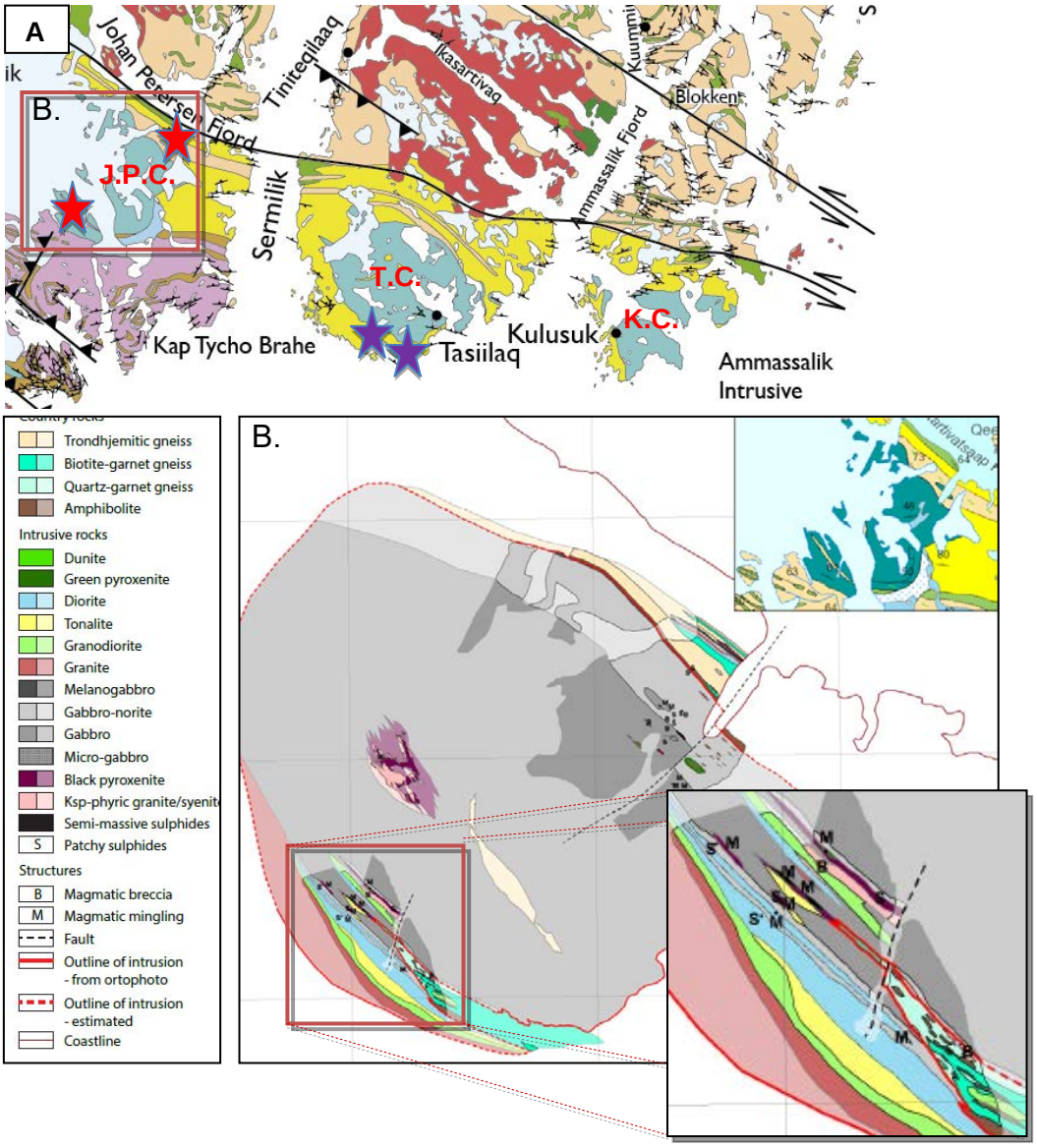

Figure 16.8 ***A.*** *Overview map of the three intrusive centres of the Ammassalik Intrusive Complex (AIC) (the intrusive centres are abbreviated in red in the figure as J.P.C. = Johan Petersen Fjord Intrusive Centre, T.C = Tasiilaq Intrusive Centre, K.C. = Kulusuk Intrusive Centre) and* ***B.*** *detail map of the Johan Petersen Intrusive Centre with indication the sulphide mineralisation. The violet stars in A. indicate the mineralised lens of serpentinized ultramafic rocks was discovered in 1997 by NunaOil A/S. The red stars indicate the sulphide mineralisation that was discovered in 2014 during the SEGMENT project. The AIC contains additional mineralised sites than the three outlined here. See Fig. 16.9 for detailed maps of the mineralisations within the Johan Petersen Fjord Intrusive Centre.*

Reconnaissance and detailed mapping of the AIC during the SEGMENT project discovered several sulphide mineral occurrences hosted by intrusive rocks of the AIC (Fig. 16.8). In the Tasiilaq Intrusive Centre, pyroxenite and olivine-bearing gabbro host interstitial sulphides (Grøtner 2014). The ore assemblage is pyrrhotite-pyrite-chalcopyrite-(magnetite). Pentlandite has not been observed in the studied samples, but whole rock geochemistry returned higher Ni and Co as predicted from modal mineral abundance, which indicates presence of pentlandite (or another Ni-Co-bearing mineral). Maximum values for mineralised samples are 770 ppm Ni, 5230 ppm Cu and 433 ppb Au (Grøtner 2014).

Smaller patches of sulphide mineralisation have also been observed in the Johan Petersen Intrusive Centre. They typically occur in less than a few metre wide shear zones, in smaller mingling zones where the pyroxenite to Hbl-gabbronorite stringers are present, in mafic-ultramafic sheets and breccia clasts and along the contact between the intrusion and the wall rocks. Three larger sulphide mineral occurrences were discovered: (1) a mingling zone of the south-western part of the intrusion (Fig. 16.9A); (2) an approx. 60 x 20 m mingling zone at the north-eastern coast of a melt water lake in the north-east; and (3) in an approx. 15 m wide melanogabbronorite sheet to the northeast of the melt water lake towards the inlet of the Johan Petersen Fjord (Fig. 16.9B).

Contact-style mineralisation of up to 5 vol.% sulphides is hosted in gabbronorite and melanogabbronorite in the north-east and Bt-Grt-gneiss in the south-western part of the intrusion (Fig. 16.9 and Fig. 16.10). The ore minerals are interstitial and consist of chalcopyrite, pyrrhotite, lesser pyrite, covellite and marcasite. Pyrrhotite and chalcopyrite are intergrown and have exsolution lamellae. A later generation of chalcopyrite-pyrite overgrows the earlier sulphide assemblage, probably during cooling and equilibration with intermediate solid solution (iss) and subsequent fractionation into chalcopyrite and pyrite. Marcasite replaces pyrrhotite at the edges and lamellae in pyrrhotite are replaced by covellite. Supergene alteration consists of goethite or other oxy-hydroxides. Both the rock samples and the sulphides are low in Ni and Cu, indicating that the magma was already depleted in Ni-Cu. Sulphur isotopes are highly variable but display very heavy values, with $\delta^{34}S$ of *c.* +11 ‰ and lack of any mass-independent sulphur isotope anomaly. These results indicate that the most probable sulphur source is derived from the wall rocks of the intrusion. More distal crustal sources such as devolatilized sulphur derived from the slab subducted underneath the Johann Petersen Intrusive Centre cannot be ruled out. However, the lack of a ^{33}S anomaly makes the interaction of Archaean crustal sulphur sources unlikely.

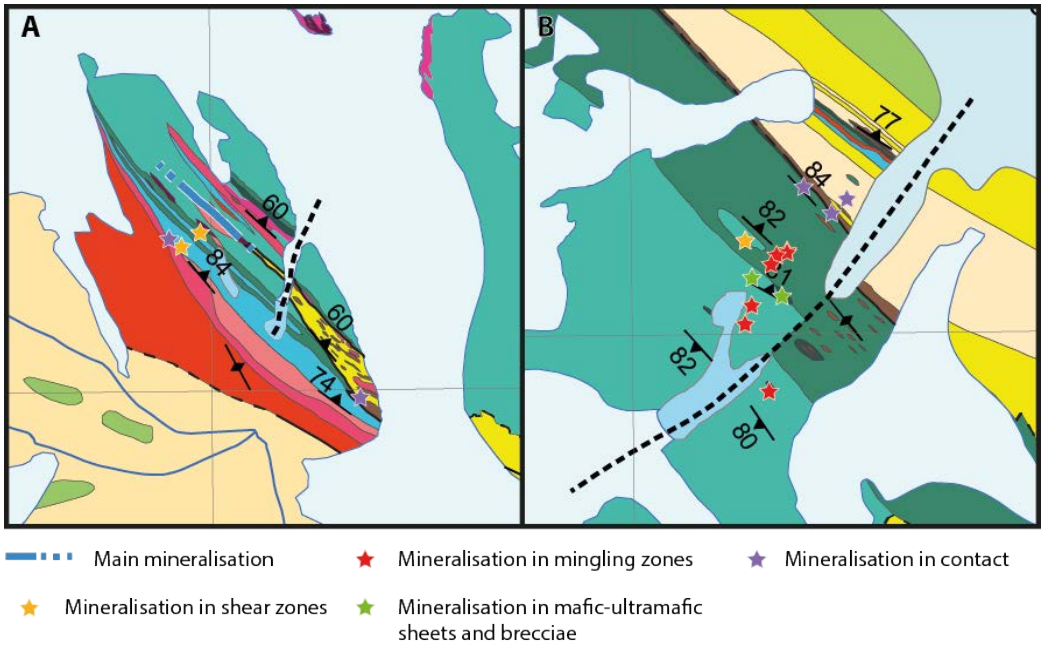

Figure 16.9 *Geological maps of the sulphide mineral occurrences. See Fig. 16.8 for location of the maps within the Johan Petersen Fjord Intrusive centre of the Ammassalik Intrusive Complex.* ***A.*** *Enlargement of the south-western part of the intrusion.* ***B.*** *Enlargement of the north-eastern part of the intrusion.*

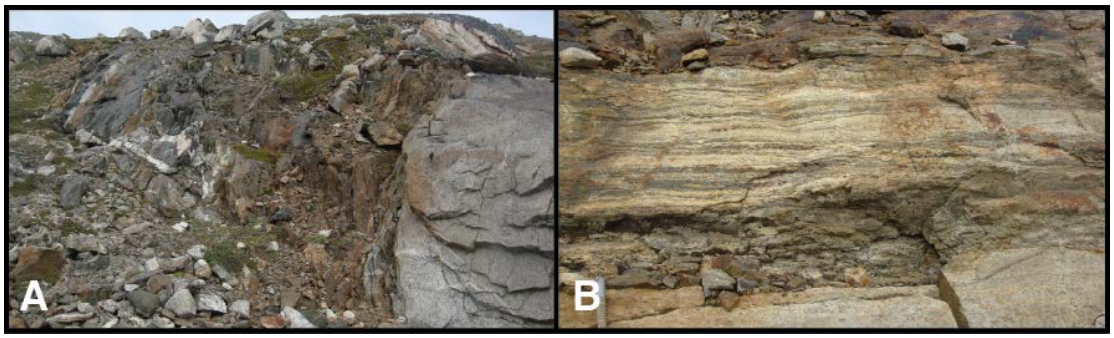

Figure 16.10 ***A.*** *Contact-style mineralisation in the north-east. The mineralisation is developed between gabbronorite to the right and melanogabbronorite to the left just adjacent to wall rocks.* ***B.*** *Contact-style mineralisation from the south-west. A rusty-wheathered band of Bt-Grt-gneiss at the top is adjacent to less mineralised Bt-Grt-gneiss*.

Mineralisation in mafic-ultramafic sheets and brecciae is on average 5-15 vol.% with maximum values at 30 vol.% sulphides (Fig. 16.11). Pyrrhotite and pyrite with lesser chalcopyrite and pentlandite form an interstitial network and local inclusions in cumulus silicates. Similar to the contact-style mineralisation, the primary sulphides are replaced by pyrite, chalcopyrite and magnetite and supergene marcasite and goethite. Ni-Cu contents are subeconomic, but the highest found so far in our study. The breccia matrix and the melanogabbronorite sheet have network-like sulphides, indicating that the sulphide melt droplets could coalesce and settle between the cumulus minerals. They differ, however in Ni#; breccia matrix and clast have a similar primitive signature, whereas the melanogabbronorite sheet has a Ni# of 0.5, indicating different processes of sulphide mineralisation and possible sulphide melt immiscibility deeper in the intrusion that was brought to the present-day surface in the breccia clasts. The sulphur isotope signature for all mineralised samples is similar in the range of the mantle composition and very different from the very heavy signature of the contact-style mineralisation.

Mineralisation in mingling zones occurs throughout the intrusion, but mostly in the northeastern part (Fig. 16.9 and Fig. 16.11). It is mainly hosted by pyroxenite, melanogabbronorite and Hbl-melanogabbro stringers. The gabbroic rocks may contain disseminated sulphides up to 10 cm away from the stringers. The sulphide content varies from a few percent up to 20 vol.% and averages at 5 vol.%. Pyrrhotite, minor chalcopyrite and traces of pentlandite are fine-grained, finely disseminated, cm-scale clusters, an interstitial network or inclusions in silicates. Similar to the other sulphide mineralisation, the primary sulphides are replaced by secondary pyrite and chalcopyrite, and supergene marcasite-goethite-(covellite). The whole rock and sulphide Ni and Cu contents are, with Cu-enrichment over Ni, possibly indicating Ni-depletion during sulphide liquid separation earlier in the magmatic history. Sulphur isotopes have mantle signature, but also weak indication of mass independent fractionation (MIF), which leaves the question of potential sulphur source open to further investigations.

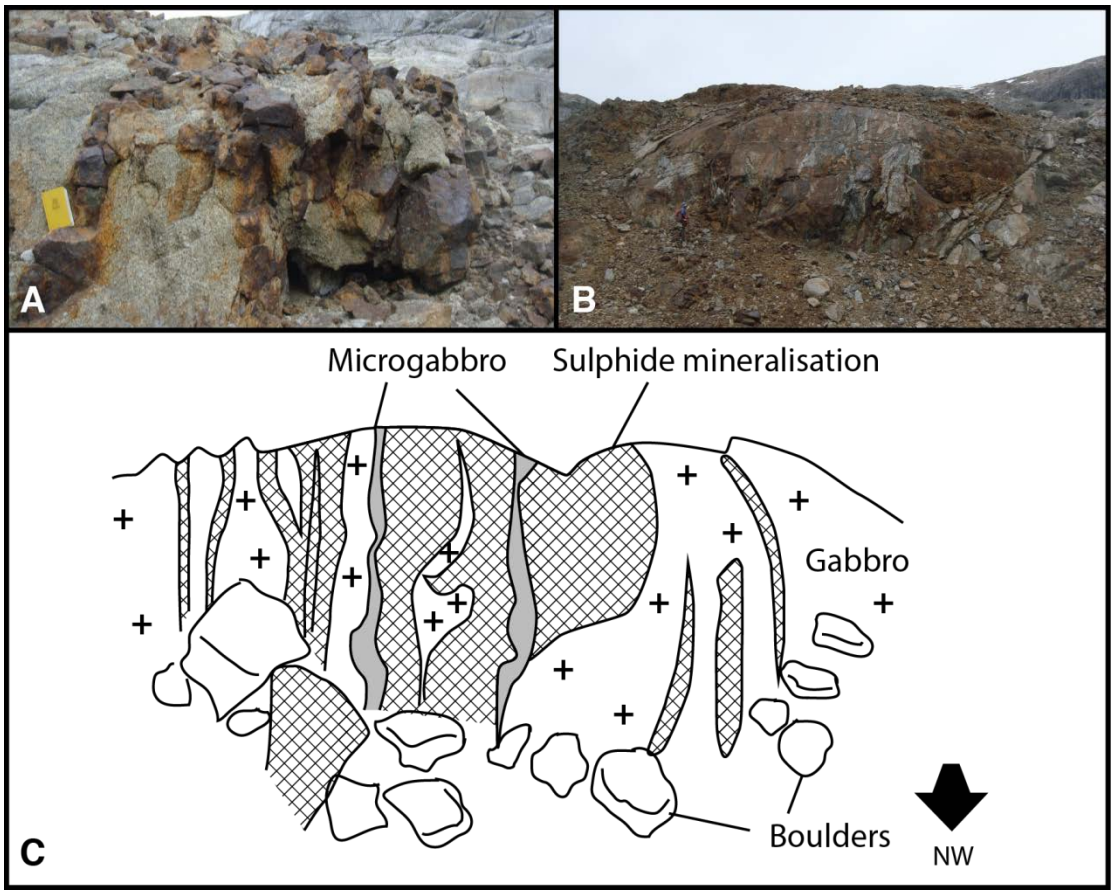

Figure 16.11 *Mingling-style sulphde mineralisation.* ***A.*** *Mineralisation in stringers mingling with gabbro.* ***B.*** *Approx. 60 x 20 m mingling zone with leucocratic gabbro, melanogabbro and amphibolite-granulite clasts, microgabbro and sulphide mineralisation (view towards SE).* ***C.*** *Sketch of B.; the sulphide mineralisation is spatially associated with most of the mafic-ultramafic clasts, stringers and xenoliths.*

A steeply dipping lens of sulphide mineralisation discovered in 2014 in the southern part of the intrusion is 500-1000 m long and 0.5-15 m wide (Fig. 16.9A). It is located in a mingling zone, where also a larger Bt-Grt-gneiss xenolith occurs. The recognition of hybrid igneous lithologies and K-feldspar-cordierite-garnet-graphite assemblages indicates magma mingling, and melting and assimilation of the wall rock. Pyrrhotite and minor chalcopyrite form net-vein textured mineralisation. Pyrrhotite contains little Ni and Cu and no pentlandite was observed. The low metal tenor of the sulphides indicates that the sulphide liquid did not interact with a large volume of silicate magma, which already formed a crystal mush at the time of intrusion or was already depleted in Ni and Cu. Sulphur isotopes are light with negative $\delta^{34}S$ in the range between -7‰ and -20‰, which together with a MIF-signature indicates a sulphur source in metasedimentary wall rocks. The favoured interpretation of the mineralisation is formation from assimilation of sedimentary sulphide in an already semi-solid magma, which was already depleted in Ni and Cu. This resulted in low R-factors and insignificant Ni-Cu enrichment.

Shear zone-related sulphide mineralisation occurs locally in 1.5-3 m wide shear zones indicated by protomylonite structures (Figs 16.9 & 16.12). Three shear zone trends are recog-

nized: (1) NE-trending dipping at 60°-80° SW; (2) NNE-trending dipping at 60°-80° SSW; and (3) NW-trending dipping 80° NE. Quartz veins and the hydrothermal quartz-biotite-epidote-chlorite-talc-muscovite-pyrite alteration assemblage point to hydrothermal overprint related to deformation. Pyrite occurs in quartz veins, breccia matrix and in protomylonite elongated along the main foliation. Distal to the shear zone, primary sulphides are replaced by pyrite, minor chalcopyrite, chalcocite and covellite. All sulphides show supergene alteration to hematite-goethite assemblages. Copper- and Ni-contents are generally low, with local Cu-enrichment to 1 wt%, indicating selective transport of Cu by the hydrothermal fluid. The sulphur isotope signature is light with $\delta^{34}S$ values peaking at -3‰ to -4‰ and -10‰ to -15‰, overlapping with adjacent primary sulphide mineralisation also in the MIF. This indicates that hydrothermal fluids remobilized the primary magmatic sulphide mineralisation into the shear zones.

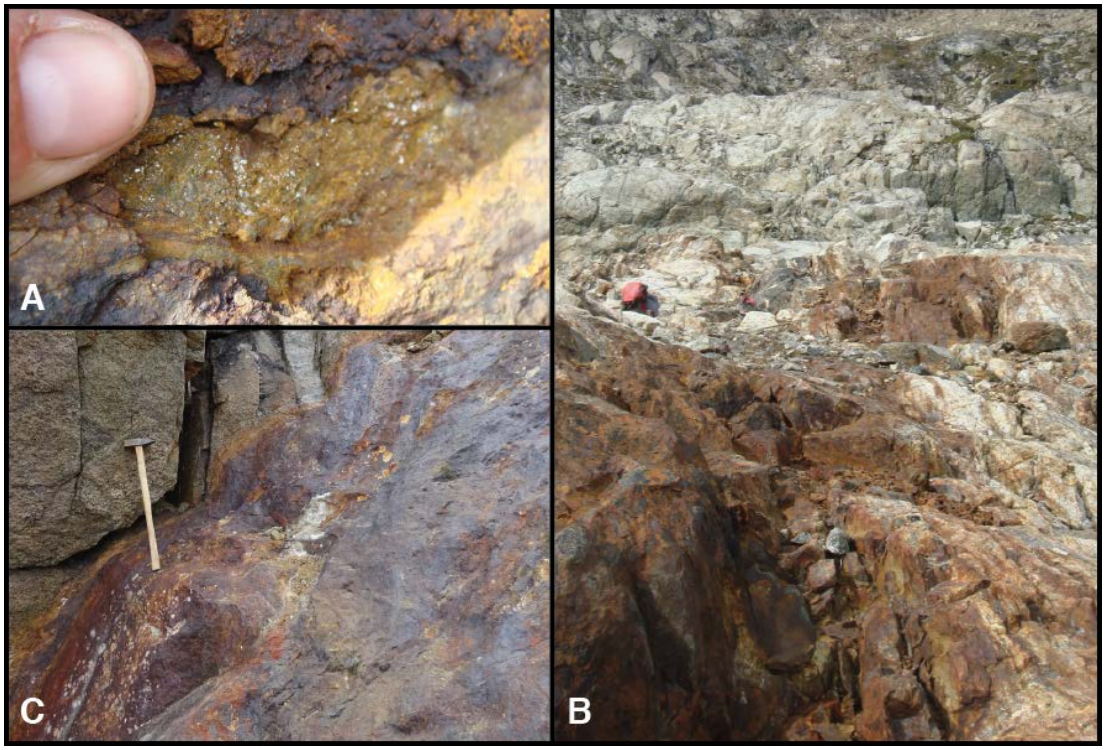

Figure 16.12 ***A.*** *Fine-grained, disseminated pyrite in relict stringer.* ***B.*** *Shear zone mineralisation.* ***C.*** *Protomylonitic shear zone with cataclasis and grain size reduction.*

Sulphide mineralisation in the intrusions of the AIC is complex, involving several processes like magma mixing, mingling and wall rock assimilation, and later hydrothermal remobilization and supergene alteration. The mineralisation is at very low Ni-Cu-PGE-Au grade and only the mafic-ultramafic sheets formed grades that may be comparable to known deposits. Several evidences support the occurrence of deeper-seated sulphides, which potentially host Ni-Cu-PGE-Au mineralisation at unexposed levels of the intrusions.

16.6 Flake graphite mineralisation in the Tasiilaq area

Flake graphite mineralisation is present in the high-grade metamorphic Kuummiut Terrane north of Tasiilaq. Graphite from Nuuk-Ilinnera has been known to the indigenous population for centuries and occurrences at Auppaluttoq and Kangikajik were recorded and investigated in some detail in earlier GGU campaigns (Fig. 16.13) (Rosing-Schow *et al.* in review). These three main occurrences have been studied in more detail during SEG.

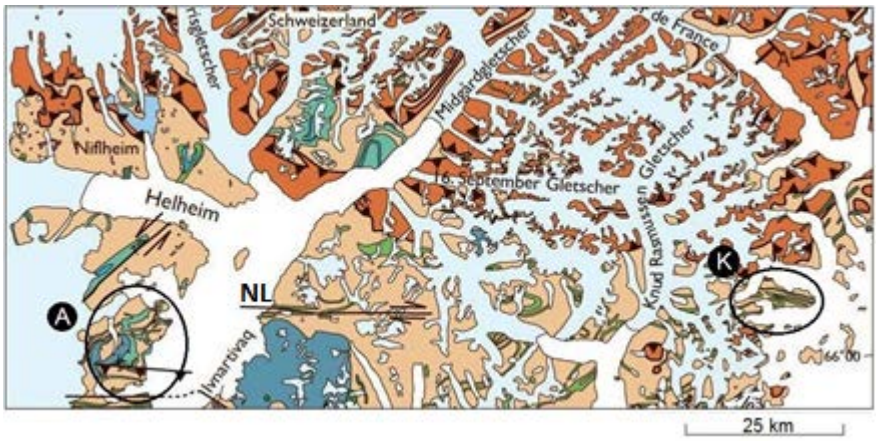

Figure 16.13 *Map with indication of the Auppaluttoq area, the Nuuk-Ilinnera area and the Kangikajik area which all carries graphite mineralisations.*

The rocks in the Auppaluttoq area (Fig. 16.14) are orthogneiss, amphibolite, paragneiss and biotite schist, which are cross-cut by pegmatite, and dolerite dykes and quartz-garnet veins. The oldest (F_1) ENE-trending folds are associated with layer sub-parallel, up to hundreds of meters long thrusts, which host the graphite mineralisation. The graphite content decreases outward from the shear zones, indicating that they acted as fluid conduits during hydrothermal mineralisation. Graphite mineralisation of > 30 vol.% graphite is hosted in 0.2 to 1.5 m-wide and 2 to 20 m long bands (Rosing-Schow *et al.* in review).

Figure 16.14 *Supergene limonite alteration zone in central Auppaluttoq. The graphite mineralised zone is approx. 300 m wide and surrounded by orthogneiss.*

The Kangikajik area (Fig. 16.13) consists of orthogneiss, amphibolite, grunerite-gneiss, paragneiss, quartzite and biotite schist, which show complex fold interference patterns. Graphite is concentrated in ~ 1.5 km wide D_1 shear zones, commonly forming anastomosing structures containing mineralised lenses draped around amphibolite, grunerite-gneiss and orthogneiss fragments. High-grade graphite mineralisation is up to 0.7 m wide and 20 m long, and locally forms rich lenses in F_1 fold hinges. Pegmatite dykes locally contain up to 2 vol. % graphite (Rosing-Schow *et al.* in review).

The Nuuk-Ilinnera area (Fig. 16.13) was a source of graphite for the local population in the early 1900s (T.F.D. Nielsen 2014 pers. comm.). The area contains metasedimentary rocks of the Kuummiut unit, which are interfolded with orthogneiss and amphibolite. Metre-scale D_1 shear zones are present sub-parallel to the trend on the F_1 fold axial traces. Graphite mineralisation of up to 10 vol.% graphite is hosted in 0.7- 20 m wide and up to 30 m long quartz-biotite-chlorite schist lenses (Rosing-Schow *et al.* in review).

Graphite mineralisation in all studied locations is flaky ranging from 0.2 to 4.0 mm across, and occurs together with quartz, plagioclase, biotite, amphibole, K-feldspar, titanite, pumpellyite and garnet (Rosing-Schow et al., in review).

X-ray diffraction shows that the graphite is well-ordered with the interlayer spacing of its crystalline structure ($d_{(002)}$) ranging from 3.352 to 3.357 Å. It is exclusively hexagonal, except for one sample in which approximately 15% of the rhombohedral polytype is observed. Raman spectroscopy shows that flake-type graphite has lower crystallinity, a higher D1/G ratio and higher D2 peaks, whereas anhedral graphite has higher crystallinity, a lower D1/G ratio with local disappearance of D1 and appearance of D2. The two types of graphite are locally intergrown. Estimated temperatures of graphite mineralisation indicate that the flaky graphite formed between 360 and 460°C, and anhedral graphite formed at 430° to > 640°C (Rosing-Schow et al., in review). The carbon isotope values of graphite are uniform and range between -31 and -18‰ (Rosing-Schow *et al.* in review). Liberation and grain-size analyses were completed on graphite ore with 13.7 wt% carbon and with 53.0 wt% carbon. Grain-size analyses show that 50% of the graphite grains are > 116 µm and > 153.71 µm, respectively. Approx. 65-71 wt% of the graphite is liberated by free surface liberation and ~60 wt% is liberated by composition liberation (Rosing-Schow *et al.* in review).

The graphite mineralisation is hosted in various rocks as well as in veins and breccia, with the richest mineralisation being located in shear zones. Hydrothermal alteration of the wall rocks associated with the graphite mineralisation indicates hydrothermal processes involved in the mineral system. Three stages of graphite mineralisation are distinguished: (1) organic matter was transformed to graphite during prograde metamorphism; (2) remobilization by hydrothermal fluids during retrograde exhumation, possibly in several stages; and (3) enrichment in supergene alteration zones. The carbon source likely is in the metasedimentary rocks of the Kuummiut unit based on the relatively low $\delta^{13}C$ values. Marble has carbon isotope composition that cannot be related to the graphite signature. The shear zones acted as pathways for metamorphic fluids, which scavenged carbon from the graphitic metasediments. Graphite precipitated from these carbon-bearing hydrothermal fluids resulted from hydration of the wall-rocks causing carbon-saturation. Supergene alteration led to enrichment in an approx. 2 m thick colluvium layer.

16.7 Gemstone corundum mineralisation in the Tasiilaq area

Corundum was first discovered by the Greenlandic Geological Survey (GGU) in the Síportôq supracrustal belt in the 1980's (see Hall *et al.* 1989a).

In 2009, the local prospector Vittus Sakæussen found corundum on a small island in the Nattivit Kangertiva, at Nattvit east of the fjord Sipportooq (Fig. 16.15), which won him the first price of the national mineral hunt Ujarassiorit. Vittus Sakæussen's locality was studied in detail in 2014 and 2015 during the SEGMENT project, and the supracrustal rocks that host this occurrence were investigated along the full length of their exposure on either side of the Nattivit Kangertiva and north of Isortoq.

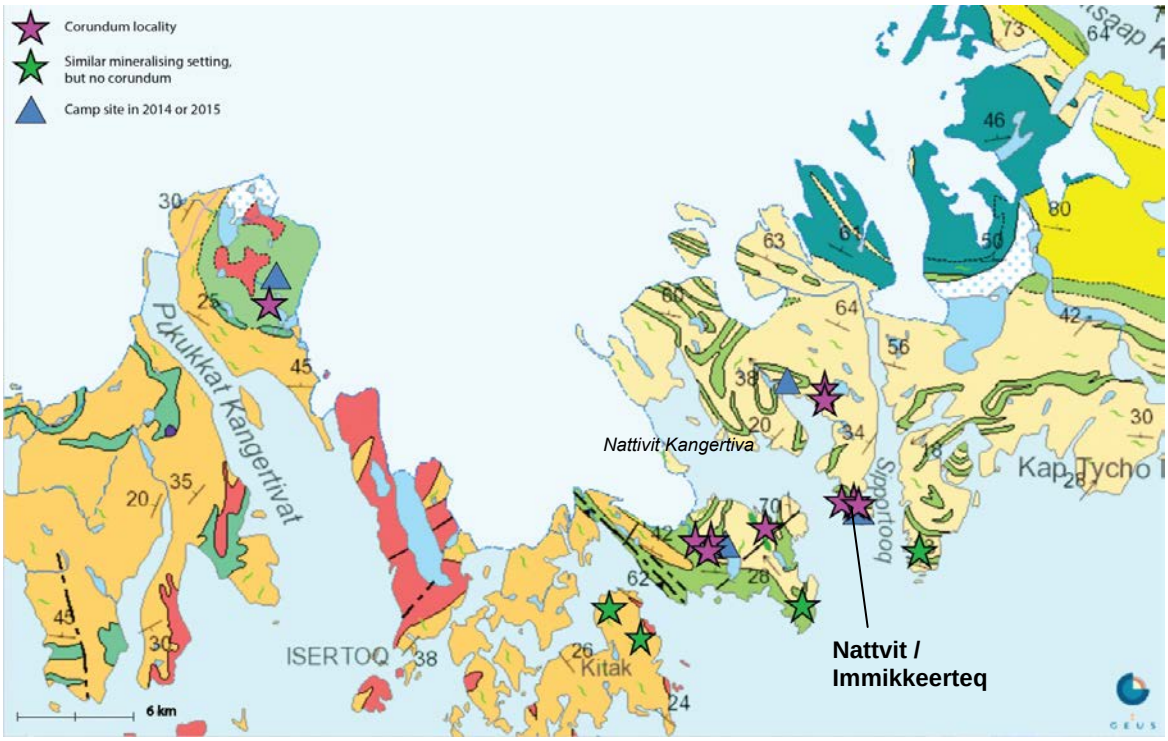

Figure 16.15 *Map of the SEGMENT 2015 follow-up on rubies in the Sipportooq area, east of Kap Tycho Brahe, with indications of the Nattivit Kangertiva (which is located close to Nattvit in the map), Immikkeerteq island, Kitak island and Nattivit Kangertiva fjord that hosts the ruby occurrences.*

The following corundum occurrences were found: (1) two floats with corundum at the coast of the inner fjord North of Isortoq, and in-situ in a roof-pendant of the Isortoq granite-diorite complex; (2) in-situ corundum occurrences on the small island in the Nattivit Kangertiva identified by Vittus Sakæussen, and equivalent lithologies on Immikkeerteq island; and (3) several occurrences in Kitak and on both sides of Nattivit Kangertiva (Fig. 16.15). The discovered corundum occurrences are of local extent and vary in size. Most of the corundum has a light pink colour with two samples having a purplish colour. However, the quality of the stones discovered so far is not of gemstone quality.

Corundum mineralisation in the Nattivit area is hosted in metamorphosed, hydrothermally altered and boudinaged ultramafic rocks that represent dykes or sills emplaced in a basement of paragneiss and amphibolite. Hydrothermal alteration and corundum mineralisation occurs, where the youngest pegmatite generation cross-cuts the ultramafic rocks (Fig. 16.16A). Notably, earlier pegmatite that is folded by regional deformation is not related to corundum mineralisation. At the contact of metamorphosed ultramafic rocks and young pegmatite, hydrothermal alteration zones developed: (1) an outer biotite or talc zone; (2) an intermediate black or green amphibole zone; and (3) an inner corundum or plagioclase zone.

The genesis of this hydrothermal alteration is interpreted to be related to fluid-assisted Si-Al exchange between the pegmatite and the metamorphosed ultramafic rocks. The amount of Si and the availability of hydrothermal fluid appear to control the style of mineralisation. The aluminium appears to come from the pegmatite and removal of silica creates new mineral zones and reaches Al_2O_3 saturation in the late-stage phases (Fig. 16.16B-D). The occurrences with corundum are local and most of the ultramafic rocks do not contain corundum (Fig. 16.16E-F). The last generation of pegmatites in the area are associated with the formation of corundum and cross-cuts the main foliation of the rocks in the area, while an earlier generation of pegmatites that is folded in the same way as the other lithologies, does not affect the ultramafic rocks at all. The amount of silica in the pegmatites are important to reach Al_2O_3 saturation during the desilification process, and in some places not all mineral stages are present due to limited fluid availability and at others the amount of fluid have been too high to reach corundum formation.

Although no occurrences of gemstone-quality corundum have been discovered, the documentation of hydrothermal corundum mineralisation in the Nattivit area shows the exploration potential for undiscovered deposits of better quality.

Figure 16.16 *Setting of the corundum formation in the Nattivit area.* ***A.*** *Partially altered ultramafic rock. Reaction zones rich in black and green amphiboles are locally corundum-bearing,* ***B.*** *Pegmatite (with person on top) crosscutting the orthogneiss and ultramafic rocks; these pegmatites trigger the corundum-forming reaction,* ***C.*** *Reaction zone in an ultramafic rock with brown, green and black amphiboles and a centre containing biotite and corundum or other minerals,* ***D.*** *close-up of a reaction zone with pink corundum grains,* ***E.*** *large corundum grains of variable quality,* ***F.*** *near-white corundum grains (e.g. above loupe) in a reaction zone rich in green amphibole.*

17 References

Andersen, T., Austrheim, H. and Bridgwater, D., 1989: P-T and fluid evolution of the Angmagssalik "charnockite" complex, SE Greenland. In: D. Bridgwater (Editor), Fluid Movements, Element Transport and the Composition of the Deep Crust. NATO Advanced Study Institute, Mathematical and Physical Sciences, Kluwer, Dordrecht, pp. 71-94.

Andersson, U.B., Rutanen, H., Johansson, Å., Mansfeld, J. and Rimša, A., 2007: Characterization of the Palaeoproterozoic mantle beneath the Fennoscandian Shield: geochemistry and isotope geology (Nd, Sr) of ~1.8 Ga mafic plutonic rocks from the Transscandinavian Igneous Belt in southeast Sweden. International Geology Review, **49**: pp. 587-625.

Andrews, J.R., Bridgwater, D., Gormsen, K., Gulson, B., Keto, L. and Watterson, J., 1973: The Precambrian of South-East Greenland. In: R.G. Park and J. Tarney (Editors), The Precambrian of Scotland and related rocks of Greenland. University of Keele, Keele, pp. 143-156.

Andrews, J.R., Bridgwater, D., Gulson, B. and Watterson, J., 1971: Reconnaissance mapping of South-East Grennland between 62 30' N and 60 30' S. Rapport Grønlands geologisk Undersøgelse, **35**: 32-38.

Árting, T.B., 2013: A detailed study of a Fe-Ti oxide band in the Njords Glacier Intrusion, Skjoldungen Alkaline Province, SE Greenland, University of Copenhagen, 30 pp.

Árting, T.B., 2016: A geochronological, petrological and geochemical investigation of the Palaeoproterozoic Tasiilaq Intrusive Centre, South-East Greenland, University of Copenhagen, unpublished 175 pp.

Baden, K., 2016: Palaeoproterozoic hydrothermal graphite-sulfide ± gold mineralization from the Tasiilaq area, South-East Greenland, Geological Survey of Denmark and Greenland Report, Copenhagen.

Bagas, L., Kolb, J., Fiorentini, M.L., Thébaud, N., Owen, J., Rennick, S. and Stensgaard, B.M., 2016: On the processes that formed Archaean Ni-Cu sulfide mineralisation inthe deep continental crust, Thrym Complex, southeastern Greenland. Precambrian Research, **277**: 68-86.

Bagas, L., Næraa, T., Kolb, J., Reno, B.L. and Fiorentini, M.L., 2013: Partial melting of the Archaean Thrym Complex of southeastern Greenland. Lithos, **160-161**: 164-182.

Bartels, A., Nielsen, T.F.D., Lee, S.R., Upton, B.G.J. and Thomsen, T.B., 2015: Petrological and geochemical characteristics of Mesoproterozoic dyke swarms in the Gardar Province, South Greenland: evidence for a major sub-continental lithospheric mantle component in the generation of the magmas. Mineralogical Magazine, **79(4)**: 909-939.

Bartels, A., Nilsson, M.K.M., Klausen, M.B. and Söderlund, U., 2016: Mesoproterozoic dykes in the Timmiarmiit area, Southeast Greenland: evidence for a continuous Gardar dyke swarm across Greenland's North Atlantic Craton. GFF, **138(1)**: 255-275.

Beckinsale, R.D., Brooks, C.K. and Rex, D.C., 1970: K-Ar ages for the Tertiary of East Greenland. Bulletin of the Geological Society of Denmark, **20**: 27-37.

Berger, A., Kokfelt, T.F. and Kolb, J. 2014 (in press): Exhumation rates in the Archaean from pressure-time paths: example from the Skjoldungen Orogen (SE Greenland). Precambrian Research: in press.

Bernstein, S. and Bird, D.K., 2000: Formation of wehrlites through dehydration of metabasalt xenoliths in layered gabbros of the Noe-Nygaard Intrusion, Southeast Greenland. Geological Magazine, **137(02)**: 109-128.

Blichert-Toft, J., Arndt, N.T. and Ludden, J.N., 1996: Precambrian alkaline magmatism. Lithos, **37**: 97-111.

Blichert-Toft, J., Rosing, M.T., Lesher, C.E. and Chauvel, C., 1995: Geochemical constraints on the origin of the Late Archaean Skjoldungen alkaline igneous province, SE Greenland. Journal of Petrology, **36(2)**: 515-561.

Bothma, R., 2013: Google Earth Mapping, Petrography and Geochemistry of Proterozoic Dyke Swarms in the Umivik Area, SE Greenland. Unpublished Honours Thesis, Stellenbosch University, 32 pp.

Bridgwater, D., 1976: Nagssugtoqidian mobile belt in East Greenland. In: A. Escher and W.S. Watt (Editors), Geology of Greenland. Geological Survey of Greenland, Copenhagen, pp. 97-103.

Bridgwater, D., Austrheim, H., Hansen, B.T., Mengel, F., Pedersen, S. and Winter, J., 1990: The Proterozoic Nagssugtoqidian mobile belt of southeast Greenland: a link between the eastern Canadian and Baltic shields. Geoscience Canada, **17(4)**: 305-310.

Bridgwater, D., Davies, F.B., Gill, R.C.O., Gorman, B.E., Henriksen, N. and Watterson, J., 1976: Field mapping of the Nagssugtoqidian of South-East Greenland. 74-83.

Bridgwater, D., Davies, F.B., Gill, R.C.O., Gorman, B.E., Henriksen, N. and Watterson, J., 1977: Field mapping in the Nagssugtoqidian of South-East Greenland. Rapport Grønlands Geologisk Undersøgelse, **85**: 74-83.

Bridgwater, D., Davies, F.B., Gill, R.C.O., Gorman, B.E., Myers, J.S., Pedersen, S. and Taylor, P., 1978: Precambrian and Tertiary geology between Kangerdlugssuag and Angmagssalik, East Greenland: a preliminary report. Rapport Grønlands Geologiske Undersøgelse **83**. 17 pp.

Bridgwater, D., Escher, A. and Watterson, J., 1973: Dyke swarms and the persistence of major geological boundaries in Greenland. In: R.G. Park and J. Tarney (Editors), The Early Precambrian of Scotland and related rocks of Greenland. Proceedings of the Conference held at the Department of Geology, University of Keele, Staffordshire, pp. 200.

Bridgwater, D. and Gormsen, K., 1968: Precambrian rocks of the Angmagssalik area, East Greenland. Rapport Grønlands Geologisk Undersøgelse, **15**: 61-71.

Bridgwater, D. and Gormsen, K., 1969: Geological reconnaissance of the Precambrian rocks of South-East Greenland. Rapport Grønlands geologisk Undersøgelse, **19**: 43-50.

Bridgwater, D. and Myers, J.S., 1979: Outline of the Nagssugtoqidian mobile belt of East Greenland. Rapport Grønlands geologisk Undersøgelse, **89**: 9-18.

Brooks, C.K., 1977: Example of magma mixing from the Kialineq district of East Greenland. Bulletin of the Geological Society of Denmark.

Brooks, C.K., 1989: The Geology of the East Greenland Margin. Springer Netherlands, Dordrecht, pp. 47-65.

Brooks, C.K., 2011: The East Greenland rifted volcanic margin, 24. Geological Survey of Denmark and Greenland Bulletin, Copenhagen, 96 pp.

Brooks, C.K. and Stenstrop, G., 1989: The Ivnartivaq complex, Sermilik, Ammassalik. In: F. Kalsbeek (Editor), Geology of the Ammassalik region, South-East Greenland. Grønlands Geologiske Undersøgelse (GGU), Copenhagen, pp. 87-91.

Brown, P.E. and Becker, S.M., 1986: Fractionation, hybridisation and magma-mixing in the Kialineq centre East Greenland. Contributions To Mineralogy And Petrology, **92(1)**: 57-70.

Brown, P.E., van Breeman, O., Noble, R.H. and Macintyre, R.M., 1977: Mid-tertiary igneous activity in east Greenland — The Kialineq complex. Contributions To Mineralogy And Petrology, **64(1)**: 109-122.

Chadwick, B., Dawes, P.R., Escher, J.C., Friend, C.R.L., Hall, R.P., Kalsbeek, F., Nielsen, T.F.D., Nutman, A.P., Soper, N.J. and Vasudev, V.N., 1989: The Proterozoic mobile belt in the Ammassalik region, South-East Greenland (Ammassalik mobile belt): an introduction and reappraisal. In: F. Kalsbeek (Editor), Geology of the Ammassalik region, South-East Greenland. Grønlands Geologiske Undersøgelse (GGU), Copenhagen.

Chadwick, B. and Vasudev, V.N., 1989: Some observations on the structure of the early Proterozoic, Ammassalik mobile belt in the Ammassalik region, South-East Greenland. In: F. Kalsbeek (Editor), Geology of the Ammassalik region, South-East Greenland Grønlands Geologiske Undersøgelse (GGU), Copenhagen, pp. 29-40.

Dawes, P.R., 1989: The Grusgraven locality: border relationships between Precambrian supracrustal rocks and orthogneisses, Kangikajik, South-East Greenland. In: F. Kalsbeek (Editor), Geology of the Ammassalik region, South-East Greenland. Grønlands Geologiske Undersøgelse (GGU), Copenhagen, pp. 23-28.

Dawes, P.R., Friend, C.R.L., Nutman, A.P. and Soper, N.J., 1989a: The Blokken gneisses: a reappraisal. In: F. Kalsbeek (Editor), Geology of the Ammassalik region, South-East Greenland. Grønlands Geologiske Undersøgelse (GGU), Copenhagen, pp. 83-86.

Dawes, P.R., Soper, N.J., Escher, J.C. and Hall, R.P., 1989b: The northern boundary of the Proterozoic (Nagssugtoqidian) mobile belt of South-East Greenland. In: F. Kalsbeek (Editor), Geology of the Ammassalik region, South-East Greenland. Grønlands Geologiske Undersøgelse (GGU), Copenhagen, pp. 54-65.

Deer, W.A., 1976: Tertiary igneous rocks between Scoresby Sund and Kap Gustav Holm, East Greenland. Geology of Greenland.

Escher, J.C., 1990: Skjoldungen 62°30'–67°00'N; 35°50'–43°15'W. Geological map of Greenland 1:500 000 (Geologisk kort over Grønland), Sheet 14. Geological Survey of Denmark and Greenland, Copenhagen.

Escher, J.C. and Hall, R.P., 1989: The Niflheim thrust: a tectonic contact between granulite and amphibolite facies gneisses, South-East Greenland. In: F. Kalsbeek (Editor), Geology of the Ammassalik region, South-East Greenland. Grønlands Geologiske Undersøgelse (GGU), Copenhagen, pp. 66-69.

Escher, J.C. and Nielsen, T.F.D., 1983: Archaean gneisses and supracrustal rocks of the Tingmiarmiut region, South-East Greenland. Rapport Grønlands geologisk Undersøgelse, **115**: 79-82.

Evans, D.A.D. and Mitchell, R.N., 2011: Assembly and breakup of the core of Palaeoproterozoic-Mesoproterozoic supercontinent Nuna. Geology, **39**: 443-446.

Friend, C.R.L. and Kinny, P.D., 2001: A reappraisal of the Lewisian Gneiss Complex: geochronological evidence for tectonic assembly of disparate terranes in the Proterozoic. Contributions to Mineralogy and Petrology, **142**: 198-218.

Friend, C.R.L. and Nutman, A.P., 1989: The geology and structural setting of the Proterozoic Ammassalik Intrusive Complex, South-East Greenland. In: F. Kalsbeek (Editor), Geology of the Ammassalik region, South-East Greenland. Grønlands Geologiske Undersøgelse (GGU), Copenhagen, pp. 41-45.

Gaina, C., Werner, S.C., Saltus, R., Maus, S. & the CAMP-GM GROUP 2011: Circum-Arctic mapping project: new magnetic and gravity anomaly maps of the Arctic. In: Spencer, A. M., Embry, A. F., Gautier, D. L., Stoupakova, A. V. & Sørensen, K. (eds) Arctic Petroleum Geology. Geological Society, London, Memoirs, **35**, 39–48.

Garde, A.A. 2007: Sydgrønland 59°30'–62°30'N; 42°00'–50°30'W. Second Edition, Geological map of Greenland 1:500 000 (Geologisk kort over Grønland), Sheet 1. Geological Survey of Denmark and Greenland, Copenhagen.

Garde, A.A., Grocott, J. and McCaffrey, K.J.W., 1999: New insights on the north-eastern part of the Ketilidian orogen in South-East Greenland. Geology of Greenland Survey Bulletin, **183**: 23-33.

Garde, A.A., Hamilton, M.A., Chadwick, B., Grocott, J. and McCaffrey, K.J.W., 2002: The Ketilidian orogen of South Greenland: geochronology, tectonics, magmatism, and fore-arc accretion during Palaeoproterozoic oblique convergence. Canadian Journal of Earth Sciences, **39**: 765-793.

Geldenhuys, P.R., 2015: Petrogenesis and magmatic evolution of intrusive complexes along the Nordre Skjoldungensund, Late Archaean Skjoldungen Alkaline Province, SE Greenland, Stellenbosch University, unpublished, 53 pp.

Gill, R.C.O., Nielsen, T.F.D., Brooks, C.K. and Ingram, G.A., 1988: Tertiary volcanism in the Kangerdlugssuaq region, E Greenland: trace-element geochemistry of the Lower Basalts and tholeiitic dyke swarms. Geological Society, London, Special Publications, **39(1)**: 161-179.

Gleadow, A.J.W. and Brooks, C.K., 1979: Fission track dating, thermal histories and tectonics of igneous intrusions in East Greenland. Contributions To Mineralogy And Petrology, **71(1)**: 45-60.

Greeff, J., 2012: Petrogenesis of late/kinematic dykes and sheets within the 2.7 Ga Skjoldungen Alkaline Province, South East Greenland, Stellenbosch University, unpublished 51 pp.

Grobbelaar, 2012: Petrographical and geochemical variations across the layered ultramafic-mafic Vend Om intrusion within the 2.7 Ga Skjoldungen Alkaline Province, southeast Greenland, Stellenbosch University, unpublished 37 pp.

Grøtner, B.D., 2014: Sulphide mineralisation in the Tasiilaq Intrusion, Ammassalik, South-East Greenland, Copenhagen University, Copenhagen, 30 pp.

Hall, R.P., Chadwick, B., Escher, J.C. and Vasudev, V.N., 1989a: Supracrustal rocks in the Ammassalik region, South-East Greenland. In: F. Kalsbeek (Editor), Geology of the Ammassalik region, South-East Greenland. Grønlands Geologiske Undersøgelse (GGU), Copenhagen, pp. 17-22.

Hall, R.P. and Hughes, D.J., 1987: Noritic dykes of southern West Greenland: early Proterozoic boninitic magmatism. Contributions to Mineralogy and Petrology, **97(2)**: 169-182.

Hall, R.P., Hughes, D.J. and Joyner, L., 1989b: Basic dykes of the southern Ammassalik region, South-East Greenland: preliminary mineralogical and geochemical results. In: F. Kalsbeek (Editor), Geology of the Ammassalik region, South-East Greenland. Grønlands Geologiske Undersøgelse (GGU), Copenhagen, pp. 79-82.

Halls, H.C., Hamilton, M.A. and Denyszyn, S.W., 2011: The Melville Bugt Dyke Swarm of Greenland: a Connection to the 1.5-1.6 Ga Fennoscandian Rapakivi Granite Province? In: R.K. Srivastava (Editor), Dyke Swarms: Keys for Geodynamic Interpretation. Springer-Verlag, Berlin, Heidelberg, pp. 509-535.

Hanghøj, K., Storey, M. and Stecher, O., 2003: An Isotope and Trace Element Study of the East Greenland Tertiary Dyke Swarm: Constraints on Temporal and Spatial Evolution during Continental Rifting. Journal of Petrology, **44(11)**: 2081-2112.

Hansen, B.T. and Kalsbeek, F., 1989: Precise age for the Ammassalik Intrusive Complex. In: F. Kalsbeek (Editor), Geology of the Ammassalik region, South-East Greenland. Grønlands Geologiske Undersøgelse (GGU), Copenhagen, pp. 46-47.

Holden, E-J., Dentith, M.& Kovesi, P. 2008: Towards the automated analysis of regional aero-magnetic data to identify regions prospective for gold deposits. Computer & Geosciences, **34**, 1505-1513.

Johansson, Å., 2013: From Rodinia to Gondwana with the 'SAMBA' model – a distant view from Baltica towards Amazonia and beyond. Precambrian Research, **244**: 226-235.

Kalsbeek, F., 1989: Geology of the Ammassalik region, South-East Greenland. Grønlands Geologiske Undersøgelse Rapport, 146. Geological Survey of Greenland, Copenhagen, 112 pp.

Kalsbeek, F., Austrheim, H., Bridgwater, D., Hansen, B.T., Pedersen, S. and Taylor, P., 1993: Geochronology of Archaean and Proterozoic events in the Ammassalik area, South-East Greenland, and comparisons with the Lewisian of Scotland and the Nagssugtoqidian of West Greenland. Precambrian Research, **62**: 239-270.

Kalsbeek, F. and Taylor, P., 1985: Age and origin of early Proterozoic dolerite dykes in South-West Greenland. Contributions to Mineralogy and Petrology, **89(4)**: 307-316.

Kalsbeek, F. and Taylor, P.N., 1986: Chemical and isotopic homogeneity of a 400 km long basic dyke in central West Greenland. Contributions to Mineralogy and Petrology, **93**: 439-448.

Kalvig, P. 1992: Geologisk undersøgelse af grafitforekomster Kangikajik, Tasiilaq Kommune. Udført for Tasiilaq Kommune og Grønlands baseselskab A/S af Mineral Development Int. A/S, marts 1992. Internal report, Tasiilaq Kommune, 41 pp., 2 app., 2 plates. (in archives of Geological Survey of Denmark and Greenland, GEUS Report File GRF **21317**).

Klausen, M.B., 2006: Similar dyke thickness variation across three volcanic rifts in the North Atlantic region: implications for intrusion mechanisms. Lithos, **92**: 137-153.

Klausen, M.B. and Kokfelt, T.F., 2014: Field report from the 2011 field season on the Skjoldungen Alkaline Province, South-East Greenland. Geological Survey of Denmark and Greenland Report, **2014/81**: 85.

Klausen, M.B. and Loreti, O.D., 2016: Coast-parallel Tertiary dykes in South-East Greenland., the Igneous and Metamorphic Study Group, Langebaan, University of Cape Town.

Klausen, M.B., Nilsson, M.K.M., Snyman, D., Bothma, R., Kolb, J., Tappe, S., Kokfelt, T.F., Nielsen, T.F.D. and Denyszyn, S.W., 2014.: The >2000 km-long 1.63 Ga Melville Bugt Dyke Swarm and its petrogenetic relationship to the ~1.8 Ga Ketilidian Orogen: evidence from SE Greenland, Nordic Geological Winter Meeting, Lund, Sweden, pp. 85.

Klausen, M.B. and Larsen, H.C., 2002: East Greenland coast-parallel dike swarm and its role in continental breakup. Geological Society of America, pp. 133-158.

Kleckner, A., 1997: Petrogenetic Implications of the Presence of Meteoric Water in the Northern Monzonite Intrusion of Kap Gustav Holm and Other Nearby East Greenland, Unpublished MSc Thesis Standford University, pp. 75.

Kokfelt, T.F., Næraa, T., Thrane, K. and Bagas, L., 2016a (in press): Zircon U-Pb and Hf isotopic constrains on the crustal evolution of the Skjoldungen region, South-East Greenland, Review of Survey activities 2015. Geological Survey of Denmark and Greenland Bulletin, Copenhagen.

Kokfelt, T.F., Thrane, K. and Næraa, T., 2016b (in press): Geochronology of basement rocks and intrusions of the larger Tasiilaq area, South-East Greenland (64° 20' – 67° N) (Volume 3), Geological Survey of Denmark and Greenland Report, Copenhagen

Kokfelt, T.F., Thrane, K., Næraa, T., Klausen, M.B. and Tegner, C., 2016c: Geochronology of the Skjoldungen Alkaline province, South-East greenland, Geological Survey of Denmark and Greenland Report, Copenhagen.

Kokfelt, T.F., Weatherley, S.M., Keiding, J.K. and Árting, T.B., 2015a: Field report for the 2014 field season, South East Greenland - intrusions in the larger Tasiilaq region, Geological Survey of Denmark and Greenland Report, Copenhagen

Kokfelt, T.F., Weatherley, S.M., Keiding, J.K. and Árting, T.B., 2015b: Magma mixing, mingling and hybridisation at different crustal levels: snapshots from 1.9 billion years of magmatism in south-eastern Greenland, Review of Survey activities 2014. Geological Survey of Denmark and Greenland Bulletin, Copenhagen, pp. 45-48.

Kolb, J., 2014: Structure of the Palaeoproterozoic Nagssugtoqidian Orogen, South-East Greenland: model for the tectonic evolution. Precambrian Research, **255**: 809-822.

Kolb, J., Thrane, K. and Bagas, L., 2013: Field relationship of high-grade Neo- to Mesoarchaean rocks of South-East Greenland: Tectonometamorphic and magmatic evolution. Gondwana Research, **23**: 471-491.

Kovesi, P. 2012: Phase preserving tone mapping of non-photographic high dynamic range images. Digital Image Computing Techniques and Applications (DICTA), 2012 International Conference on Digital Image Computing Techniques and Applications (DICTA). Vol. **1** USA: IEEE, 2012. p. 1-8.

Lally, B.D., 2013: Geological mapping and tectonostratigraphy of mineralised mafic bands of the Timmiarmiut region of South-East Greenland. South-East Greenland Mineral Endowment

Task Project, SEGMENT 2009–2014, Geological Survey of Denmark and Greenland Report, Copenhagen.

Larsen, H.C., 1978: Offshore continuation of East Greenland dyke swarm and North Atlantic Ocean formation. Nature, **274(5668)**: 220-223.

Lassen, B., Bridgwater, D., Bernstein, S. and Rosing, M.T., 2004: Assimilation and high-pressure fractional crystallization (AFC) recorded by Paleo-proterozoic mafic dykes, Southeast Greenland. Lithos, **72**: 1-18.

Le Maitre, R.W., 2002: Igneous Rocks: A Classification and Glossary of Terms. Cambridge University Press, 236 pp.

Lenoir, X., Féraud, G. and Geoffroy, L., 2003: High-rate flexure of the East Greenland volcanic margin: constraints from 40Ar/39Ar dating of basaltic dykes. Earth and Planetary Science Letters, **214(3-4)**: 515-528.

Lenskjold, A., 2015: Petrologisk og geokemisk undersøgelse af Sulugssut komplekset, SØ Grønland, Unpublished BSc Thesis.

Lie, A. 1997: Reconnaissance scale geochemical exploration and compilation of regional data from the Ammassalik area, South-East Greenland. Nunaoil A/S (Exploration Licence 15/96). 22p. + 32 enclosed thematic maps, 1 disc (in archives of Geological Survey of Denmark and Greenland, GEUS Report File GRF **21520**).

Lie, A., 1998: Nickel, Gold and PGE-Discoveries on the Ammassalik Island, South East Greenland, and Results of the VLF-EM Test Survey, NunaMinerals A/S, 43 pp., 8 appendices. (in archives of Geological Survey of Denmark and Greenland, GEUS Report File GRF **21690**).

Loreti, O.D., 2015: Onshore distribution, magma compositions and petrogenesis of potential Tertiary mafic dykes along the rifted margin of southern SE Greenland, Unpublished Honours Thesis, 52 pp.

Meen, J.K., 1987: Formation of shoshonites from calcalkaline basalt magmas: geochemical and experimental constraints from the type locality. Contributions to Mineralogy and Petrology, **97**: 333-351.

Murphy, J.B., 2013: Appinite suites: a record of the role of water in the genesis, transport, emplacement and crystallization of magma. Earth-Science Reviews, **119**: 35-59.

Myers, J.S., 1980: Structure of the coastal dyke swarm and associated plutonic intrusions of East Greenland. Earth and Planetary Science Letters, **46(3)**: 407-418.

Myers, J.S., 1984: The Nagssugtoqidian mobile belt of Greenland. In: A. Kröner and R. Greiling (Editors), Precambrian Tectonics Illustrated. Schweitzerbart, Stuttgart, pp. 237-250.

Myers, J.S., 1987a: The East Greenland Nagssugtoqidian mobile belt compared with the Lewisian complex. In: R.G. Park and J. Tarney (Editors), Evolution of the Lewisian and comparable Precambrian high-grade terranes. Special Publication of the Geological Society of London, London, pp. 235-246.

Myers, J.S., Austrheim, H., Gill, R., Gorman, B.E. and Rex, D., 1979a: Field work on the Nagssugtoqidian boundary north of Angmagssalik and Tertiary igneous rocks of Kialineq and Kap Gustav Holm, East Greenland. Rapp. Grønl. Geol. Unders.

Myers, J.S., Austrheim, H., Gill, R.C.O., Gorman, B.E. and Rex, D.C., 1979b: Field work on the Nagssugtoqidian boundary north of Angmagssalik and Tertiary igneous rocks of Kialineq and Kap Gustav Holm, East Greenland. Rapport Grønlands geologisk Undersøgelse, **95,** pp. 82-85.

Myers, J.S., Dawes, P.R. & Nielsen, T.F.D. 1988: Kangerdlugssuaq 66°00'–69°00'N; 24°00'–36°30'W. Geological map of Greenland 1:500 000 (Geologisk kort over Grønland), Sheet 13. Geological Survey of Denmark and Greenland, Copenhagen.

Myers, J.S., Gill, R.C.O., Rex, D.C. and Charnley, N.R., 1993: The Kap Gustav Holm Tertiary Plutonic Centre, East Greenland. Journal Of The Geological Society, **150(2)**: 259-276.

Müller, S., Dziggel, A. and Kolb, J., 2016: Metamorphic evolution of relict eclogite-facies rocks in the Nagssugtoqidian Orogen, Southeast Greenland, North Atlantic Craton Conference, NAC+ 2016, Edinburgh, pp. 26.

Maarupgaard, B.P., 2015: Petrology of the 2.7 Ga Vend Om Intrusion, Skjoldungen Alkaline Province, SE Greenland, Aarhus University, unpublished, 90 pp.

Nielsen, T., Soper, N.J., Brooks, C.K., Faller, A.M., Higgins, A.C. and Matthews, D.W., 1981: The pre-basaltic sediments and the Lower Basalts at Kangerdlugssuaq, East Greenland: their stratigraphy, lithology, palaeomagnetism, and petrology. Meddelelser om Grønland Geoscience, **6**.

Nielsen, T.F.D., 1975: Possible mechanism of continental breakup in the North Atlantic. , Published online: 17 January 1975; doi:10.1038/253182a0, **253(5488)**: 182-184.

Nielsen, T.F.D., 1978: The Tertiary dike swarms of the Kangerdlugssuaq area, East Greenland. An example of magmatic development during continental break-up. Contributions to Mineralogy and Petrology, **67**: 63-78.

Nielsen, T.F.D., 1990: Melville Bugt dyke swarm: a major 1645 Ma alkaline magmatic event in West Greenland. In: A.J. Parker, P.C. Rickwood and D.H. Tucker (Editors), Mafic dykes and emplacement mechanisms. A.A. Balkema, Rotterdam, pp. 497-505.

Nielsen, T.F.D., 2002: Palaeogene intrusions and magmatic complexes in East Greenland, 66 to 75° N, **2002/113**. Geological Survey of Denmark and Greenland Report, 249 pp.

Nielsen, T.F.D. and Brooks, C.K., 1981: The E Greenland rifted continental margin: an examination of the coastal flexure. Journal Of The Geological Society, **138(5)**: 559-568.

Nielsen, T.F.D. and Escher, J.C., 1985: Preparations for the South-East Greenland mapping project 1986-1987. Rapport Grønlands geologisk Undersøgelse, **125**: 84-87.

Nielsen, T.F.D. and Rosing, M.T., 1990: The Archaean Skjoldungen alkaline province, South-East Greenland. Rapport Grønlands geologisk Undersøgelse, **148**: 93-100.

Nielsen, T.F.D., Rosing, M.T. and Vasudev, V.N., 1988: The nephelinitic Singertat Complex. The Archaean terrains in South-East Greenland. GGU.

Nilsson, M.K.M., 2016: New constraints on paleoreconstructions through geochronology of mafic dyke swarms in North Atlantic Craton. Lund: Lund University, Faculty of Science, Department of Geology, Lithosphere and Biosphere Science, PhD Thesis, pp. 104.

Nilsson, M.K.M., Klausen, M.B., Söderlund, U. and Ernst, R.E., 2013: Precise U–Pb ages and geochemistry of Palaeoproterozoic mafic dykes from southern West Greenland: Linking the North Atlantic and the Dharwar cratons. Lithos, **174**: 255-270.

Nutman, A.P., Dawes, P.R., Kalsbeek, F. and Hamilton, M.A., 2008a: Palaeoproterozoic and Archaean gneiss complexes in northern Greenland: Palaeoproterozoic terrane assembly in the High Arctic. Precambrian Research, **161**: 419-451.

Nutman, A.P., Kalsbeek, F. and Friend, C.R.L., 2008b: The Nagssugtoqidian Orogen in South-East Greenland: evidence for Palaeoproterozoic collision and plate assembly. American Journal of Science, **308**: 529-572.

Nutman, A.P. and Rosing, M.T., 1994: SHRIMP U-Pb zircon geochronology of the late Archaean Ruinnæsset syenite, Skjoldungen alkaline province, South-East Greenland. Geochimica et Cosmochimica Acta, **58**: 3515-3518.

Næraa, T., Kokfelt, T. and Thrane, K., 2016: Geochronology of the larger Skjoldungen area, South-East Greenland (62°30'-64°N), Geological Survey of Denmark and Greenland Report, Copenhagen.

Næraa, T., Kokfelt, T.F. and Thrane, K., 2014: Zircon geochronology of the Skjoldungen region, SE Greenland, 31st Nordic Geological Winter Meeting. Geological Society of Sweden, Lund, pp. 92.

Owen, J. and Kolb, J., 2012: Characterisation of the Nickel Sulphide Mineralisation between Graah Fjord and Bernstorff Isfjord, South-East Greenland, **2012/66**. Geological Survey of Denmark and Greenland Report, Copenhagen.

Pedersen, S. and Bridgwater, D., 1979: Isotopic re-equilibration of Rb-Sr whole rock systems during reworking of Archaean gneisses in the Nagssugtoqidian mobile belt, East Greenland. Rapport Grønlands Geologisk Undersøgelse, **89**: 133-146.

Pesonen, L.J., Mertanen, S. and Veikkolainen, T., 2012: Paleo-Mesoproterozoic Supercontinents – a Paleomagnetic View. Geophysica, **48**: 5-47.

Pedersen, M., Weng, W.L., Keulen, N. Kokfelt, T.F. 2013: A new seamless digital 1:500 000 scale geological map. Geological Survey of Denmark and Greenland Bulletin 28, 65–68. (open access to arcticle: www.geus.dk/publications/bull; open access to map: http://data.geus.dk/map2/geogreen)

Petersen. J. & Thomsen, L.L. 2014: Results in South-East Greenland from Ujarassiorit-program In: Stensgaard, B.M. (ed.) 2014: South-East Greenland Mineral Endowment Task (SEGMENT): 2014 Workshop Abstract Volume and Status Primo-2014. Danmarks og Grønlands Geologiske Undersøgelse Rapport **2014/79**. GEUS, p. 65-66.

Philpotts, A.R., 1967: Origin of certain iron-titanium oxide and apatite rocks. Economic Geology, **62**: 303-315.

Poulsen, P.B., 2016: Mineralisation in a volcanic succession in the Kialineq magmatic complex, East Greenland, Unpublished MSc thesis, University of Aarhus

Rennick, S. and Kolb, J., 2012: Structural control and stratigraphy of the mafic and ultramafic units between Graah Fjord and Bernsto[r]ff Isfjord, South-East Greenland. South-East Greenland Mineral Endowment Task Project, SEGMENT 2009–2014., Geological Survey of Denmark and Greenland Report, Copenhagen.

Rasmussen, T.M. 2013: Airborne geophysical surveys in Greenland. Exploration and Mining in Greenland. Fact Sheet No.**27**, 2 pp.

Rasmussen, T.M., Thorning, L., Riisager, P. and Tukiainen, T. 2013: Airborne geophysical data from Greenland. Geology and Ore, Exploration and Mining in Greenland, **22**, 12 pp.

Riisager, P. & Rasmussen, T.M. 2013: Aeromagnetic survey in south-eastern Greenland: project Aeromag 2013. Geological Survey of Denmark and Greenland Bulletin, **31**, 63–67.

Rosa, D. and Ulrich, T., 2015: A quartz-wolframite-molybdenite vein and scheelite in amphibolite horizons from Thrudvang peninsula, Skjoldungen, SE Greenland. Geological Survey of Denmark and Greenland Bulletin, **33**: 49-52.

Rosing-Schow, N., Bagas, L., Kolb, J., Balić-Žunić, T., Korte, C. and Fiorentini, M.L.: in review. Hydrothermal flake graphite mineralisation in Palaeoproterozoic rocks of South-East Greenland. Mineralium Deposita.

Rucklidge, J.C., Brooks, C.K. and Nielsen, T., 1980: Petrology of the coastal dykes at Tugtilik, southern East Greenland. Meddelelser om Grønland Geoscience, **3**: 17.

Rutanen, H., Anderssson, U.B., Väisänen, M., Johansson, Å., Fröjdö, S., Lahaye, Y. and Eklund, O., 2011: 1.8 Ga magmatism in southern Finland: strongly enriched mantle and juvenile crustal sources in a post-collisional setting. International Geology Review, **53**: 1622-1683.

Rämö, O.M., 1991: Petrogenesis of the Proterozoic rapakivi granites and related basic rocks of southeastern Fennoscandia: Nd and Pb isotopic and general geochemical constraints. Geological Survey of Finland Bulletin, **355**: 1-161.

Snyman, D., 2013: Petrogenesis of Precambrian dikes and sheets within the Timmiarmiut Alkaline Province of South-East Greenland. Unpublished Honours Thesis, Stellenbosch University, 72 pp.

Srivastava, R.J., 2008: Global Intercratonic Boninite-Norite Magmatism during the NeoArchaean-Palaeoproterozoic: Evidence from Central Indian Bastar Craton. International Geology Review **50**, 61-74.

St-Onge, M., van Gool, J.A.M., Garde, A.A. and Scott, D., 2009: Correlation of Archaean and Palaeoproterozoic units between northeastern Canada and western Greenland: constraining the pre-collisional upper plate accretionary history of the Trans-Hudson orogen. Accretionary Orogens in Space and Time, **318**. Geological Society Special Publications, London.

Steenfelt, A. 2013: Overview of stream sediment geochemistry data with focus on gold and its pathfinders. Presentation at "Assessment of the orogenic gold potential in Greenland" workshop, 19 - 21 November 2014, GEUS, Copenhagen. In: Kolb et al. (in prep.) Assessment of orogenic gold mineralization in Greenland: Report of the "Assessment of the orogenic gold potential in Greenland" workshop, 19 - 21 November 2014, GEUS, Copenhagen.

Stensgaard, B.M. 2015: South-East Greenland Mineral Endowment Task (SEGMENT) - Project status 2014. Danmarks og Grønlands Geologiske Undersøgelse Rapport. **2015/32**. GEUS, 58 pp.

Stensgaard, B.M., Kolb, J., Nielsen, T.F.D., Olsen, S.D., Pilbeam, L., Lieber, D. and Clausen, A., 2010: The mineral resource assessment project, South-East Greenland: year one. Geological Survey of Denmark and Greenland Bulletin, **20**: 59-62.

Stensgaard, B.M. & Kolb, J. 2015: Assessing one of the last frontiers in mineral exploration. Greenland Day in Perth. 9 December, 2015. Perth, Australia. Government of Greenland - Ministry of Mineral Resources & Center of Exploration Targeting, University of Western Australia. Exploration Connect - Exploration Advice (www.explorationconnect.com.au).

Storey, M., Duncan, R.A. and Tegner, C., 2007: Timing and duration of volcanism in the North Atlantic Igneous Province: Implications for geodynamics and links to the Iceland hotspot. Chemical Geology, **241(3-4)**: 264-281.

Sun, S.S. and McDonough, W.F., 1989: Chemical and isotopic systematics of oceanic basalts. In: A.D. Saunders and M.J. Norry (Editors), Magmatism in the Ocean Basins. Geological Society Special Publication, London, pp. 313-345.

Tegner, C., Duncan, R.A., Bernstein, Brooks, C.K., Bird, D.K. & Storey, M. 1998: 40Ar-39Ar geochronology of Tertiary mafic intrusions along the East Greenland rifted margin: Relation to flood basalts and the Iceland hotspot track, Earth and Planetary Science Letters, **156**, 75 -88.

Tegner, C., Brooks, C.K., Heister, L.E. and Bernstein, S., 2008: 40Ar-39Ar ages of intrusions in East Greenland: rift-to-drift transition over the Iceland hotspot. Lithos, **101**: 480-500.

Thrane, K. 2014: Characterisation of the South East Greenland basement – an ICPMS detrital zircon study. In: Stensgaard, B.M. (ed.) 2014: South-East Greenland Mineral Endowment Task (SEGMENT): 2014 Workshop Abstract Volume and Status Primo-2014. Danmarks og Grønlands Geologiske Undersøgelse Rapport. **2014/79**. GEUS, p. 80.

Thompson, R.N., 1982: Magmatism of the British Tertiary volcanic province. Scottish Journal of Geology, **18**: 49-107.

Thomsen, H.S., 1998: Geological and experimental constraints on the formation of the Late Archaean Skjoldungen Alkaline Province, Southeast Greenland and petrogenetic implications of late stage amphibole growth in arc environments, University of Copenhagen, unpublished 134 pp.

Thorning, L. 2009: Preparations for a mineral resource assessment programme in South-East Greenland (MRAPSEG). Danmarks og Grønlands Geologiske Undersøgelse Rapport. 2014/79. GEUS, 47 pp.

Tukiainen, T. 2014: The Archaean Skjoldungen Alkaline Province, South East Greenland – carbonatite intrusions confined to a specific 60 km long zone of the basement? [presentation without accompanying abstract; on CD-ROM] In: Stensgaard, B.M. (ed.) 2014: South-East Greenland Mineral Endowment Task (SEGMENT): 2014 Workshop Abstract Volume and

Status Primo-2014. Danmarks og Grønlands Geologiske Undersøgelse Rapport. **2014/79**. GEUS, p. 90.

Wager, L.R., 1934: Geological investigations in east Greenland, part 1. General geology from Angmagssalik to Kap Dalton. . Meddelelser om Grønland, 105.

Wager, L.R. and Deer, W.A., 1938: A Dyke Swarm and Crustal Flexure in East Greenland. Geological Magazine, **75(01)**: 39-46.

Wright, A.E., Tarney, J., Palmer, K.F., Moorlock, B.S.P. and Skinner, A.C., 1973: The geology of the Angmagssalik area, East Greenland and possible relationships with the Lewisian of Scotland. In: R.G. Park and J. Tarney (Editors), The Early Precambrian of Scotland and related rocks of Greenland. University of Keele, Keele, pp. 157-177.

18 Appendix I: SEGMENT Data Package

The SEGMENT Data Package that is accessible on the USB memory-stick that is enclosed in this report contains the following datasets (see also section 2):

18.1.1 Revised 1:500 000 scale geological map

The exsisting published 1:500 000 scale geological maps that covers the SEGMENT project area has been revised during the project. The resulting map is accessible in the ArcMap project on the memory-stick that is enclosed to this report. Also; a pdf file (scaled for A0 format) is also accessible for printing.

The basic of the revision is the parts of the earlier 1:500 000 published map sheets (sheet 1, 13 and 14; Garde 2007, Myers, Dawes & Nielsen 1988, and Escher 1990) and the 1:500 000 seamless digital representation of entire Greenland (version as of January 2016; see Pedersen 2013; http://data.geus.dk/map2/geogreen) which covers the SEGMENT project area. The revision covers the onshore ice-free areas between 62°00'N – 67°00'N and 33°00'W – 44°00'W.

The revision is based on a review of exsiting data and information as well as all available new acquired data, etailed mapping in selected areas and new knowledge obtained during the SEGMENT project. All earlier defined rock units and most established boundaries/structurs was visited and revised if necessary according to field observations, new data sets and knowledge.

18.1.2 Localities and oblique photos

Photographs have been taken by field participants taken during the field campaigns, only the relevant ones and those having coordinates are included, these are labelled *Photos_locality_YYYY*. Campaigns of photoflying have also been undertaken around the Skjoldungen area in 2009 and 2011. There are about 15,500 photographs (10,000 photos from different localities and 5,500 aerial photos).

18.1.3 Structural measurements

Structures measured in the field are included under this heading. Data has been collected by the field participants. The participants have laid various emphases on it, and are reflected in the data set. The attribute table lists name of sampler, dip and direction, plus detail description. In all there are 1734 lines of structural readings.

18.1.4 Digital Field Data – description of localities, samples, etc.

Two separate systems have been used to capture field data. Both data sets are available here and can be opened as Fieload and Ganfeld. In all there are c. 6,000 lines of data. Fieload hold 75 columns, and the Ganfeld c. 160 columns.

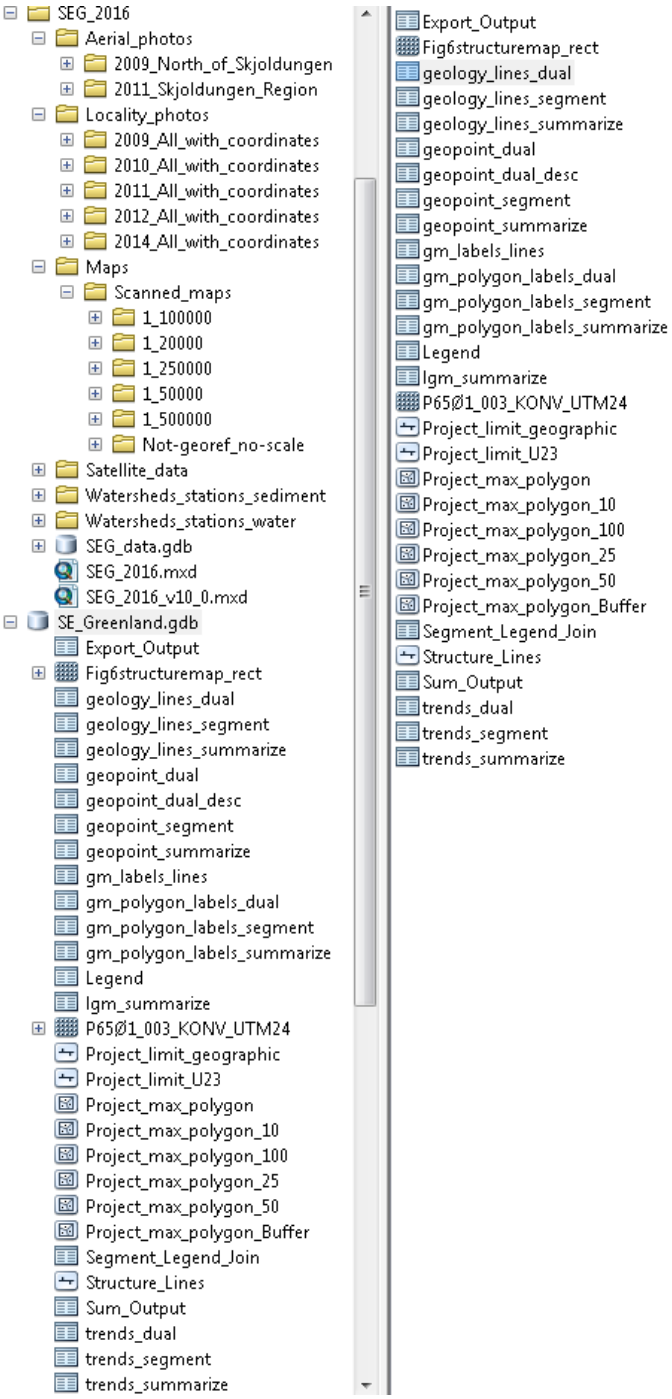

Figure 18.1. *Tree structure of the SEG_2016 folder, showing the sub-folders and the geodatabase (SEG_data.gdb) hosting data that can be shown in ArcMap and ArcCatalog environment.*

18.1.5 Lithogeochemistry

Lithogeochemistry is geochemical analyses of rock samples, collected from outcrops or float. In addition they may be chip samples. There are 1156 lines of data, hosting major elements and trace element analyses. Elements that are not analysed are not empty, but hold null values. Values below detection limit are negative.

18.1.6 Fine-fraction sediment sample geochemistry

Campaigns of stream sediment samples collection was launched in 2009 and 2010. In all 998 samples were collected, including duplets. The various attributes are included in the tables as well as the geochemical data that was analysed. Later stream sediment samples may have been taken later, but do not occur in these two tables.

18.1.7 Stream- and surface water chemistry

Along with the stream sediment sampling water samples were also undertaken. These data are found in three tables: *Water_2009_pH_chem_cond*, *Water_2010_chem* and *Water_2010_pH_cond*. I.e. the 2009 dataset includes pH and conductivity readings along with geochemical analyses, while the 2010 data set has been spilt up into geochemistry in one table and pH and conductivity in a second one. In all there are 997 lines of data regarding the water samples.

18.1.8 Indicator minerals from till samples

Till sample campaign was only undertaken in 2009 and sampled the area around Skjoldungen and Timmiarmiut. The total number of till samples is 132. The till samples have been analysed for kimberlite indicator minerals (listed as *TILL_KIM* in ArcMap), magmatic or metamorphic massive sulphide (*TILL_MMS*), precious group metals (*TILL_PGM*) and gold (*TILL_AU*).

18.1.9 Watershed in Skjoldungen region

Watershed_stations is the hinterland areas that the stream or water samples collected drained. Thus there are two subsets, one for stream sediment samples and the other water samples (*watershed_stations_sediment* and *watershed_stations_water,* respectively). The Watershed is only defined for the Skjolungen region.

18.1.10 Scanned maps from previous field campaigns

Scanned maps from previous field campaigns are listed in this theme and sorted according to scale. The sub-layers (*1:20,000*; *1:50,000*; *1:100,000*; *1:250,000* and *1:500,000*) hold maps that are in or between the scale of the sub-layer names. Non georeferenced maps are stored in a separate folder, visible in File Manager, and located under \SEG_2016\Maps\Scanned_maps\Not-georef_no-scale

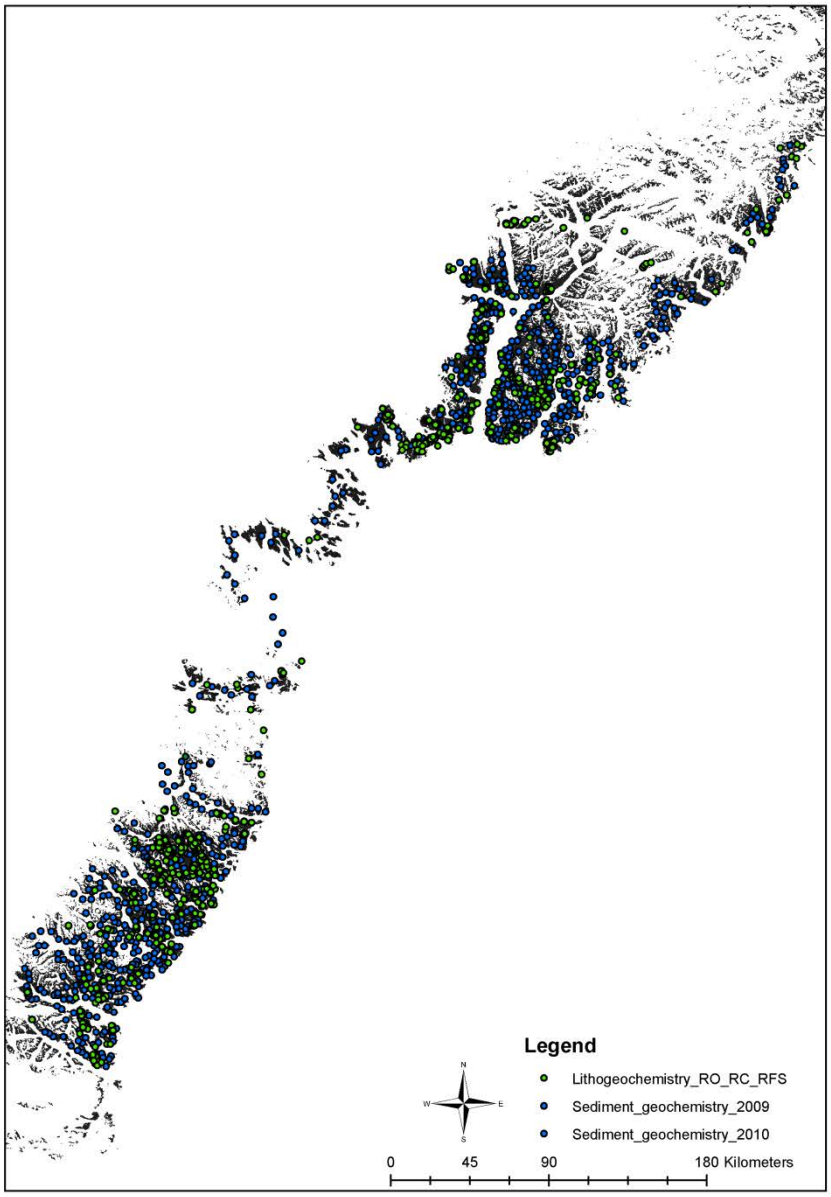

Figure 18.2. *Project area, showing lithological (green) and stream sediment (blue) samples. Background is silica index (white is low, black is high) from satellite data.*

18.1.11 Satellite data

Two subsets of satellite data (ASTER) are provided: *VNIR MOSAIC@15M*, consists of two false coloured mosaic files from 62° to 68°N, and *Mineral_indices*, consisting of processed showing the silica and mafic index, obtained from similar scenes as the mosaic images.

18.1.12 Geochronology

Age determinations have been performed on 193 samples from the Skjoldungen area and 53 from the Tasiilaq area (total 246 samples). These data are located in *Skjoldungen_U_Pb* and *Tasiilaq_U_Pb*.

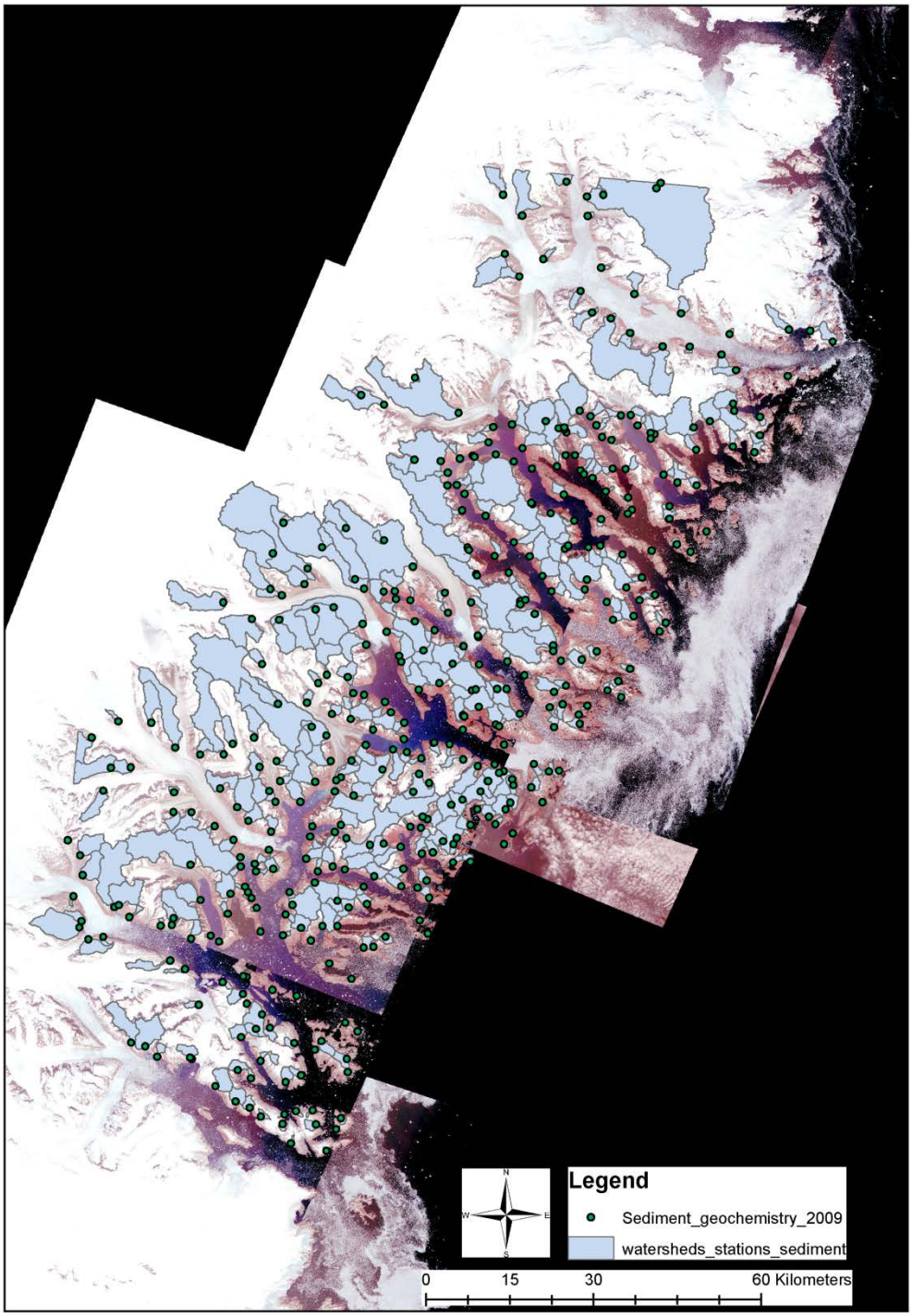

Figure 18.3. *Skjoldungen-Timmiarmiut area, with watershed_stations_sediment and sediment sample points overlain on VNIR MOSAIX@15M.*

TERMS OF DELIVERY

The following terms of delivery cover data and documentation (hereafter referred to as 'Data') available from the data storage device, in this case a 64 Gb MicroSD memory card, attached to this GEUS Report (hereafter referred to as the "Data Storage Device"), including (but not limited to) geophysical and geochemical data, reports, maps and photos.

The report is made under a joint research project between the Geological Survey of Denmark and Greenland (hereafter referred to as GEUS) and the Ministry of Mineral Resources under the Government of Greenland (hereafter referred to as MMR).

1. 'Data'

'Data' available on the 'Data Storage Device' are derived from the databases, processed or worked up by GEUS and/or MMR through systematization, quality control, interpretation, digitalisation, and/or other data processing. 'Data' may consist of data reported to GEUS and/or MMR or produced/gathered by GEUS and/or MMR.

2.1 Proprietary Rights and Copyrights

The 'Data Storage Device' contains data and documentation (hereafter referred to as the 'Data'), which are covered by copyrights. This agreement only transfers the proprietary rights to the delivered copy of the 'Data' and a limited right of use, as specified in Section 5.2 to the Customer. No proprietary rights, copyrights or other rights contained in the 'Data' are transferred to the Customer or user of the GEUS Report and/or the attached Data Storage Device.

The rights of the parties according to these terms include the 'Data' in any shape, including the digital format.

2.2 Customer's Rights

The Customer has a non-exclusive right to use the 'Data' for internal purposes only, including the right to process the 'Data', the right to data extraction from the 'Data', and the right to make one safety copy of the 'Data' for own use only.

The Customer is not entitled to produce or transfer to third parties products based on processed 'Data', unless it is for pure non-commercial information purposes within the Customer's field of business/field of competence. However, the Customer is not entitled to produce or transfer to third parties new maps based fully or partly on processed 'Data'.

The rights according to these terms of delivery include the rights to 'Data' in digital form as well as in any other form.

The Customer's rights according to these terms of delivery may be utilised by individuals employed by the Customer or with any fully controlled subsidiaries of the Customer. Furthermore, the Customer is entitled to make the 'Data' available to contractors, consultants and the like in connection with work undertaken for the Customer. In this event, the 'Data' may only be made available to others to the extent dictated by the specific purpose.

If the Customer is a consultant or the like, who purchases/downloads the 'Data' for the purpose of performing work for a customer, the "for internal purposes" may be extended to cover "the customer's internal purposes", which is conditioned upon the term that 'Data' (original as well as processed 'Data') is transferred to one customer only. If the Customer is a municipality, county or another governmental body within the Kingdom of Denmark, including Greenland and the Faroe Islands, "for internal purposes" may include the Customer's right to use the 'Data' for administrative purposes within its jurisdiction, including handling of specific cases, and for planning purposes, including preparation of regional plans etc. Furthermore, the Customer is entitled to make the 'Data' (original as well as processed 'Data') available to other governmental bodies or private individuals as part of the handling of specific cases for the Customer.

2.3 Redistribution

The Customer is not entitled to copy, publish, resell, lend or rent samples of the 'Data' or part hereof or otherwise redistribute the 'Data' (original as well as processed 'Data') in any other way than described in article 5.2 without the prior written consent of the copyright holder. This includes redistribution to collaboration partners in exploration or production partnerships or transfer of data from one company to another if changes occur in exploration or production partnerships.

If the 'Data' are redistributed or otherwise made available to third parties in accordance with article

5.2 above or in accordance with a specific written agreement, the Customer is obliged to inform the third party of and impose on him the obligation to respect GEUS' and MMR's rights according to the present terms of sale and delivery.

2.4 Source Reference etc.
The Customer is obliged to duly acknowledge GEUS and MMR (and any other rightful co-owner) as data source in accordance with the Danish law on copyrights and common practice.

3 Liability and Force Majeure
GEUS and MMR warrant that 'Data' are in accordance with GEUS' and MMR's databases at the time of delivery.

'Data' produced by GEUS and/or MMR are collected and interpreted in accordance with the scientific practice at the time of the data collection. However, GEUS and MMR disclaim any responsibility for the quality of the 'Data' and the applicability of the 'Data' to the Customer's purposes. Therefore, GEUS and MMR do not assume any liability in respect of the consequences of the Customer's use of the 'Data', whether the consequences are caused by defects or shortcomings of the 'Data', the Customer's handling or use of the 'Data', or by any other reason. The same applies to 'Data' reported to GEUS and/or MMR by third party. These conditions apply notwithstanding the information regarding exactness, use etc. of the data in the agreement between the parties, the order confirmation or the order form.

GEUS and MMR are not responsible towards the Customer for conditions due to circumstances beyond GEUS' and MMR's control and which GEUS and MMR, upon entering the agreement, should not have taken into consideration nor have avoided or overcome, including interruption of work, strikes and lockout at GEUS and MMR etc.

GEUS and MMR are not liable for business loss, loss of profits, loss of earnings or other indirect losses. GEUS' and MMR's liability for errors and shortcomings is in any case limited to DKK 10,000.

4 Disputes
In case of disputes between the parties in connection with the agreement, each party is obliged to solve these disputes amicably. Disputes, which are not solved amicably, must be referred to Københavns byret (Copenhagen City Court). Danish law is applicable.